ASTIA Document No. 05000 5-T

THE UNIVERSITY OF MICHIGAN

NOISE IN MULTI-DIMENSIONAL ELECTRON STREAMS

TECHNICAL REPORT NO. 59

ELECTRON PHYSICS LABORATORY
Department of Electrical Engineering

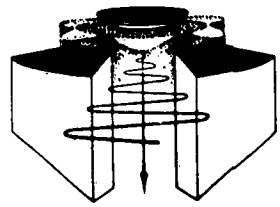

By: C. P. Wen

Approved by: J. E. Row

March, 1963

CONTRACT WITH:

ELECTRONIC TECHNOLOGY LABORATORY, AERONAUTICAL SYSTEMS DIVISION, WRIGHT-PATTERSON AIR FORCE BASE, OHIO. DEPARTMENT OF THE AIR FORCE, PROJECT NO. 4156, TASK NO. 415603, CONTRACT NO. AF-33(657)-8050

OFFICE OF RESEARCH ADMINISTRATION • ANN ARBOR

Qualified requesters may obtain copies of this report from ASTIA.

THE UNIVERSITY OF MICHIGAN
ANN ARBOR, MICHIGAN

NOISE IN MULTI-DIMENSIONAL ELECTRON STREAMS

TECHNICAL REPORT NO. 59

Electron Physics Laboratory
Department of Electrical Engineering

By

Cheng P. Wen

Approved by: J. E. Rowe

J. E. Rowe, Director
Electron Physics Laboratory

Project 05000

CONTRACT NO. AF-33(657)-8050
DEPARTMENT OF THE AIR FORCE
PROJECT NO. 4156, TASK NO. 415603
PLACED BY: ELECTRONIC TECHNOLOGY LABORATORY
AERONAUTICAL SYSTEMS DIVISION
WRIGHT-PATTERSON AIR FORCE BASE, OHIO

March, 1963

This report has also been submitted as a dissertation in partial fulfillment of the requirements for the degree of Doctor of Philosophy in The University of Michigan, 1963.

ABSTRACT

The purpose of this investigation is to study the noise transport and reduction phenomena in multivelocity electron beams with significant potential variations in the transverse direction. Correlations between the noise reduction mechanism and the multi-dimensional nature of the electron beams are sought. The investigation was carried out by means of a high-speed digital computer employing two different numerical methods. The mathematical model assumes an infinite confining magnetic field so that transverse motions are not allowed. In addition a one-dimensional half-Maxwellian velocity distribution function is considered for the electrons at the potential minimum.

Details of the derivation of a small-signal linearized Boltzmann equation in terms of a statistical electron density function and the electric field in a two-dimensional space-charge-limited diode are presented, together with some discussion on the singularities in the boundary conditions and the formulation of the a-c electric fields. To facilitate a solution of the transport equation, velocity classes are introduced as an approximation so that digital techniques become applicable. Haus's noise theory for small-signal longitudinal beam devices is employed to evaluate the noise transport characteristics of the two-dimensional electron beam.

In parallel with the density function analysis, the transport phenomena in a two-dimensional diode are treated with the Monte Carlo technique in which random numbers are generated to simulate the stochastic emission process and each electron emitted from the thermionic cathode is traced in phase space by numerical integration methods. The methods employed to evaluate the d-c and a-c electric fields are discussed, especially the implications of the widely used open-circuit assumption. A brief description of the generalized harmonic analysis is included and Haus's noise parameters are estimated statistically by means of sampling techniques. Because of the thin beam assumption, the axial a-c electric field is assumed to be uniform in the transverse direction. Only the d-c multi-dimensional effects are actually included in the Monte Carlo calculations.

Results from the density function calculations are presented. No reduction from the thermionic emission shot noise is observed, nor is there any evidence of the multi-dimensional noise reduction effects expected. Re-examination of the coupling mechanism employed reveals that the z-directed a-c electric field decays too rapidly in the transverse direction to bring forth any significant two-dimensional effects. Because of the velocity dependent characteristics of the coupling fields, the heavy emphasis placed on the fluctuations associated with the slow electrons results in a net reduction of the kinetic power carried by the electron beam, causing deterioration in noise performance.

Substantial noise reduction at low frequencies for the two-dimensional diode is found by means of the Monte Carlo calculations. A minimum noise figure of less than 2 db is predicted for O-type devices. The reduction in beam noise is believed to be a result of the large Π/S ratio developed in the extended multivelocity region created by the two-dimensional space-charge effects. Comparisons are made between the results obtained here and previous results from the analyses employing one-dimensional diodes of similar d-c configurations.

The large discrepancy between the results from the two numerical methods of noise transport calculations in two-dimensional diodes of identical d-c characteristics pointed out the extreme importance of the coupling mechanism approximations. Further improvement of the electron beam noise transport theory would depend on a thorough understanding of the actual coupling mechanism in a multi-dimensional realistic electron beam model.

ACKNOWLEDGMENTS

The author wishes to express his gratitude to Professor Joseph E. Rowe, the chairman of his doctoral committee, for his guidance and encouragement during the course of the work and to Professor Gunnar Hok for many stimulating discussions and helpful suggestions. Special thanks should also go to Messrs. E. Fronczak and A. Pajas for their contributions in programming the computer. Finally, the administrative staff of the laboratory is gratefully acknowledged for their assistance in the preparation of the text and the figures.

This work was made possible through the sponsorship of the Rome Air Development Center, Contract No. AF-30(602)-2303, and the Electronic Technology Laboratory of the Aeronautical Systems Division at Wright-Patterson Air Force Base under Contract No. AF-33(657)-8050.

TABLE OF CONTENTS

LIST OF ILLUSTRATIONS

LIST OF TABLES

CHAPTER I. INTRODUCTION

1.1 Noise in Longitudinal Beam-Type Amplifiers

Ever since the invention of such electronic communication systems as telegraphy, telephone, radio, etc., much effort has been exerted on the improvement of the reliability and sensitivity of the receivers. For ideal systems, a receiver consists of one or more amplifiers and a detector designed to recover the original signal. Unfortunately, it is impossible to avoid a certain amount of uncertainty introduced by those imperfect amplifiers or detectors, and the undesirable fluctuations thus introduced will reduce the reliability and especially the sensitivity of the entire receiving system.

Prior to the discovery of such ultra-low-noise devices as masers, parametric amplifiers and other solid-state amplifiers, the longitudinal beam-type device has been the only device with which appreciable amplification of an electronic signal at microwave frequencies could be accomplished without introducing an excessive amount of uncertainty in the signal. However, because of the presence of velocity and current fluctuations in the electron beam, the kinetic-energy source, a certain amount of noise* will be detected at the output superposed on the amplified signal. In small-signal detection the sensitivity of a longitudinal-beam amplifier is limited by the shot noise current and the velocity fluctuations originating at the thermionic cathode.

---

* Noise is generally considered to be the amount of uncertainty existing in a physical process; it may be represented by a chance variable whose instantaneous behavior is not predictable from its past history. In this dissertation, the representation of noise is limited to stationary ergodic random processes only.

Various investigations on noise transport phenomena have been carried out in the past starting with low-frequency diodes and carrying on to accelerated electron beams. The one-dimensional single-velocity model gave a beam noise conservation theory predicting a theoretical minimum noise figure of longitudinal beam-type devices of 6-1/2 db. On the other hand, with the distribution of velocities in the electron beam taken into account, nearly a 3 db reduction in noise figure was predicted by Watkins' multivelocity analysis. Currently the best experimental noise performance of 2-1/2 db noise figure at frequencies near 3 Gc is still unaccounted for by the existing one-dimensional noise theories. In view of the fact that a substantial reduction in noise temperature has been observed in amplifiers with a controlled potential distribution near the cathode and that hollow electron beams are employed in the ultra-low-noise amplifiers, a question is raised as to how the noise characteristics of an electron beam will be affected by the multi-dimensional potential distribution.

1.2 Thermionic Emission and the Origins of Noise in Electron Beams

Thermionic emission is defined as the phenomenon by which some electrons in a metal or semiconductor material held at an elevated temperature escape from the surface into the neighboring space. The emission mechanism can be represented as stationary random processes. At the cathode plane, two kinds of fluctuations are observed, namely, the fluctuations of the emission current and the initial velocities of the electrons. In noise transport analyses the interest is primarily directed to the frequency domain, where the noise properties are conventionally represented and the spectral densities of the two variables are the significant characteristics.

At low frequencies, where the transit angles of the electrons across a diode are negligible compared to 2π, Schottky[1] obtained a formula for the self-power spectral density of the current fluctuations, under temperature-limited conditions, which are referred to as shot noise.

$$S_1(f) = 2eI_o \quad \text{for} \quad f \to 0 \ , \tag{1.1}$$

where I_o is the average current. Meanwhile, an expression for the power spectral density of the velocity fluctuations created by shot noise in the emission current was derived by Rack[2].

$$S_2(f) = \frac{|e|kT_c}{mI_o}(4-\pi) \quad \text{for} \quad f \to 0 \ , \tag{1.2}$$

where m = mass of an electron,

T_c = temperature of the cathode in degrees K,

k = Boltzmann's constant.

The equipartition of energy in frequency so indicated is valid only for low frequencies ($kT \gg \hbar\omega$). For the noise transport investigation carried out in this report, both Eqs. 1.1 and 1.2 are assumed valid.

1.3 Survey of Previous Noise Transport Studies

Previous noise studies were carried out for one-dimensional electron beam models and they could be classed generally in one of two categories. In one category the single-velocity assumption was employed in a small-signal perturbation analysis for diodes or electron beams in which the thermal velocity spread was negligible; in the other category, the formation of a potential minimum away from the surface of the cathode constituted a multivelocity electron beam in which a portion of the electrons emitted would eventually be returned to the cathode because of the negative potential gradient.

1.3.1 Space-Charge Reduction of Noise in Diodes of Small Transit Angle. The phenomenon of space-charge reduction of shot noise in diodes was first treated by Rack[2] based on the Llewellyn-Peterson[3,4] equations. At low frequencies, where the transit time effect is small, a shot noise reduction factor of 0.644 was obtained for space-charge-limited diodes operated under Child's law.

Pierce[5] made use of the open-circuit assumption and showed that the fluctuations in current density at the cathode produce no significant effects on the fluctuations at the anode. An identical noise smoothing factor was derived in his simplified single velocity model diode in which similarity between the potential distribution beyond the minimum and Child's law was assumed.

The mechanism of noise reduction by space charge has long been recognized to be the gating action of the potential minimum in regulating the number of electrons passing through. In a diode operated under full space charge, any instantaneous increase over the average number emitted from the cathode would result in lowering the potential minimum immediately and in turn decrease the percentage of electrons passing through. Noise reduction is accomplished by the establishment of the compensation currents opposite to the original disturbance.

Thomson, North and Harris[6] made an attempt to evaluate the smoothing factor for a multivelocity model diode assuming independent fluctuations for each velocity class at the cathode. For a moderate anode potential, the noise reduction factor thus obtained is the same as the single-velocity approximation.

1.3.2 Noise Transport in High-Frequency Diodes. At high frequencies the transit time effect becomes important and the noise reduction mechanism must be treated from a somewhat different approach.

Rack[2] has extended his single-velocity analysis to include the effects of finite transit angles. Later on, Peterson[7] applied the Llewellyn-Peterson equations to evaluate the noise reduction in a tetrode, and Pierce[8] employed the same method to estimate the noise in an electron beam with zero velocity at the potential minimum, realizing that such an assumption would lead to the elimination of the effects produced by current fluctuations at the cathode plane. However, his assumption contradicts the fact that the average electron velocity at the potential minimum is small but finite, and the velocity fluctuations there are not the only source of noise.

Whinnery[9], Siegman and Watkins[10,11] attempted to establish the boundary conditions at the potential minimum of a multivelocity flow model for both zero and finite transit angles. An equivalent noise was obtained from a macroscopic point of view; unfortunately, it is rather doubtful that the reduced noise obtained by the multivelocity analysis would be applicable to the single-velocity theory.

1.3.3 Reduction of Noise in Beam-Type High-Frequency Devices and the Minimum Noise Figure in the Single-Velocity Theory. An artificial method for noise reduction was first suggested by Watkins[12] at the time when velocity fluctuations were still considered to be the only effective noise source at the potential minimum. Because of the invariant characteristic of the kinetic potential,

$$V_1 = -\frac{u_o v_1}{h} ,$$

where h is the absolute value of electron charge-to-mass ratio, the magnitude of the a-c velocity v may be reduced in the case of a sudden increase in d-c potential at the velocity fluctuation maxima. Following this argument, Watkins proposed that periodically repeated sudden

accelerations and decelerations placed a quarter plasma wavelength apart may in the limit reduce the velocity fluctuations to zero, i.e., the theoretical minimum noise figure would be zero according to this theory.

Peter and Bloom[13,14] derived the transmission-line analog for space-charge-wave propagation in univelocity accelerated electron beams. The r-f impedance of a thermionic cathode may be matched to the electron beam impedance at the input of the amplifier through one or more exponential transformer sections. Theoretically this is an ideal method of noise reduction because of the smooth transition of the d-c potential along the electron beam in an exponential impedance transformation region. The minimum achievable noise figure of a one-dimensional longitudinal beam-type amplifier as predicted by the preceding transport analysis is approximately 6-1/2 db with current fluctuations also taken into account.

Meanwhile, Haus and Robinson[15,16] carried out a general study of noise transport behavior in a single-velocity electron beam using the kinetic power theorem. A noise invariance theory was established together with the introduction of some characteristic noise parameters representing the self-power-spectral density and the cross-power-spectral density. Haus concluded from his theory that correlations between velocity and current fluctuations should remain unchanged in the propagation direction of the electron beam.

1.3.4 Multivelocity Theories. Siegman, Watkins and Hsieh[17,18] in a series of two papers described the formulation and the method of solution of the noise transport problem in a multivelocity flow diode utilizing the density function analysis. A set of linearized small-signal multi-coupled differential equations governing the behavior of the density functions was solved numerically by a forward integration

method for an open-circuit diode operated under Child's law. Contrary to the single-velocity theories, a certain amount of correlation was developed between the current and velocity fluctuations previously supposed to be independent in the region where multivelocity flow prevailed. Neither the noise parameters nor the theoretical minimum noise figure were found to be invariant by the authors and the question of the existence of a theoretical minimum was again raised.

Vivian[19] performed similar computations on a space-charge-limited diode with a potential minimum, knowing that linear transformation methods could be applied to evaluate the boundary conditions at the potential minimum plane. Due to the rough approximations employed in his discrete beam model, the inclusion of the reflected flows failed to show appreciable effects on the end results.

Following the invention of the ultra-low-noise electron gun by Currie[20], extensive studies of noise propagation in low-velocity drifting electron beams were carried out both analytically and numerically by various authors. The nonconservative nature of the noise parameters was demonstrated by Berghammer and Bloom[21] in a low-potential multivelocity drifting electron beam; and by means of the kinetic power theorem in electron beams with appreciable velocity spread, Hok[22] showed that the real part of the kinetic power is not necessarily an invariant. Similar results were also obtained by Shaw[23] and others while solving the Boltzmann transport equation for a drifting beam with square velocity distributions.

The Monte Carlo approach to the noise problem in electron beams was first investigated by Tien and Moshman[24] to calculate the shot effect at a plane just beyond the potential minimum of a short-circuited diode.

A direct simulation of the emission process and the mechanism of establishing the self-consistent electric fields in a one-dimensional diode was performed by means of a high-speed electronic computer. Instead of studying the macroscopic behavior of the smoothed out quantities like currents or density functions, the electrons were traced in phase space after emission which was simulated by some stochastic processes with appropriate distributions. Fluctuations in the electron beam would then be evaluated at several planes beyond the potential minimum using statistical methods. Appreciable noise reduction was found at low frequencies and a sudden dip in the noise reduction factor was observed just below the plasma frequency corresponding to the electron concentration at the potential minimum. Besides these, no coupling was observed between the noise current and the velocity fluctuations.

The same approach was again employed by Lambert and Dayem[25] to analyze the transport problem in an open-circuit diode which has dimension and emission characteristics identical to Tien and Moshman's diode. Similar to other open-circuit diode noise analyses, the dip in noise reduction factor no longer exists and some correlations between the two independent noise sources were observed.

1.3.5 Reactive Damping of Noise in an Electron Beam with Finite Diameter. Berghammer[26] demonstrated the possibility of the existence of a new noise reduction mechanism in a low average velocity electron beam of finite diameter using the square velocity distribution. It is believed that in addition to the two space-charge waves described by Ramo and Hahn[27,28], two decaying waves propagating in opposite directions might exist. This is similar to the damping mechanism proposed by Landau in plasma physics.

In summary, the literature contains numerous noise transport and reduction analyses in electron beams. However, each of the above analyses, except the newly developed reactive damping hypothesis, is limited to one-dimensional models. It appears that a thorough study of the multi-dimensional effects on the noise characteristics of an electron beam has not yet been carried out. An investigation of this type would be desirable because the extremely low-noise figures achieved experimentally are still unaccounted for by existing noise theories.

1.4 Noise Transport in a Two-Dimensional Space-Charge-Limited Diode

During the past three years noise figures lower than 3 db have been achieved in longitudinal beam amplifiers at S-band frequencies. Because of the discrepancy between experimental results and the existing one-dimensional theories, in which the Fry-Langmuir potential distribution was adopted, it was suggested to the writer by Professor J. E. Rowe that the multi-dimensional effect in the vicinity of the potential minimum may better explain the transport and reduction phenomena in a space-charge-limited hollow-beam diode.

1.4.1 Two-Dimensional Model. In the following chapters, the noise transport characteristics of a theoretical multi-dimensional high-frequency diode will be studied by two different numerical methods. Since the noise characteristics of thin annular beams are found to be superior to the conventional pencil beams, a mathematical model is chosen to simulate a hollow beam with a small thickness-to-radius ratio. If all the variations in the circumferential direction are neglected, each small section of this actual electron beam may be expanded and developed into a thin ribbon beam of infinite width as shown in Fig. 1.1, resulting in a reduction by one dimension. Noise analyses are to be carried out for

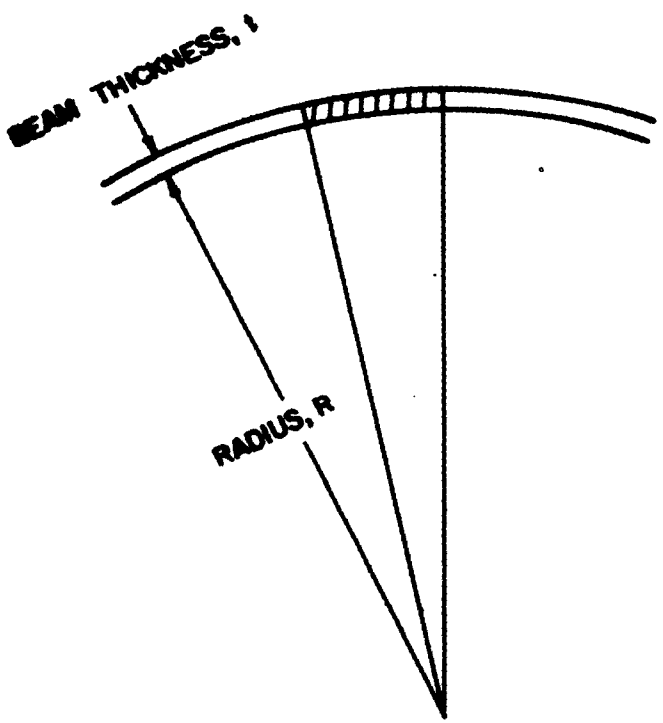

A SECTION OF A HOLLOW ELECTRON BEAM.
ACTUAL MODEL.

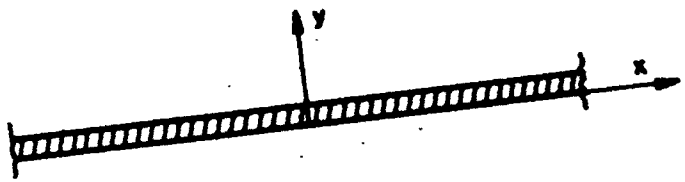

THIN RIBBON BEAM OF INFINITE WIDTH.
A THEORETICAL MODEL FOR A TWO-
DIMENSIONAL NOISE TRANSPORT ANALYSIS.

FIG. 1.1 THEORETICAL TWO-DIMENSIONAL BEAM MODEL.

the two-dimensional electron beam model thus obtained, flowing between two parallel plane electrodes.

1.4.2 Methods of Investigation. Among the methods of analysis adapted by previous workers only the density function method and the Monte Carlo techniques are valid in the cathode-potential minimum region where reflected flows exist. Both methods will be employed in the following chapters to solve the problem of noise propagation for a two-dimensional discrete-beam diode with identical emission characteristics to the one-dimensional diode selected by Tien and Moshman and Lambert and Dayem.

In the density function method, the analysis of noise or signal propagation along an electron beam depends on the simultaneous solution of a set of linearized multi-coupled a-c transport equations corresponding to various velocity classes in the discrete beam. Numerical solutions may be obtained with the aid of a high-speed electronic computer. Because of the linear nature of the working equations, the well established linear transformation theories may be applied to establish the boundary conditions for the transmitted flows at the potential minimum, making it possible to evaluate the effects due to the electrons returning to the cathode. Coupling between streams not experiencing the same d-c electric field is accomplished by the a-c electric field associated with the convection current in the diode. It is believed that correlations between velocity and current fluctuations will be developed through the a-c coupling electric fields.

The Monte Carlo method of noise transport calculation is, on the other hand, extremely simple in mathematical formulation. Random numbers are generated corresponding to the stochastic emission process and each

electron emitted is traced in phase space throughout by numerical integrations. Both linearization and singularity extractions are avoided and hence the true nature of electrons inside a beam is preserved. Coupling between streams is achieved by the open-circuit assumption. Potential distribution inside a two-dimensional diode with certain boundary conditions are evaluated by taking the time average of the self-consistent potential profile under space-charge-limited conditions and the instantaneous electric fields are computed by the image method summing over all electrons inside the diode.

Noise parameters at some planes where only transmitted flows exist are evaluated and the results obtained by these two methods of analysis are compared with previous ones derived using the one-dimensional theory.

CHAPTER II. DENSITY-FUNCTION FORMULATION

2.1 Introduction

In the following sections, the Boltzmann transport equation is formulated in terms of the density function, the electric fields and the operating frequency for a space-charge-limited thermionic diode in two-dimensional space. The density function is defined as the density of electrons in a six-dimensional phase space in which electric charges and masses are considered to have a continuous probabilistic distribution. Instead of studying the microscopic movements of individual electrons, the density-function method of noise transport studies deals with the average macroscopic behavior of the density functions which is in turn governed by the Boltzmann transport equation. Discrete velocity classes and a discrete beam model are introduced to reduce the nonlinear transport equation to a set of linear small-signal differential equations mutually coupled through the space-charge electric fields. Linear transform techniques are thus applicable in solving the boundary-value problems with uncorrelated (independent) inputs.

The method of extraction of singularities is described in detail and the source of the singularities is also investigated. Special attention is directed to the disappearance of Watkins's[18] low-frequency limit in the transport equation for a two-dimensional electron beam.

Details of the density-function formulation are included and the expressions for the noise parameters in terms of the density functions are developed. Haus's noise theory for small-signal longitudinal-beam devices is employed to evaluate the minimum achievable noise figure

for an amplifier in which important quantities depend upon two space dimensions.

2.2 A Discrete Beam Model Two-Dimensional Diode

In the following noise transport analyses, the actual two-dimensional electron beam is replaced by a mathematically discrete beam model to facilitate solution by digital computer techniques. In two-dimensional models, all variations in one of the transverse directions are ignored. For a z-directed electron beam of finite thickness in the y-direction, no variation of any kind is allowed from $x = -\infty$ to $x = \infty$. If the ribbon beam illustrated in Fig. 2.1 is divided into small sections of thickness Δy, the total current per unit length in the x-direction may be replaced by a current sheet of equal magnitude at the center of the corresponding increment Δy. The resulting model thus consists of layers of current sheets of infinitesimal thickness located at $y = 0$, $y = \pm \Delta y$, $y = \pm 2\,\Delta y$ ... etc., separated by a small incremental distance Δy. The mathematical electron beam model may be made an arbitrarily close approximation to the real ribbon electron beam flowing between two electrodes of a diode immersed in a strong axial magnetic field by reducing the magnitude of each current sheet and increasing the number of current sheets per unit length in the y-direction.

The discrete beam method used in the analysis gives good approximations as long as Δy is small compared to the wavelength of the highest frequency of interest. In the density function method of investigation, only the z-directed current density is of importance, the width of the electron beam in the x-direction is taken to be unity at all times. Due to geometric symmetry, sheet beams of the same distance from the center of the ribbon beam should be identical in d-c characteristics.

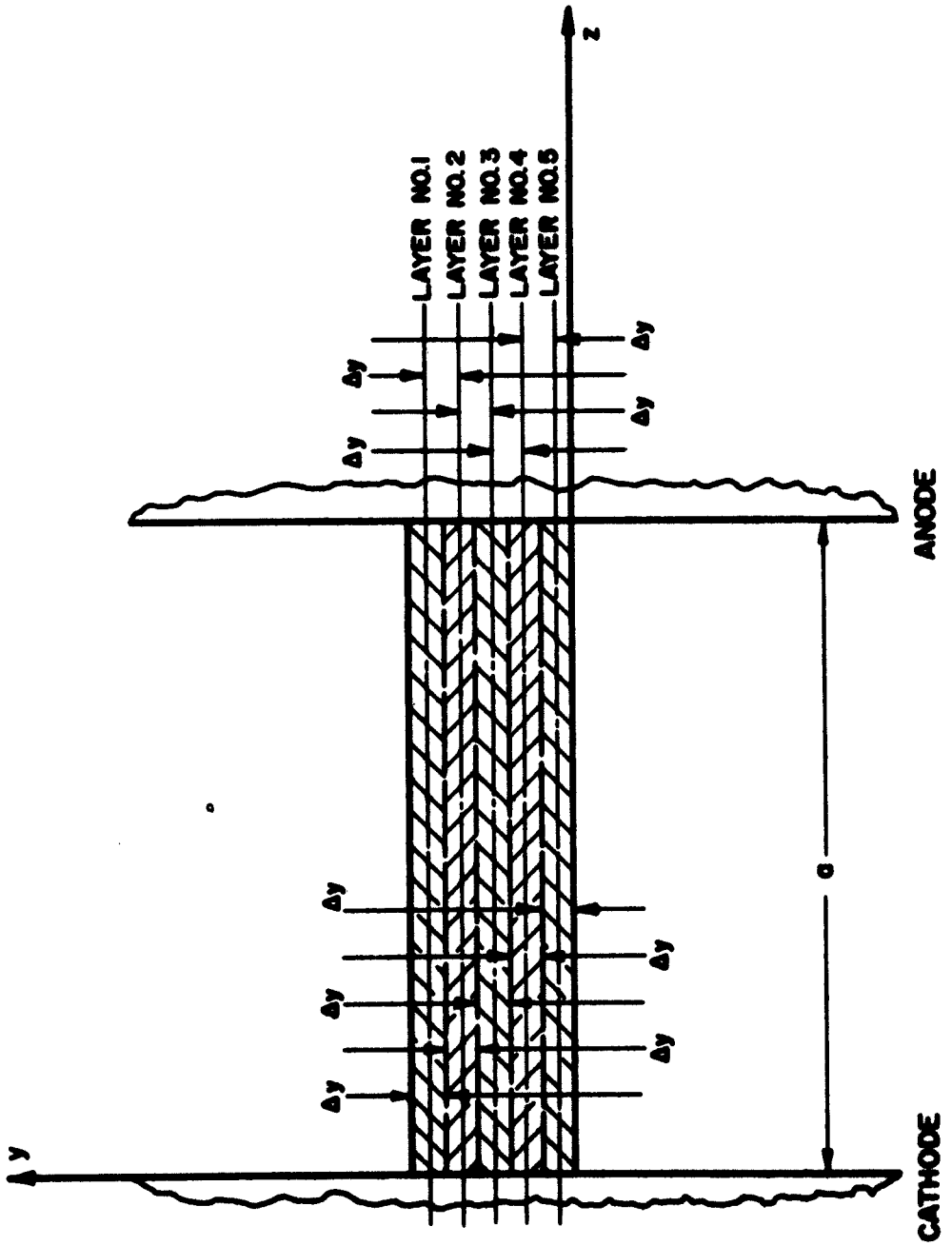

FIG. 2.1 TWO-DIMENSIONAL DISCRETE BEAM DIODE.

2.3 Assumptions

Certain assumptions are made to simplify the problem which is to be solved numerically on a digital computer.

1. The analysis is two dimensional, yet, no transverse motion of electrons is allowed. An infinite magnetic field parallel to the direction of the electron beam is assumed.

2. There are no direct collisions between electrons; this, together with the previous assumption, limits the coupling mechanism to space-charge forces alone.

3. Nonrelativistic assumption prevails.

4. The initial velocity distribution at the cathode is taken to be the Rayleigh distribution.

5. As shown in Fig. 2.2 the beam model is divided into many velocity classes; the number of velocity classes is large enough to insure a small velocity spread within each velocity class compared to its respective mean velocity.

6. The linearized small-signal Boltzmann transport equation is used in the analysis.

7. The fluctuation at the cathode plane in any one velocity class is assumed to be uncorrelated with the fluctuation in any other velocity class.

8. Those electrons returning to the cathode before reaching the potential minimum produce no effect on cathode emission. There is no secondary emission at either of the two electrodes.

9. There is no accumulation of electrons at the potential minimum. The probability that an electron should possess just enough energy to reach the potential minimum and stay there is zero.

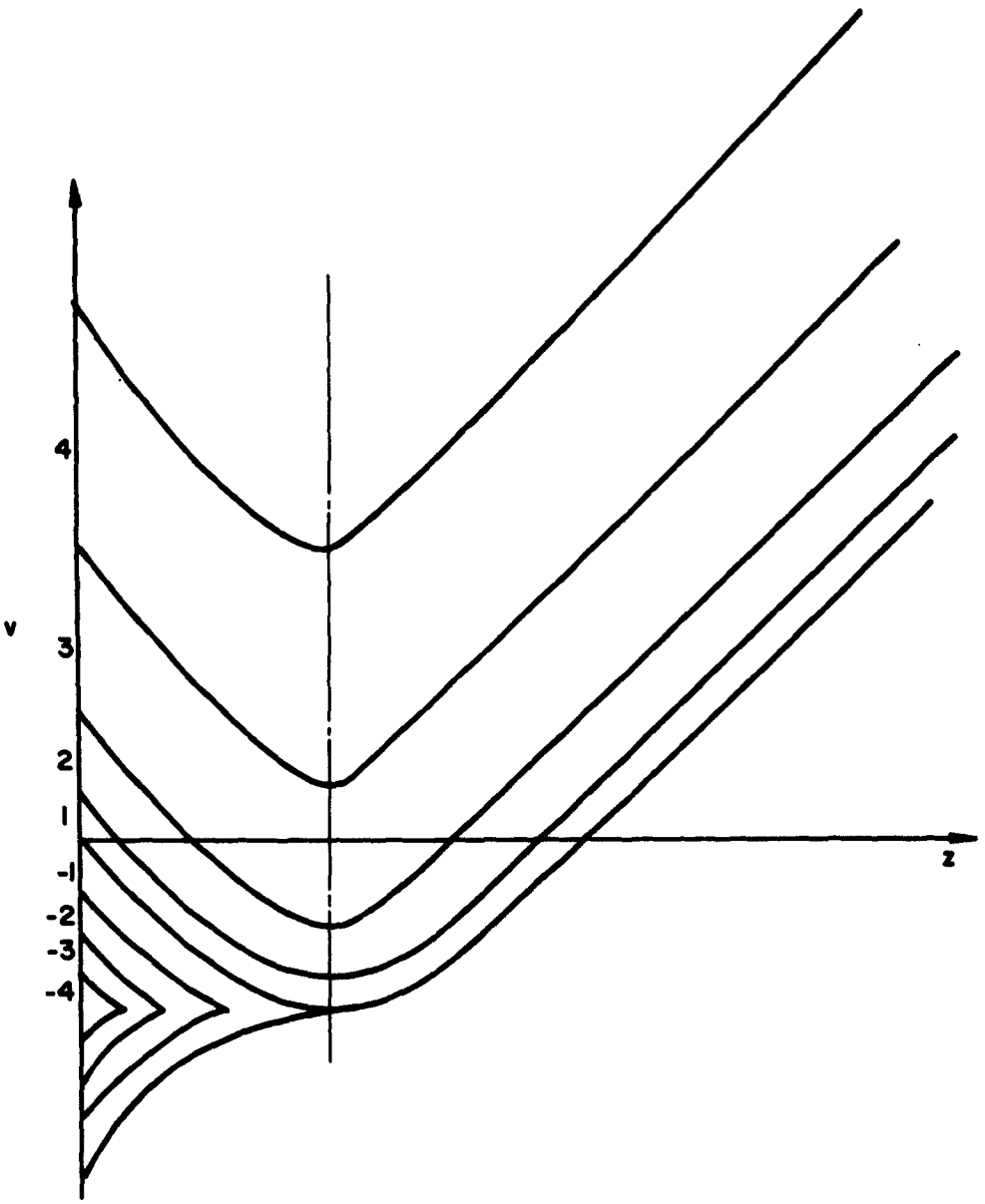

FIG. 2.2 RETARDING FIELD DIODE WITH DISCRETE VELOCITY CLASS. VELOCITY VS. DISTANCE FOR EACH LAYER OF THE ELECTRON BEAM.

10. The d-c potential distribution is obtained from the time average of the potential distributions from the Monte Carlo calculations.

2.3.1 Transport Equations. The transport equations written in terms of the density functions, the electric fields and the operating frequency are obtained from the combination of Liouville's theorem, the force laws and the small-signal assumption. The density function $F(y,z,\dot{y},\dot{z},t)$ for a two-dimensional model is defined such that $[F(y,z,\dot{y},\dot{z},t)\, dy\, dz\, d\dot{y}\, d\dot{z}]$ represents the number of electrons found between y and y + dy, z and z + dz with y-directed velocities between $\dot{y}$ and $\dot{y} + d\dot{y}$ and z-directed velocity components between $\dot{z}$ and $\dot{z} + d\dot{z}$ at time t. According to Liouville's theorem, the density function $F(y,z,\dot{y},\dot{z},t)$ in phase space is invariant with respect to time; i.e., the total derivative of $F(y,z,\dot{y},\dot{z},t)$ with respect to time is identically zero.

$$\frac{dF(y,z,\dot{y},\dot{z},t)}{dt} = \frac{\partial F(y,z,\dot{y},\dot{z},t)}{\partial t} + \frac{\partial F(y,z,\dot{y},\dot{z},t)}{\partial y}\,\dot{y} + \frac{\partial F(y,z,\dot{y},\dot{z},t)}{\partial \dot{y}}\,\ddot{y}$$

$$+ \frac{\partial F(y,z,\dot{y},\dot{z},t)}{\partial z}\,\dot{z} + \frac{\partial F(y,z,\dot{y},\dot{z},t)}{\partial \dot{z}}\,\ddot{z} = 0 \quad . \qquad (2.1a)$$

With the infinite z-directed magnetic field assumption introduced,

$$\frac{\partial F(y,z,\dot{z},t)}{\partial z}\,\dot{z} + \frac{\partial F(y,z,\dot{z},t)}{\partial \dot{z}}\,\ddot{z} + \frac{\partial F(y,z,\dot{z},t)}{\partial t} = 0 \quad , \qquad (2.1b)$$

wherever $F(y,z,\dot{z},t)$ is differentiable.

The acceleration $\ddot{z}$ is related to the z-directed electric field according to the force law

$$\ddot{z} = -hE_z(y,z,t) \quad , \qquad (2.2)$$

where h is the absolute value of the charge-to-mass ratio of electrons.

For a linear small-signal perturbation analysis, the density function as well as the electric field is assumed to be separable into a d-c component and a sinusoidal time-varying component in such a manner that the magnitude of the r-f component is very small compared to that of the d-c part.

$$F(y,z,\dot{z},t) = F_o(y,z,\dot{z}) + F_1(y,z,\dot{z})\, e^{j\omega t} \quad , \tag{2.3}$$

where

$$F_1(y,z,\dot{z}) \triangleq F_o(y,z,\dot{z})\, F_{11}(y,z,\dot{z})$$

and

$$F_{11}(y,z,\dot{z}) \ll 1 \quad .$$

$$E_z(y,z,t) = E_{oz}(y,z) + E_{1z}(y,z)\, e^{j\omega t} \quad , \tag{2.4}$$

where ω is the radian frequency of interest. The subscripts "o" and "1" denote the d-c and the a-c parts respectively.

The nonlinear partial differential equation, Eq. 2.1, may now be reduced to two linear transport equations which govern the behavior of the d-c and the a-c components of the density functions by neglecting the cross product term involving two a-c quantities.

$$\dot{z}\,\frac{\partial F_o(y,z,\dot{z})}{\partial z} - hE_{oz}(y,z)\,\frac{\partial F_o(y,z,\dot{z})}{\partial \dot{z}} = 0 \tag{2.5}$$

and

$$j\omega F_1(y,z,\dot{z}) + \dot{z}\,\frac{\partial F_1(y,z,\dot{z})}{\partial z} - hE_{oz}(y,z)\,\frac{\partial F_1(y,z,\dot{z})}{\partial \dot{z}} - hE_{1z}(y,z)\,\frac{\partial F_o(y,z,\dot{z})}{\partial \dot{z}} = 0 \quad . \tag{2.6}$$

Equation 2.6 is the basic transport equation for the multivelocity electron beam in which the third term describes the effect due to the potential gradient while the last term specifies the amount of coupling between

various velocity classes and adjacent electron streams through the r-f electric field E_{1z}. For a two-dimensional model, E_{1z} may be expressed in terms of the density functions (see Appendix A.1).

$$E_{1z}(y,z) = -\frac{e}{2j\omega\epsilon_o} \int_{-\infty}^{\infty} \int_{-\infty}^{\infty} \beta' \dot{z}' F_1(y',z,\dot{z}') e^{-\beta'|y-y'|} \, dy' \, d\dot{z}' \quad , \tag{2.7}$$

where the y'-integration is actually taken across the thickness of the electron beam.

$E_{1z}(y,z)$ is the a-c electric field at (y,z) due to the existence of an a-c density function at (y',z) which belongs to the $u' = \dot{z}'$ velocity class.

$$\beta' \triangleq \left| \frac{\omega}{\dot{z}'} \right| \quad .$$

For a drifting beam without coupling between density functions of different classes, a solution for Eq. 2.6 may be obtained by setting E_{1z} to zero.

$$F_1(y,z,t) = F_1(y) \, e^{j(\omega t - \beta z)} \quad , \tag{2.8}$$

where

$$\beta = \frac{\omega}{\dot{z}} \quad .$$

This is designated as the solution of the homogeneous transport equation in which signals travel along the stream with only a change in phase angle.

2.3.2 Excess Energy Parameter. In noise transport studies, a new parameter W, the excess energy parameter, is often introduced to replace the velocity parameter $\dot{z}$ for identification purposes.

$$W \triangleq \dot{z}^2 - 2h[V(y,z) - V'(y)] \quad , \tag{2.9}$$

where V(y,z) (see Appendix A.II) is the d-c potential at (y,z) with respect to the cathode, V'(y) is the potential minimum at plane y, and V'(y) is generally negative. W represents the amount of excess energy of an electron over its potential energy in the electrostatic field; it is, in the steady state, determined solely by the initial velocity of the associated electron and is invariant throughout. The introduction of W, a scalar parameter, to replace a vector variable $\dot{z}$ however raises some complications in the region where reflected flows exist. Because the amount of excess energy possessed by an electron of a reflected flow class is independent of its direction of propagation, a plus or minus sign must be attached to the differential of the parameter W indicating whether the group of electrons is traveling in the forward or reversed direction, i.e., toward the anode or cathode.

$$dW = \pm 2\dot{z}\, d\dot{z} \quad . \tag{2.10}$$

2.3.3 Dimensionless Parameters. The following dimensionless parameters are brought together with Eqs. 2.7 through 2.10 to reduce the a-c transport equation into dimensionless form.

$$\eta(\zeta,\xi) \triangleq \frac{e[V(y,z) - V'(y)]}{kT_c} \qquad \text{Potential Parameter,}$$

$$\left.\begin{aligned} \zeta &\triangleq \beta\alpha^{3/4}\, y \\ \xi &\triangleq \beta\alpha^{3/4}\, z \end{aligned}\right\} \qquad \text{Real Space Coordinate Parameters,}$$

$$g \triangleq \frac{\omega}{\beta\alpha^{1/4}} \qquad \text{Frequency Parameter,}$$

$$P(\zeta,\xi,w) \triangleq \left(\alpha \frac{I_o}{e}\right)^{-1} F(y,z,W) \qquad \text{Density Function Parameter,}$$

$$w = \alpha W \qquad \text{Excess Energy Parameter,} \tag{2.11}$$

where $\alpha \triangleq m/2kT_c$,

$$\beta \triangleq 2\pi^{1/4}\left(\frac{e|I_o|}{\epsilon_o m}\right)^{1/2},$$

m = mass of an electron,

I_o = average current density of the electron beam,

T_c = cathode temperature in degrees K,

k = Boltzmann's constant,

ϵ_o = dielectric constant of free space.

The transport equation may now be written as (see Appendix A.III):

$$\frac{\partial P_1(\zeta,\xi,w)}{\partial \xi} = \mp \frac{jgP_1(\zeta,\xi,w)}{\sqrt{w(\zeta,\xi)+\eta(\zeta,\xi)}} - \left\{\frac{\partial P_o(\zeta,\xi,w)}{\partial w}\right\}\left\{\frac{\pm 1}{j\beta\sqrt{\pi}}\int_{-\infty}^{\infty}\int_{-\infty}^{\infty}\right.$$

$$\left.\cdot\exp\left[\frac{-g|\zeta-\zeta'|}{\sqrt{w(\zeta',\xi)+\eta(\zeta',\xi)}}\right]\frac{P_1(\zeta',\xi,w)}{\sqrt{w(\zeta',\xi)+\eta(\zeta',\xi)}}\,dw\,d\zeta'\right\} . \quad (2.12)$$

The upper signs are for the forward going electrons of the density function parameter immediately following, while the lower signs are for the reflected flows.

2.4 Velocity Classes

The concept of velocity classes is introduced to split the transport equation into a set of linear small-signal multi-coupled differential equations in the multivelocity region. As shown in Fig. 2.3, all electrons emitted with an excess energy parameter between $w_i - \Delta w_i/2$ and $w_i + \Delta w_i/2$ are considered to be in the velocity class characterized by w_i. If the rms fluctuation within each velocity class is small compared to the mean velocity, a delta function can be placed at the center

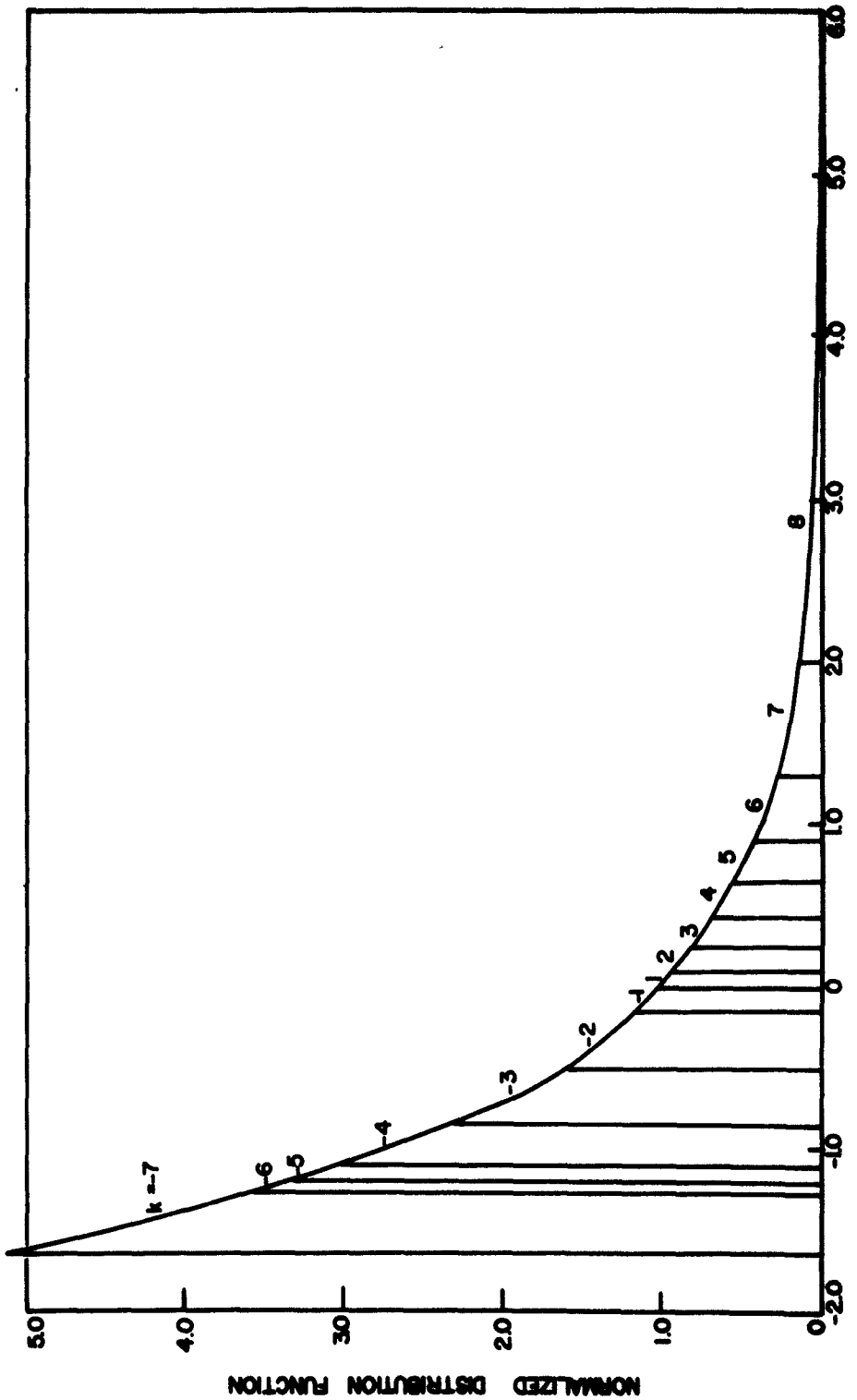

FIG. 2.3 NORMALIZED DISTRIBUTION OF THE D-C DENSITY FUNCTION VS. EXCESS ENERGY PARAMETER w_k FOR FIFTEEN VELOCITY CLASSES (HALF-MAXWELLIAN DISTRIBUTION).

of each of the velocity classes to represent their respective rms fluctuations. This means of incorporating the fluctuations into the mean velocity of every velocity class may be accomplished by choosing a large number of classes to make certain of a negligibly small deviation from the mean in each class. Since no correlations between initial fluctuations from different velocity classes are postulated, the sum of the mean square current fluctuations at the cathode plane is taken to be the full shot noise input.

One of the most controversial problems brought forth by the discrete velocity class model is the existence of the zero velocity class whose characteristic excess energy parameter W is zero. In a space-charge-limited diode with the formation of a potential minimum, only those electrons emitted with $W > 0$ have enough energy to go past the potential minimum. $W = 0$ merely implies that the group of electrons possesses just enough energy to reach the potential minimum and stay there. In an actual diode, the probability measure of all electrons having $W = 0$ is zero. The accumulation of electrons is therefore not a true representation of what really happens. Velocity classes should be rearranged so that electrons are either in the lowest $W > 0$ class or the lowest $W < 0$ class. Similar argument may also be applied to the $W = -\eta_c$ velocity class in which electrons are emitted with zero velocity from the cathode.

2.5 Extraction of Singularities (see Appendix A.IV)

In density function analysis, the step function discontinuities in the d-c part of the density function $F_o(W)$ would make any function involving the term $\partial F_o(W)/\partial W$ nonanalytic at one or more values of W. The presence of this ill-behaved factor often introduces some undesirable

complications in solving the transport equation by certain numerical techniques. Fortunately, a method was derived by Siegman[17] by which the singularity factor in the a-c density functions may be extracted leaving only analytic functions in the Boltzmann equation.

The a-c density function may be separated into two parts which will be called the homogeneous part and the response part respectively. The homogeneous or kinematic part consists of a Dirac delta function corresponding to the current fluctuations originating from the thermionic emission process. This part undergoes no change in magnitude and propagates along the electron beam under d-c effects alone. The response part of the a-c density function is the result of intercoupling through the a-c electric fields. If the singularities of the response parts are postulated to be of the same nature as $\partial F_o/\partial W$, a new variable $p_1(\zeta,\xi,w)$ may be defined for a unit a-c current input at the velocity class characterized by an excess energy parameter w_1,

$$P_1(\zeta,\xi,w) = \left[-\frac{\partial P_o(\zeta,\xi,w)}{\partial w_+} \frac{I_o}{I_o(\zeta)} p_1(\zeta,\xi,w) - 2\delta(w-w_1) e^{-j\theta_1} \left| \frac{1}{I_o} \right| \right], \quad (2.13)$$

where $p_1(\zeta,\xi,w)$ does not contain any singularity,

$I_o(\zeta)$ is the average current density of the beam layer, centered at ζ,

$$\theta_1 \triangleq g \int_0^{\xi} \frac{d\xi}{\pm(w_1 + \eta)^{1/2}} ,$$

"±" signs are for the forward and reflected flow respectively.

$\delta(w-w_1)$ is defined as the Dirac delta function with the following properties:

$$\delta(w-w_1) \triangleq 0 \quad \text{for} \quad w \neq w_1,$$
$$\triangleq \infty \quad \text{for} \quad w = w_1,$$

$$\int_{w_i-\epsilon}^{w_i+\epsilon} \delta(w-w_i)\, dw \triangleq 1 \ ,$$

$$\int_{w_i-\epsilon}^{w_i+\epsilon} \delta(w-w_i)\, F(w)\, dw = F(w_i) \ ,$$

From Eq. A.24

$$\frac{\partial P_o(w)}{\partial w_+} = -2\frac{I_o(\zeta)}{I_o}\left[\delta(w_+) - S(w_+)\right]\int_{-\eta_c}^{\infty}\frac{\partial P_o(w)}{\partial w_+}\, dw$$

$$= -2\frac{I_o(\zeta)}{I_o}\left\{\int_{-\eta_c}^{\infty}\left[\delta(w_+ + \eta) - S(w_+ + \eta_c)\right] dw_+ - \int_{-\eta_c}^{0}\left[\delta(w_- + \eta_c) - S(w_- + \eta_c)\right] dw_-\right\} \ ,$$

$$dw_+ = -\, dw_- \ ,$$

where $S(w_+)$ = a unit step function,

$S(w_+) \triangleq 1$ for $w_+ \geq 0$, $\dot{z} > 0$

$S(w_+) \triangleq 0$ for $w_+ < 0$.

Equation 2.12 may now be expressed in terms of the response part $p_1(\zeta,\xi,w)$ of the a-c density functions. In the preceding section, an argument was presented showing that the population of electrons characterized by the energy parameters $w = -\eta_c$ and $w = 0$ are zero. The current fluctuations brought forth by the singularities in $\partial P_o(w)/\partial w$ at these two values of w are actually included in their respective adjacent velocity classes. After some simplification, the transport equations may be written for an input at velocity class w_1 as

$$\pm \frac{\partial p_1(\zeta,\xi,w)}{\partial \xi} = \frac{-jg p_1(\zeta,\xi,w)}{\sqrt{w+\eta(\zeta,\xi)}}$$

$$\pm \frac{I_o(\zeta)}{I_o} \left\{ \frac{\mp \left|\frac{1}{I_o}\right|}{j4\sqrt{\pi}} \int_{-\infty}^{\infty} \int_{-\eta_c}^{\infty} \frac{\delta(w-w_i)}{\sqrt{w+\eta(\zeta',\xi)}} \exp\left[\frac{-g|\zeta-\zeta'|}{\sqrt{w+\eta(\zeta',\xi)}} \right] e^{-j\theta_i} \, dw \, d\zeta' \right.$$

$$- \frac{1}{j4\sqrt{\pi}} \int_{-\infty}^{\infty} \int_{0}^{\infty} \exp\left[\frac{-g|\zeta-\zeta'|}{\sqrt{w(\zeta',\xi)+\eta(\zeta',\xi)}} \right] \frac{p_1(\zeta',\xi,w)}{\sqrt{w(\zeta',\xi)+\eta(\zeta',\xi)}} \exp\left[-w(\zeta',\xi)\right]$$

$$\cdot dw d\zeta' - \frac{(\pm 1)}{j4\sqrt{\pi}} \int_{-\infty}^{\infty} \int_{-\eta_c}^{0} \exp\left[\frac{-g|\zeta-\zeta'|}{\sqrt{w(\zeta',\xi)+\eta(\zeta',\xi)}} \right] \frac{p_1(\zeta',\xi,w)}{\sqrt{w(\zeta',\xi)+\eta(\zeta',\xi)}}$$

$$\left. \cdot \exp\left[-w(\zeta',\xi)\right] dw \, d\zeta' \right\} . \quad (2.14)$$

where η_c is the potential parameter at the cathode.

2.6 Boundary Conditions for the A-c Density Functions

The following conditions are attached to the a-c transport equations:

1. Full thermionic emission shot noise is assumed at the cathode of the diode, and the response part of the density function for all the forward going electrons is identically zero at the cathode plane for all velocity classes.

2. Continuity of the a-c density functions is assumed at the potential minima as well as the points where the $w > 0$ velocity classes reverse their direction of propagation. The a-c density function

associated with the forward going electrons is equal to that associated with the backward going electrons of the same velocity class at the point of reflection.

3. The initial conditions specified are insufficient if numerical solutions are to be evaluated by the step-by-step forward integration method starting from the cathode plane, because of the difficulties encountered in an attempt to determine uniquely the response part of the a-c density functions associated with the backward going electrons of the reflected flows at the cathode. Another boundary is selected as the starting point instead. As a matter of convenience, the integrations will be carried out beginning at the potential minima and the points of reflection. A method by which the boundary conditions of the a-c density functions are determined at the newly selected boundary will be fully described in Section 2.8.

2.7 Working Equations

A mathematically discrete beam model which can be made to approximate the d-c density function arbitrarily well in the velocity domain is introduced so that the integrations in the a-c transport equation may be replaced by summations during numerical computations. The discrete beam model, as shown in Fig. 2.4, consists of a number of velocity classes each characterized by an excess energy parameter w_i and a d-c density function parameter $P_o(w_i)$, where $P_o(w)$ is assumed to be a constant for all electrons inside any velocity class. In Section 2.9 the a-c current and the kinetic potential are shown to be proportional to the first and third velocity moments of the d-c density function, respectively. Therefore, a satisfactory discrete beam model may be obtained provided its

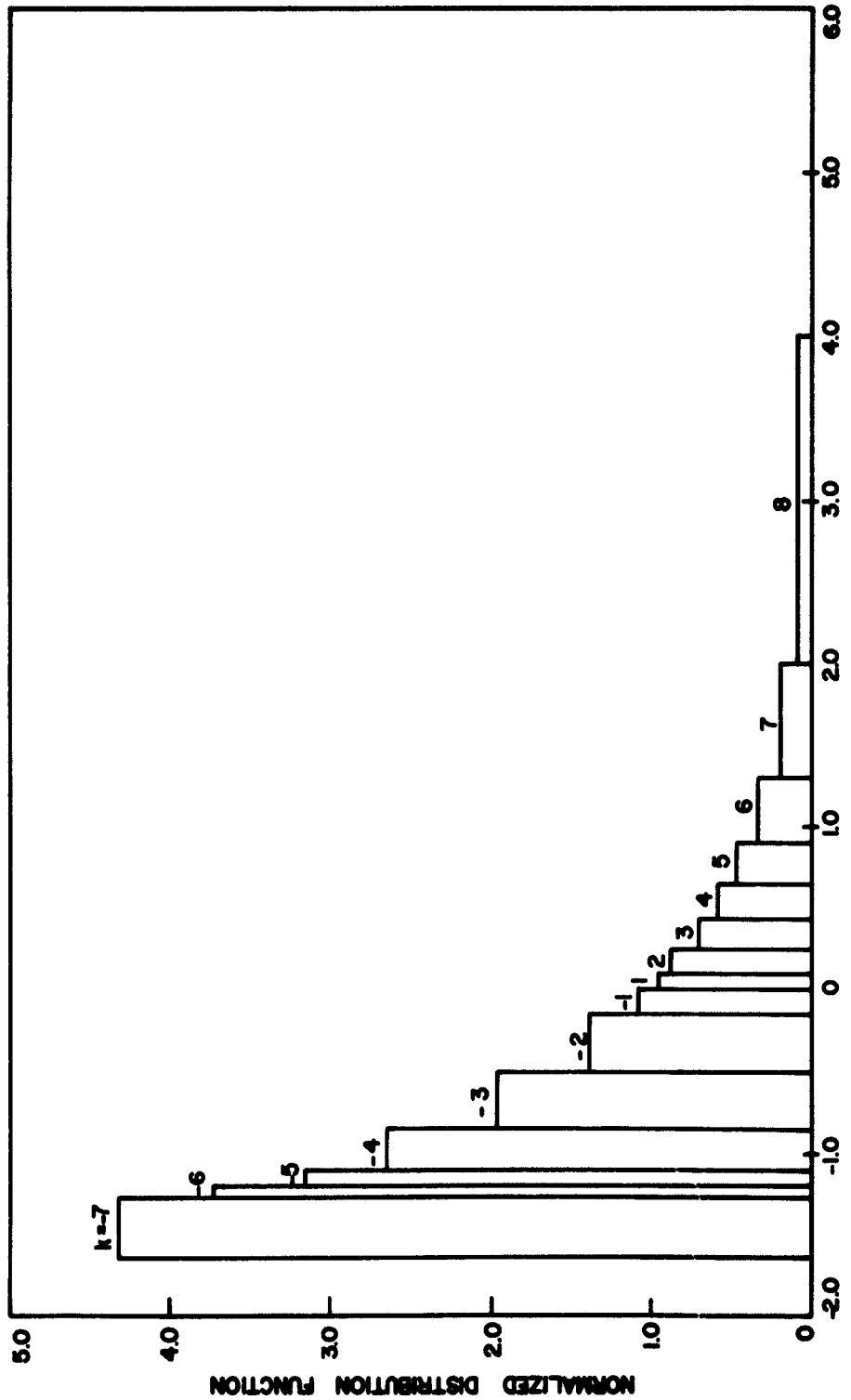

FIG. 2.4 NORMALIZED DISTRIBUTION OF THE D-C DENSITY FUNCTION VS. EXCESS ENERGY PARAMETER w_k FOR THE DISCRETE BEAM MODEL WITH FIFTEEN VELOCITY CLASSES.

first and third velocity moments are equal to the same moments of the half-Maxwellian distribution for each velocity class.

From Eq. 2.14, working equations for electrons going in both forward and reversed directions are derived with a unit input to the homogeneous part of the a-c density function at layer ζ_m and velocity class w_i.

$$\frac{\partial p^{+}_{1H}(\zeta_j,\xi,w_k;\zeta_m,w_i)}{\partial \xi} = \frac{-jap^{+}_{1H}(\zeta_j,\xi,w_k;\zeta_m,w_i)}{\sqrt{w_k+\eta(\zeta_j,\xi)}} - \frac{I_o(\zeta_j)}{I_o} M_H \Delta\zeta \quad (2.15a)$$

and

$$\frac{\partial p^{-}_{1H}(\zeta_j,\xi,w_k;\zeta_m,w_i)}{\partial \xi} = \frac{jap^{-}_{1H}(\zeta_j,\xi,w_k;\zeta_m w_i)}{\sqrt{w_k+\eta(\zeta_j,\xi)}} - \frac{I_o(\zeta_j)}{I_o} M_H \Delta\zeta \quad . \quad (2.15b)$$

Similarly, with a unit input to the response part of the a-c density function at layer ζ_m and velocity class w_i, the working equations are:

$$\frac{\partial p^{+}_{1R}(\zeta_j,\xi,w_k;\zeta_m,w_i)}{\partial \xi} = \frac{-jap^{+}_{1R}(\zeta_j,\xi,w_k;\zeta_m,w_i)}{\sqrt{w_k+\eta(\zeta_j,\xi)}} - \frac{I_o(\zeta_j)}{I_o} M_R \Delta\zeta \quad (2.15c)$$

and

$$\frac{\partial p^{-}_{1R}(\zeta_j,\xi,w_k;\zeta_m,w_i)}{\partial \xi} = \frac{jap^{-}_{1R}(\zeta_j,\xi,w_k;\zeta_m,w_i)}{\sqrt{w_k+\eta(\zeta_j,\xi)}} - \frac{I_o(\zeta_j)}{I_o} M_R \Delta\zeta \quad , \quad (2.15d)$$

where

$$-M_H = \frac{-Y[\eta(\zeta_m,\xi),w_i]}{j4|I_o|\sqrt{\pi}} \exp\left[\frac{-g|\zeta_j-\zeta_m|}{\sqrt{w_i+\eta(\zeta_m,\xi)}} - j\theta_i^+\right]\frac{\Delta w_i}{\sqrt{w_i+\eta(\zeta_m,\xi)}}$$

$$+\frac{X[\eta,w_i]}{j4|I_o|\sqrt{\pi}} \exp\left[\frac{-g|\zeta_j-\zeta_m|}{\sqrt{w_i+\eta(\zeta_m,\xi)}} - j\theta_i^-\right]\frac{\Delta w_i}{\sqrt{w_i+\eta(\zeta_m,\xi)}}$$

$$-\frac{Y[\eta,w_h]}{j4\sqrt{\pi}}\sum_{\ell=-2}^{\ell=2}\sum_{h=-7}^{8} \exp\left[\frac{-g|\zeta_j-\zeta_\ell|}{\sqrt{w_h+\eta(\zeta_\ell,\xi)}} - w_k\right]\frac{p_{iH}^+(\zeta_\ell,\xi,w_h;\zeta_m,w_i)}{\sqrt{w_h+\eta(\zeta_\ell,\xi)}}\Delta w_h$$

$$+\sum_{\ell=-2}^{2}\sum_{h=-7}^{-1}\frac{X[\eta,w_h]}{j4\sqrt{\pi}} \exp\left[\frac{-g|\zeta_j-\zeta_\ell|}{\sqrt{w_h+\eta(\zeta_\ell,\xi)}}\right.$$

$$\left. - w_h\right]\frac{p_{iH}^-(\zeta_\ell,\xi,w_h;\zeta_m,w_i)}{\sqrt{w_h+\eta(\zeta_\ell,\xi)}}\Delta w_h \quad ,$$

$$-M_R = \frac{-1}{j4\sqrt{\pi}}\sum_{\ell=-2}^{2}\sum_{h=-7}^{8} Y(\eta,w_h) \exp\left[\frac{-g|\zeta_j-\zeta_\ell|}{\sqrt{w_h+\eta(\zeta_\ell,\xi)}}\right.$$

$$\left. - w_h\right]\frac{p_{iR}^+(\zeta_\ell,\xi,w_h;\zeta_m,w_i)}{\sqrt{w_h+\eta(\zeta_\ell,\xi)}}\Delta w_h + \sum_{\ell=-2}^{2}\sum_{h=-7}^{-1}\frac{X[\eta,w_h]}{j4\sqrt{\pi}} \exp\left[\frac{-g|\zeta_j-\zeta_\ell|}{\sqrt{w_h-\eta(\zeta_\ell,\xi)}}\right.$$

$$\left. - w_h\right]\frac{p_{iR}^-(\zeta_\ell,\xi,w_h;\zeta_m,w_i)}{\sqrt{w_h+\eta(\zeta_\ell,\xi)}}\Delta w_h$$

and the superscripts "+" or "-" are indications of the propagation directions, $p_{iH}^{\pm}(\zeta_j,\xi,w_k;\zeta_m,w_i)$ is defined as the response part of the a-c

density function at (ζ_j,ξ) belonging to velocity class w_k due to a unit input to the homogeneous part of the a-c density function at layer ζ_m and velocity class w_i, $p^{\pm}_{iR}(\zeta_j,\xi,w_k;\zeta_m,w_i)$ is the response part of the a-c density function of velocity class w_k at (ζ_j,ξ) due to a unit input to the response part of the a-c density function at layer ζ_m and velocity class w_i,

$$\theta_i^+ = -\theta_i^- = g\int_0^{\xi} \frac{d\xi}{\sqrt{w_i + \eta(\zeta_m,\xi)}} ,$$

where θ = the phase shift per unit time of the homogeneous part of the a-c density function,

$X(\eta,w) \triangleq 1$ if $w < 0$, $w + \eta \geq 0.02$,

$\triangleq 0$ otherwise,

$Y(\eta,w) = 1$ if $w > 0$ or $w < 0$ and $w + \eta \geq 0.02$.

Only fifteen discrete velocity classes are employed because of the limitation in computer time and expense. For a beam of m layers and n velocity classes, a [2 x n x m] x [2 x n x m] square matrix will have to be solved for the initial conditions at the new boundary. (The factor of two comes from the complex nature of the density functions.) The amount of computing time required goes up as the square of the number of velocity classes.

2.8 Linear Transformations

The linear characteristics of the working equations and the simultaneous emission assumption allow the application of the superposition theorem at the cathode to determine the boundary conditions at the newly chosen boundary. For the m-layer n-beam model, the set of coupled transport equations defines a unique linear transformation between two sets of 2n x m linearly independent functions, i.e., the homogeneous and

the response parts of the a-c density functions associated with the forward going electrons at the cathode plane and those at the new boundary. Due to the second boundary condition, the a-c density functions associated with flows of opposite directions are mutually dependent in nature. Now if n x m sets of linearly independent inputs consisting of "ones" and "zeros" for the response parts are injected at the potential minima and the reflection points, the boundary conditions of the a-c density functions at the cathode plane must be satisfied by a linear combination of the n x m sets of transforms thus obtained plus the transform of a full shot noise input (homogeneous part) at the potential minima. In Appendix A.VI the weighting factor $R(\zeta_m,w_i)$ for the homogeneous part of the a-c density function at layer m and velocity class i is evaluated using the shot noise formula by Schottky and the uncorrelated input assumption at the cathode plane for different velocity classes.

For each input in the homogeneous part of the a-c density function at layer m and velocity class i, a weighting factor $G(\zeta_m,w_i;\zeta_n,w_\ell)$ for the response part of the a-c density function $p^+_{1R}(\zeta_j,\xi,w_k;\zeta_n,w_\ell)$ at the potential minimum may be obtained from the following equation. At the cathode plane where the algebraic sum of the response parts in each velocity class is identically zero,

$$p^+_{1H}(\zeta_j,0;w_k;\zeta_m,w_i) + \sum_{n=-2}^{2}\sum_{\ell=-7}^{8} G(\zeta_m,w_i;\zeta_n,w_\ell) \cdot p^+_{1R}(\zeta_j,0,w_k;\zeta_n,w_\ell) \equiv 0 \quad . \quad (2.16)$$

The weighting factor G needed to satisfy the boundary conditions at the cathode then specifies the initial conditions at the new boundary selected for the transmitted flow induced by the unit noise current input at (ζ_m,w_i).

2.9 Computation of Noise Parameters and the Minimum Noise Figure

Noise parameters expressed in terms of the self-power spectral density (SPSD) and the cross-power spectral density (CPSD) of the z-directed a-c current and voltage fluctuations according to the small-signal univelocity theory of Haus and Robinson are employed in the noise transport analysis in a two-dimensional multivelocity discrete beam model provided that the equivalent current fluctuations and the kinetic potential are properly defined.

2.9.1 Current Fluctuations. The noise current density at any point (ζ,ξ) per unit bandwidth associated with a unit current input at the w_i velocity class is defined such that

$$i_1(\zeta,\xi;\zeta_m,w_i) \triangleq -\frac{e}{2}\int_0^\infty F_1(\zeta,\xi,w;\zeta_m,w_i)\,dw \quad , \tag{2.17}$$

or in terms of dimensionless parameters,

$$i_{1R}(\zeta_j,\xi;\zeta_m,w_i)$$

$$= I_o \sum_{k=1}^{8}\left[\sum_{n=-2}^{2}\sum_{\ell=-7}^{8} G(\zeta_m,w_i;\zeta_n,w_\ell)\, p^+_{1R}(\zeta_j,\xi,w_k;\zeta_n,w_\ell)e^{-w_k}\Delta w_k\right] \quad , \tag{2.18}$$

where H and R indicate the homogeneous input and response input respectively. For full shot noise input at the cathode, the variance of the noise current at any point (ζ_j,ξ) downstream is, by the superposition theorem,

$$< i_1^2(\zeta_j,\xi) > = \sum_{m=-2}^{2} \sum_{i=-7}^{8} \Big\{ R(\zeta_m,w_i)\,\Delta w_i(\Delta\zeta)^2 \cdot \Big[i_{1H}(\zeta_j,\xi;\zeta_m,w_i) + i_{1R}(\zeta_j,\xi;\zeta_m,w_i) \Big] \cdot \Big[i^*_{1H}(\zeta_j,\xi;\zeta_m,w_i) + i^*_{1R}(\zeta_j,\xi;\zeta_m,w_i) \Big] \Big\} \quad , \quad (2.19)$$

where "*" denotes complex conjugates.

2.9.2 Kinetic Potential. In noise transport analyses, the velocity fluctuation in an electron beam is often replaced by a variable V_1 which has the dimension of voltage and is designated as the kinetic potential. From an energy standpoint, V_1 may be regarded as the kinetic energy density expressed in electron-volts and it is therefore continuous through a velocity jump, i.e., a sudden acceleration or deceleration of the electron beam. In a single-velocity perturbation analysis, the kinetic potential is defined to be

$$V_1 \triangleq -\frac{u_o v_1}{h} \quad , \quad (2.20)$$

where u_o is the d-c or average velocity of the electrons in the beam, and v_1 is the a-c velocity component.

In a multivelocity region, the expression for the kinetic potential is not nearly as unique. It can be shown that a direct substitution of the density function into Eq. 2.20 does not yield a quantity with the invariant characteristic over potential gaps. In Appendix A.V, V_1 is shown to be

$$V_1(y,z) = -\frac{1}{2h}\left\{\frac{-e}{I(y)}\int_0^\infty \dot{z}^3\left[F_o(y,z,\dot{z}) + F_1(y,z,\dot{z})\right]d\dot{z}\right.$$

$$\left. + \frac{e}{I_o(y)}\int_0^\infty \dot{z}^3 F_o(y,z,\dot{z})d\dot{z}\right\} \quad , \qquad (2.21)$$

where $I_o(\zeta)$ and $I(\zeta)$ are the d-c current density and the total current density at layer ζ respectively. After some algebraic manipulations,

$$V_1(\zeta,\xi) = \frac{e}{4hI_o(\zeta)\Delta\zeta}\int_0^\infty (W+\overline{W})\, F_1(\zeta,\xi,W)\, dW\Delta\zeta \quad , \qquad (2.22)$$

where

$$\overline{W} = \frac{e}{2I_o(\zeta)}\int_0^\infty WF_o(\zeta,\xi,W)\, dW = \frac{-1}{\alpha}$$

for half-Maxwellian velocity distributions.

It can be seen that Eq. 2.22 will not reduce to Eq. 2.20, the univelocity definition of kinetic potential, unless the velocity spread involved is negligibly small. Similarly, a direct substitution of the density functions into Eq. 2.20 will not give a satisfactory equivalent kinetic potential for a multivelocity electron beam, since the quantity V_1 thus obtained will not be invariant over a velocity gap.

In terms of dimensionless parameters, the kinetic potential at (ζ_j,ξ) due to a unit homogeneous input at ζ_m and the w_i velocity class is

$$V_{1H}(\zeta_j,\xi;\zeta_m,w_i) = \frac{-kT_c}{e}\,\frac{I_o}{I_o(\zeta)}\left[\sum_{k=1}^{s}(w_k - 1)\, p^+_{1H}(\zeta_j,\xi,w_k;\zeta_m,w_i)e^{-w_k}\Delta w_k\right.$$

$$\left. + \frac{\delta_{j,m}}{|I_o|}(w_i - 1)e^{-j\theta_i}\Delta w_i\right] \qquad (2.23)$$

and for unit response input,

$$V_{1R}(\zeta_j,\xi;\zeta_m,w_i) = \frac{-kT_c}{e}\,\frac{I_o}{I_o(\zeta)}\sum_{k=1}^{8}\Bigg[\sum_{n=-2}^{2}\sum_{\ell=-7}^{8} G(\zeta_m,w_i;\zeta_n,w_\ell)$$

$$\cdot p^{+}_{1R}(\zeta_j,\xi,w_k;\zeta_n,w_\ell)\ (w_k - 1)e^{-w_k}\Delta w_k\Bigg] .$$

The variance of the kinetic potential at (ζ_j,ξ) inside a diode with full shot noise input at the cathode is then

$$\langle V_1^2(\zeta_j,\xi)\rangle = \sum_{m=-2}^{2}\sum_{i=-7}^{8}\Big\{R(\zeta_m,w_i)\,\Delta w_i$$

$$\cdot\Big[V_{1H}(\zeta_j,\xi;\zeta_m,w_i) + V_{1R}(\zeta_j,\xi;\zeta_m,w_i)\Big]$$

$$\cdot\Big[V^{*}_{1H}(\zeta_j,\xi;\zeta_m,w_i) + V^{*}_{1R}(\zeta_j,\xi;\zeta_m,w_i)\Big]\Big\} \qquad (2.24)$$

and the covariance between the current and voltage fluctuations is defined as

$$\langle i_1(\zeta_j,\xi)V_1(\zeta_j,\xi)\rangle = \sum_{m=-2}^{2}\sum_{i=-7}^{8}\Big\{R(\zeta_m,w_i)\,\Delta w_i\,\Delta\zeta$$

$$\cdot\Big[i^{*}_{1H}(\zeta_j,\xi;\zeta_m,w_i) + i^{*}_{1R}(\zeta_j,\xi;\zeta_m,w_i)\Big]$$

$$\cdot\Big[V_{1H}(\zeta_j,\xi;\zeta_m,w_i) + V_{1R}(\zeta_j,\xi;\zeta_m,w_i)\Big]\Big\} . \qquad (2.25)$$

Slightly different expressions for the fluctuations, their respective variances and the covariance will be obtained if all layers are taken into account simultaneously. Comparisons may be made between the noise parameters of the individual layers and those of the whole beam. Noise current densities at ξ are

$$i_{1H}(\xi;\zeta_m,w_i) = \frac{I_o}{5}\Bigg[\sum_{j=-2}^{2}\sum_{k=1}^{8} p^{+}_{1H}(\zeta_j,\xi,w_k;\zeta_m,w_i)e^{-w_k}\Delta w_k + \frac{\delta_{j,m}}{|I_o|}e^{-j\theta_i(\zeta_m,\xi,w_i)}\Delta w_i\Bigg] \quad (2.26a)$$

and

$$i_{1R}(\xi;\zeta_m,w_i) = \frac{I_o}{5}\sum_{j=-2}^{2}\sum_{k=1}^{8}\Bigg[\sum_{n=-2}^{2}\sum_{\ell=-7}^{8} G(\zeta_m,w_i;\zeta_n,w_\ell)\cdot p^{+}_{1R}(\zeta_j,\xi,w_k;\zeta_n,w_\ell)e^{-w_k}\Delta w_k\Bigg] . \quad (2.26b)$$

Similarly, the voltage fluctuations are written as

$$V_{1H}(\xi;\zeta_m,w_i) = \frac{-kT_c}{e}\frac{1}{5}\Bigg[\sum_{j=-2}^{2}\sum_{k=1}^{8}(w_k-1)p^{+}_{1H}(\zeta_j,\xi,w_k;\zeta_m,w_i)e^{-w_k}\Delta w_k + \frac{\delta_{j,m}}{|I_o|}(w_i-1)e^{-j\theta_i}\Delta w_i\Bigg] \quad (2.27a)$$

and

$$V_{1R}(\xi;\zeta_m,w_i) = \frac{-kT_c}{e}\frac{1}{5}\sum_{j=-2}^{2}\sum_{k=1}^{8}\Bigg[\sum_{n=-2}^{2}\sum_{\ell=-7}^{8}\cdot G(\zeta_m,w_i;\zeta_n,w_\ell)\ p^{+}_{1R}(\zeta_j,\xi,w_k;\zeta_n,w_\ell)(w_k-1)e^{-w_k}\Delta w_k . \quad (2.27b)$$

The respective variances are respectively

$$< V_1^2(\xi) > = \sum_{m=-2}^{2} \sum_{i=-7}^{8} \Big\{ R(\zeta_m, w_i)\, \Delta w_i \cdot \Big[V_{1H}(\xi;\zeta_m,w_i) + V_{1R}(\xi;\zeta_m,w_i) \Big] \cdot \Big[V^*_{1H}(\xi;\zeta_m,w_i) + V^*_{1R}(\xi;\zeta_m,w_i) \Big] \Big\} \quad (2.28)$$

and

$$< i_1^2(\xi) > = \sum_{m=-2}^{2} \sum_{i=-7}^{8} \Big\{ R(\xi_m, w_i)\, \Delta w_i (5\Delta\zeta)^2 \cdot \Big[i_{1H}(\xi;\zeta_m,w_i) + i_{1R}(\xi;\zeta_m,w_i) \Big] \cdot \Big[i^*_{1H}(\xi;\zeta_m,w_i) + i^*_{1R}(\xi;\zeta_m,w_i) \Big] \Big\} \ , \quad (2.29)$$

and the covariance between the two variables is

$$< i_1(\xi) V_1(\xi) > = \sum_{m=-2}^{2} \sum_{i=-7}^{8} \Big\{ R(\zeta_m, w_i)\, \Delta w_i (5\Delta\zeta) \cdot \Big[i^*_{1H}(\xi;\zeta_m,w_i) + i^*_{1R}(\xi;\zeta_m,w_i) \Big] \cdot \Big[V_{1H}(\xi;\zeta_m,w_i) + V_{1R}(\xi;\zeta_m,w_i) \Big] \Big\} \ . \quad (2.30)$$

Since the kinetic power density is a function of the cathode temperature alone, $< i_1(0)\ V_1(0) >$ should be equal to $< i_1(\zeta_j,0)\ V_1(\zeta_j,0) >$ at the cathode.

2.9.3 Noise Parameters. Normalized noise parameters $\psi(\zeta_j,\xi)$, the self-power spectral density of the current fluctuations, $\Phi(\zeta_j,\xi)$, the self-power spectral density of the voltage fluctuations, $\Pi(\zeta_j,\xi)$, the real part of the cross-power spectral density of the current and the voltage fluctuations, $\Lambda(\zeta_j,\xi)$, the imaginary part of the cross-power spectral density and $S(\zeta_j,\xi)$ for each individual layer of the electron beam are defined according to Haus's[16] notations.

$$\psi(\zeta_j,\xi) \triangleq \langle i_1^2(\zeta_j,\xi)\rangle / 2e|I(\zeta_j)|\Delta\zeta \ ,$$

$$\Phi(\zeta_j,\xi) \triangleq [\langle V_1^2(\zeta_j,\xi)\rangle / 2(kT_c)^2]e|I(\zeta_j)|\Delta\zeta \ ,$$

$$\Pi(\zeta_j,\xi) \triangleq \mathrm{Re}[\langle i_1(\zeta_j,\xi)\ V_1(\zeta_j,\xi)\rangle / 2kT_c] \ ,$$

$$\Lambda(\zeta_j,\xi) \triangleq I_m[\langle i_1(\zeta_j,\xi)\ V_1(\zeta_j,\xi)\rangle / 2kT_c]$$

and

$$S^2(\zeta_j,\xi) \triangleq \Phi(\zeta_j,\xi)\psi(\zeta_j,\xi) - \Lambda^2(\zeta_j,\xi) \ , \qquad (2.31)$$

where S and Π are invariant quantities in one-dimensional single-velocity flow perturbation theory. As will be pointed out in the Monte Carlo method of noise transport calculations, the noise parameters are the Fourier transforms of the auto-correlation functions and the cross-correlation functions of the a-c current and the equivalent a-c voltage.

The minimum noise figure of a longitudinal-beam microwave amplifier with one of the m layers of the electron beam is again, according to Haus's theory:

$$F_{min}(\zeta_j,\xi_{in}) \triangleq 1 + \frac{T_c}{T}\left[S(\zeta_j,\xi_{in}) - \Pi(\zeta_j,\xi_{in})\right] \qquad (2.32)$$

for a fixed frequency, where

T is the ambient temperature, and

ξ_{in} is the distance between the input plane of the interacting circuit and the cathode.

Considering all layers together, theoretically, it is possible to match the a-c impedance of the electron beam (all layers and all velocity classes) simultaneously provided the lengths of the transformation region and the drift regions are unlimited.

Noise parameters similar to those for one layer beams are written in terms of the total current fluctuations and the kinetic potential.

$$\Psi(\xi) \triangleq \langle i_1^2(\xi)\rangle / 2e|I_o|(5\Delta\zeta) \quad ,$$

$$\Phi(\xi) \triangleq [\langle V_1^2(\xi)\rangle / 2(kT_c)^2]\, e|I_o|(5\Delta\zeta) \quad ,$$

$$\Pi(\xi) \triangleq \mathrm{Re}[\langle i_1(\xi)V_1(\xi)\rangle]/2kT_c \quad ,$$

$$\Lambda(\xi) \triangleq I_m[\langle i_1(\xi)V_1(\xi)\rangle]/2kT_c$$

and

$$S^2(\xi) \triangleq \Phi(\xi)\Psi(\xi) - \Lambda^2(\xi) \quad . \qquad (2.33)$$

The minimum noise figure is given by the expression

$$F_{min}(\xi) \triangleq 1 + \frac{T_c}{T}\left[S(\xi) - \Pi(\xi)\right] \qquad (2.34)$$

for a fixed operating frequency.

The minimum noise figure will cease to be a function of distance as soon as the average velocity of the electrons becomes very large compared to the equivalent velocity fluctuations. From then on, the small-signal single-velocity theory will take over and no further reduction in electron beam noise content may be achieved.

2.10 Choice of Velocity Classes and Integration Steps

A compromise must be made between two contradictory factors governing the number of velocity classes selected and the sizes of the numerical integration steps. The available computing time limits the maximum number of discrete velocity classes in the theoretical beam model; computing time varies as the square of the number of classes and inversely with the size of integration steps. On the other hand, the small-signal assumption poses a lower limit on the number of velocity classes employed.

2.10.1 Choice of Velocity Classes. For the two-dimensional diode, 15 velocity classes are employed in the noise transport calculations. In Fig. 2.4 and Table 2.1, the first and third moments of each velocity class in the discrete beam model described in Section 2.7 are identically set to the corresponding elements of the actual beam with a half-Maxwellian velocity distribution at the cathode.

The slowest velocity class in the transmitted flow is characterized by $w_k = 0.04961$ and the slowest initial velocity class has a w of approximately -1.5.

Table 2.1

The First and Third Moments of the Velocity Classes

in the Discrete Beam Model

Velocity Class K	Δw_k	Mean Excess Energy Parameter w_k	First Velocity Moment $e^{-w_k}\Delta w_k$	Third Velocity Moment $w_k e^{-w_k}\Delta w_k$
1	0.100	0.0496105	0.09516	0.0047209
2	0.150	0.174360	0.12604	0.0219763
3	0.180	0.338663	0.12829	0.0434471
4	0.220	0.538010	0.12846	0.0691128
5	0.250	0.7723636	0.11548	0.0891925
6	0.400	1.093326	0.13404	0.1465494
7	0.700	1.629713	0.13719	0.223580
8	2.000	0.693112	0.13534	0.3644858
-1	0.150	-0.0757257	0.1618	-0.0122524
-2	0.350	-0.3299202	0.4868	-0.16060515
-3	0.350	-0.6800619	0.6909	-0.4698547
-4	0.250	-0.9777244	0.6646	-0.649795
-5	0.100	-1.150256	0.3159	-0.363366
-6	0.073	-1.317179	0.255	-0.358931
-7 Layer II & IV	0.278	-1.396850	1.1238	-1.56978
Layer III	0.373	-1.465326	1.6147	-2.36606

2.10.2 Integration Steps for the A-c Density Functions.

2.10.2a Computation Method. The set of linear small-signal differential equations is solved by the step-by-step integration method. Variations of the a-c density functions with respect to distance are governed by the following formula:

$$p_1(\zeta,\xi_{s+1},w) = p_1(\zeta,\xi_s,w) + \frac{\partial p_1(\zeta,\xi_s,w)}{\partial \xi}\Delta\xi_s + \frac{1}{s!}\frac{\partial^2 p_1(\zeta,\xi_s,w)}{\partial \xi^2}(\Delta\xi_s)^2 , \tag{2.35}$$

where

$$\xi_{s+1} = \xi_s + \Delta\xi_s$$

and

$$\frac{\partial p_1(\zeta,\xi_s,w)}{\partial \xi^2} = \frac{\frac{\partial p_1(\zeta,\xi_{s+1},w)}{\partial \xi} - \frac{\partial p_1(\zeta,\xi_s,w)}{\partial \xi}}{\Delta\xi_s} .$$

This is actually the Taylor's series approximation taken to second-order terms. In order to avoid large computation errors, integration steps $\Delta\xi_s$ are chosen to be extremely small with their magnitudes being determined by the increment of transit angles at the frequency of interest.

2.10.2b Integration Steps in ξ. Errors introduced by the discrete step-by-step integration method may be minimized if the transit angles of the slow electrons are limited to only a small fraction of a cycle for any step taken. The transit angle is defined as

$$\theta \triangleq g\int_0^{\xi} \frac{d\xi}{\sqrt{w + \eta(\xi)}} \tag{2.36}$$

and

$$\Delta\theta = \frac{g\Delta\xi}{\sqrt{w + \eta(\xi)}} ,$$

$$\Delta\xi = \frac{\Delta\theta}{g}\left[w + \eta(\xi)\right]^{1/2} . \tag{2.37}$$

For the transmitted flows, $w \geq 0.02$. If $\Delta\theta$ is chosen to be less than 0.20 radian,

$$\Delta\xi_{max} = \frac{0.20}{g}\left[\eta(\xi) + 0.002\right]^{1/2} . \qquad (2.38)$$

For the reflected flows, $w + \eta$ is chosen to be larger than 0.02 at all times so that the problem of infinite phase shift at the points of reflection may be by-passed. It can be shown mathematically (see Appendix A.VII) that the phase shift would not really increase without bound when $(w+\eta)$ approaches zero as a limit. The singularities encountered here are believed to be the result of the discrete beam analysis. Physically, not all the electrons in a velocity class change their direction of propagation simultaneously and those reflected electrons actually spend no time (or undergo no phase change) at the point of reflection.

2.11 High-Frequency and Low-Frequency Limits

In the two-dimensional diode, the noise-transport analysis is valid as long as both the distance between the discrete beam layers and the spacing between the electrodes are small compared to a free space wavelength corresponding to the highest frequency of interest. On the other hand, at low frequencies, the limitation described by Watkins[18], Siegman and Hsieh for one-dimensional models with an open-circuit assumption fails to appear in the present formulation. According to Eq. A.9, the z-directed a-c electric field in a two-dimensional diode no longer varies inversely as frequency and it stays in bound when the operating frequency drops to zero.

$$E_{1z}(y,z) = \frac{e}{2j\omega\epsilon_o}\int_{-\infty}^{\infty}\int_{-\infty}^{\infty}\beta'\dot{z}'\,F_1(y',z,\dot{z}')e^{-\beta'|y-y'|}dy'd\dot{z}' \quad , \quad (A.9)$$

where

$$\beta' = \left|\frac{\omega}{\dot{z}'}\right| \quad .$$

Therefore,

$$E_{1z}(y,z) = \frac{e}{2j\,\epsilon_o} \int_{-\infty}^{\infty} \int_{-\infty}^{\infty} F_1(y',z,\dot{z}')e^{-\beta'|y-y'|} \frac{\dot{z}'}{|\dot{z}'|}\, dy'd\dot{z}' \quad , \tag{2.39}$$

which is independent of the radian frequency ω for $y = y'$. The a-c electric field evaluated this way depends on the a-c space charge in a way quite similar to the dependence of the d-c electric field on the d-c space charge.

CHAPTER III. MONTE CARLO FORMULATION

3.1 Introduction

The Monte Carlo method is a numerical method of approximation with which investigations in stochastic models of physical or mathematical processes may be carried out by direct simulation. The method by itself is far from new, nor is there any novelty in the theory of stochastic processes. Yet, the application of the Monte Carlo techniques did not gain popularity until high-speed electronic computers with a large memory capacity became available.

For some equations arising in a nonprobabilistic context, neither a closed form nor a numerical solution is easily obtainable although there may exist a stochastic process with a proper distribution which satisfies the equation. Also it may be more efficient to construct such a process and compute statistically than to attempt using the more conventional mathematical tools. In the noise analyses where the physical process involved is stochastic in nature, the Monte Carlo method is generally found adaptable. Because of the low average electron velocity near the potential minimum of a thermionic diode operated under space-charge-limited conditions, the velocity spread causes nonlinearity in the transport equation governing the macroscopic propagation phenomena. It is rather doubtful that the linear small-signal assumption made in most other methods of analysis (e.g., density function) for a practical model is valid. The Monte Carlo techniques employed here in solving the multivelocity transport problem would not only by-pass the difficulties which arise from nonlinearity, but would also preserve the particle

nature of the electrons and have the singularity factors eliminated from the mathematical formulation.

Simple as it may sound, the Monte Carlo calculations are usually extremely lengthy if a high degree of resolution is demanded. Sufficient samples must be taken so as to make the statistical approach feasible. One of the prerequisites for the application of the method is that all physical or mathematical stochastic processes satisfy the ergodic theorem in which the time average of a stationary random process is equal with a probability one to the statistical average. In this way, the stochastic features are dominated by a statistical approach with time as the independent parameter. Data obtained over a long period of time are interpreted the same as a large sample drawn at an arbitrary moment. The rather extensive arithmetic involved in the average is easily carried out by modern machine methods.

All in all, the Monte Carlo method is, with the aid of high-speed automatic computing machinery, a means of returning to the stochastics in phase space to obtain the thermodynamic functions required rather than averaging over all the phase space to deal with the thermodynamic quantities directly. During the process of calculations, all the work is carried out in the time domain; it is therefore quite difficult to observe the real mechanism in noise reduction which is a function of frequency. In spite of this disadvantage, this method of calculation is still considered to be the most accurate numerical method for noise transport investigations in the low-potential region of a multivelocity electron beam. Due to the similarities between a two-dimensional immersed flow model and its one-dimensional counterpart, it is convenient to describe the noise transport problem in one-dimensional formulation first

and add on some necessary modifications required by the multi-dimensional model.

3.2 One-Dimensional Analysis

In a two-dimensional noise transport problem, the immersed-flow assumption is necessarily made; otherwise the model diode would generalize into a three-dimensional model automatically once transverse velocities of any kind begin to interact with the axial magnetic field. Mixing of electrons which originate at various parts of the cathode will increase the complexity of the problem to such a degree that it is unlikely to be solved in a reasonable amount of time even by the highest speed computer available. In the present analysis an infinite magnetic-field assumption is made and the two-dimensional model may be approximated by a set of tightly coupled electron sheet beams with slightly different d-c characteristics. Each sheet beam is regarded as if it were a one-dimensional electron beam in the Monte Carlo treatment.

Some assumptions are made for the theoretical electron beam model employed to simplify the analysis.

1. Transverse motion of electrons is not allowed, a direct consequence of the infinite axial magnetic field assumption.

2. All random processes involved are ergodic stationary stochastic processes with equal time averages and ensemble averages.

3. Electrons are emitted normal to the cathode surface with a Rayleigh initial velocity distribution.

4. A potential minimum exists just outside of the cathode surface. A full space-charge-limited condition prevails.

5. No effect is produced by the returning electrons on the emission characteristics of the cathode.

6. Direct collisions between electrons are prohibited. The coupling mechanism between electrons comes from the space-charge fields.

7. There is no secondary emission.

8. Accumulation of electrons at the potential minimum is disallowed. Electrons emitted either will eventually reach the anode or return to the cathode.

9. Relativistic effects are not considered.

3.3 The Open-Circuit and the Short-Circuit Assumption

As will be shown later, coupling between convection current density and velocity fluctuations is achieved by the relationship between the a-c electric fields and the a-c current through Ampere's law, and

$$\nabla \times H = J = \epsilon_o \frac{\partial E}{\partial t} + i_c = \frac{V_{a\text{-}c}}{ZA} , \qquad (3.1)$$

where $\epsilon_o(\partial E/\partial t)$ is the displacement current density, i_c is the convection current density, $V_{a\text{-}c}$ is the a-c voltage across the diode, Z is the r-f impedance of the diode as seen by the electron beam, and A is the area of the cathode. The r-f impedance Z of a high-frequency diode is generally considered to be either an open circuit or a short circuit in noise transport problems because it is otherwise difficult to determine a unique finite equivalent impedance independent of frequency variations. In the short-circuit diode theory, the argument is based on the fact that the large inter-electrode capacitance represents virtually a short circuit at high frequencies. Both the a-c electric fields and the a-c potential across the diode approach zero as a limit in a short-circuit diode, yet

$$\lim_{f \to \infty} \frac{V_{a\text{-}c}}{ZA} = i_c \qquad (3.2)$$

is assumed to hold true always. It is easy to see that no correlation between the current fluctuations and velocity fluctuations can be obtained in a short-circuit diode because of the absence of a-c electric fields. In the open-circuit assumption, coupling between the electron beam and the diode circuit is assumed to be negligible and the impedance of an electron beam is taken to be an open circuit at high frequencies where the average transit angle for the electrons becomes appreciable.

$$\frac{V_{a\text{-}c}}{ZA} = 0 \tag{3.3}$$

and

$$\frac{\partial E}{\partial t} = -\frac{1}{\epsilon_o} i_c \quad . \tag{3.4}$$

Since

$$\frac{dv}{dt} = -\frac{e}{m} E$$

the correlations between the current and the velocity fluctuations are a direct result of the a-c space-charge effect. In the Monte Carlo analysis presented in this chapter the open-circuit assumption similar to the one employed by Dayem and Lambert is adopted because it seems to be a better approximation to the real physical phenomenon than the short-circuit assumption made by Tien and Moshman. In Section 3.5, further discussion on the subject of the a-c impedance of two-dimensional diodes will be presented.

3.4 Statistical Numbers

3.4.1 Generation and Transformation of Random Numbers. There are countless number of ways by which random numbers can be generated. In the modern digital computers, random numbers are internally generated using built-in routines. To name a few there are the mid-square method,

the modulus method, the Rand method, etc. Because the end result of the Monte Carlo calculation depends heavily on the quality of the random numbers, it is necessary to make sure the subroutines are checked statistically prior to application.

By means of a random number transformation, a set of positive random numbers $v_i (i = 1,2,3...)$ may be obtained having a desirable distribution function $f(v)$, where $f(v)$ denotes the probability of finding a number between v and v+dv and $f(v)$ is called the distribution function of v. If an integral distribution function $F(v)$ is defined such that

$$F(v) = \int_{-\infty}^{v} f(v)\, dv \quad , \tag{3.5}$$

$F(v)$ must fall between zero and one and it must be a single-valued monotone increasing function of v. In other words, there exists a one-to-one correspondence between v and $F(v)$. For a set of equally probable random numbers $R_i (i = 1,2,3...)$ generated so that

$$0 \leq R_i \leq 1 \tag{3.6}$$

a transformation may be accomplished by giving this set of random numbers a one-to-one correspondence with $F(v_i)$,

$$F(v_i) = R_i \quad . \tag{3.7}$$

The set of variables v_i corresponding to $F(v_i)$ thus obtained would then have the characteristics of random numbers governed by a distribution function $f(v)$.

3.4.2 Velocity Distribution of Thermionic Emission. With the infinite axial magnetic field assumption, all transverse velocities may be neglected and the initial velocity of electrons emitted normal to the

surface of the cathode follows approximately a Rayleigh distribution provided that the temperature of the emitting surface is reasonably high compared to the equivalent temperature of its work function. In Fig. 3.1 the probability density function that an electron be emitted with velocity between v and v+dv is plotted against its initial velocity v. This function is

$$f(v)\,dv = \frac{mv}{kT_c} \exp\left(-\frac{mv^2}{2kT_c}\right) dv \quad . \tag{3.8}$$

The integrated distribution function is shown in Fig. 3.2 as,

$$\begin{aligned} F(v) &= \int_0^v f(v)\,dv \\ &= \int_0^v \exp\left(-\frac{mv^2}{2kT_c}\right) d\left(\frac{mv^2}{2kT_c}\right) \\ &= 1 - \exp\left[-\frac{mv^2}{2kT_c}\right] \quad . \end{aligned} \tag{3.9}$$

If R is a random number between zero and one, it is easy to see that 1-R is also a random number in the same range. As long as R is uniformly distributed, a set of random numbers $R_i (i = 1,2,\ldots)$ may be transformed in the following manner.

$$\begin{aligned} 1 - R_i &= R(v_1) \\ &= 1 - \exp\left(-\frac{mv_i^2}{2kT_c}\right) \end{aligned} \tag{3.10}$$

or

$$\exp\left(-\frac{mv_i^2}{2kT_c}\right) = R_i \quad , \tag{3.11a}$$

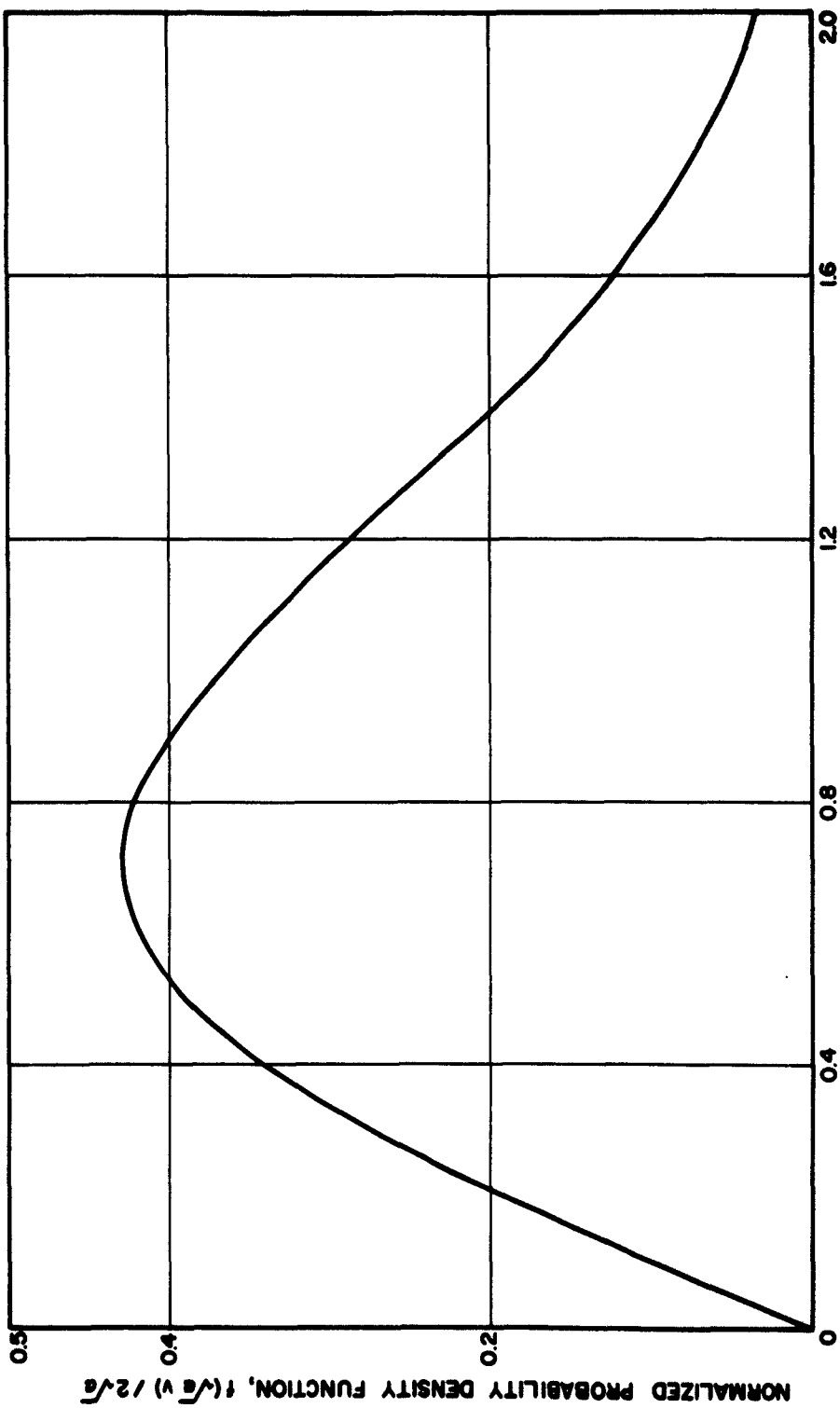

FIG. 3.1 NORMALIZED INITIAL VELOCITY DISTRIBUTION AT THE CATHODE (RAYLEIGH DISTRIBUTION).

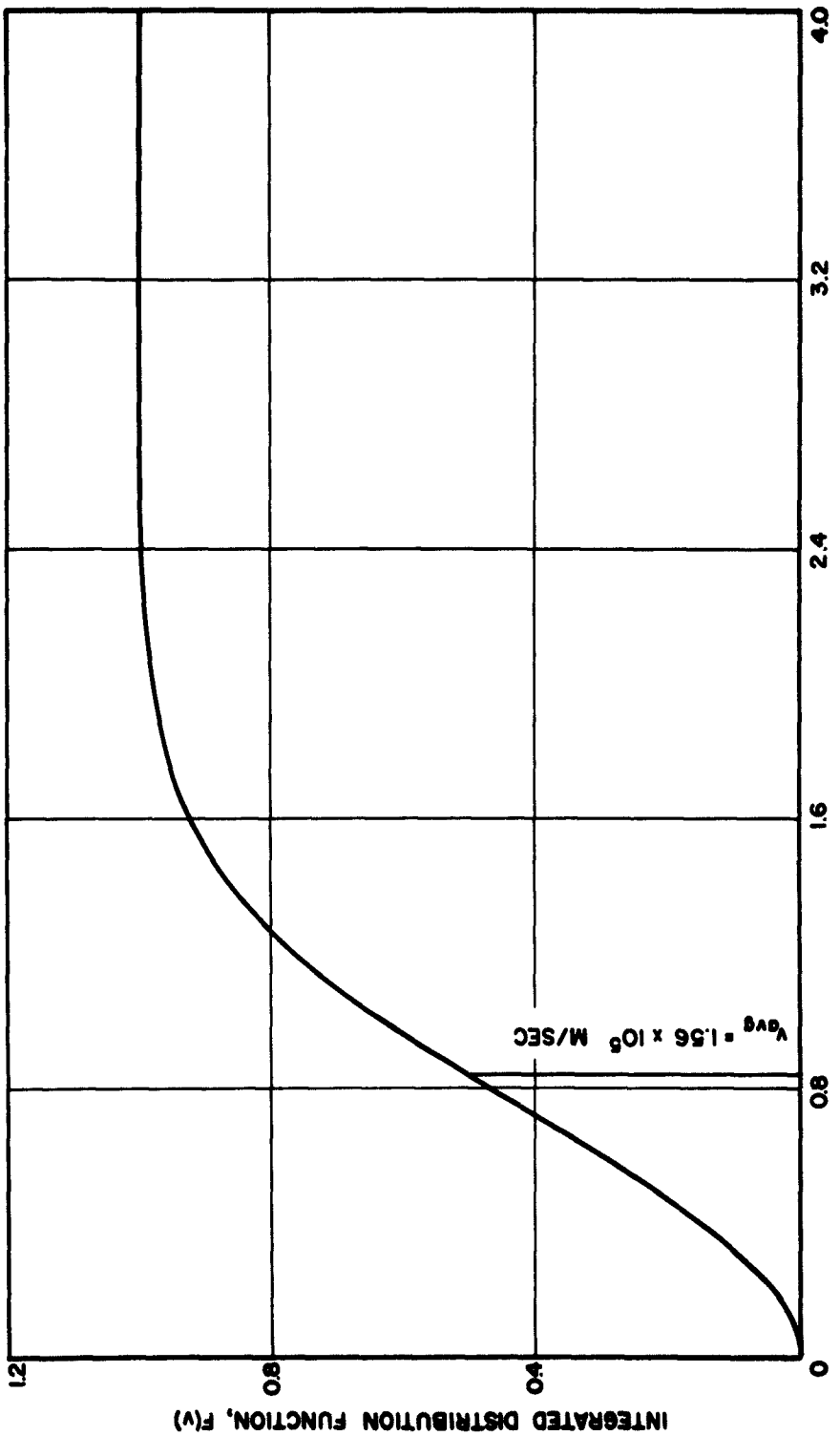

FIG. 3.2 INTEGRATED INITIAL VELOCITY DISTRIBUTION VS. NORMALIZED VELOCITY.

$$v_i = \left(\frac{2kT_c}{m}\right)^{1/2} (-\ln R_i)^{1/2} \quad , \tag{3.11b}$$

where v_i is the initial velocity of the ith electron and the velocity distribution is governed by a probability density function f(v). In emission processes, a random number must be generated corresponding to the initial velocity of every electron emitted.

3.4.3 Emission Probability. The instantaneous rate of emission during a very small time interval Δt follows Poisson's distribution as shown in Fig. 3.3, because of the postulate that the emission process of thermionic cathodes is stationary. From a unit area on the surface of the cathode, if the average number of electrons emitted during a time interval Δt is n, the probability that s electrons will be emitted during a time interval between t and $t+\Delta t$ is

$$f(s) = \frac{e^{-n} \cdot n^s}{s!} \quad . \tag{3.12}$$

Since s assumes only discrete values, the integration in Eq. 3.5 must be replaced by a series summation, such that

$$F(s) = \sum_{s} f(s) \quad . \tag{3.13}$$

The plot of F(s) versus s in integer values is shown in Fig. 3.4. After a numerical integration is carried out,

$$F(s) = \frac{1}{2} f(0) + f(1) + f(2) + \ldots + f(s-1) + \frac{1}{2} f(s) \quad . \tag{3.14}$$

It is convenient to designate the number of electrons emitted per time interval Δt to be s if

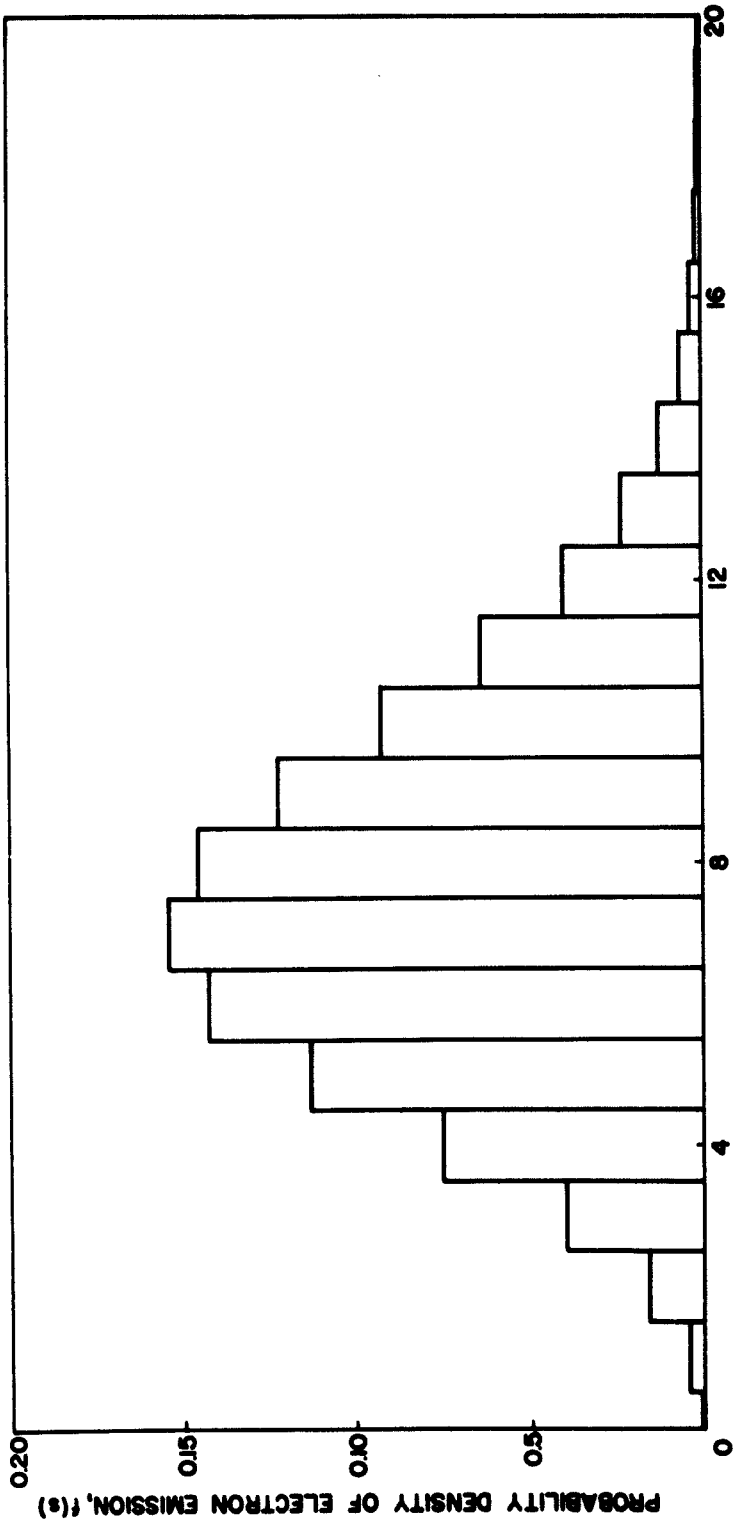

FIG. 3.3 PROBABILITY DENSITY OF ELECTRON EMISSION PER UNIT TIME INTERVAL. ($n = 7.5509$ ELECTRONS)

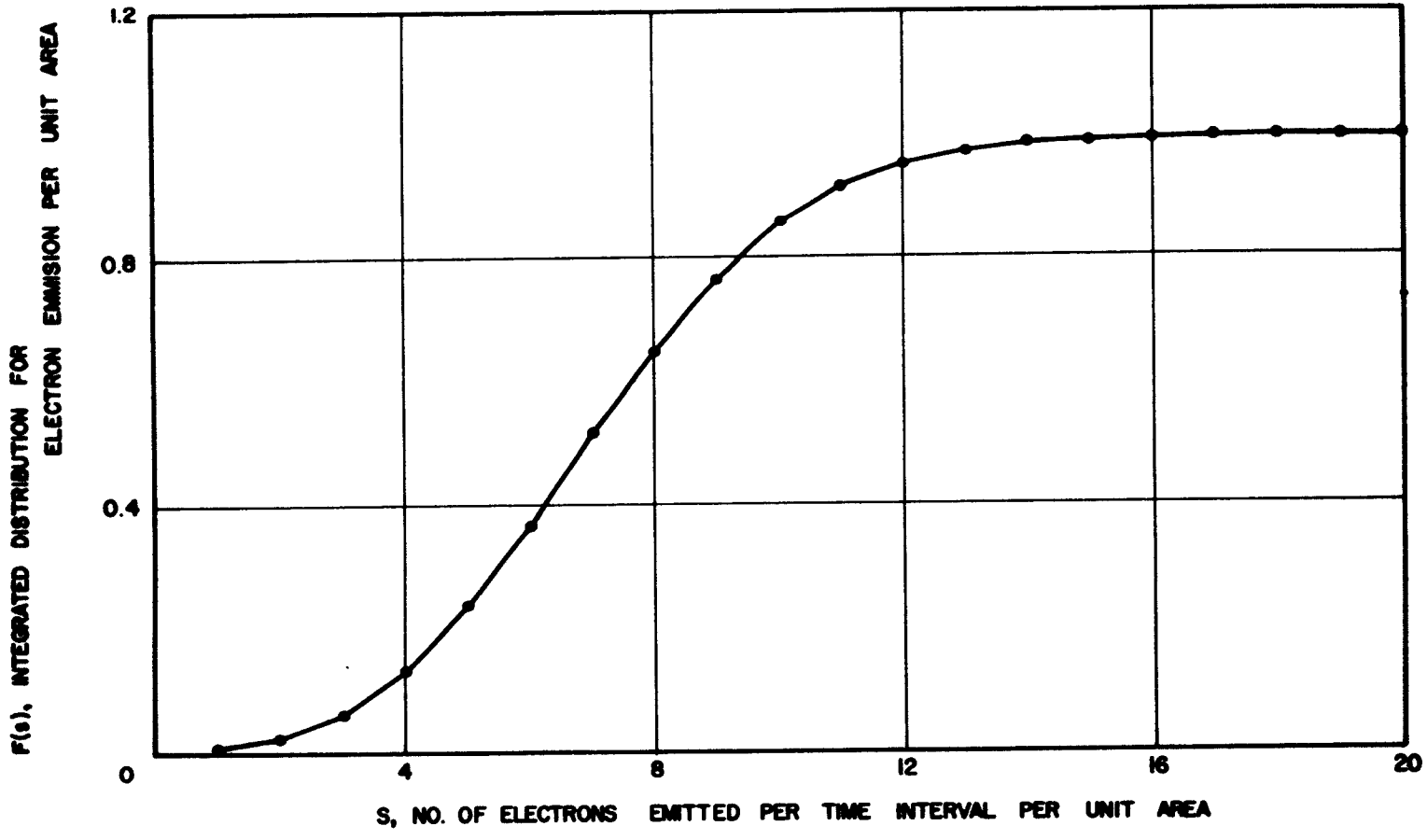

FIG. 3.4 INTEGRATED DISTRIBUTION CURVE FOR EMISSION PROBABILITY PER UNIT AREA PER UNIT TIME INTERVAL.

(n = 7.5509 ELECTRONS)

$$F\left(s - \frac{1}{2}\right) \leq R_s < F\left(s + \frac{1}{2}\right) , \qquad (3.15)$$

where R_s is a random number.

$F(s - 1/2)$ and $F(s + 1/2)$ may be obtained by means of graphical method from the $F(s)$ versus s curve.

3.4.4 Emission Time of Electrons. Because of the discrete nature of the digital computer techniques, the exact emission time of all electrons during a time interval Δt may be simulated by a random variable with a uniform distribution function. However, for computation purposes it would be much more convenient if all the electrons are considered to be emitted at the end of each time interval at a small distance z_i from the surface of the cathode, where i = 1,2,... corresponding to the ith number of electrons emitted during the immediately preceding time interval. The small displacement z_i is actually the distance traveled by the ith electron during the fraction of Δt between the time of its emission and the end of the time interval.

$$z_i = \frac{R_i \Delta t\, v_i - h\, E_{cathode} \dfrac{(R_i \Delta t)^2}{2}}{1 + \dfrac{h}{4} \dfrac{\partial E_{cathode}}{\partial z} (R_i \Delta t)^2} , \qquad (3.16)$$

where v_i is the initial velocity of the ith electron at the cathode plane, R_i is the random number corresponding to the emission time of the ith electron, $E_{cathode}$ is the electric field as seen by electrons at the cathode surface. No random number transformation is needed for the set of random numbers corresponding to the emission time of electrons.

The velocity of the ith electron at z_i is then

$$v_i' = v_i - h \left[E_{cathode} + \frac{1}{2} \frac{\partial E_{cathode}}{\partial z} z_i \right] R_i \Delta t . \qquad (3.17)$$

3.5 Electric Fields in a Two-Dimensional Diode

Inside the diode, electric fields experienced by each electron due to the presence of the space charge are to be evaluated at the beginning of every unit time interval and the d-c electric fields are assumed to be unchanged throughout Δt. Because of the divergence conditions encountered in an attempt to evaluate the electric field inside a two-dimensional diode through term-wise differentiation of the Fourier series representation of the potential function, the image method is instead employed to solve Poisson's equation. Details of both the Fourier series method and the image method are presented in Appendix B.I.

As a result of the infinite axial magnetic field assumption, the only current flowing perpendicular to the two-dimensional ribbon beam is the displacement current induced by the variations of the surface space-charge density of the z-directed sheet beams. According to the equation of continuity which requires the net current flowing out of any volume in space to be zero, the existence of a net current in the transverse direction must be accompanied by a nonzero algebraic sum for the longitudinal currents from the same volume. In other words, the impedance of a truly two-dimensional diode will remain finite.

In the present analysis, since it is difficult to determine how rapidly the a-c electric fields will decay in the transverse direction, some additional assumption on their boundary conditions are made. Consider a ribbon beam whose thickness is very small compared to a free-space wavelength corresponding to the highest frequency of interest, where the induced a-c electric fields may be assumed uniform across the electron beam. Outside of the beam boundaries, where the large inter-electrode capacitance of the diode behaves like a short circuit

at high frequencies, no z-directed a-c electric fields or displacement current is allowed. Now if the electron beam is divided axially into many sections, the transverse displacement current flowing from any section may be made arbitrarily small compared to the respective z-directed component by reducing the ratio between the axial dimension of the section and the thickness of the electron beam. Under such conditions, a close approximation of the axial a-c electric field may be obtained by means of the open-circuit assumption. It follows from the added boundary conditions that one-dimensional a-c electric fields are actually employed in the Monte Carlo noise transport analysis in a diode with a two-dimensional d-c potential distribution. A comparison of the results from the present analysis with those from the one-dimensional diodes will therefore reveal the effects on the noise transport characteristics by the d-c space charge.

3.5.1 Grouping of Electrons. The effects of space charge on d-c electric fields and potential distribution may be obtained by equations derived in Appendix B.I. Unfortunately, the large amount of time needed to compute the d-c electric fields alone makes the Monte Carlo analysis highly impractical even for the highest speed computer available. One way of reducing the length of the problem is to divide the diode into some compartments, each containing a few electrons as illustrated in Appendix B.II. These small groups of electrons are in turn replaced by x-directed line charges equal to the sum of all the electric charges in the respective compartments and are located at their respective effective centroids. After the potential distribution and the electric field are computed for all the boundary lines between compartments, the d-c

space-charge field anywhere inside the diode may be evaluated by linear interpolation methods.

Further simplification of the computation procedure may be achieved by fixing the centroids at their corresponding compartments regardless of the actual space-charge configurations. Techniques of linear transform are applicable once the centroids are considered fixed in space, because the resulting electric field is a linear combination of all the electric fields due to the presence of space charge at the various centroids.

3.5.2 Potential Distributions. Due to the absence of space charge outside of a two-dimensional ribbon beam, the potential distribution inside a two-dimensional space-charge-limited diode will deviate considerably from Langmuir's curve for one-dimensional diodes in which a uniform space-charge distribution in the transverse direction is assumed, unless an appropriate applied potential distribution is introduced to replace the potential depression effect of the missing electrons. In a synthetic model, the desirable potential distribution may be realized by properly placing a fixed fictitious space charge between the electrodes. An applied potential distribution corresponding to Child's law is assumed in the two-dimensional diode employed in the present analysis to account for the effect of the missing space charge. As a result of the image method, the potential at a point between compartments (i,j) and (i,j+1) is

$$V(i,j) = \sum_{m=1}^{5} \sum_{n=1}^{24} V(i,j;m,n) + V_{anode} \left(\frac{z_j}{a} \right)^{4/3} , \qquad (3.18)$$

where $V(i,j;m,n)$ is the potential at a point (y_i,z_j) due to the electric charge at the centroid of the (m,n) compartment, the last term is the applied potential at z_j according to Child's law, a is the distance

between the cathode and the anode and V_{anode} is the applied potential at the anode.

$$V(i,j;m,n) = \frac{\rho_{m,n}}{4\pi\epsilon_o}\left\{\ell n\left[\frac{(z_j+z_n)^2+(y_i-y_m)^2}{(z_j-z_n)^2+(y_i-y_m)^2}\right]+\ell n\left[\frac{(2a)^2-(z_j-z_n)^2}{(2a)^2-(z_j+z_n)^2}\right]\right.$$

$$+\frac{z_j}{a}\ell n\left[\frac{[2a+(z_j-z_n)][2a-(z_j+z_n)]}{[2a-(z_j-z_n)][2a+(z_j+z_n)]}\right]$$

$$\left.+\frac{z_n}{a}\ell n\left[\frac{[2a-(z_j+z_n)][2a-(z_j-z_n)]}{[2a+(z_j+z_n)][2a+(z_j-z_n)]}\right]\right\}, \quad (3.19)$$

$\rho_{m,n}$ is the charge per unit length in the (m,n) compartment. For $z_j + z_n \leq 0.2a$

$$V(i,j;m,n) \simeq \frac{\rho_{m,n}}{4\pi\epsilon_o}\left\{\ell n\left[\frac{(z_j+z_n)^2+(y_i-y_m)^2}{(z_j-z_n)^2+(y_i-y_m)^2}\right]-\frac{3z_jz_n}{a^2}\right\}. \quad (3.20)$$

The time average of the discrete potential functions thus obtained will be put into series form for each layer of the electron beam so that a continuous potential distribution will be available for the noise transport analysis in Chapter II where the density function method is employed.

3.5.3 D-c Electric Fields. The z-directed d-c electric field experienced by an electron within the (i,j) compartment is obtained by term-by-term differentiation of the potential function. Electric fields at points between compartments are first evaluated, then, linear interpolation in-between will be made for each individual electron inside the compartments.

The z-directed electric field at a point between (i,j) and (i,j+1) may be written as

$$E(i,j) = \sum_{m=1}^{5} \sum_{n=1}^{24} E(i,j;m,n) - \frac{4V_{anode}}{3a}\left(\frac{z_j}{a}\right)^{1/3} , \qquad (3.21)$$

where $E(i,j;m,n)$ is the electric field at (y_i,z_j) due to the presence of a charge $\rho_{m,n}$ at the centroid of compartment (m,n), and $-(4V_{anode}/3a)(z_j/a)^{1/3}$ is the d-c applied electric field corresponding to the last term in Eq. 3.18.

Again from Appendix B.I

$$E(i,j;m,n) = \frac{\rho_{m,n}}{2\pi\epsilon_o}\left\{(z_j-z_n)\left[\frac{1}{(z_j-z_n)+(y_i-y_m)^2} + \frac{1}{(z_j-z_n)^2-(2a)^2}\right] - (z_j+z_n)\left[\frac{1}{(z_j+z_n)^2+(y_i-y_m)^2} - \frac{1}{(z_j+z_n)^2-(2a)^2}\right] + \frac{1}{2a}\ln\left[\frac{(2a+z_j+z_n)[2a-(z_j-z_n)]}{(2a+z_j-z_n)[2a-(z_j+z_n)]}\right]\right\} \qquad (3.22)$$

or, if $z_j+z_n \leq 0.2a$, the equation above may be reduced to

$$E(i,j;m,n) = \frac{\rho_{m,n}}{2\pi\epsilon_o}\left\{\frac{z_j-z_n}{(z_j-z_n)^2+(y_i-y_m)^2} - \frac{z_j+z_n}{(z_j+z_n)^2+(y_i-y_m)^2} + \frac{z_n}{a^2}\right\} . \qquad (3.23)$$

For an electron in compartment (i,j) such that $z \geq z_j$, where (y_i,z_j) are the coordinates of the centroid of compartment (i,j), the d-c electric field may be evaluated by linear interpolation.

$$E(y,z) = E(i,j) + [E(i,j+1) - E(i,j)]\frac{z-z_j}{z_{(j+1)}-z_j} , \qquad (3.24)$$

or, if $z \leq z_j$,

$$E(y,z) = E(i,j) + [E(i,j-1) - E(i,j)] \frac{z_j - z}{z_j - z_{(j-1)}} \quad . \qquad (3.25)$$

3.5.4 Initial Potential Distribution in the Diode. A one-dimensional potential distribution as illustrated in Fig. 3.5 is assumed in the two-dimensional diode for the first two-hundred time intervals so that the diode may be properly filled up with electrons before formulas listed in the previous sections are employed to compute the electric fields. Approximation of Langmuir's one-dimensional space-charge-limited diode potential distribution curve is made for various sections of the diode. In dimensionless form

1. $0 \leq \xi \leq 1.9$.

$$\eta = 0.25(1.9-\xi)^2 + 0.045(1.9-\xi)^4 + 0.0045(1.9-\xi)^6$$

and

$$-\frac{d\eta}{d\xi} = 0.50(1.9-\xi) + 0.18(1.9-\xi)^3 + 0.027(1.9-\xi)^5 \quad .$$

2. $1.9 \leq \xi \leq 6$.

$$\eta = [0.424(\xi-1.9)]^{1.735} \quad ,$$

$$-\frac{d\eta}{d\xi} = -1.735\ [0.424(\xi-1.9)]^{0.735} \times 0.424 \quad .$$

3. $6 \leq \xi \leq 12$.

$$\eta = [0.4405(\xi-1.9)]^{1.618} \quad ,$$

$$-\frac{d\eta}{d\xi} = -1.618 \times 0.4405\ [0.4405(\xi-1.9)]^{0.618} \quad .$$

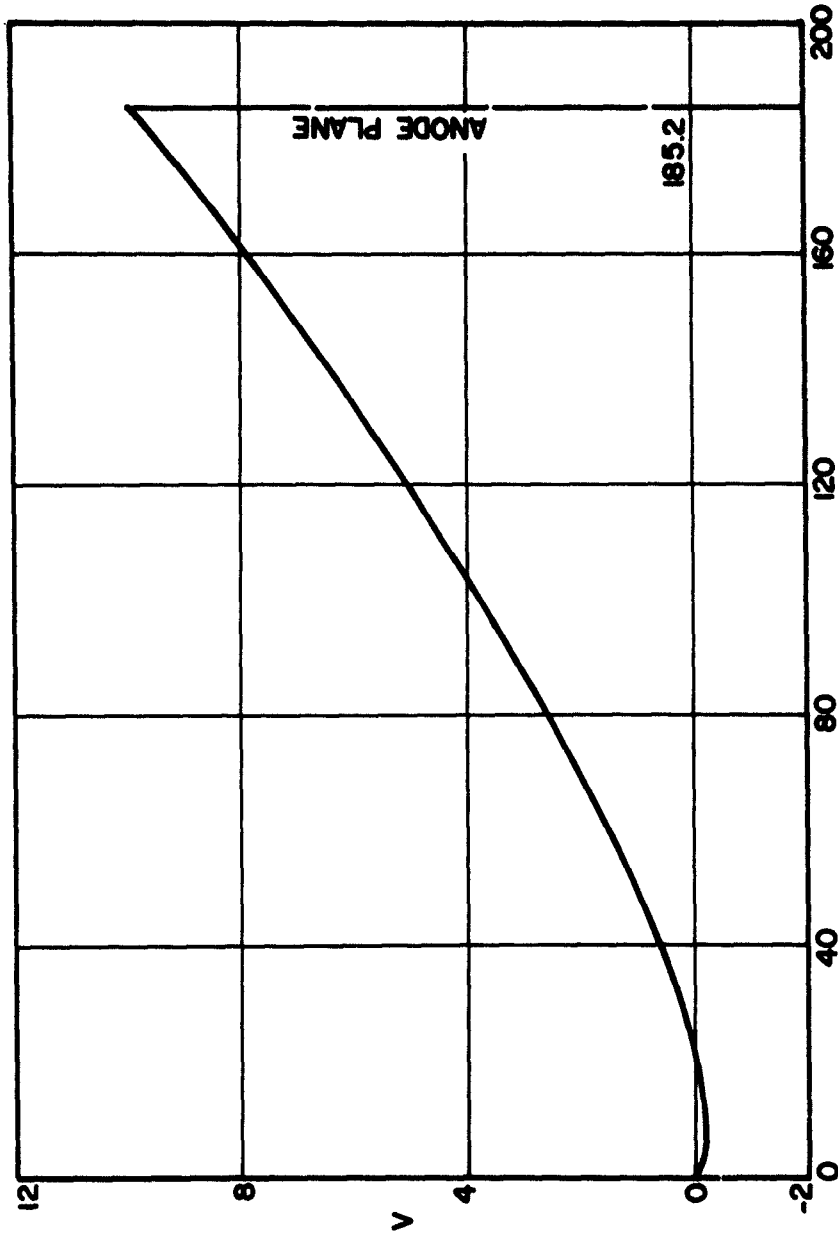

FIG. 3.5 POTENTIAL DISTRIBUTION INSIDE LANGMUIR'S ONE-DIMENSIONAL DIODE.

4. $12 \leq \xi \leq 42.$

$$\eta = [0.5035(\xi-1.9)]^{1.483} ,$$

$$-\frac{d\eta}{d\xi} = -1.483 \times 0.5035\,[0.5035(\xi-1.9)]^{0.483} .$$

5. $42 \leq \xi \leq 200.$

$$\eta = [0.5925(\xi-1.9)]^{1.408} ,$$

$$-\frac{d\eta}{d\xi} = -1.408 \times 0.5925\,[0.5925(\xi-1.9)]^{0.408} ,$$

where η and ξ are the potential and distance parameters defined in Chapter II, $-(d\eta/d\xi)$ is proportional to the d-c electric field.

The potential minimum plane for a one-dimensional diode with the same emission characteristic as the model employed here is located at approximately $\xi_m = 1.9$. In a two-dimensional model the potential minimum of the center layer of the electron beam is expected to be approximately the same distance away from the cathode surface.

3.5.5 A-c Electric Fields. Since the diode is assumed to be an open circuit at high frequencies, the total r-f current flowing across any plane parallel to the surface of the cathode is zero. Or in terms of current densities,

$$\epsilon_o \frac{\partial E(y_i,z_j)}{\partial t} + \frac{1}{5}\sum_{i=1}^{5} [\rho v](y_i,z_j) + J_{d\text{-}c} = 0 , \qquad (3.26)$$

where $[\rho v](y_i,z_j)$ is the convection current density carried by the electrons in compartment (i,j), $J_{d\text{-}c}$ is the average current density of the electron beam, $\partial E/\partial t$ is the time rate of change of the electric field experienced by all electrons in compartments (i,j), where $i = 1,2,\ldots 5$.

$$[\rho v](y_i, z_j) = \sum_{\ell} \frac{-e}{\Delta z_j (\Delta y)^2} \cdot v_{\ell} \quad , \tag{3.27}$$

where ℓ is the number of electrons in compartment (i,j), $\partial E/\partial t$ is computed at the beginning of each time interval Δt and is assumed to be a constant throughout.

The relation given between the a-c electric fields and the current fluctuations in this two-dimensional model suggests that the a-c electric fields drop off abruptly beyond the boundaries of the electron beam in the y-direction. In a real diode, the field strength is expected to decay exponentially instead.

3.6 Numerical Integration

Electrons are traced in phase space by means of numerical integration techniques. The incremental changes in velocity and distance are governed by the electric field through the use of Newton's force laws to the first-order approximation in both time and space.

$$\ddot{z} = -hE = -h\left(E_{d\text{-}c} + \frac{\partial E}{\partial t}\Delta t\right) , \tag{3.28}$$

$$\Delta \dot{z} = -h\left[\left(E_{d\text{-}c} + \frac{1}{2}\frac{\partial E}{\partial z}\Delta z\right)\Delta t + \frac{1}{2}\frac{\partial E}{\partial t}(\Delta t)^2\right] \tag{3.29}$$

and

$$\Delta z = \left\{-h\left[E_{d\text{-}c}\frac{\Delta t^2}{2} + \frac{1}{6}\frac{\partial E}{\partial t}(\Delta t)^3\right] + \dot{z}\Delta t\right\} \frac{1}{1 + \frac{h}{2}\frac{\partial E}{\partial z}\frac{(\Delta t)^2}{2}} \quad , \tag{3.30}$$

where $\dot{z}$ is the velocity of an electron at the beginning of a time interval Δt.

E_{d-c} is the total d-c electric field at the point where the electron is located. $E_{d-c} = E_{applied} + E_{space\ charge}$.

$\partial E/\partial t$ is the rate of change of the a-c electric field obtained by the open-circuit diode assumption. It is assumed to be constant over a small time interval Δt, i.e., $f\Delta t$ is much smaller than unity if f is the highest frequency of interest.

$\partial E/\partial z$ is the slope of the d-c electric field at the initial position of the electron at the beginning of the time interval.

$\Delta \dot{z}$ is the incremental change of velocity during Δt for an electron traveling with a velocity $\dot{z}$ and located at z at the beginning of the time interval.

Δz is the incremental change of distance occurring during Δt.

Numerical integrations are carried out for every electron between the two electrodes for every time interval Δt until they cross the anode plane or return to the cathode. Positions and velocities of electrons are stored temporarily and then updated at the end of each iteration.

The second-order term $1/6\ (\partial^2 E/\partial t^2)(\Delta t)^3$ is assumed to be negligible compared to the first-order effect of the a-c electric field in the Monte Carlo analysis.

3.7 Computation of Noise Parameters

Noise parameters are evaluated at several planes beyond the potential minimum for a set of discrete frequencies. According to the noise theory derived by Haus and Robinson, the minimum noise figure achievable by a longitudinal-beam amplifier depends solely on these parameters, which are the Fourier transforms of the correlation functions of the convection current density and the voltage fluctuations.

3.7.1 Current and Velocity Fluctuations. The current and the velocity fluctuations are computed for planes located at $z = z_1, z_2, \ldots z_n$ for each time interval between t_i and $t_i+\Delta t$. The current fluctuations at (y_m, z_n) during the ith time interval may be expressed as

$$i_1(y_m, z_n, t_i) = \frac{-e}{\Delta t}\left[N(y_m, z_n, t_i) - N_o(y_m, z_n)\right] , \qquad (3.31)$$

where the subscript "1" denotes an r-f quantity, and "o" denotes a d-c quantity, $N(y_m, z_n, t_i)$ is the number of electrons crossing z_n at layer y_m between t_i and $t_i+\Delta t$, and $N_o(y_m, z_n)$ is the average number of electrons crossing plane z_n at the y_mth layer for an interval Δt. Similarly, for the electron beam as a whole, the current fluctuation at z_n during the ith time interval is

$$i_1(z_n, t_i) = \frac{-e}{\Delta t}\sum_{m=1}^{5}\left[N(y_m, z_n, t_i) - N_o(z_n)\right] , \qquad (3.32)$$

where

$$N_o(z_n) = \frac{1}{5}\sum_{m=1}^{5} N_o(y_m, z_n) .$$

As to velocity fluctuations, the problem is much more complicated if the retarding field region of the diode is considered. Because of the reflected flows, it will be necessary to assign each electron a name tag and follow through to see whether it will eventually pass the potential minimum or not. However, it is less difficult to determine velocity fluctuations at planes beyond the potential minimum. Chu's kinetic potential may be introduced in place of velocity fluctuations. By definition

$$2h\, V_1(y_m,z_n,t_i) = \frac{-1}{N_o(y_m,z_n)} \sum_{\ell} \left[v_\ell^2(y_m,z_n,t_{ic}) - \overline{v_o^2}(y_m,z_n) \right] , \tag{3.33}$$

where ℓ is the number of electrons crossing plane z_n at layer y_m between t_i and $t_i+\Delta t$, $v_\ell(y_m,z_n,t_{ic})$ is the velocity of the ℓth electron at z_n as shown in Appendix B.III, and $\overline{v_o^2}(y_m,z_n)$ is the mean square velocity of electrons at the z_n plane of the layer y_m.

$$\overline{v_o^2}(y_m,z_n) = \frac{1}{\sum_{t_i} N(y_m,z_n,t_i)} \cdot \sum_{t_i} \sum_{\ell} v_\ell^2(y_m,z_n,t_{ic})$$

and for the whole beam,

$$2h\, V_1(z_n,t_i) = \frac{-1}{\sum_{m=1}^{5} N_o(y_m,z_n)} \sum_{m=1}^{5} \sum_{\ell} \left[v_\ell^2(y_m,z_n,t_{ic}) - \overline{v_o^2}(z_n) \right] , \tag{3.34}$$

where

$$\overline{v_o^2}(z_n) = \frac{1}{\sum_{t_i} \sum_{m=1}^{5} N(y_m,z_n,t_i)} \cdot \sum_{t_i} \sum_{m=1}^{5} \sum_{\ell} v_\ell^2(y_m,z_n,t_{ic}) .$$

The noise power carried by the two-dimensional electron beam as a whole is expected to be somewhat higher than that carried by individual layers, because of the non-Maxwellian velocity distribution in the multi-layer model.

3.7.2 Time Auto-Correlation and Time Cross-Correlation Functions. The time auto-correlation function is an indication of the amount of mean-square fluctuations as well as the time dependence characteristics of a

sample function of a random process. On the other hand, the time cross-correlation function of the sample functions of two random processes describes the dependency of the two random processes.

From the definitions given in Appendix B.IV.1, the time auto-correlation and cross-correlation functions of the kinetic potential and the noise current density fluctuations are given by the following equations:

$$\varphi(y_m,z_n,s) = \frac{1}{p-s} \sum_{t=0}^{(p-s)\Delta t} V_1(y_m,z_n,t)\, V_1(y_m,z_n,t+s\Delta t) \quad , \qquad (3.35)$$

$$\Psi(y_m,z_n,s) = \frac{1}{p-s} \sum_{t=0}^{(p-s)\Delta t} i_1(y_m,z_n,t)\, i_1(y_m,z_n,t+s\Delta t) \qquad (3.36)$$

and

$$\theta(y_m,z_n,s) = \frac{1}{p-s} \sum_{t=0}^{(p-s)\Delta t} i_1(y_m,z_n,t)\, V_1(y_m,z_n,t+s\Delta t) \quad , \qquad (3.37)$$

where s is an integer less than or equal to q such that $q < p$, and p is the maximum number of computer time intervals (total number of iterations carried out). It is postulated that negligible correlation can be found between events separated by a time interval larger than $q\Delta t$. The magnitude of p is limited mainly by the available time and money for computer operations.

The choice of q depends on two conflicting considerations. First of all, the frequency resolution of the statistical noise analysis increases with q; no new information in frequency domain may be extracted at discrete values of frequency less than Δf apart, where $\Delta f = 1/q\Delta t$. On the contrary, the confidence interval of the statistical approximation

deteriorates with any increase of the ratio of q/p. It is therefore necessary to make some kind of compromise between the two limiting factors keeping in mind that q should be of the order of one hundred so that Δf is much smaller than $1/\Delta t$, the upper frequency limit of the spectral analysis.

3.7.3 Power Spectral Density and the Noise Parameters. The application of the power spectral densities and the correlation functions of random processes are usually referred to as the generalized harmonic analysis. For a stationary random process such as a signal or noise, the power spectral density may be considered as the power distribution in the frequency domain. The normalized self-power spectral density and the normalized cross-power spectral density may be obtained by expanding the auto-correlation and the cross-correlation functions respectively in Fourier series as shown in Appendix B.IV.2.

$$\Phi(y_m,z_n,\Omega) = \frac{eI(y_m)\Delta t}{(kT_c)^2}\left[\varphi(y_m,z_n,0) + 2\sum_{s=1}^{q-1}\varphi(y_m,z_n,s)\cos\left(\frac{\pi\Omega s}{q}\right) + \varphi(y_m,z_n,q)\cos(\pi\Omega)\right], \quad (3.38)$$

$$\Psi(y_m,z_n,\Omega) = \frac{\Delta t}{eI(y_m)}\left[\psi(y_m,z_n,0) + 2\sum_{s=1}^{q-1}\psi(y_m,z_n,s)\cos\left(\frac{\pi\Omega s}{q}\right) + \psi(y_m,z_n,q)\cos(\pi\Omega)\right], \quad (3.39)$$

$$\Theta(y_m,z_n,\Omega) = \frac{\Delta t}{kT_c}\left\{\theta_1(y_m,z_n,0) + \sum_{s=1}^{q-1}\left[\theta_1(y_m,z_n,s) + \theta_2(y_m,z_n,s)\right]\cos\left(\frac{\pi\Omega s}{q}\right) + \frac{\theta_1(y_m,z_n,q) + \theta_2(y_m,z_n,q)}{2}\cos(\pi\Omega)\right\}$$

$$- j\frac{\Delta t}{kT_c}\left\{\sum_{s=1}^{q-1}\left[\theta_1(y_m,z_n,s) - \theta_2(y_m,z_n,s)\right]\sin\left(\frac{\pi\Omega s}{q}\right) + \frac{\theta_1(y_m,z_n,q) - \theta_2(y_m,z_n,q)}{2}\sin(\pi\Omega)\right\} , \quad (3.40)$$

where $\Omega = 2qf\Delta t$, a frequency parameter,

f = the frequency variable.

If $f = 0, 1/2q\Delta t, 1/q\Delta t, 3/2\,(1/q\Delta t), 5/2\,(1/q\Delta t)$, $\Omega = 0,1,2,\ldots q$, the last term in Eq. 3.40 vanishes identically. $\Phi(y_m,z_n,\Omega)$ is the power spectral density of the kinetic potential at (y_m,z_n), $\Psi(y_m,z_n,\Omega)$ is the power spectral density of the convection current density fluctuation at (y_m,z_n), $\Theta(y_m,z_n,\Omega)$ represents the cross-power spectral density of the kinetic potential and the convection current density fluctuations at (y_m,z_n).

$$\theta_1(y_m,z_n,s) = \frac{1}{p-s}\sum_{t=0}^{(p-s)\Delta t} i_1(y_m,z_n,t)\, V_1(y_m,z_n,t+s\Delta t) ,$$

$$\theta_2(y_m,z_n,s) = \frac{1}{p-s}\sum_{t=0}^{(p-s)\Delta t} i_1(y_m,z_n,t+s\Delta t)\, V_1(y_m,z_n,t) .$$

Similar expressions may be obtained for the power spectral densities of the entire electron beam if the parameter y_m is dropped from Eqs. 3.35 through 3.40.

The noise parameters defined by Haus and Robinson are employed in the noise transport analysis.

$$\Pi(y_m,z_n,\Omega) = \mathrm{Re}\left[\Theta(y_m,z_n,\Omega)\right] , \tag{3.41}$$

$$\Lambda(y_m,z_n,\Omega) = \mathrm{Im}\left[\Theta(y_m,z_n,\Omega)\right] \tag{3.42}$$

and

$$S^2(y_m,z_n,\Omega) = \Phi(y_m,z_n,\Omega)\,\Psi(y_m,z_n,\Omega) - \Lambda^2(y_m,z_n,\Omega) . \tag{3.43}$$

For one-dimensional longitudinal beam single velocity amplifiers, both $S(y_m,z_n,\Omega)$ and $\Pi(y_m,z_n,\Omega)$ are independent of z_n, i.e., they are invariant quantities. $S(\Omega)$ represents the total a-c power carried by the fluctuations and $\Pi(\Omega)$ specifies the amount of correlation between velocity and current fluctuations. In general, $\Pi(y_m,0,\Omega)$ is assumed to be zero at the cathode plane for a diode with uncorrelated velocity and current fluctuations at the input.

3.7.4 Frequency Aliasing and Lag Windows.

3.7.4a Cutoff Frequency f_c. In a generalized harmonic analysis for a random time process with samples drawn at equally spaced intervals in time, part of the information contained by the real continuous process is lost because of the assumption of the invariance of fluctuations and their correlation functions within small unit time intervals Δt. If the correlation function $R(\tau)$ is an absolutely integrable function of τ, the Fourier transform of $R(\tau)$ exists and is called the power spectral density $S_R(f)$,

$$S_R(f) = \int_{-\infty}^{\infty} R(\tau)\, e^{-j\omega\tau}\, d\tau \quad . \tag{3.44}$$

If the average value of $R(\tau)$ in a time interval between $t - (\Delta t/2)$ and $t + (\Delta t/2)$ is designated as $\bar{R}(\tau)$, then

$$\bar{R}(\tau) = \frac{1}{\Delta t} \int_{t - \frac{\Delta t}{2}}^{t + \frac{\Delta t}{2}} R(\zeta)\, d\zeta \quad . \tag{3.45}$$

$S_{\bar{R}}(f)$ is defined as the estimated spectrum of $R(\tau)$, such that

$$\begin{aligned}
S_{\bar{R}}(f) &= \int_{-\infty}^{\infty} \bar{R}(\tau)\, e^{-j\omega\tau}\, d\tau \\
&= \int_{-\infty}^{\infty} \frac{1}{\Delta t} \int_{t - \frac{\Delta t}{2}}^{t + \frac{\Delta t}{2}} R(\zeta)\, d\zeta\, e^{-j\omega\tau}\, d\tau \\
&= \int_{-\infty}^{\infty} \frac{1}{\Delta t} \int_{\zeta - \frac{\Delta t}{2}}^{\zeta + \frac{\Delta t}{2}} R(\zeta)\, e^{-j\omega\tau}\, d\tau\, d\zeta \\
&= \int_{-\infty}^{\infty} R(\zeta)\, e^{-j\omega\zeta}\, \frac{\left[e^{j\frac{\omega\Delta t}{2}} - e^{-j\frac{\omega\Delta t}{2}} \right]}{j\omega\Delta t}\, d\zeta \\
&= S_R(f) \cdot \frac{\sin\left(\frac{\omega\Delta t}{2}\right)}{\frac{\omega\Delta t}{2}} \\
&= S_R(f)\, \frac{\sin(\pi f \Delta t)}{\pi f \Delta t} \quad .
\end{aligned} \tag{3.46}$$

From Fig. 3.6 it can be shown that $\sin(\pi f\Delta t)/\pi f\Delta t$ is approximately equal to one for small arguments. The estimated spectrum falls off very rapidly as $f\Delta t$ approaches unity. At $f_c = 1/\Delta t$, the estimated spectrum $S_{\bar{R}}(f_c)$ drops off to zero, and f_c is called the cutoff frequency of the spectrum analysis. Therefore the true spectrum may be recovered only at frequencies very low compared to the cutoff frequency f_c.

3.7.4b Aliasing Effects. As seen in Fig. 3.7, aliasing between spectra centered at different frequencies arises from the discrete nature of the parameter τ of the correlation functions. If $s = j\omega$, the Fourier transform of an equally spaced Dirac comb (a set of delta functions equally spaced in the time domain) may be expressed in the following manner.

$$S(s) = \int_{-\infty}^{\infty} \sum_{n=-\infty}^{\infty} R(\tau)\, \delta(\tau - n\Delta t) e^{-s\tau}\, d\tau \quad . \tag{3.47}$$

The right-hand side of Eq. 3.48 is called a two-sided Laplace transform, a generalized case of the Fourier transform. If the transforms of both $R(\tau)$ and $\delta(\tau - n\Delta t)$ exist, then

$$S_R(s) = \int_{-\infty}^{\infty} R(\tau) e^{-s\tau} d\tau = \int_{-\infty}^{0} R(\tau) e^{-s\tau} d\tau + \int_{0}^{\infty} R(\tau) e^{-s\tau} d\tau$$

$$= S_{R1}(s) + S_{R2}(s) \quad , \tag{3.48}$$

$$S_\delta(s) = \int_{-\infty}^{\infty} \sum_{n=-\infty}^{\infty} \delta(\tau - n\Delta t) e^{-s\tau} d\tau = \sum_{n=-\infty}^{\infty} e^{-sn\Delta t} \quad . \tag{3.49}$$

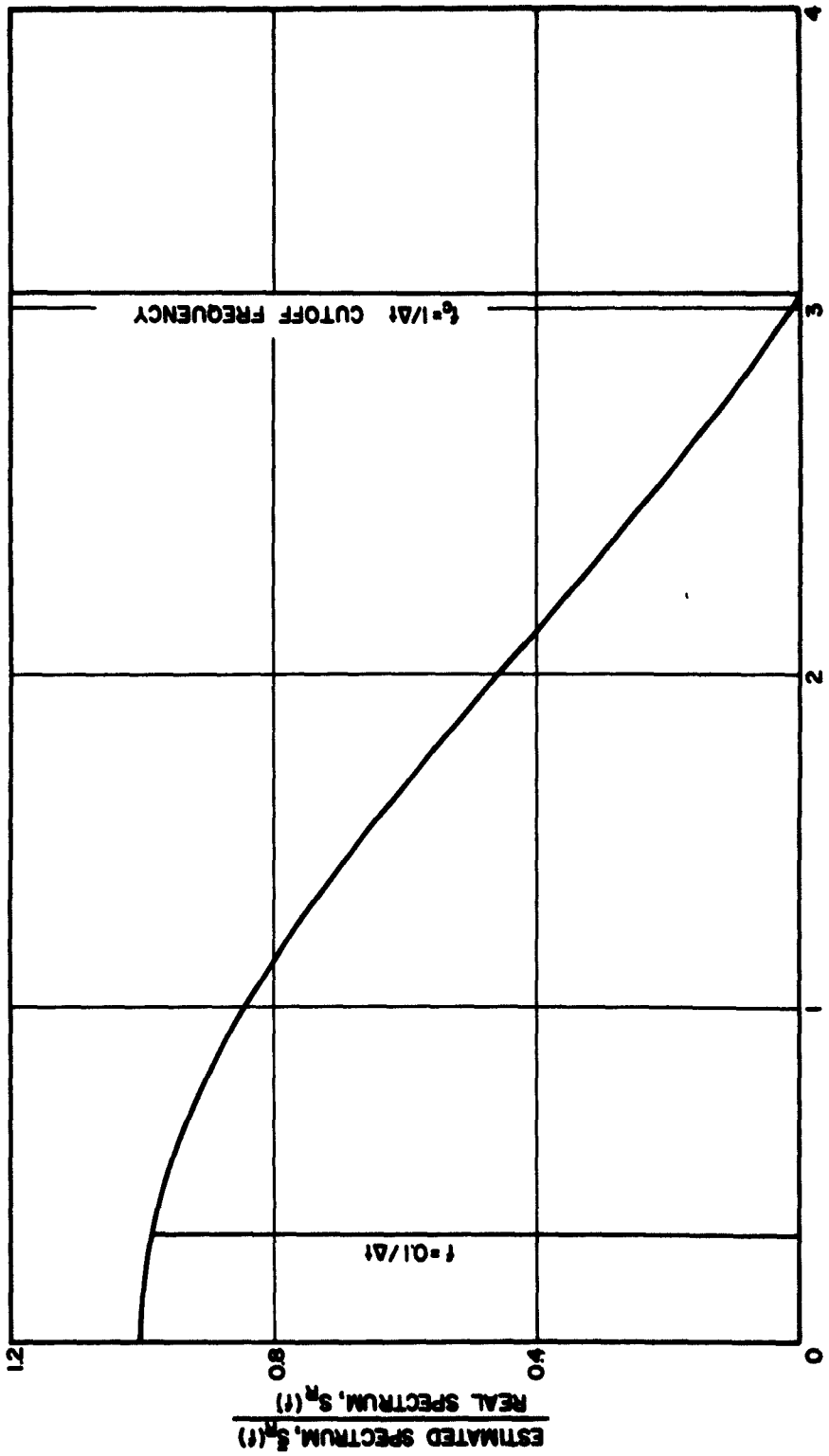

FIG. 3.6 THE RATIO OF THE MAGNITUDES OF THE ESTIMATED SPECTRUM AND THE REAL SPECTRUM VS. $\pi f \Delta t$ FROM A SET OF EQUALLY SPACED SAMPLES IN THE TIME DOMAIN.

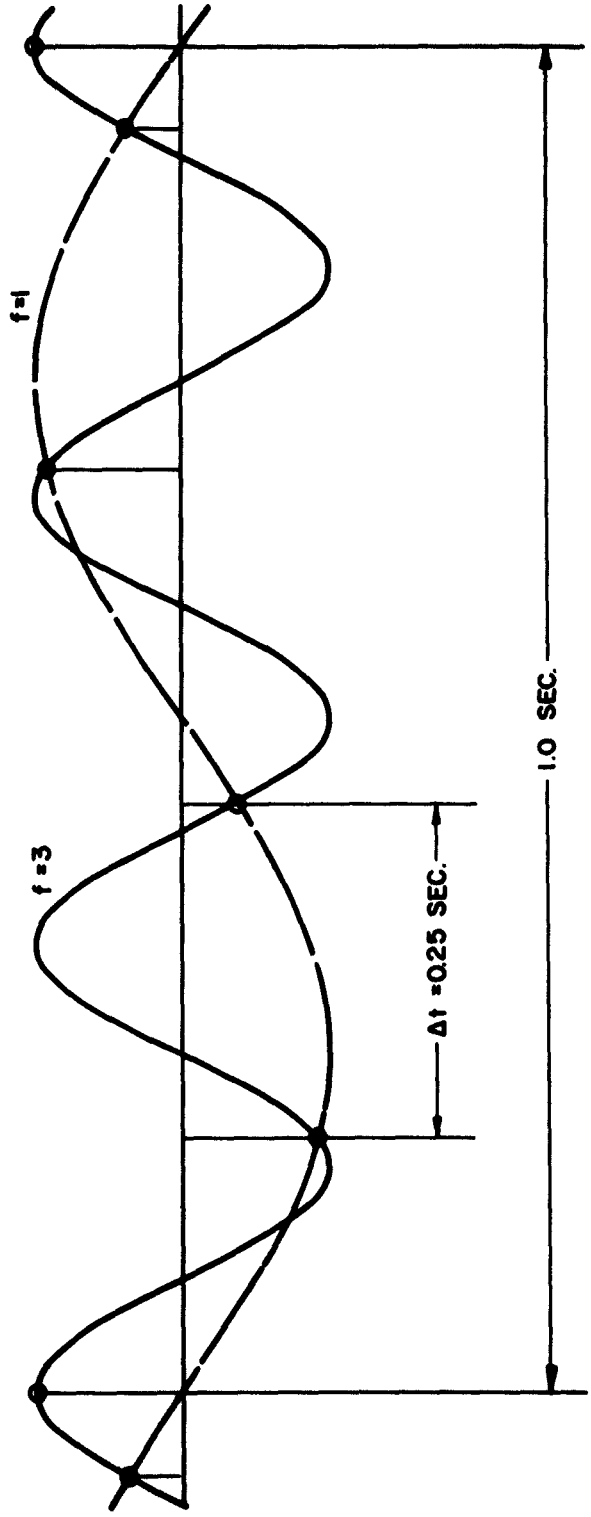

FIG. 3.7 ALIASING EFFECT OF EQUALLY SPACED SAMPLES.

By the convolution theorem,

$$S(s) = \frac{1}{2\pi j} \oint S_R(s-u)\, S_\delta(u)\, du \quad . \tag{3.50}$$

By the convolution theorem,

$$S(s) = \frac{1}{2\pi j} \oint S_{R_1}(s-u) \left[\frac{1}{1-e^{-u\Delta t}}\right] du$$

$$+ \frac{1}{2\pi j} \oint S_{R_2}(s-u) \left[\frac{1}{1-e^{-u\Delta t}}\right]_2 du \quad , \tag{3.51}$$

where the first line integral is taken along the jω-axis and a semicircle of infinite radius on the right half plane to account for all the poles in the right half plane. Then, a second integration is performed along the jω-axis and a semicircle of infinite radius on the left half of the S plane (Fig. 3.8). For $e^{-u\Delta t} = 1$

$$u = j\frac{2\pi n}{\Delta t} \qquad n = 0, \pm 1, \pm 2, \ldots \tag{3.52}$$

Therefore

$$S(s) = \sum \text{Residues of } \frac{S_R(s-u)}{1-e^{-u\Delta t}}$$

$$= \sum_{n=-\infty}^{\infty} S_R\left(s - \frac{j2n\pi}{\Delta t}\right)$$

$$S(f) = \sum_{n=-\infty}^{\infty} S_R\left(f - \frac{n}{\Delta t}\right) \quad . \tag{3.53}$$

The resulting spectrum in Fig. 3.9 consists of a fundamental mode centered at zero frequency and repeats itself every $f = n/\Delta t$. The

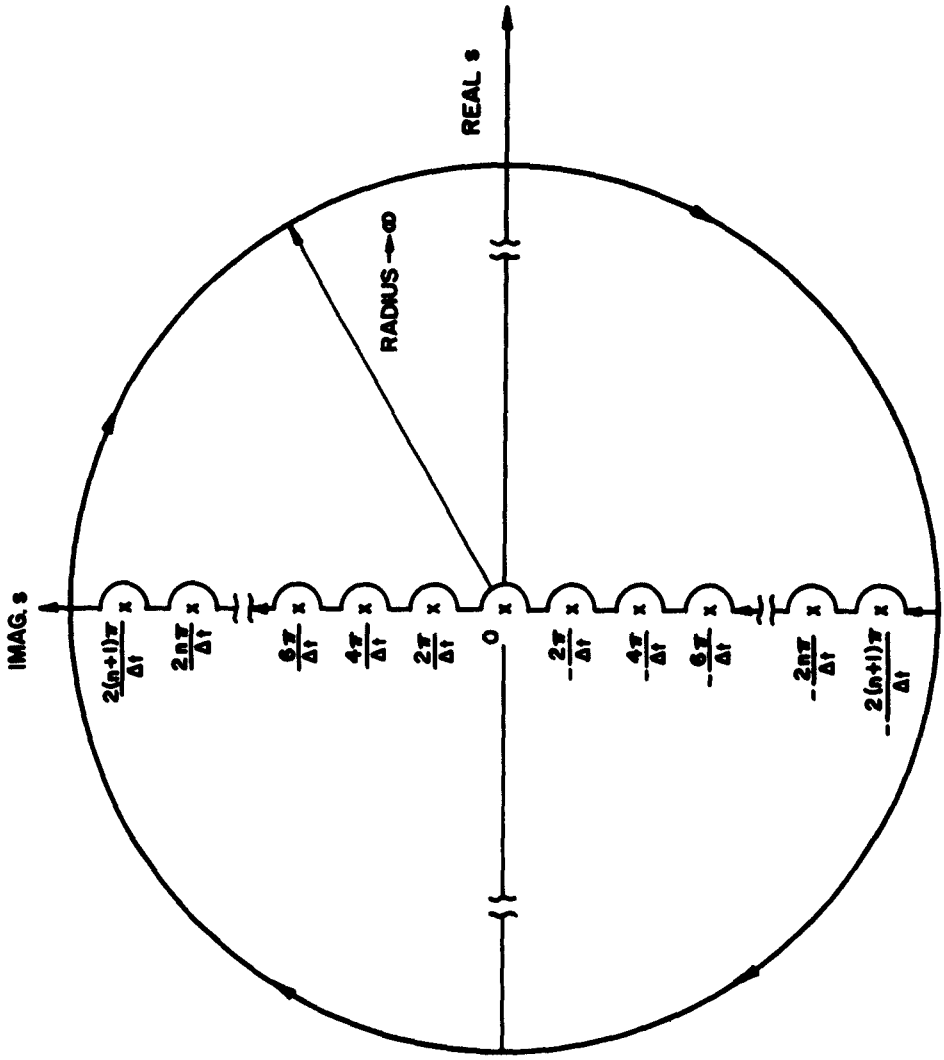

FIG. 3.8 LOCI FOR CONTOUR INTEGRATION IN S-PLANE (COMPLEX FREQUENCY PLANE).

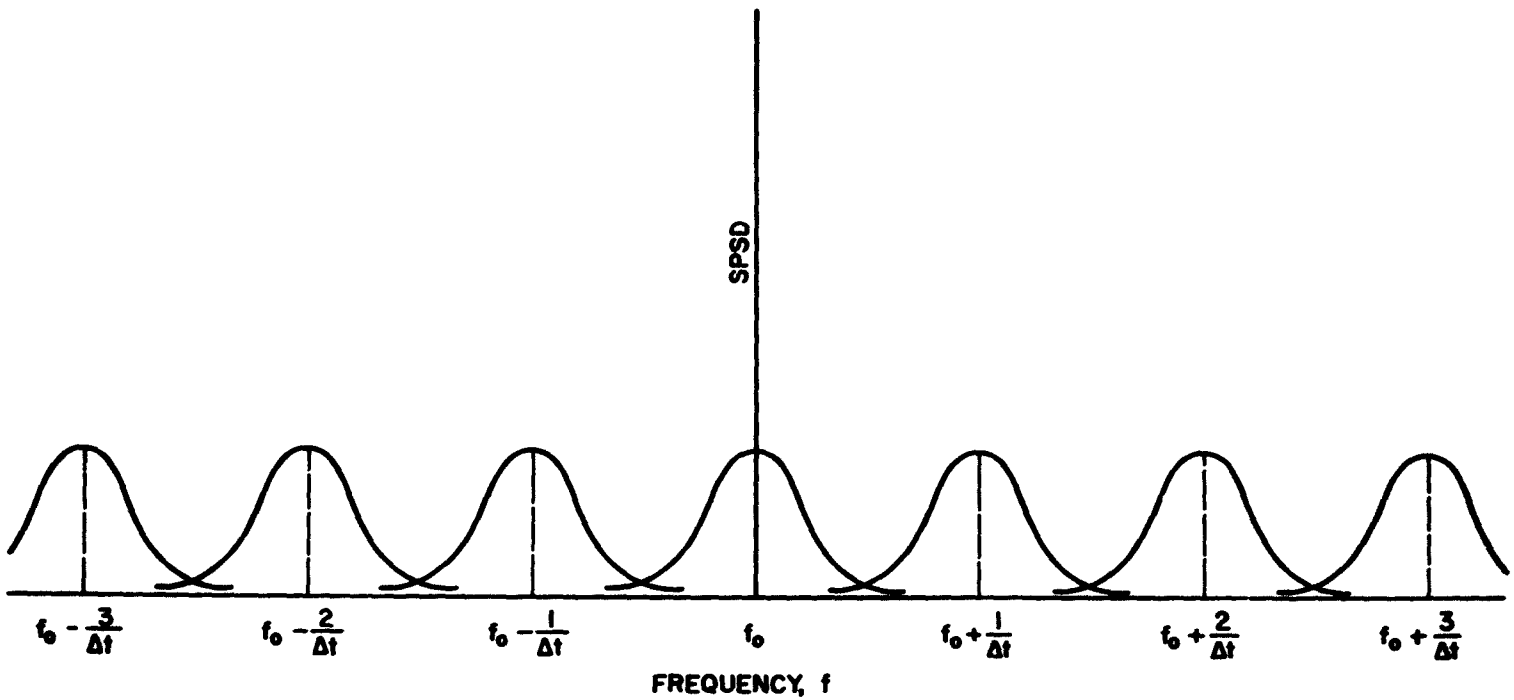

FIG. 3.9 ALIASING EFFECTS, SELF-POWER SPECTRAL DENSITY OF AN EQUALLY SPACED RECORD IN THE TIME DOMAIN.

spectrum observed anywhere will therefore include a certain amount of undesirable effects from all the modes other than the fundamental. It is recalled from the previous section that the fundamental mode drops off rapidly to zero as f approaches $n/\Delta t$. If a good approximation to the true spectrum is desired, the highest frequency of interest should be taken to be less than $1/10\Delta t$ where all aliasing modes are negligible compared to the fundamental.

3.7.4c Lag Windows. During the computation of the noise parameters, all samples taken farther than a time interval $q\Delta t$ apart are assumed to be completely uncorrelated. Power spectral densities under such as assumption may be written as

$$\tilde{S}(s) = \int_{-\infty}^{\infty} \sum_{n=-\infty}^{\infty} R(\tau)\, D_o(\tau)\delta(\tau - n\Delta t)e^{-s\tau}\, d\tau \quad , \tag{3.54}$$

where $D_o(\tau) \equiv 1$ for $|\tau| < q\Delta t$,

$\equiv 0$, otherwise,

$D_o(\tau)$ is called the lag window (Fig. 3.10).

By the convolution theorem

$$\tilde{S}(s) = \int_{-\infty}^{\infty} Q_o(f-\nu)S(\nu)\, d\nu \quad , \tag{3.55}$$

where $Q_o(f) = 2q\Delta t(\sin 2\pi f q\Delta t)$ approaches a delta function as $q\Delta t \to \infty$ and the introduction of the finite time correlation lag window constitutes an averaging process with $Q_o(f-\nu)$ as the weighting factor on the frequency spectrum. Unfortunately, this function has positive and negative peaks of appreciable magnitudes compared to the main peak at $f = \nu$ and these undesirable characteristics make it difficult to relate $\tilde{S}(s)$ to $S(s)$.

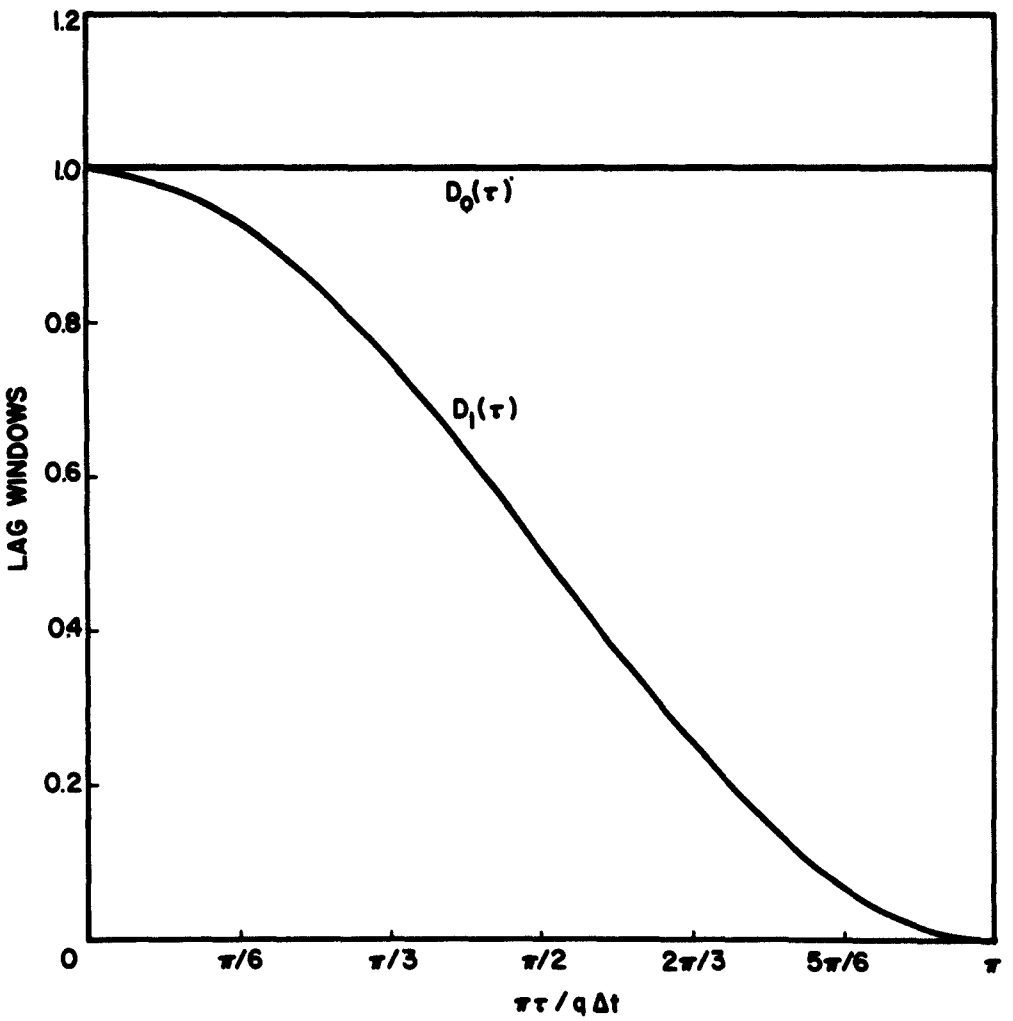

FIG. 3.10 LAG WINDOWS $D_0(\tau) = 1$, $\tau \leq q\Delta t$; $D_0(\tau) = 0$, $\tau > q\Delta t$; $D_1(\tau) = 1/2\ (1 + \cos \pi\tau/q\Delta t)$.

In this analysis a new lag window $D_1(\tau) = 1/2\ [1 + \cos \pi\tau/q\Delta t]$ is selected which has the Fourier transform

$$Q_1(f) = \frac{1}{4}\left[Q_o\left(f + \frac{1}{2q\Delta t}\right) + Q_o\left(f - \frac{1}{2q\Delta t}\right)\right] + \frac{1}{2}\,Q_o(f) \quad .$$

As illustrated in Fig. 3.11, the side loops drop off much more rapidly than those of the $Q_o(f)$.

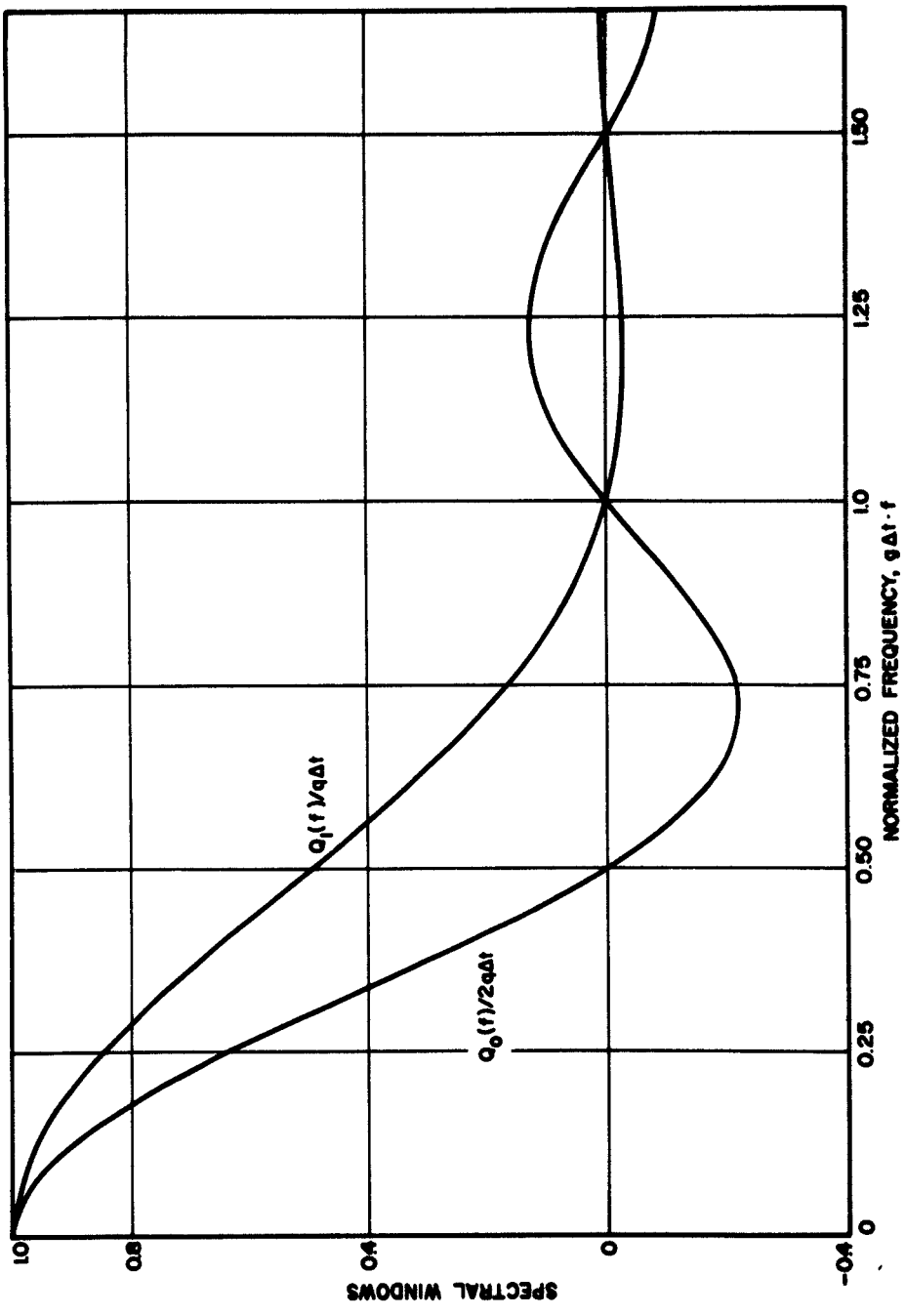

FIG. 3.11 SPECTRAL WINDOW VS. NORMALIZED FREQUENCIES.

CHAPTER IV. RESULTS AND INTERPRETATIONS OF THE DENSITY FUNCTION CALCULATIONS

4.1 Introduction

In this chapter, the results of the noise transport analysis of a discrete beam two-dimensional space-charge-limited diode by means of the density function method are presented. Correlations between the transport phenomena and the coupling mechanism are sought. A comparison is made between the a-c coupling term employed in the two-dimensional density function calculations and the one-dimensional a-c coupling term resulting from the open-circuit assumption.

Calculations are performed for three discrete values of the frequency parameter a = 0.25, 0.5 and 1.0, corresponding to 2 Gc, 4 Gc and 8 Gc respectively. Equivalent noise parameters Ψ, Φ, Π, S and F_{min} for the transmitted flows are evaluated at eight planes located at

$$z_1/z_m = 0.009 ,$$
$$z_2/z_m = 0.25 ,$$
$$z_3/z_m = 0.75 ,$$
$$z_4/z_m = 1.05 ,$$
$$z_5/z_m = 1.95 ,$$
$$z_6/z_m = 3.5 ,$$
$$z_7/z_m = 10.5 ,$$
$$z_8/z_m = 30.5 ,$$

where z_m is the average distance between the cathode and the potential minima of beam layers Nos. 2 and 4, $z_m = 6 \times 10^{-6}$ m. Because of the

multivelocity nature of the electron beam, especially in the vicinity of the potential minimum, the meaning of the equivalent noise parameters must be interpreted with great care. According to the noise theory by Haus, the noise parameters were originally defined for single-velocity one-dimensional electron beams. The noise parameters presented in this chapter are actually the equivalent noise parameters evaluated after the electron beam is suddenly accelerated to a very high velocity. In the retarding field region between the cathode and the potential minimum where reflected flows exist, the real physical meaning of the noise parameters corresponding to the transmitted flow is not clearly established and neither are these quantities physically measurable. However, they may still serve to give some indication of the noise transport characteristics of the electron beam.

It takes approximately 82 minutes of computing time on an IBM 7090 computer to complete the calculations for each selected value of the frequency parameter. No attempt has been made to refine the calculation for better accuracy.

4.2 Noise Parameters

Normalized noise parameters for the entire beam are plotted against the normalized distance from the cathode for the three chosen frequencies. At the cathode plane,

$$S(0) = Y(0) = \Phi(0) = 1.0$$

$$\Pi(0) = \Lambda(0) = 0$$

according to the initial conditions and the minimum noise figure is 6.96 db corresponding to full thermionic-emission shot noise.

Little variation in noise transport characteristics is observed from layer to layer of the electron beam. As will be pointed out in Section 4.3, the coupling a-c electric field decays too rapidly in the transverse direction to bring forth any significant two-dimensional effects.

4.2.1 Self-Power Spectral Density (SPSD). The normalized self-power spectral density Ψ of the convection current density fluctuations and the normalized self-power spectral density Φ of the kinetic potential are shown as functions of normalized distance from the cathode in Figs. 4.1 and 4.2 respectively. Spatial variations are observed for both Ψ and Φ for all frequencies. In the low potential region, the spatial variations of Ψ and Φ appear to be in quadrature, in agreement with the transmission-line analog of electron beams. In addition, the wavelengths of the spatial variations are inversely proportional to frequency. For a = 1.0, equivalent to 8.23 Gc, a full wavelength is measured to be approximately 24×10^{-6} meter. The velocity v may be evaluated from

$$\begin{aligned} v &= f\lambda \\ &= 8.23 \times 10^{-9} \times 24 \times 10^{-6} \\ &= 1.9752 \times 10^{5} \text{ m/sec.} \end{aligned}$$

This turns out to be the average velocity of electrons in the vicinity of the potential minimum of the diode. Large amplitude variations of Ψ are observed; in fact, the convection current density fluctuations tend to dominate the noise characteristics of the electron beam as evidenced by the following discussion. The basic noise reduction mechanism, namely, the fluctuating potential minimum effect, is not found. The spatial variation of the fluctuations seems to have come from some beating-wave effects instead.

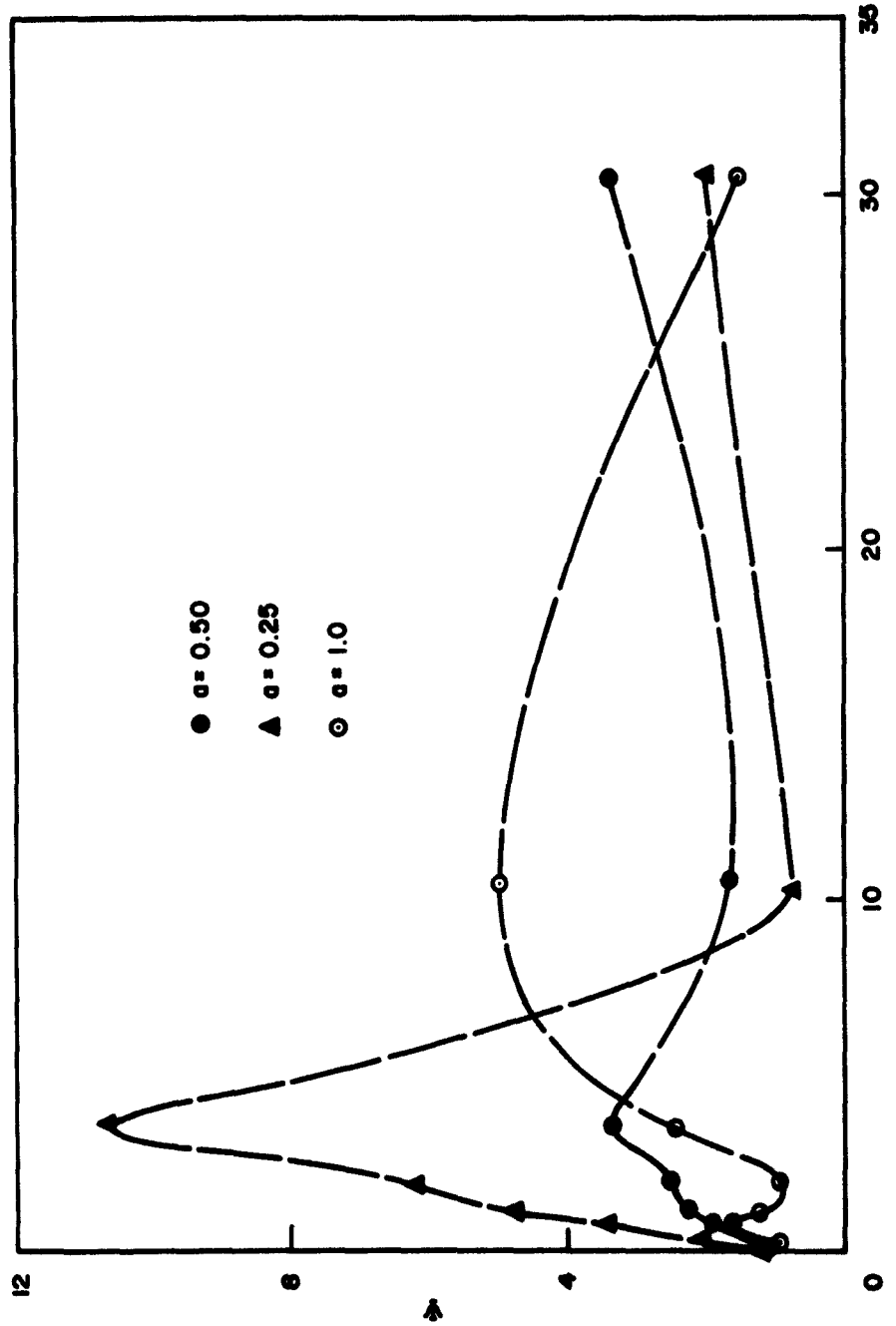

FIG. 4.1 NORMALIZED SELF-POWER SPECTRAL DENSITY OF CONVECTION CURRENT DENSITY FLUCTUATIONS VS. NORMALIZED DISTANCE FROM THE CATHODE.

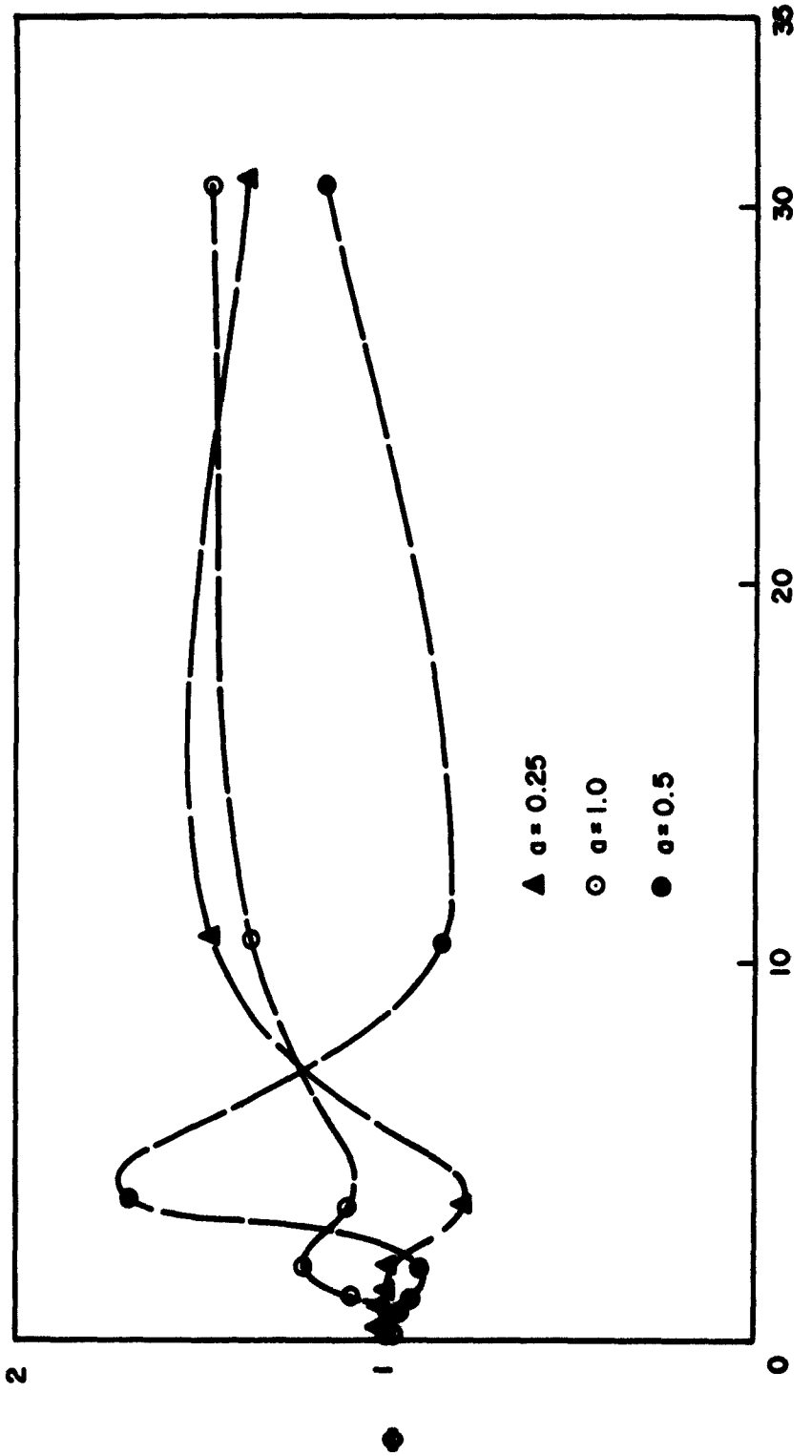

FIG. 4.2 NORMALIZED SELF-POWER SPECTRAL DENSITY OF KINETIC POTENTIAL VS. NORMALIZED DISTANCE FROM THE CATHODE.

4.2.2 Noise Parameters S and Π. In Fig. 4.3, normalized noise parameters S and Π are shown as functions of normalized distance from the cathode with frequency as a parameter. Because of the dominating role played by the convection current density fluctuations, both S and Π seem to have a similar spatial variation as Ψ. As a result, the sum S+Π is far from invariant with respect to distance, contrary to the one-dimensional linear multivelocity electron beam noise theory which predicts an invariance of S+Π for electron beams with a half-Maxwellian velocity distribution. It must be pointed out that the velocity distribution in a two-dimensional diode is no longer half-Maxwellian when the space-charge potential depression effects are taken into account. Beyond the multi-velocity region little change in Π takes place and the kinetic power remains slightly negative.

The ratio of Π and S for the three frequencies are shown in Fig. 4.4 as a function of normalized distance. Unlike the results from the Monte Carlo calculations presented in the next chapter, the absolute value of Π/S remains less than 0.2 most of the time.

4.2.3 Theoretical Minimum Noise Figure in a Two-Dimensional Diode. The equivalent minimum noise figures F_{min} computed in terms of the noise parameters S and Π are shown in Fig. 4.5 as a function of normalized distance. Little or no reduction from thermionic emission shot noise is observed across the two-dimensional diode. At 2 Gc ($a = 0.25$) the small increase of noise figure near the anode is probably due to small errors accumulated in the process of numerical integration. The second derivative term of the Taylor's series employed in the numerical step-by-step forward integration process is found to be quite influential beyond $z/z_m = 10.5$ for low frequencies. The minimum noise

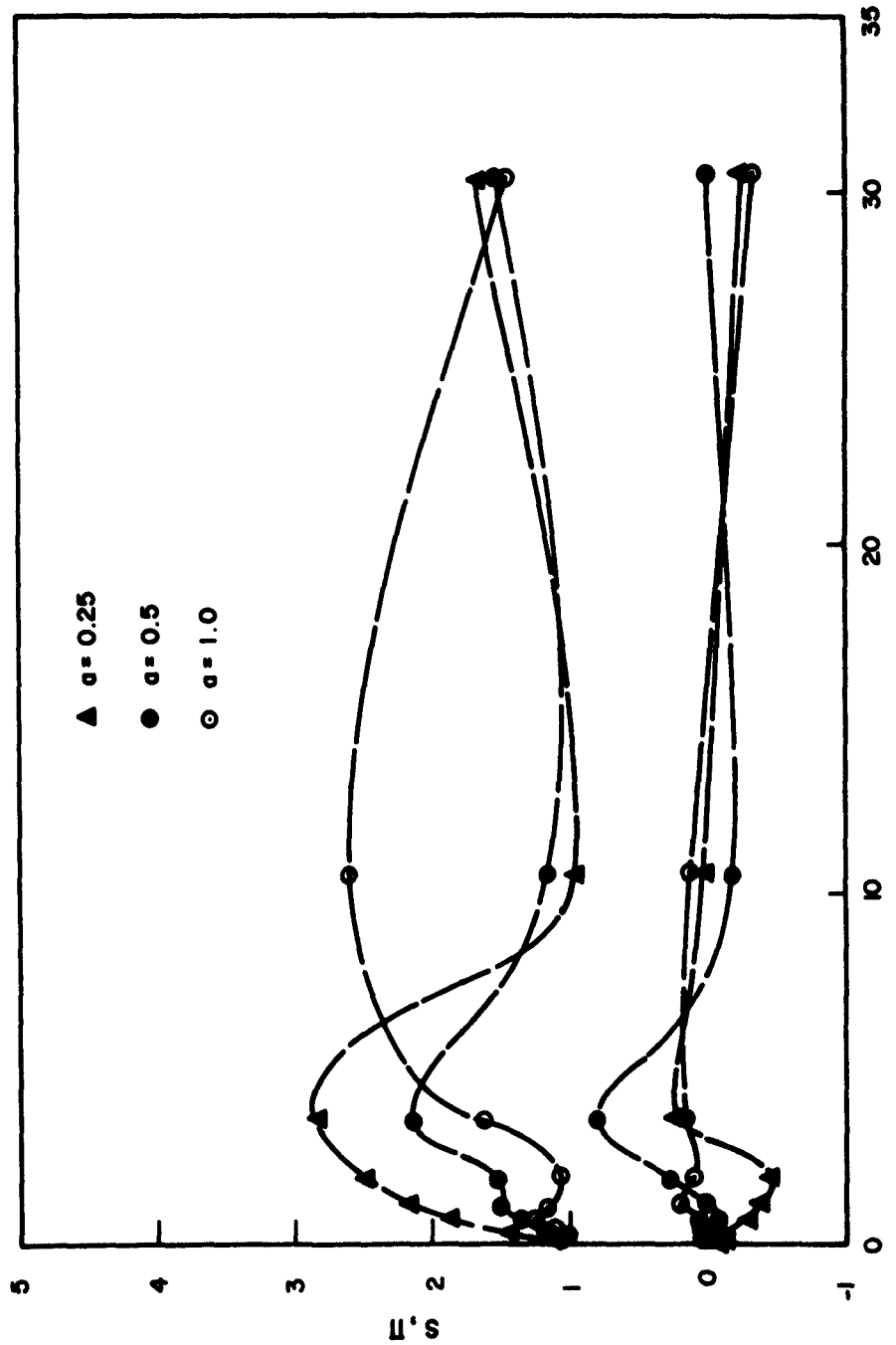

FIG. 4.3 NORMALIZED NOISE PARAMETERS S AND Π VS. NORMALIZED DISTANCE FROM THE CATHODE.

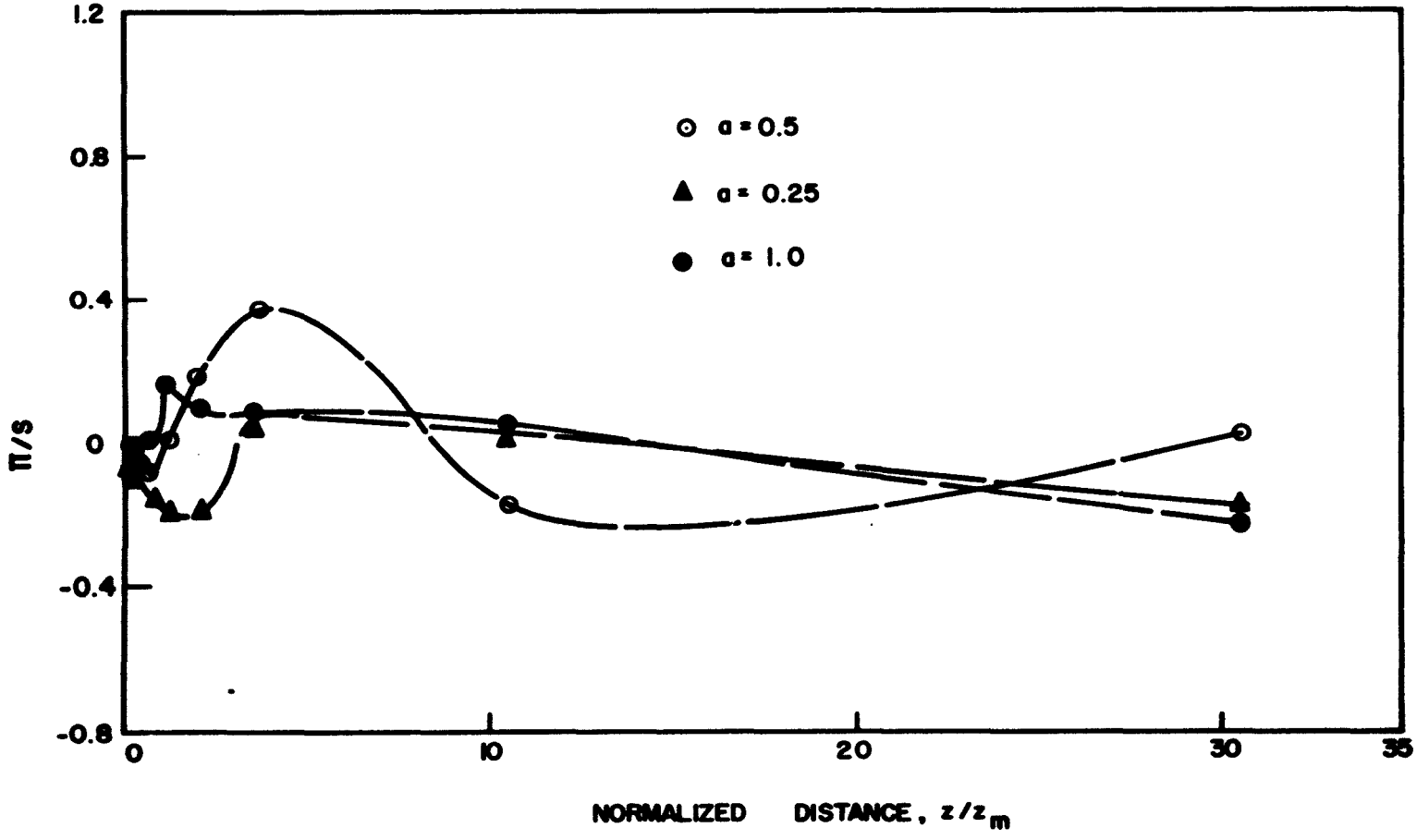

FIG. 4.4 RATIO OF Π/S VS. NORMALIZED DISTANCE FROM THE CATHODE.

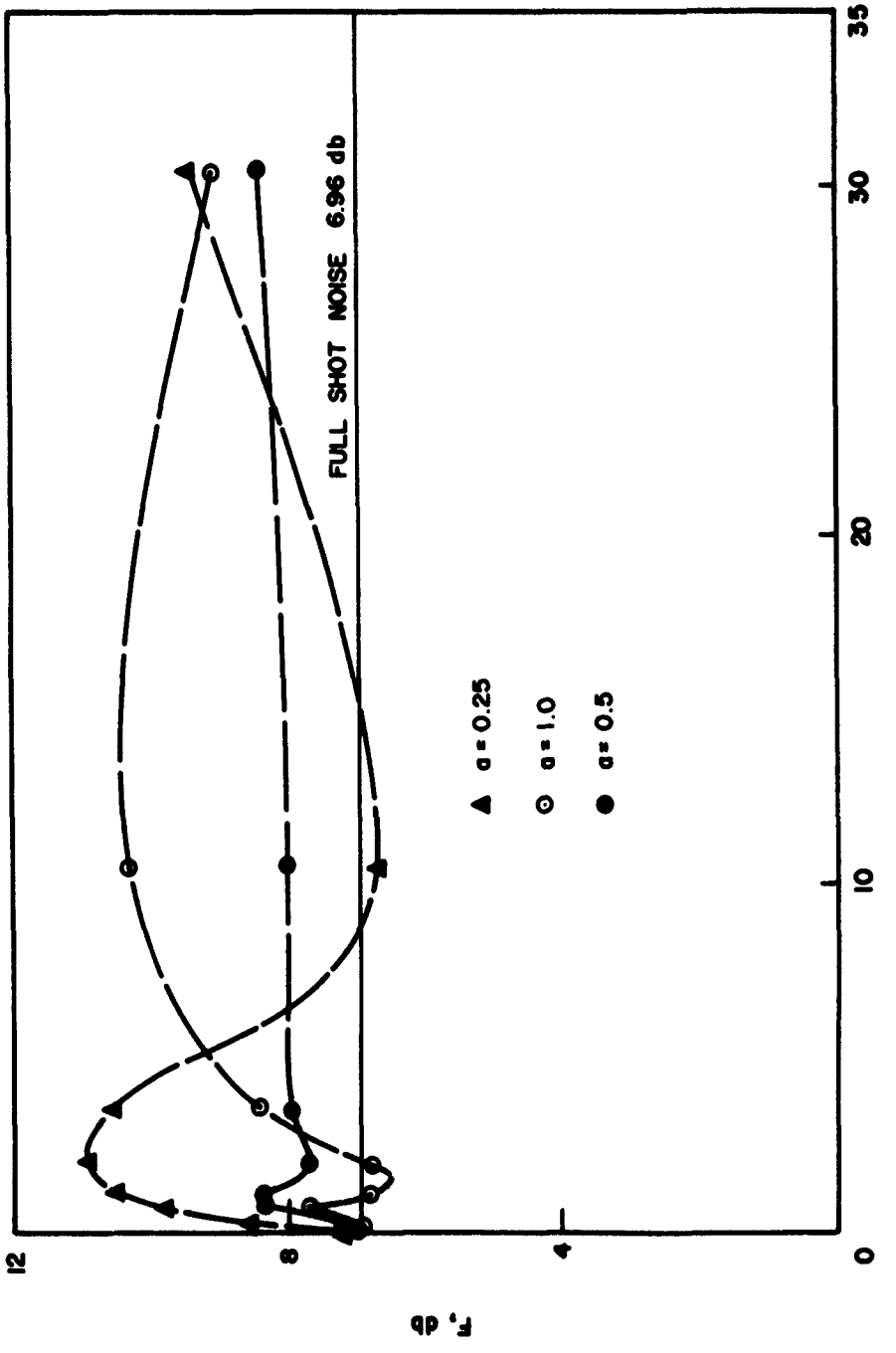

FIG. 4.5 THEORETICAL MINIMUM NOISE FIGURE VS. NORMALIZED DISTANCE FROM THE CATHODE.

figure versus normalized distance curves also take on a similar shape as the convection current density fluctuation curves.

In Fig. 4.6, the minimum noise figure is presented as a function of frequency at three z-planes, located at $z/z_m = 1.05$, $z/z_m = 10.5$ and $z/z_m = 30.5$, the anode plane. At the anode of the two-dimensional diode, a general deterioration of noise performance from 1.5 db to 2.5 db is observed.

4.3 The Two-Dimensional Coupling Mechanism

After the density calculation results are reviewed, an attempt is made to correlate the two-dimensional electron beam noise transport characteristics with the coupling mechanism. From Eq. A.9, the z-directed a-c electric field at (y,z) induced by a current sheet at (y',z) is

$$E_{1z}(y,z) = \frac{e}{2j\omega\epsilon_o} \int_{-\infty}^{\infty} \int_{-\infty}^{\infty} \beta' \dot{z}' \, F_1(y',z,\dot{z}') \, e^{-\beta'|y-y'|} \, dy' \, d\dot{z}' \quad , \quad (A.9)$$

where $\beta' = |\omega/\dot{z}|$.

In the one-dimensional noise transport analysis, the coupling z-directed a-c electric field based on the open-circuit assumption may be expressed as follows:

$$E_{1z}(\text{ONE-D}) = \frac{e}{j\omega\epsilon_o} \int_{-\infty}^{\infty} F_1(z,\dot{z}) \, \dot{z} \, d\dot{z} \quad . \quad (4.1)$$

A comparison of the two expressions shows that the two-dimensional induced a-c electric field depends not only on the convection current density of the original disturbance, but it also varies inversely as the velocity of the moving electrons. Fluctuations associated with slow electrons are given more weight in the a-c coupling, equivalent to an

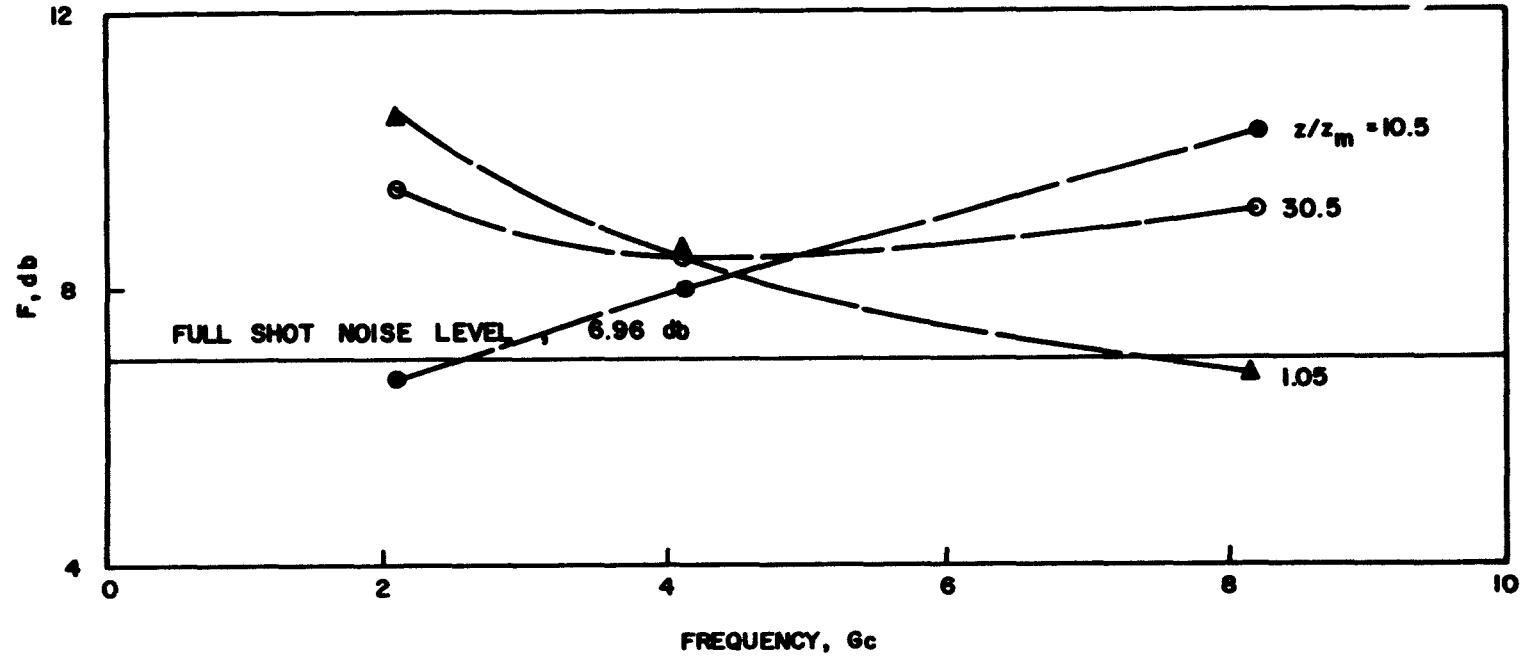

FIG. 4.6 THEORETICAL MINIMUM NOISE FIGURE VS. FREQUENCY.

effective alteration of the d-c distribution function in the velocity domain. A net reduction of the kinetic power carried by the electron beam will therefore result, causing deterioration in the noise characteristics of the electron beam.

The optimum ratio of the two-dimensional a-c electric field to the one-dimensional a-c electric field is, for $y \neq y'$,

$$\frac{E_{1z}}{E_{1z}(\text{ONE-D})} = \frac{1}{2} \frac{\omega \Delta y}{\dot{z}} e^{-\frac{\omega}{\dot{z}'} \Delta y} \tag{4.2}$$

and

$$\left.\frac{E_{1z}}{E_{1z}(\text{ONE-D})}\right|_{\max} = \frac{1}{2} e^{-1} = \frac{1}{5.436} \quad . \tag{4.3}$$

A conclusion may be reached based on Eq. 4.3 that the coupling between beam layers is weak. The rapid decay of the a-c coupling fields in the transverse direction prevents significant interactions between beam layers. In the density function calculations of noise transport in a two-dimensional diode, the lack of reduction in shot noise may be explained on the basis of the coupling mechanism employed.

CHAPTER V. RESULTS AND INTERPRETATIONS OF THE MONTE CARLO CALCULATIONS

5.1 Introduction

In the following sections the results pertaining to the noise transport characteristics of a two-dimensional discrete-layer space-charge-limited diode obtained by means of the Monte Carlo technique are presented. Special attention is devoted to the interpretation and the evaluation of the data. An attempt is made to correlate the noise transport and reduction phenomena observed with the physical properties of the electron beam under various conditions. Previous results from the analyses employing one-dimensional diodes of similar d-c configurations are often brought forth for the purpose of comparison so that the multi-dimensional space-charge effects may be revealed.

Before the results are reviewed, it is necessary to point out that the accuracy of the Monte Carlo method depends heavily on the equivalent size of the sample selected. In the present calculation, sample collection is carried out for a period of two thousand time intervals, Δt, after a quasi-stationary condition is established inside the diode. The total length of the collection period together with the maximum allowable time lag q would serve to determine the quality of the estimates made. If Gaussian error is assumed, for $q = 125$, the frequency resolution is 4 Gc and the equivalent size of the sample corresponds to a X-square distribution of 32 degrees of freedom. The confidence interval of the estimated spectra is, according to Fig. 5.1, $\pm$ 32 percent at 80 percent probability. In other words, the estimated spectra fall within $\pm$ 32

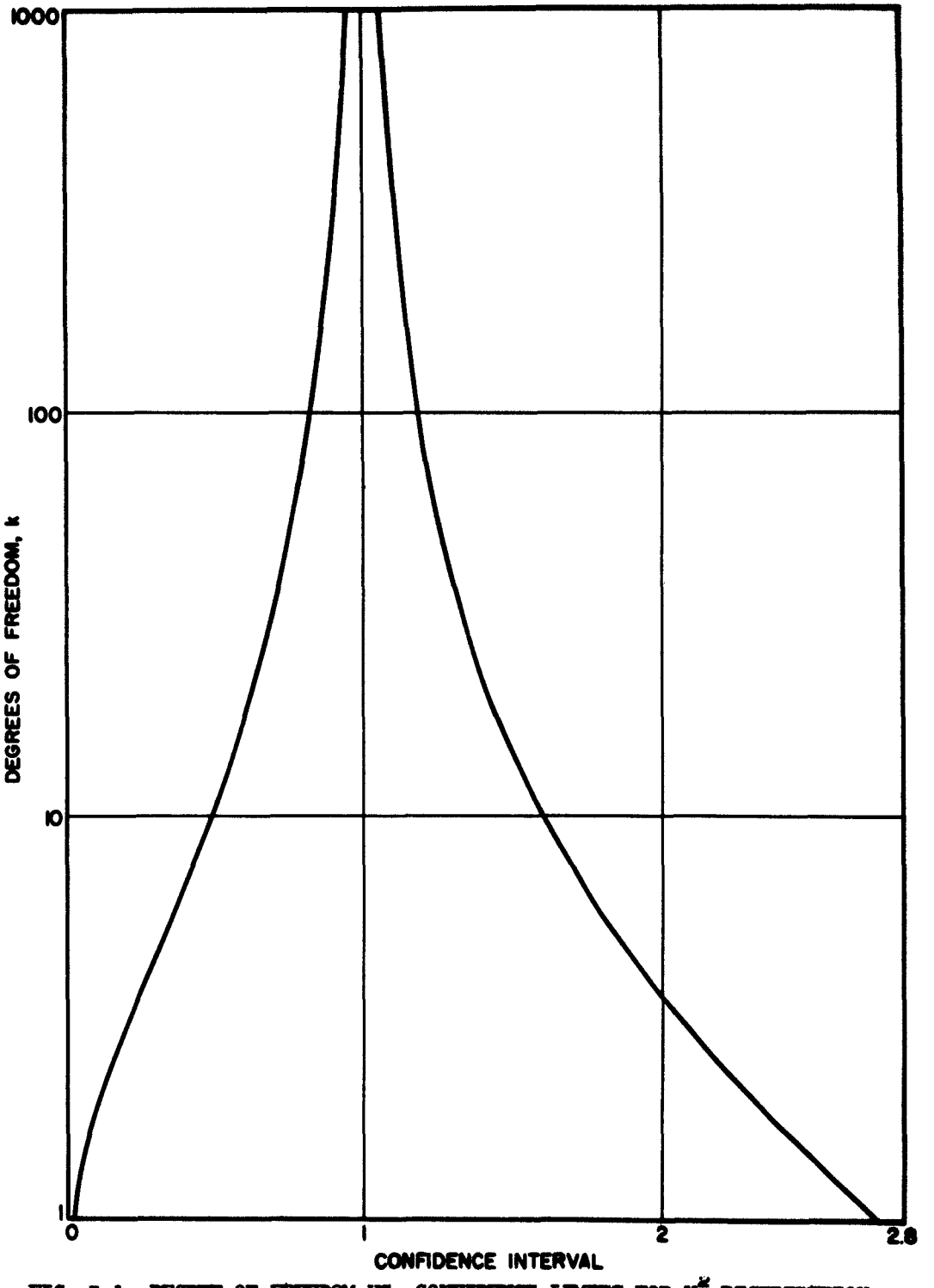

FIG. 5.1 DEGREE OF FREEDOM VS. CONFIDENCE LIMITS FOR X^{2} DISTRIBUTION, 80 PERCENT PROBABILITY.

percent of the true spectra 80 percent of the time disregarding errors introduced by the nonstatistical approximations.

From the same figure it is shown that the confidence interval may be reduced to ± 20 percent with 81 degrees of freedom in the X-square distribution, corresponding to five thousand time intervals. The slow improvement of the quality of the estimates and the expense involved in the lengthy computations limit the accuracy obtainable by this statistical method of noise transport analysis.

All the noise parameters Ψ, Φ, Π, Λ and S in the frequency domain are presented in normalized lag window average forms as described in Eqs. 3.39 through 3.44. Spectral estimations are made at discrete frequencies from 0 Gc to 40 Gc at 2 Gc intervals. Because of the 4 Gc frequency resolution, no additional information may be obtained if the spectral densities are evaluated at frequencies less than 2 Gc apart.

Following the one-dimensional diode model employed by Tien and Moshman, the temperature ratio T_c/T is taken to be 3.96, equivalent to a theoretical minimum noise figure of 6.96 db at the cathode plane. Limitation in computing time prevents numerical evaluation of the noise parameters at the cathode. However, since the random numbers employed in the mathematical model are statistically checked beforehand, there is no reason to doubt the behavior of the noise parameters at the plane of emission. From the initial conditions at the cathode, the fluctuations in kinetic potential and current are uncorrelated at emission which leads to

$$\Psi(\Omega,0) = \Phi(\Omega,0) = S(\Omega,0) = 1$$

$$\Pi(\Omega,0) = \Lambda(\Omega,0) = 0 \ . \qquad (5.1)$$

Noise parameters are computed for four z-planes located at

$$z_1/z_m = 1.5$$

$$z_2/z_m = 3.5$$

$$z_3/z_m = 10.5$$

$$z_4/z_m = 30.5 \quad , \tag{5.2}$$

where z_m is the average distance between the cathode and the potential minima of layers, Nos. 2 and 4.

$$z_m = 6 \times 10^{-6} \text{ meter} \quad .$$

Due to the variations in distance between the cathode and the potential minima, spectra at the first z-plane ($z/z_m = 1.5$) for different beam layers should be viewed separately to avoid unnecessary confusion. At the first z-plane, the effective z/z_{min} changes from layer to layer.

As pointed out in Chapter II, the noise parameters are originally defined for small-signal one-dimensional electron beams with no velocity spread. At the first two z-planes where the multivelocity nature of the electron beam prevails, the results presented are actually the noise parameters evaluated after the electron beam is given a sudden acceleration to reduce the velocity spread to the mean velocity ratio. As was shown previously, both the current fluctuations and the kinetic potential in an electron beam are continuous over a sudden change in d-c potential.

Due to the rapid change in potential gradient in the vicinity of the cathode, it is necessary to reduce the basic time interval for numerical integration steps to 4×10^{-13} seconds for the electrons inside the first compartment of each of the beam layers. For the two thousand time intervals the average convection current density measured at the

anode plane agrees with the computed current density corresponding to the average potential minima of the layers to within five percent. Because of the half-Maxwellian velocity distribution of the electrons any fluctuation of the potential minima about their respective averages tends to increase the number of electrons crossing slightly beyond the value corresponding to the average potential minima. The five percent discrepancy indicated is not considered to be very significant due to the short time average employed in the estimation of the average potential profile.

5.2 The Two-Dimensional Potential Distribution

Both the space-charge distribution and the potential profile of the two-dimensional space-charge-limited diode are shown compared with their respective one-dimensional predictions in Figs. 5.2 and 5.3. A great deal of similarity is found between the curves for the center layer of the two-dimensional model and their one-dimensional counterparts. However, an appreciable amount of variation in both space-charge density and d-c potential are observed in the transverse direction, which causes a 30 percent difference in current density between the center layer and the edge layers.

As a direct result of the two-dimensional space-charge effect, certain discrepancies in d-c potential are found between neighboring layers at the same distance from the cathode. In the region beyond the potential minima, each layer has its own low velocity cutoff; in other words, additional velocity spread is effectively induced and the nonlinear region of the electron beam is greatly extended. At the four z-planes the average d-c potentials are -0.12 volts, +0.12 volts, 1.7 volts and 10 volts, respectively. The existence of the artificial multivelocity region is shown vital to noise reduction later in this chapter.

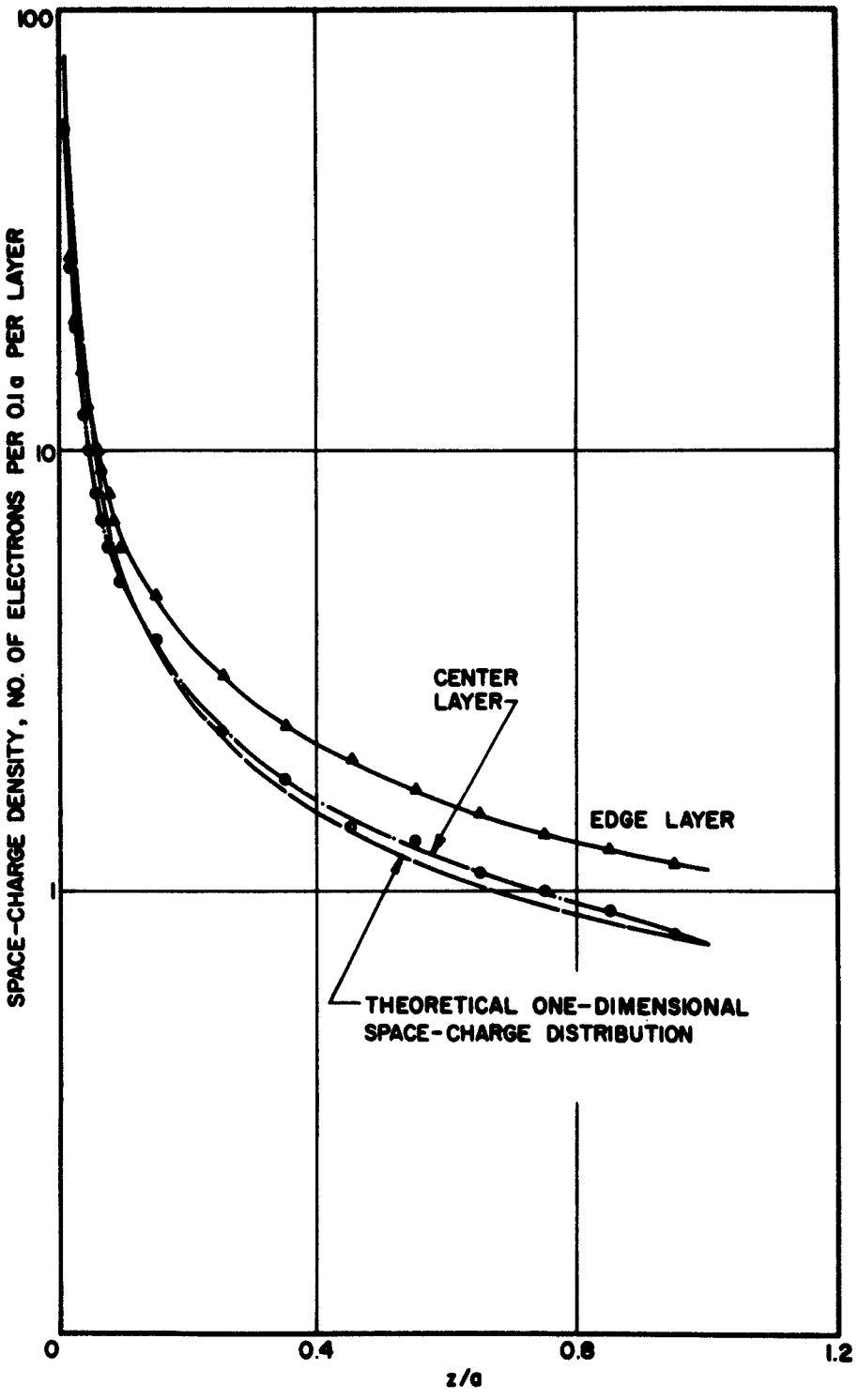

FIG. 5.2 AVERAGE SPACE-CHARGE DISTRIBUTION IN A TWO-DIMENSIONAL DIODE.

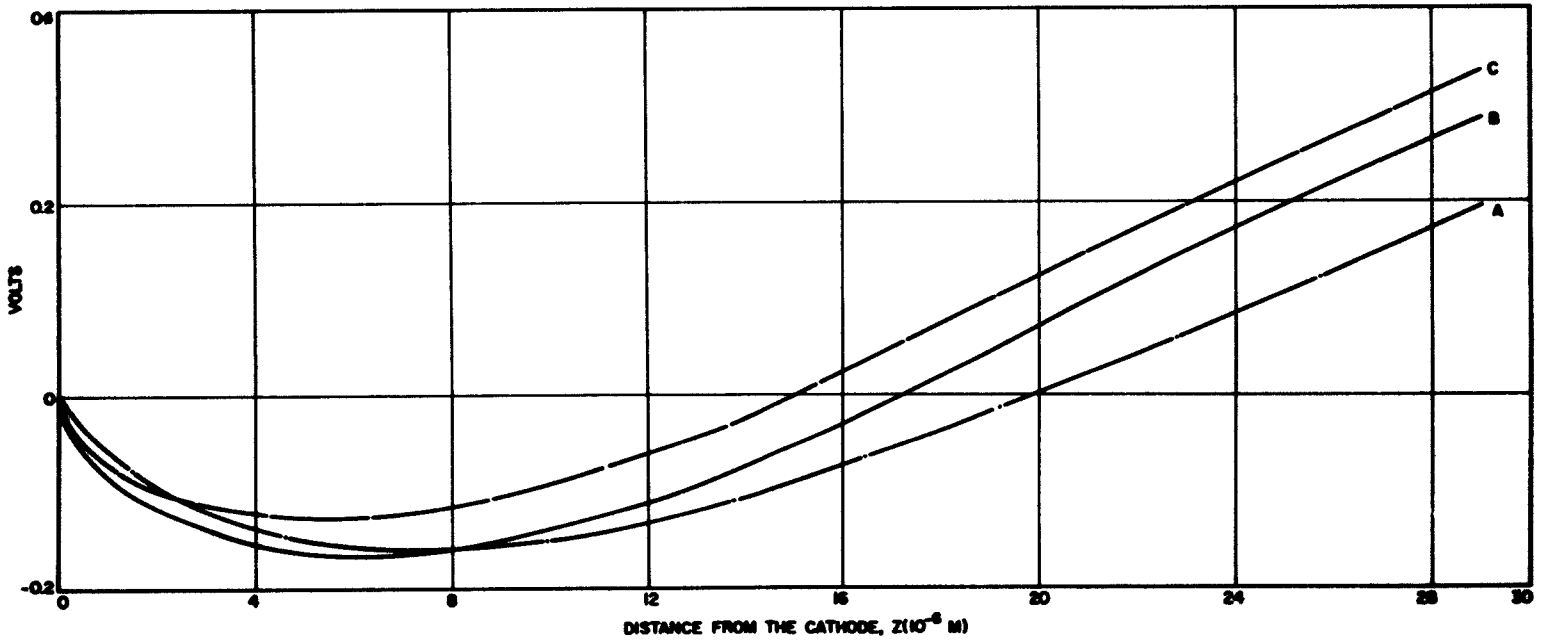

A. Langmuir's Potential Profile for a One-Dimensional Diode
B. Potential Profile at the Center Layer of the Electron Beam
C. Potential Profile at the Edge Layer of the Electron Beam

FIG. 5.3 POTENTIAL DISTRIBUTION IN A TWO-DIMENSIONAL SPACE-CHARGE-LIMITED DIODE.

5.3 Correlation Functions

Auto-correlation functions for both the kinetic potential and the current fluctuations in the time domain are displayed in Figs. 5.4 and 5.5. Appreciable deviations from the ideal delta function are observed. A certain amount of correlation has developed between fluctuations separated by short time intervals. From these two figures, negligible amounts of correlation between fluctuations are detected farther than 30 time intervals apart; therefore, the 125 Δt maximum time lag assumption seems to be justified.

5.4 Noise Parameters

Noise parameters are generally presented in two different forms. They are shown first as a function of frequency with the distance from the cathode as a parameter. In addition, they are plotted against distance for a selected number of discrete frequencies. Comparisons between noise parameters of individual beam layers and those of the whole electron beam are also made at the anode.

5.4.1 Self-Power Spectral Density (SPSD). The normalized self-power spectral density Φ of the kinetic potential is shown as a function of frequency and then as a function of normalized distance in Figs. 5.6 and 5.7, respectively. At the first z-plane, Φ is approximately unity as expected, in agreement with the theory that the gating action of the fluctuating potential minimum does not alter the velocity distribution of the electrons. Formation of the peak and the valley of 4 Gc and 8 Gc seems to have originated in the low potential region just beyond the potential minima and the causes of their existence are not yet known. Probably these points are outside of the confidence interval by chance as indicated at the beginning of this chapter.

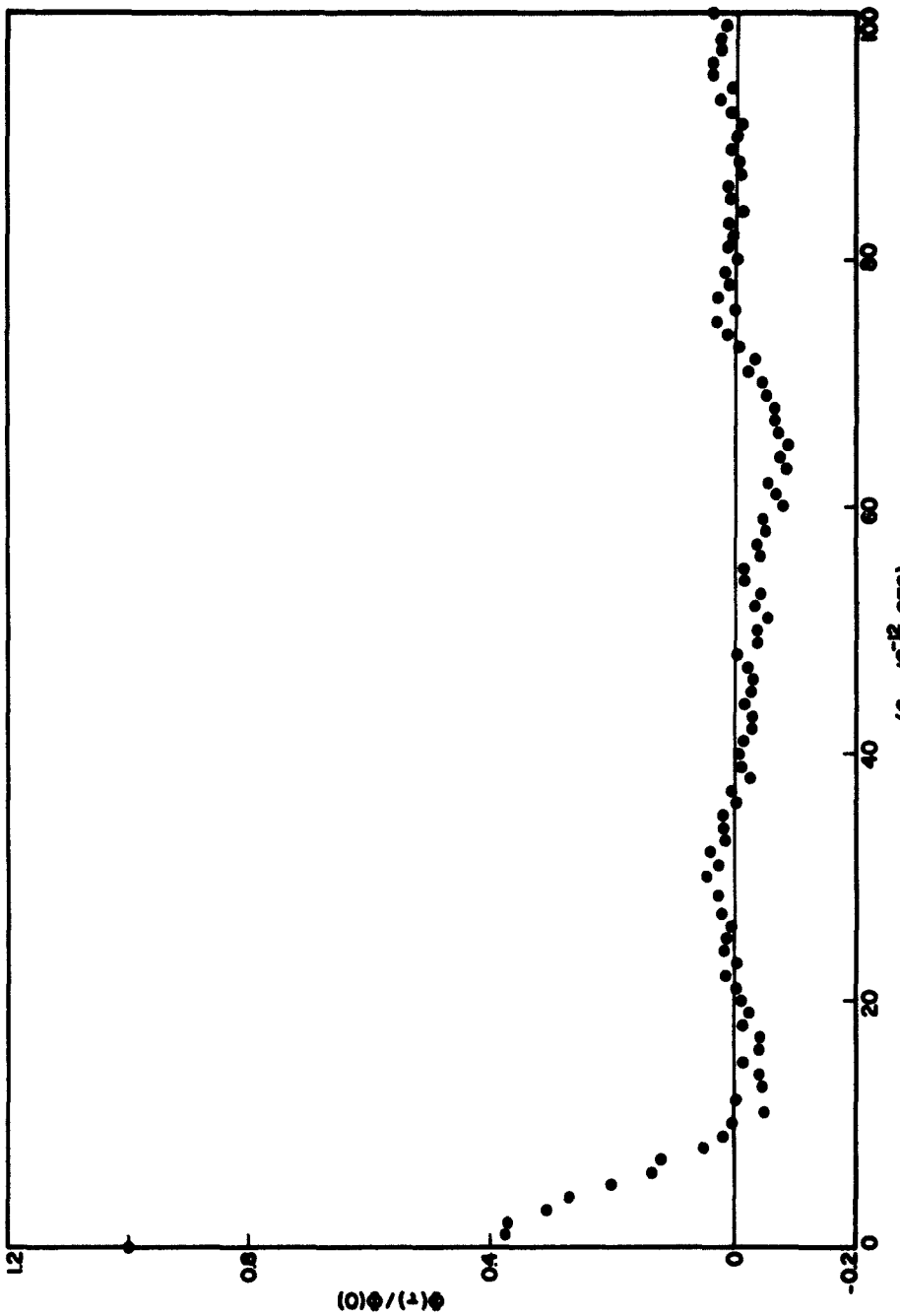

FIG. 5.4 NORMALIZED AUTO-CORRELATION FUNCTION FOR KINETIC POTENTIAL FLUCTUATIONS VS. TIME LAG AT THE ANODE PLANE.

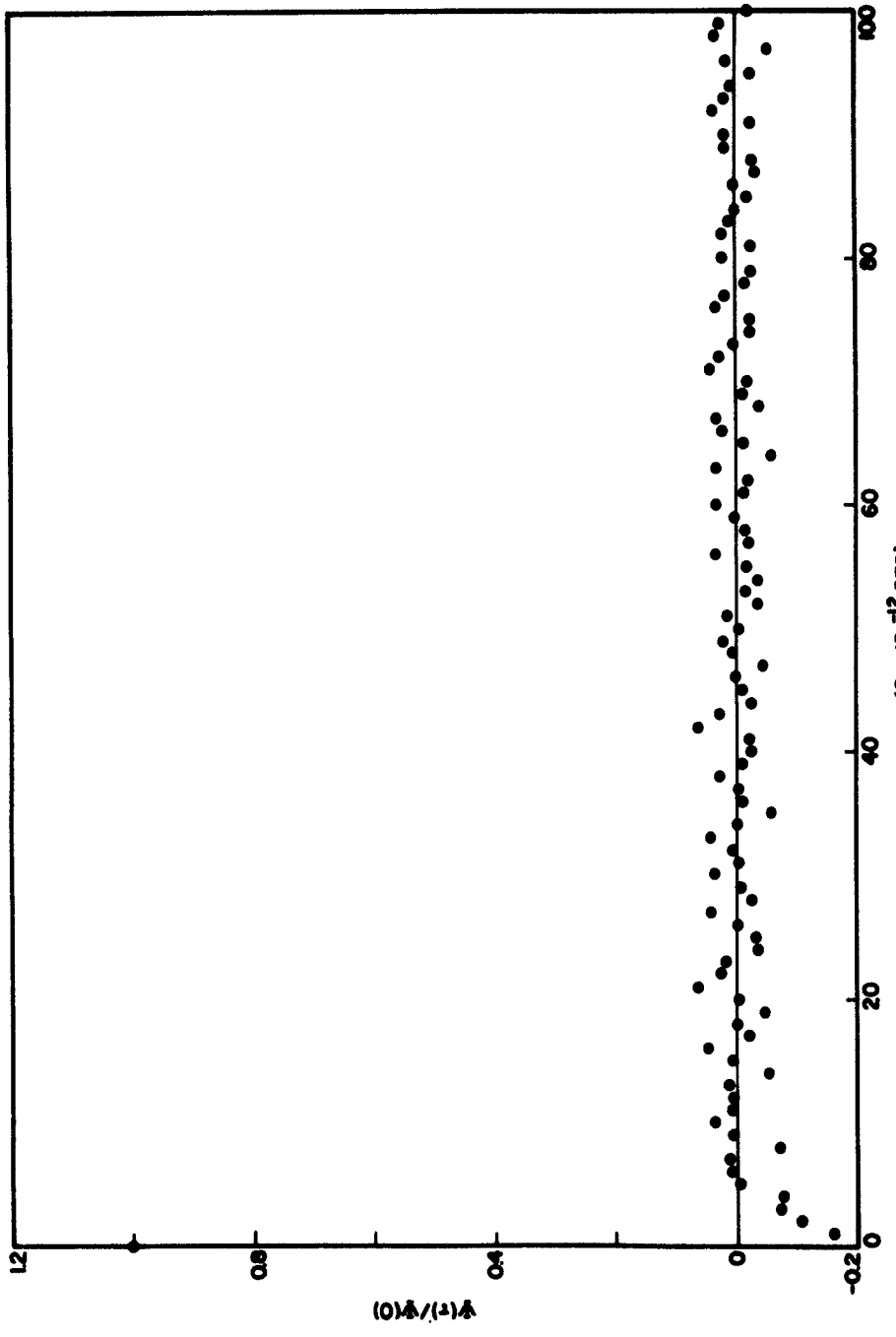

FIG. 5.5 NORMALIZED AUTO-CORRELATION FUNCTION FOR CURRENT FLUCTUATIONS VS. TIME LAG AT THE ANODE PLANE.

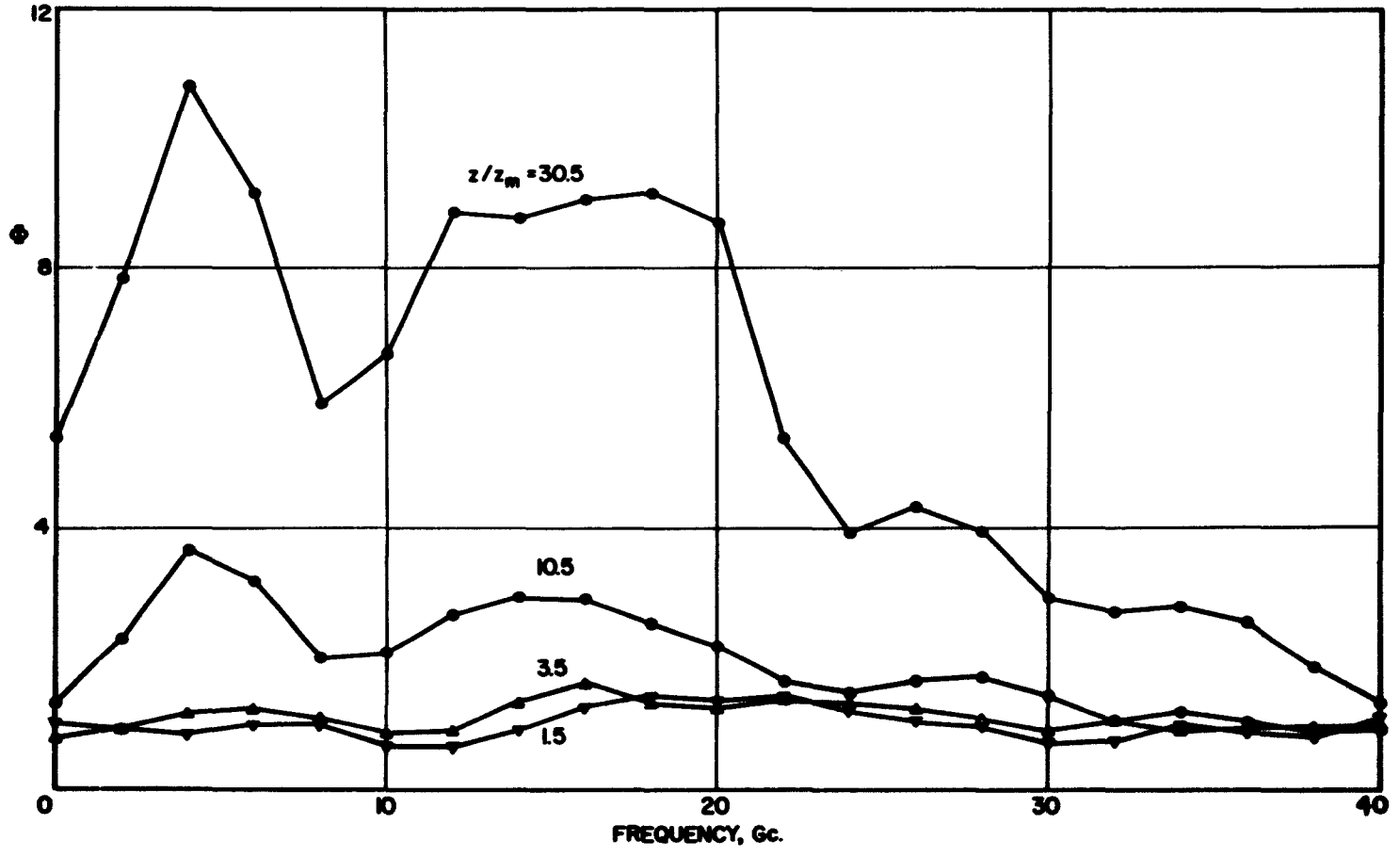

FIG. 5.6 NORMALIZED SELF-POWER SPECTRAL DENSITY OF KINETIC POTENTIAL VS. FREQUENCY (THE WHOLE BEAM).

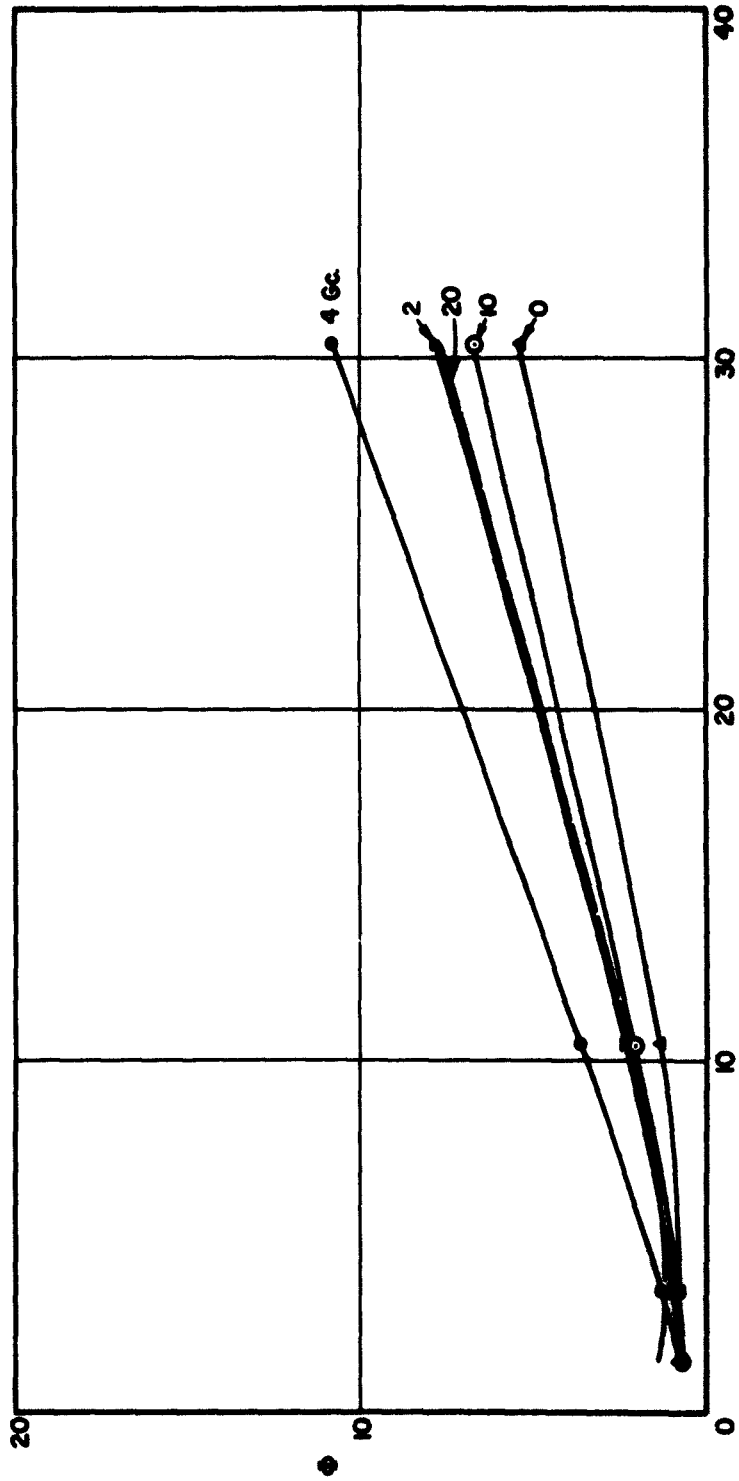

FIG. 5.7 NORMALIZED SELF-POWER SPECTRAL DENSITY OF KINETIC POTENTIAL VS. NORMALIZED DISTANCE FROM THE CATHODE.

The SPSD's of kinetic potential are found to be growing functions with respect to distance and d-c potential which is similar to the results obtained from the one-dimensional multivelocity beam analysis.

In a similar manner the normalized self-power spectral density Ψ of the current fluctuations is shown for the whole beam, the edge layer and the center layer as a function of frequency in Figs. 5.8, 5.9, 5.10 and 5.11, respectively. Also included are the respective shot noise reduction factors Γ^2 calculated by Tien and Moshman and by Dayem and Lambert. Since the SPSD of the kinetic potential is essentially unity in the vicinity of the potential minima, the normalized SPSD of the current fluctuations taken at $z/z_m = 1.5$ may be regarded equivalent to Γ^2. Results from the two-dimensional diode are found to be quite different from those obtained for either the open-circuit or the short-circuit one-dimensional diode except at the extremely high-frequency limit where there is little reduction in shot effect. No sharp rise and fall similar to Tien's dip is observed in the self-power density spectrum of current fluctuations. At the anode plane there is a substantial amount of reduction in current fluctuations below the full shot noise level up to 40 Gc which is at least ten times the electron plasma frequency corresponding to the electron concentration at the potential minimum of the center layer.

A comparison is made for the SPSD of the current fluctuations for the edge layer, the center layer and the whole beam at the anode plane. At low frequencies, a lesser amount of reduction in shot noise current takes place at the individual layers compared to the r-f current reduction in the whole beam. This phenomenon may be readily explained by recalling the a-c coupling mechanism described in Chapter III in which the a-c electric field is considered to be a function of the total a-c current.

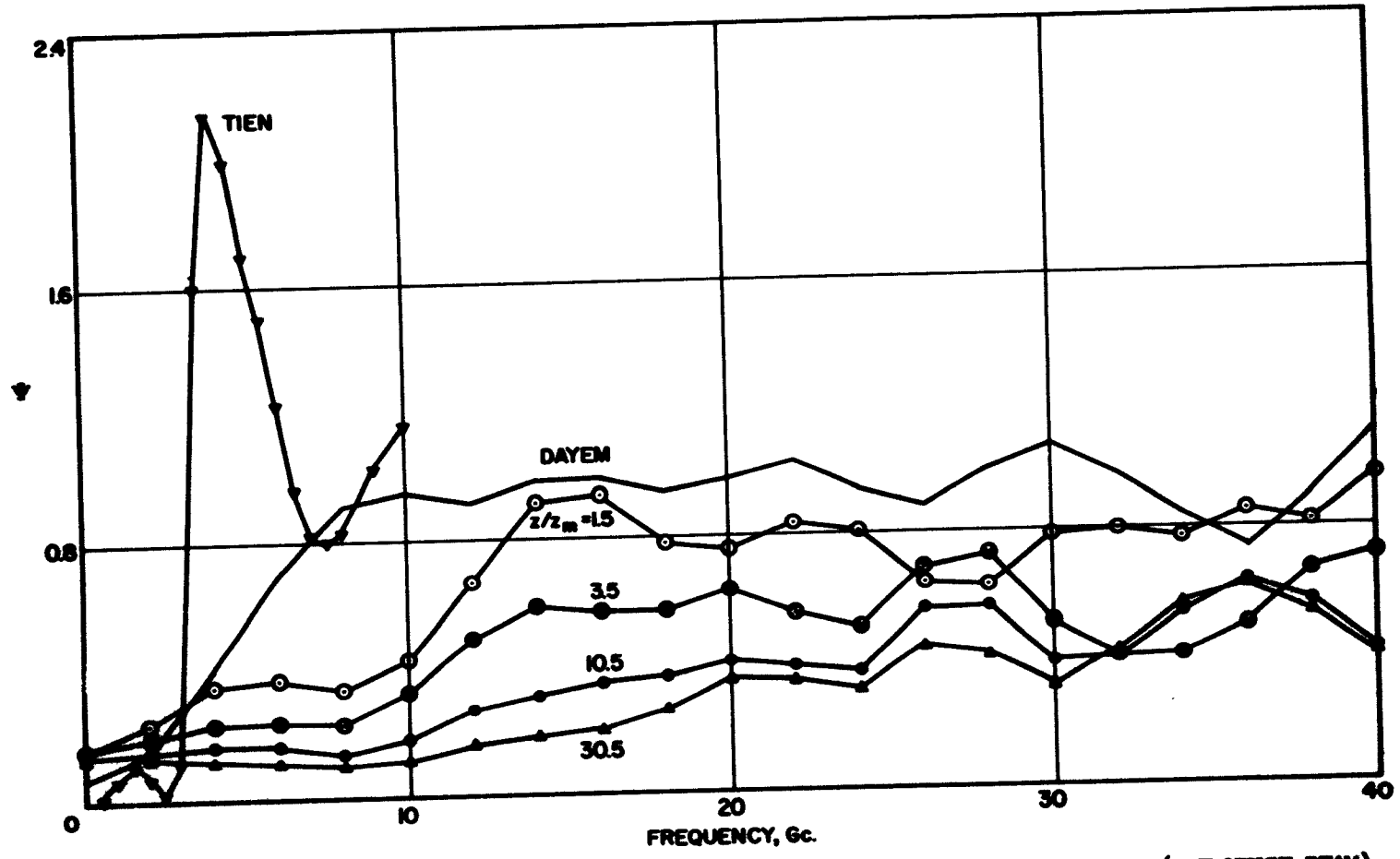

FIG. 5.8 NORMALIZED SELF-POWER SPECTRAL DENSITY OF CURRENT FLUCTUATIONS VS. FREQUENCY (THE WHOLE BEAM).

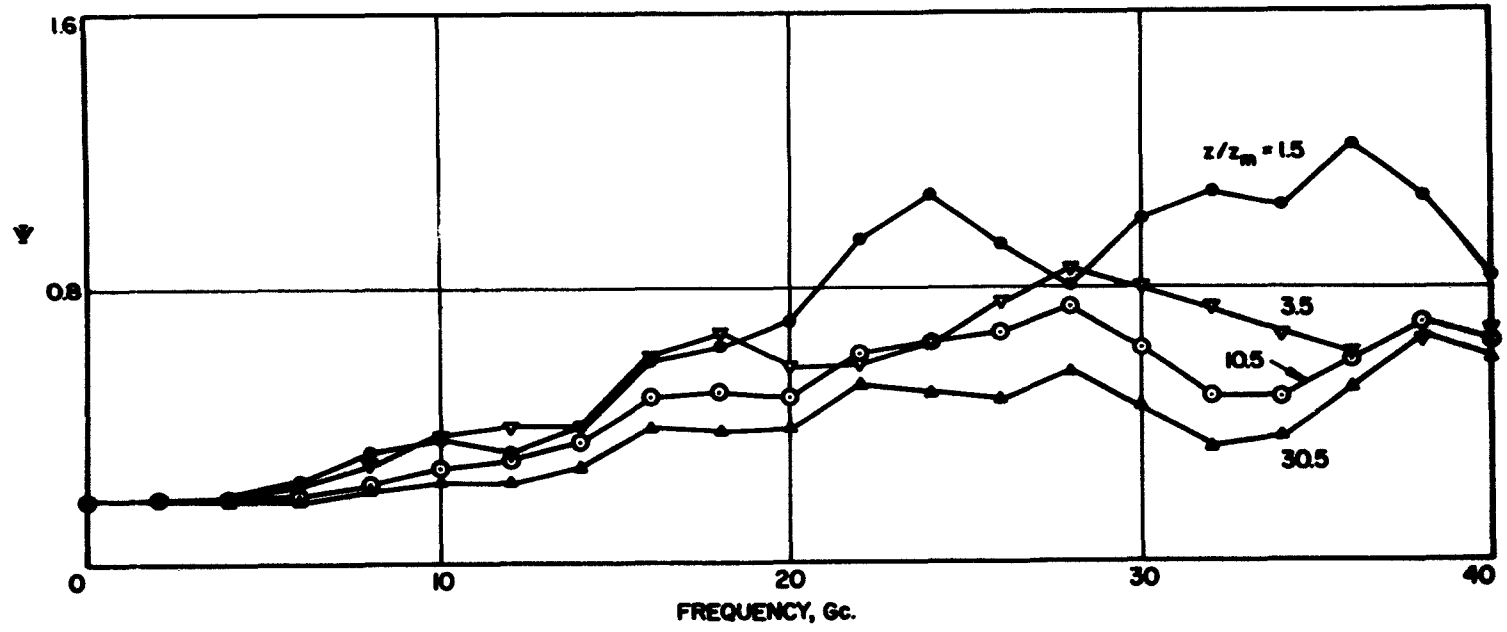

FIG. 5.9 NORMALIZED SEIF-POWER SPECTRAL DENSITY OF CURRENT FLUCTUATIONS VS. FREQUENCY (EDGE LAYER OF THE ELECTRON BEAM).

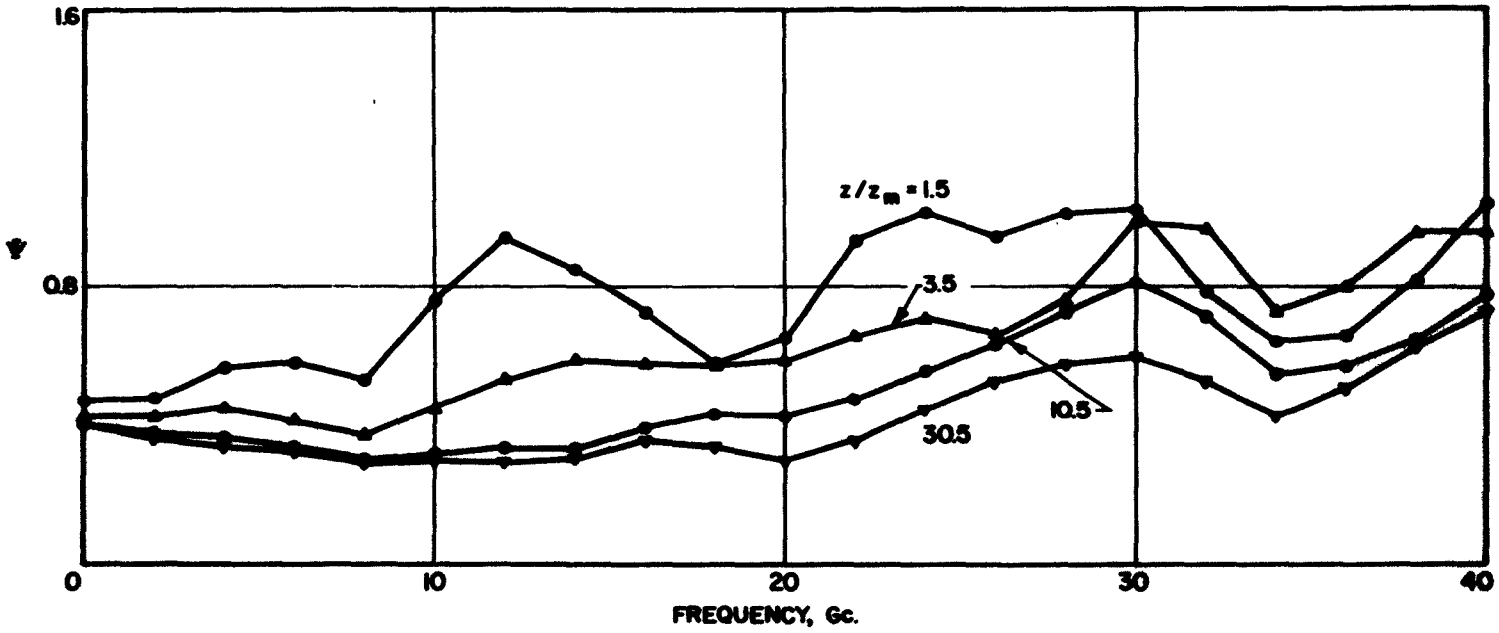

FIG. 5.10 NORMALIZED SELF-POWER SPECTRAL DENSITY OF CURRENT FLUCTUATIONS VS. FREQUENCY (CENTER LAYER OF THE ELECTRON BEAM).

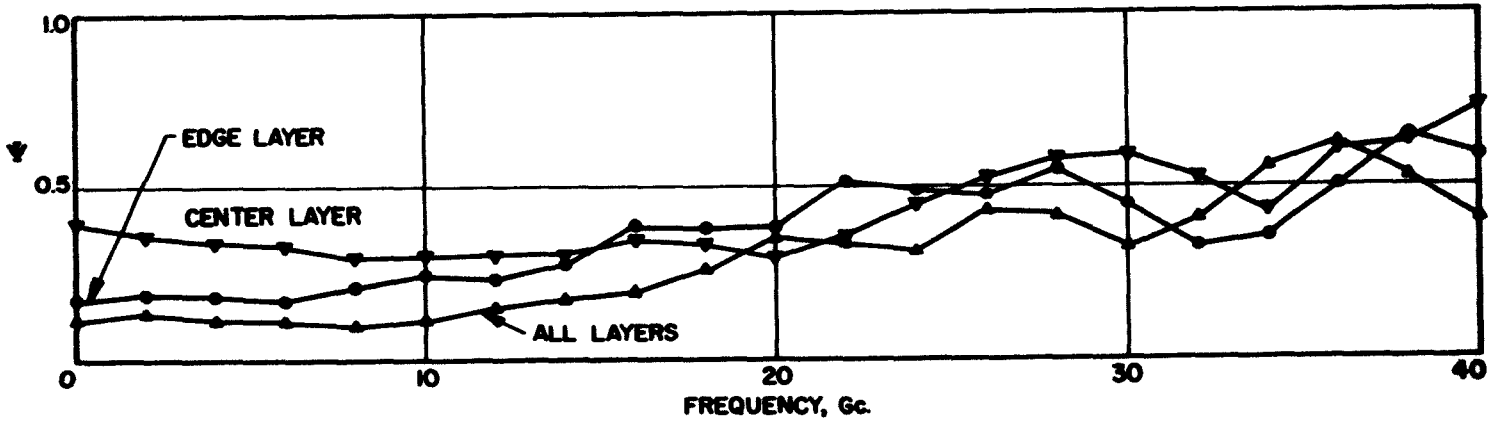

FIG. 5.11 NORMALIZED SELF-POWER SPECTRAL DENSITY OF CURRENT FLUCTUATIONS VS. FREQUENCY AT THE ANODE PLANE (THE WHOLE BEAM).

The normalized self-power spectral density of the current fluctuations in individual beam layers and the whole beam are presented as a function of normalized distance in Figs. 5.12 and 5.13. Very little reduction in noise current is found beyond the potential minimum at low frequencies. On the other hand the gating action of the potential minimum does not effectively cut down the high frequency component of the noise current which is in turn rapidly damped in the low potential multivelocity region. Beyond the 10.5 z_m plane, where the average potential reaches 1.7 volts, Ψ settles down and becomes independent of distance as predicted by the single velocity theory.

Similar to the results obtained by Dayem and Lambert, the reduction in current in the low potential region is accompanied by a rise in kinetic potential, contrary to the reduction mechanism offered by the gating motion of the potential minimum.

5.4.2 Cross-Power Spectral Density (CPSD). The real and the imaginary part of the cross-power spectral density between the kinetic potential and the current fluctuations are presented in Figs. 5.14 through 5.16, respectively. According to the postulated input conditions, both Π and Λ are equal to zero at the cathode plane. In the retarding-field region, hardly any correlations are developed between the two types of fluctuations as evident by the small values of Π and Λ at the first z-plane. Negative values for Π are observed at the low frequency end of the spectrum in the vicinity of the potential minimum, which, according to Appendix C, indicates that the magnitude of the slow wave is larger than that of the fast wave. Some kind of damping or gradual reflection must have happened to the fast space-charge wave in the low potential region, leaving an excessive amount of slow wave with negative power.

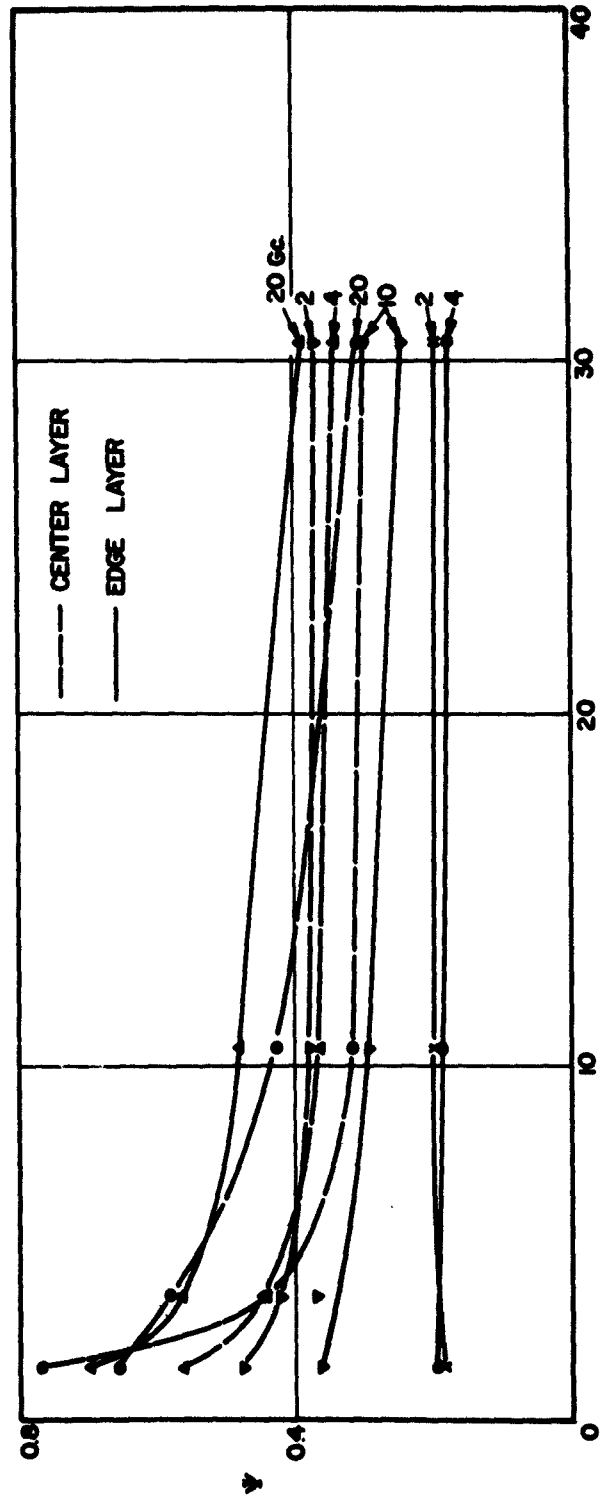

FIG. 5.12 NORMALIZED SELF-POWER SPECTRAL DENSITY OF CURRENT FLUCTUATIONS VS. NORMALIZED DISTANCE FROM THE CATHODE.

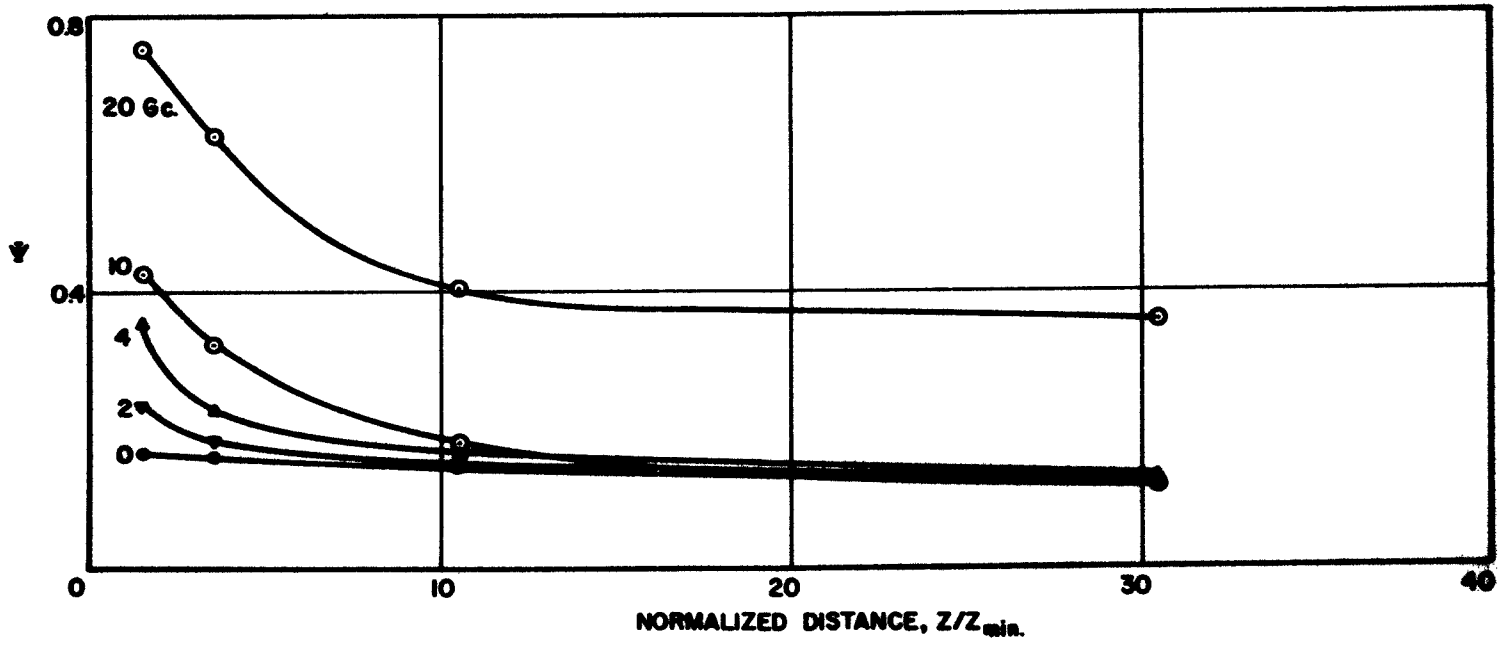

FIG. 5.13 NORMALIZED SELF-POWER SPECTRAL DENSITY OF CURRENT FLUCTUATIONS VS. NORMALIZED DISTANCE FROM THE CATHODE (THE WHOLE BEAM).

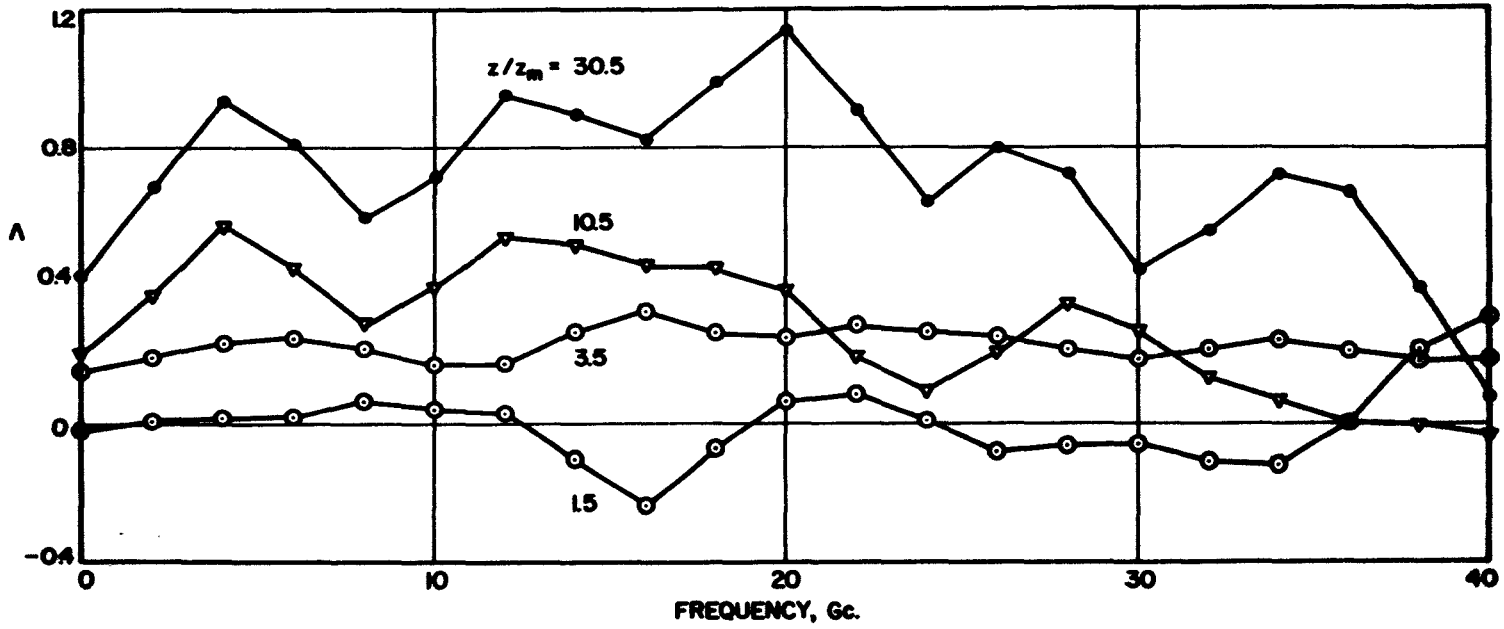

FIG. 5.14 NORMALIZED NOISE PARAMETER Λ VS. FREQUENCY (THE WHOLE BEAM).

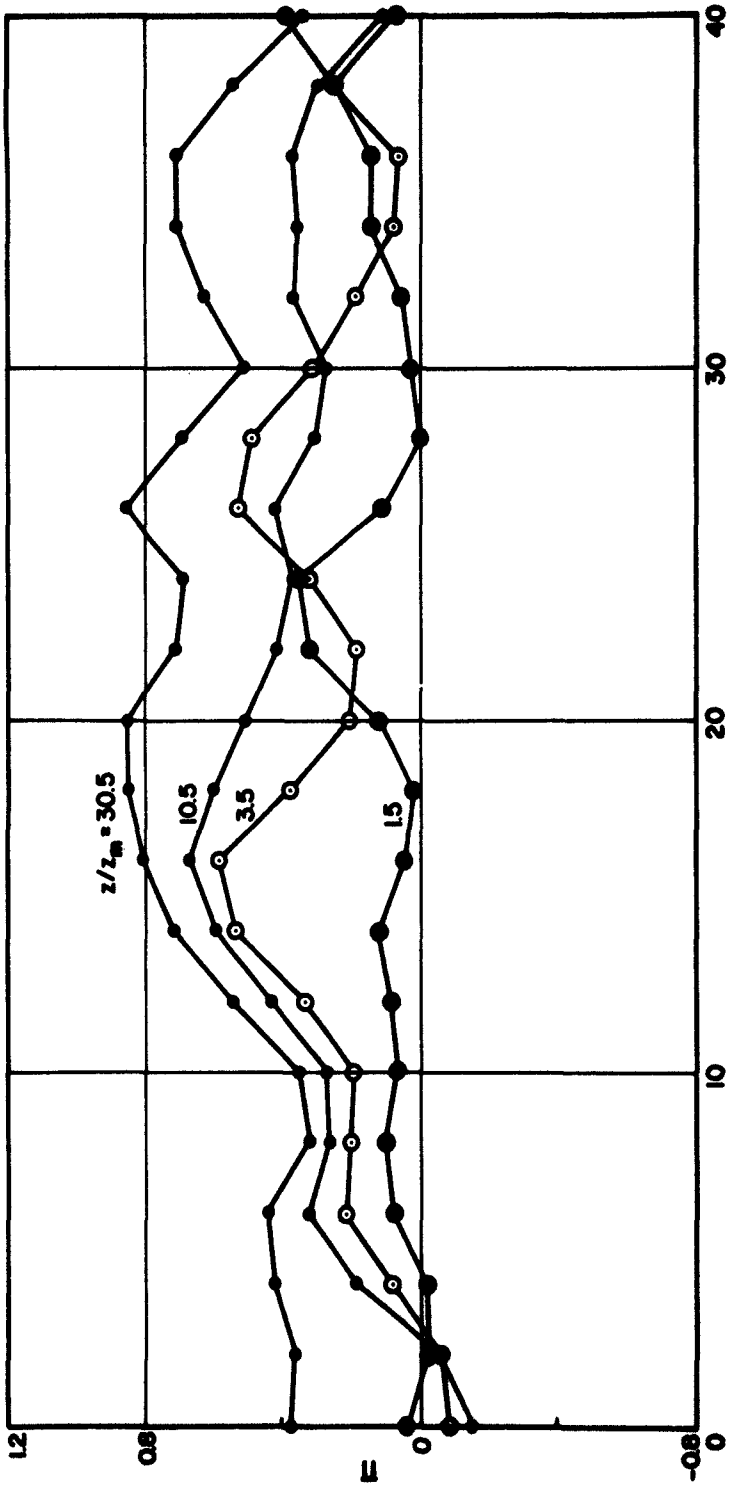

FIG. 5.15 NORMALIZED NOISE PARAMETER Π VS. FREQUENCY.

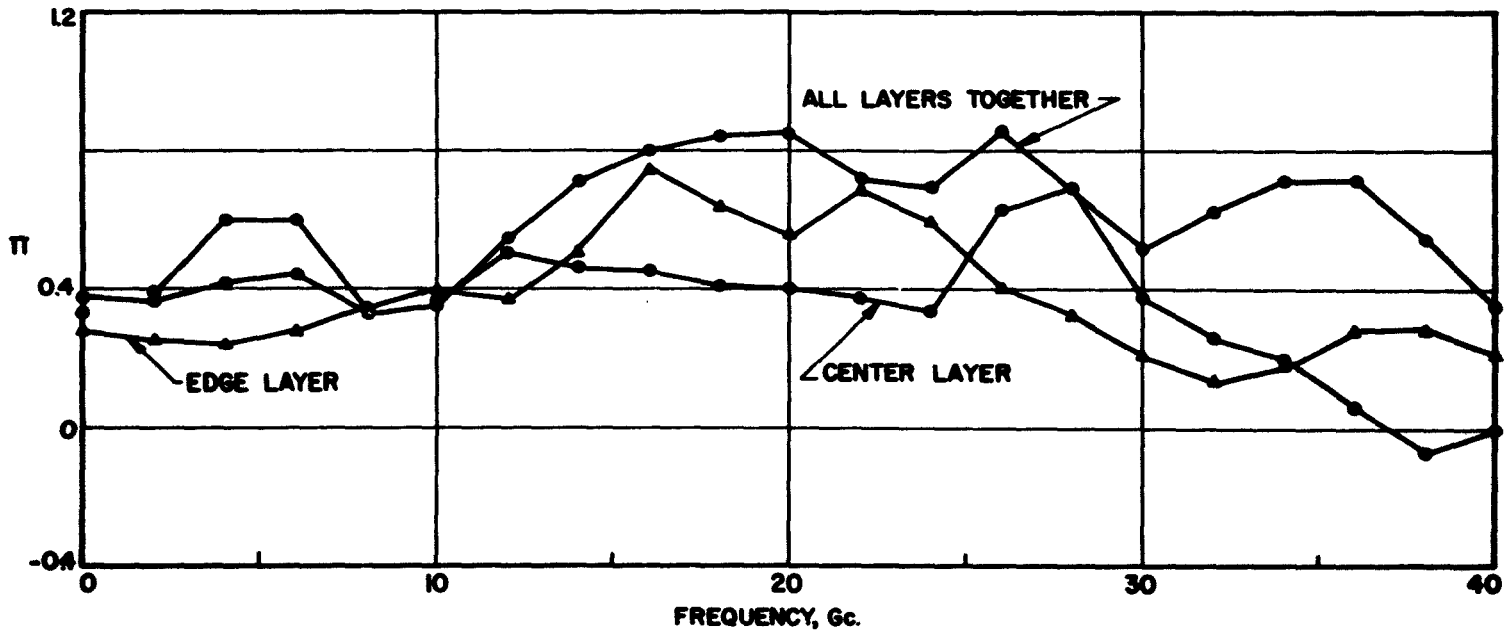

FIG. 5.16 NORMALIZED NOISE PARAMETER Π VS. FREQUENCY AT THE ANODE PLANE.

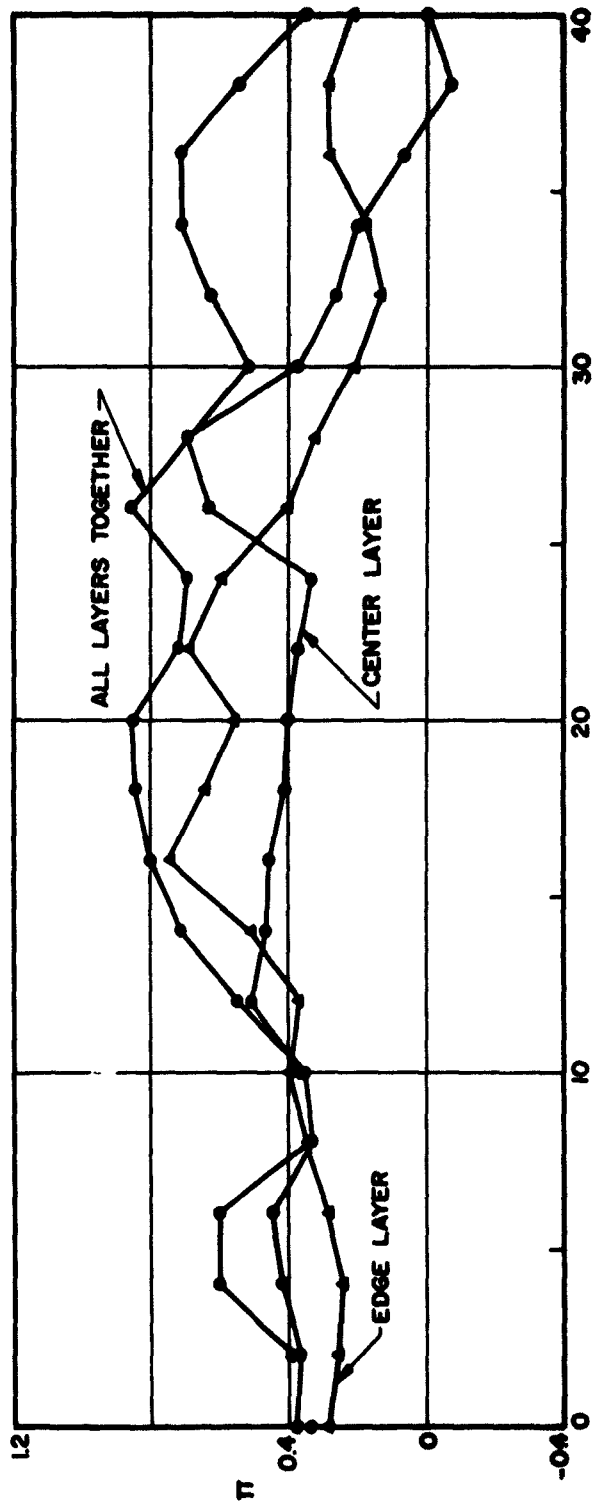

FIG. 5.16 NORMALIZED NOISE PARAMETER Π VS. FREQUENCY AT THE ANODE PLANE.

It is observed that the real part of Π, the normalized cross-power spectral density, varies between 0.32 and 0.86 at the anode plane. At low frequencies Π is asymptotic to 0.4 which is rather high compared to the results by Watkins, Siegman and Hsieh[11] or Dayem and Lambert[25]. The rapid development of the large amount of correlation in the region beyond the potential minimum is likely to be a direct result of the d-c velocity spread injected by the two-dimensional space-charge effects. The CPSD's of the center and edge layers at the anode plane are found to be slightly less than the previously mentioned figures, therefore less correlation between the kinetic potential and the current fluctuations is expected.

5.4.3 Noise Parameter S. Only a small reduction in S takes place at the center beam layer across the two-dimensional diode. In Fig. 5.17, S of the center layer is shown to be relatively independent of frequency. On the other hand, similarities are found between the noise parameter S versus frequency curves illustrated in Figs. 5.18 through 5.20 for the edge layer and the whole electron beam and the self-power spectral density Ψ versus frequency curves in Figs. 5.8 and 5.9. At zero frequency, S is reduced to 0.43 at the anode plane compared to 0.23 obtained by Dayem and Lambert. At very high frequencies, S approaches unity as expected.

In the small-signal single-velocity theory, both S and Π are invariants under any d-c acceleration. However, these two noise parameters are found to be nonconservative even beyond the $z = 10.5\, z_m$ plane of the two-dimensional beam model. The noise parameters are shown in Fig. 5.21 as a function of distance. In the multivelocity region, nearly identical growth rates of S and Π are observed at some chosen frequencies and the cause is traced back to the growth phenomenon of Ψ or the increase in magnitude of kinetic potential with distance. A

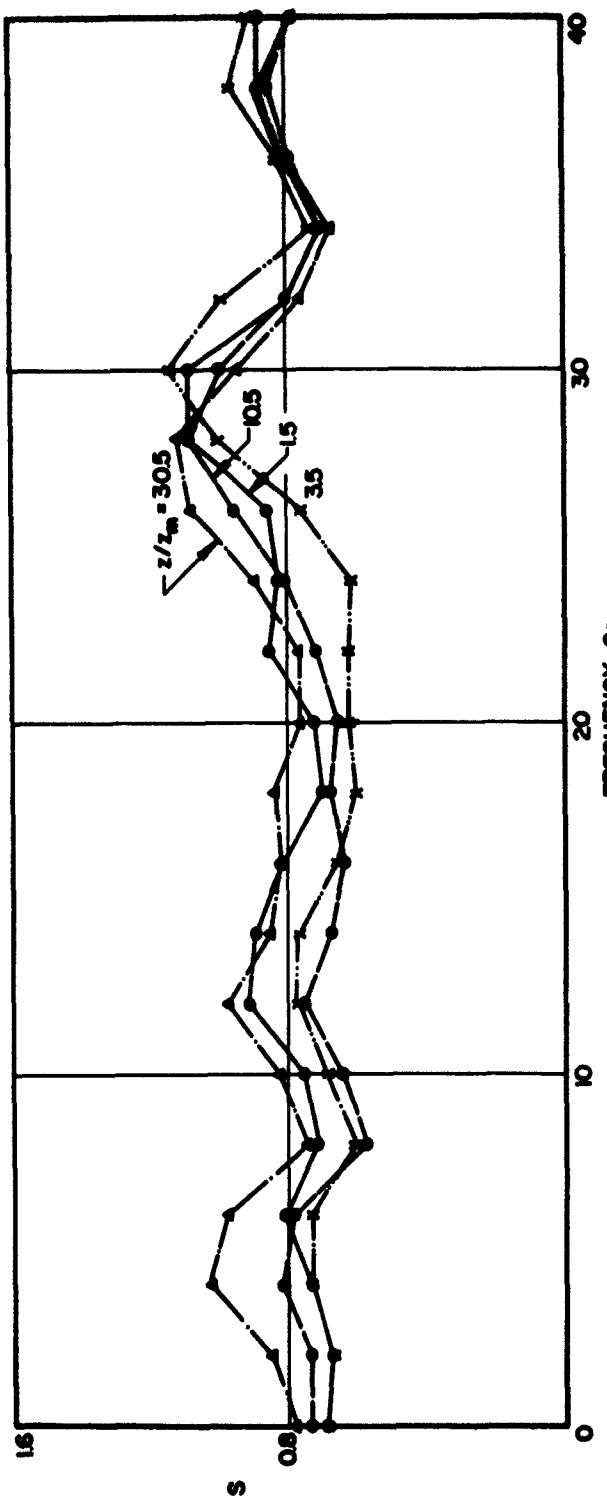

FIG. 5.17 NORMALIZED NOISE PARAMETER S VS. FREQUENCY (CENTER LAYER OF THE ELECTRON BEAM).

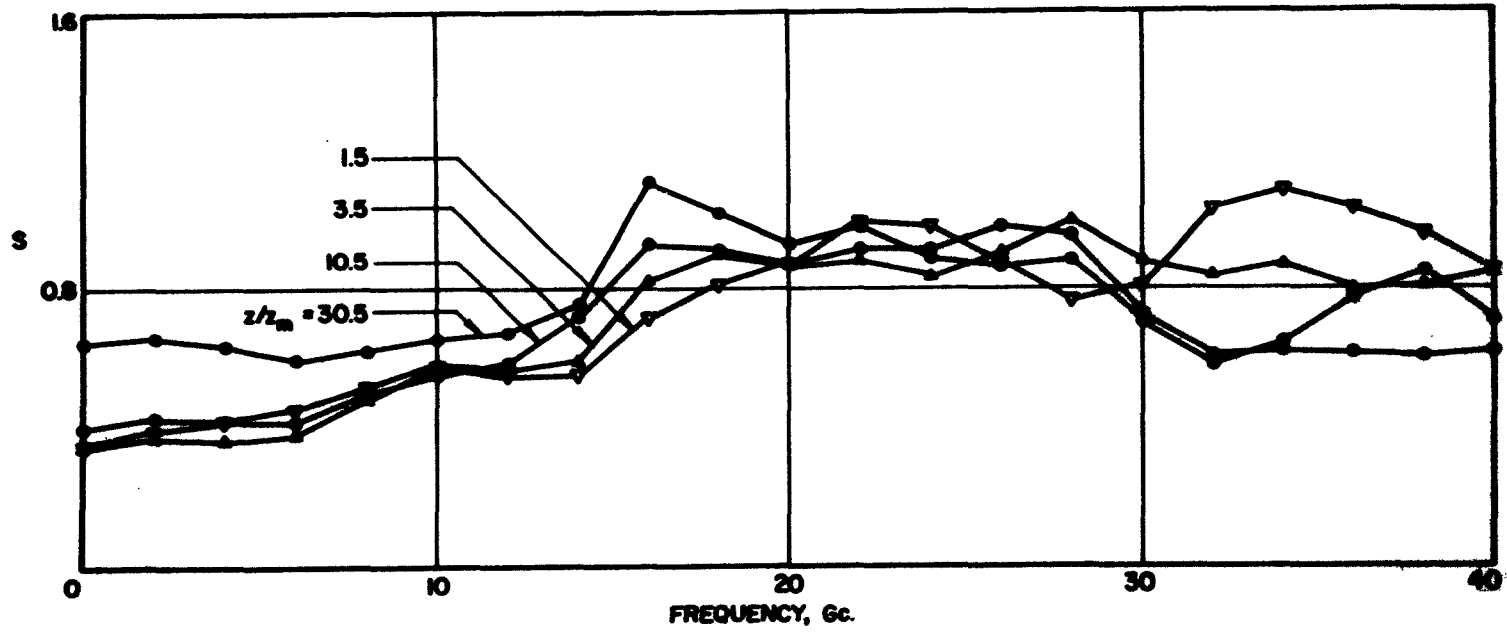

FIG. 5.18 NORMALIZED NOISE PARAMETER S VS. FREQUENCY (EDGE LAYER OF THE ELECTRON BEAM).

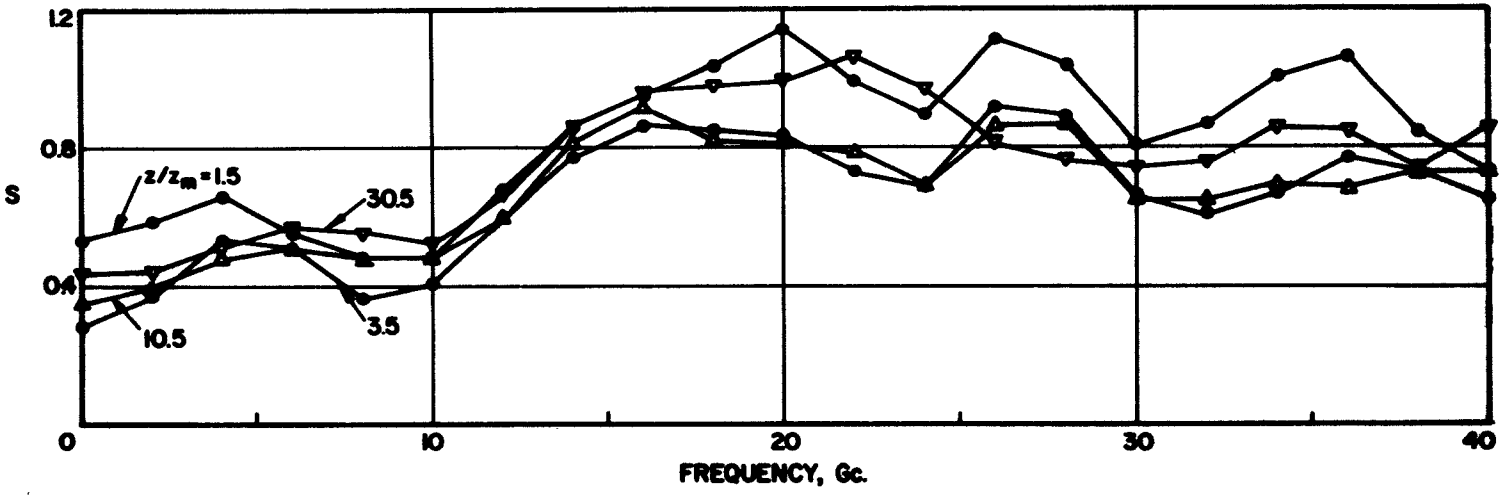

FIG. 5.19 NORMALIZED NOISE PARAMETER S VS. FREQUENCY (THE WHOLE BEAM).

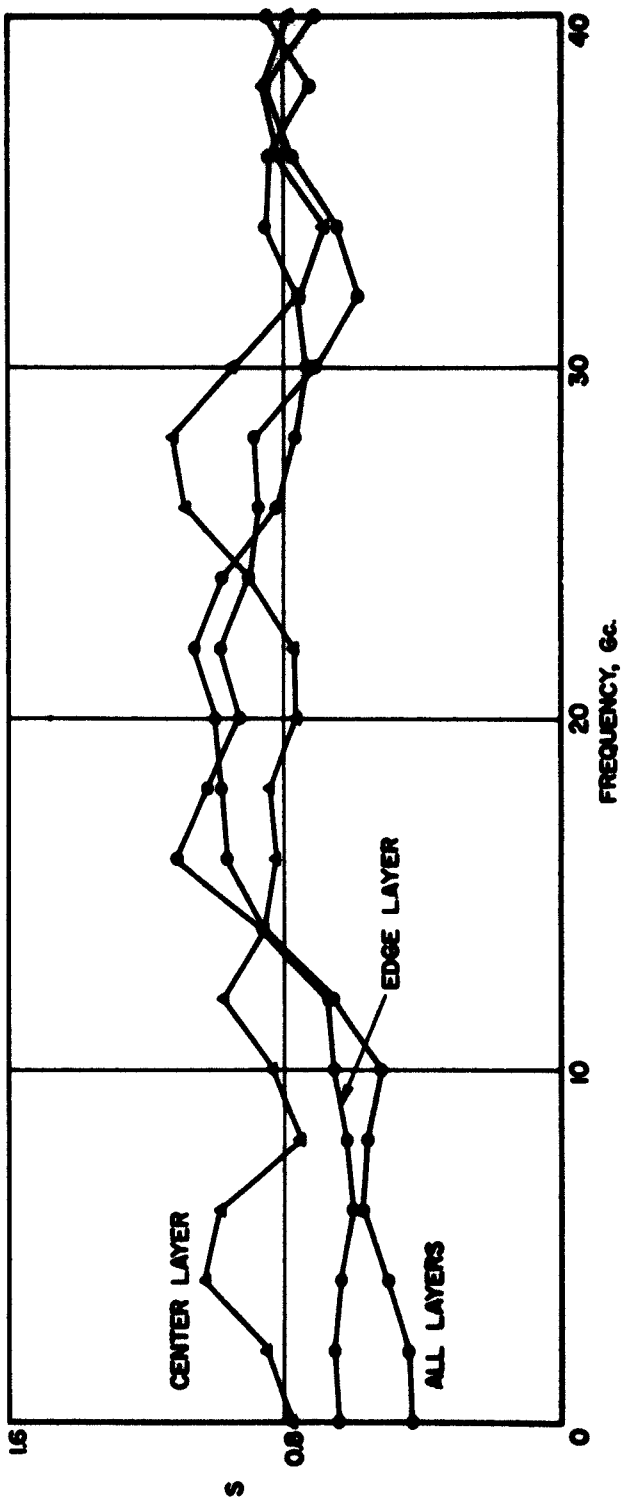

FIG. 5.20 NORMALIZED NOISE PARAMETER S VS. FREQUENCY AT THE ANODE PLANE.

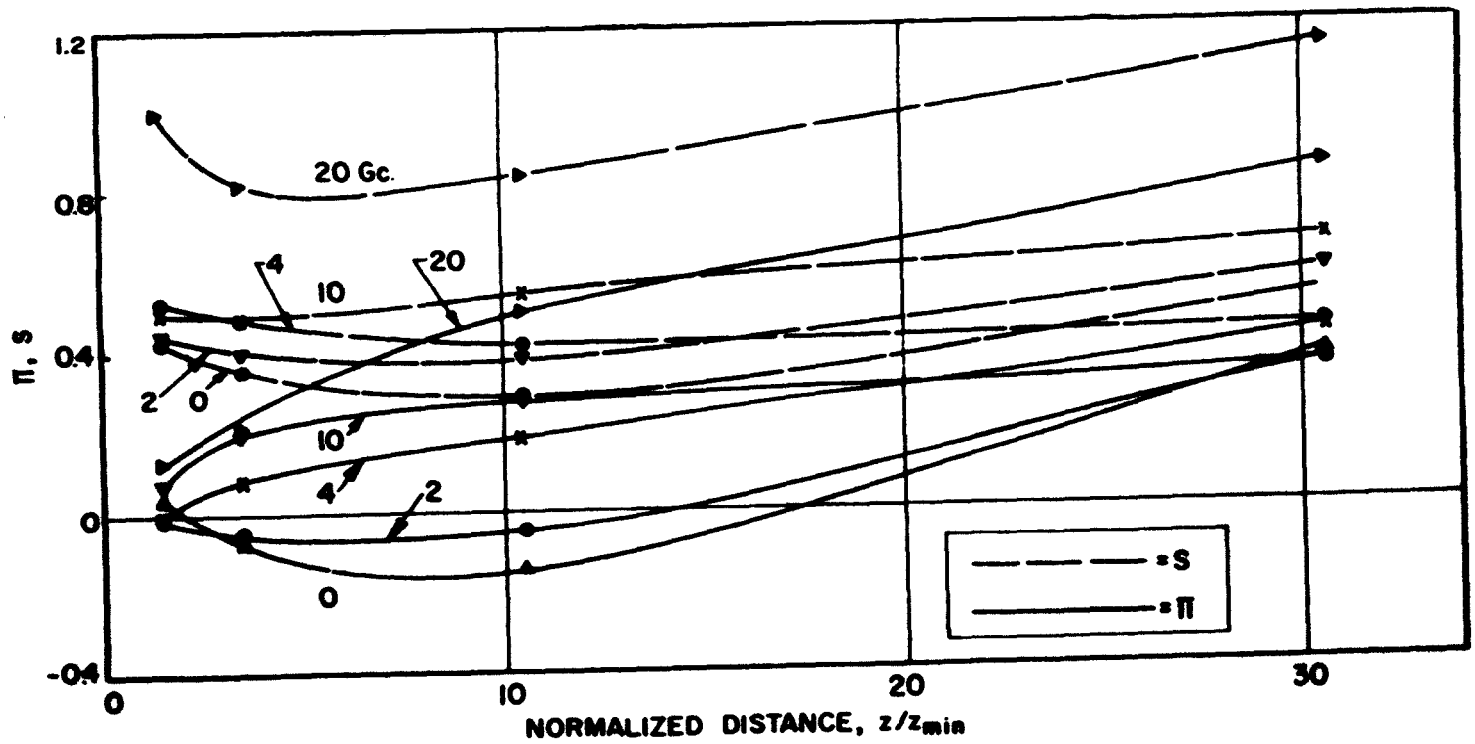

FIG. 5.21 NORMALIZED NOISE PARAMETERS S AND Π VS. NORMALIZED DISTANCE FROM THE CATHODE (THE WHOLE BEAM).

persistent amount of additional velocity spread induced by the space-charge potential depression may change the noise parameters S and Π by the same amount upon acceleration, leaving S-Π practically invariant.

A similar display of the noise parameters S and Π may be seen in Figs. 5.22 and 5.23 for the center layer and the edge layer of the ribbon beam. More gentle slopes for the S and Π curves are observed. As it was previously pointed out, the edge layer is actually farther away from its potential minimum compared to the center layer at the same normalized z-plane. Consequently, less variations in magnitude are found in the noise parameter versus distance curves for the edge layers.

5.4.4 Noise Parameters S-Π, S+Π and Π/S. From the small-signal noise theory by Haus, the theoretical minimum noise figure of a longitudinal beam-type amplifier is directly proportional to the difference of the two normalized noise parameters S and Π

$$F_{min} = 1 + \frac{T_c}{T}(S-\Pi) \quad . \tag{5.3}$$

The same equation may also be written as

$$F_{min} = 1 + \frac{T_c S}{T}\left(1 - \frac{\Pi}{S}\right) \tag{5.4}$$

separating the bracket into two independent terms S and 1 - Π/S. There has always been a controversy as to how noise reduction is accomplished, whether S or the factor (1 - Π/S) is responsible for the nonconvervative noise transport phenomena in electron beams.

Curves for S-Π, S+Π and Π/S at the anode plane are presented in Figs. 5.24 and 5.25, respectively. In a linearized one-dimensional analysis both S-Π, the amount of negative energy carried by the slow space-charge wave, and S+Π, the amount of positive energy carried by

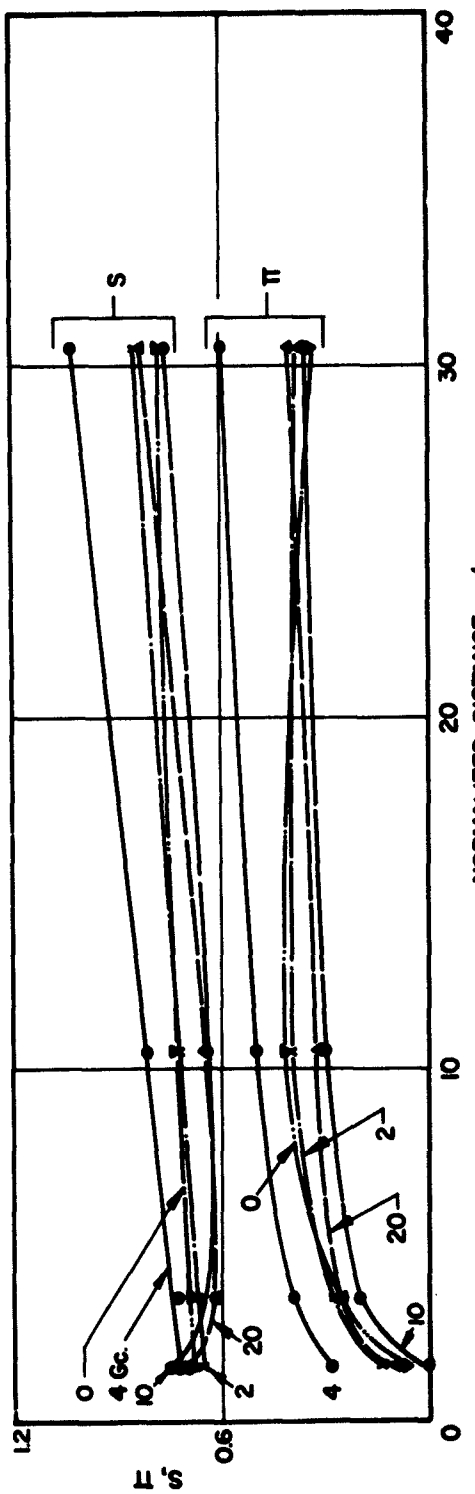

FIG. 5.22 NORMALIZED NOISE PARAMETERS S AND Π VS. NORMALIZED DISTANCE FROM THE CATHODE (CENTER LAYER OF THE ELECTRON BEAM).

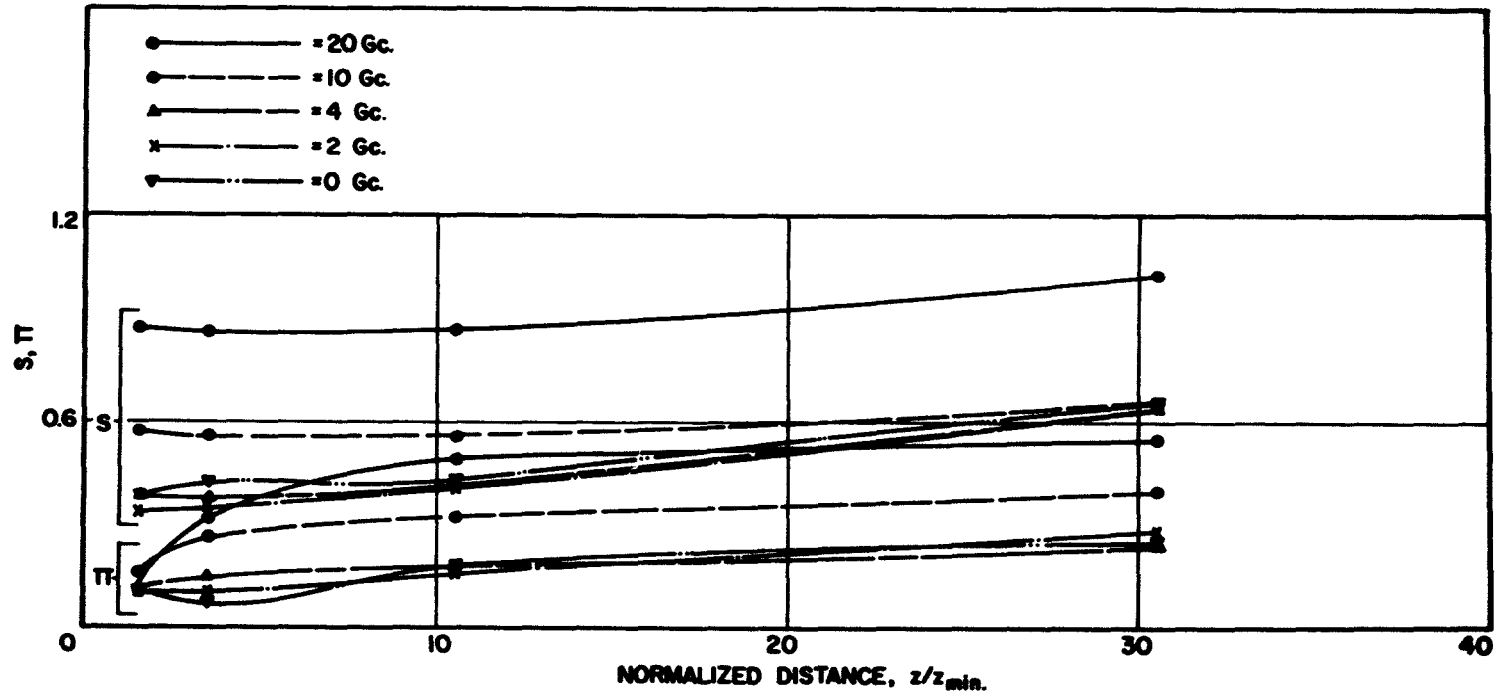

FIG. 5.23 NORMALIZED NOISE PARAMETERS S AND Π VS. NORMALIZED DISTANCE FROM THE CATHODE (EDGE LAYER OF THE ELECTRON BEAM).

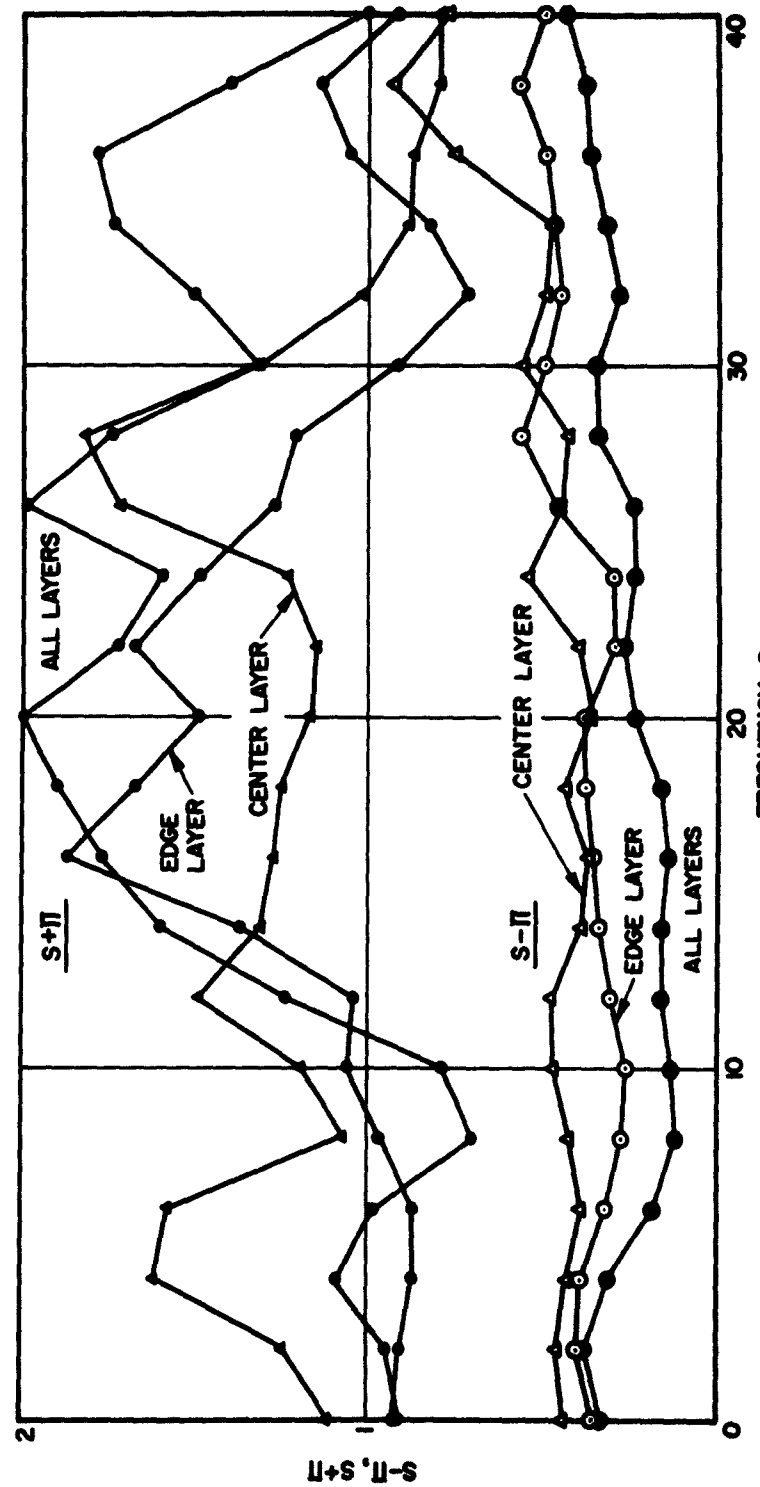

FIG. 5.24 NORMALIZED NOISE PARAMETERS S-Π AND S+Π VS. FREQUENCY AT THE ANODE PLANE.

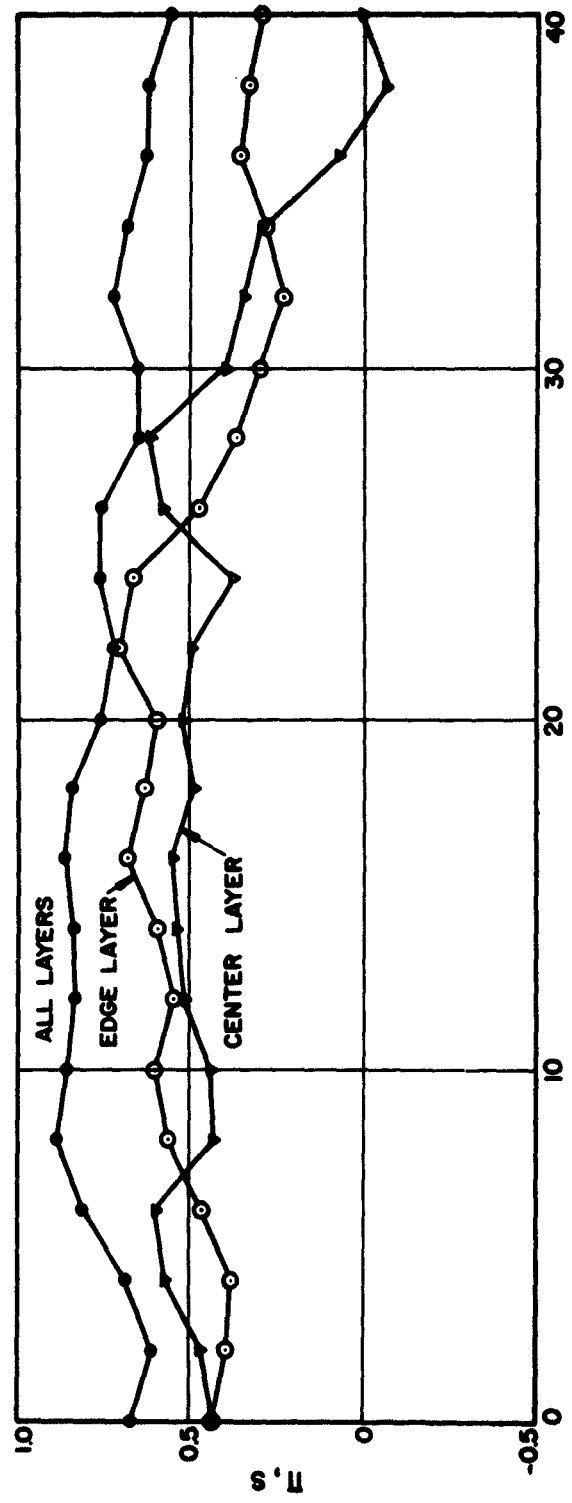

FIG. 5.25 RATIO OF Π/S VS. FREQUENCY AT THE ANODE PLANE.

the fast space-charge wave, should stay constant throughout. For the two-dimensional diode S-Π is found to be under 0.4 in the frequency range of interest and up to 3 db increase in S+Π is observed between 10 and 40 Gc. Accompanying the growth of Π, the increase in fast wave amplitude is attributed to the multi-dimensional space-charge effects.

Unprecedentedly large values for the ratio Π/S for the two-dimensional model are observed, fluctuating between 0.6 and 0.9 up to 40 Gc. The Π/S curves for the individual layers are found to be somewhat below that of the whole beam, indicating that the a-c coupling effects through the open-circuit assumption is the important mechanism in bringing forth the correlations between the velocity fluctuations and current fluctuations.

The same ratio is again shown as a function of distance in Figs. 5.26 through 5.28. For the region beyond the third z-plane, very little change in Π/S is observed for the individual layers. On the other hand, a substantial increase in Π/S for the whole beam tends to compensate for the effects introduced by S on the right-hand side of Eq. 5.4 making it constant with distance at frequencies above 4 Gc. The decay in S(1 - Π/S) for low frequencies will be discussed in the following section.

5.5 Theoretical Minimum Noise Figure in a Two-Dimensional Diode

Theoretical minimum noise figures F computed in terms of the noise parameters S and Π are presented in Figs. 5.29 through 5.36 for the two-dimensional diode operating under conditions described in Chapter III. Approximately 3 db noise reduction is found at the anode plane for the edge and the center layer of the electron beam up to 20 Gc. At low frequencies, a small rise in F is observed beyond the multivelocity region

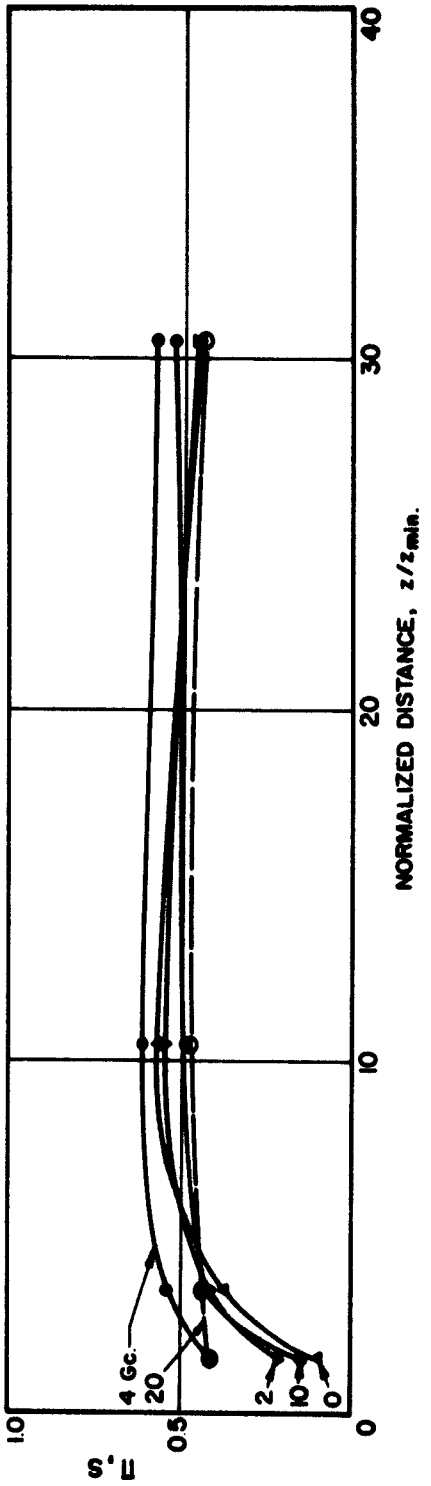

FIG. 5.26 RATIO OF Π/S VS. NORMALIZED DISTANCE FROM THE CATHODE (CENTER LAYER OF THE ELECTRON BEAM).

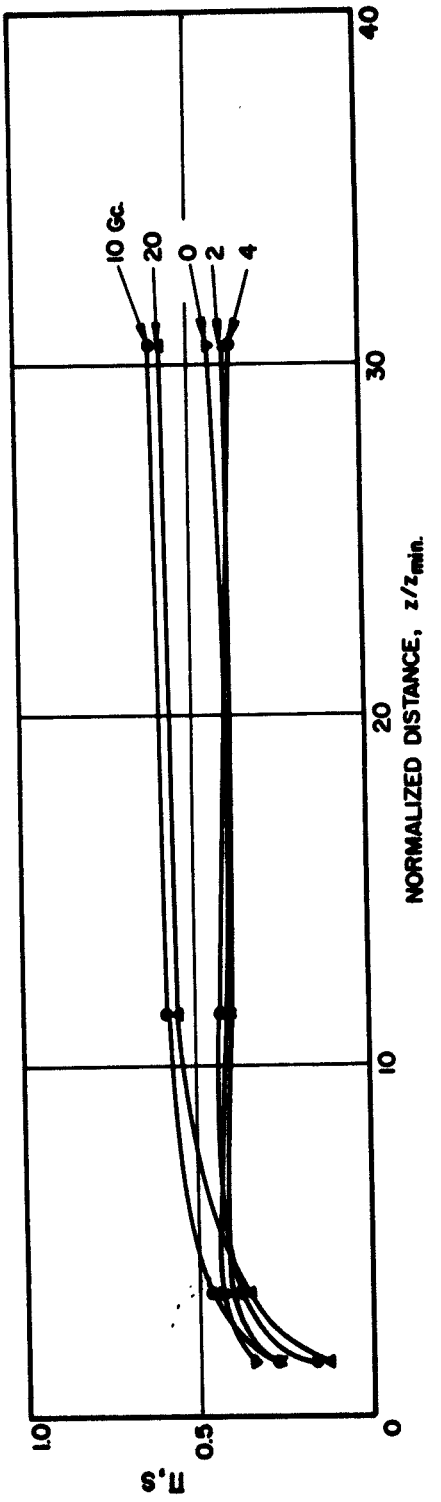

FIG. 5.27 RATIO OF Π/S VS. NORMALIZED DISTANCE FROM THE CATHODE (EDGE LAYER OF THE ELECTRON BEAM).

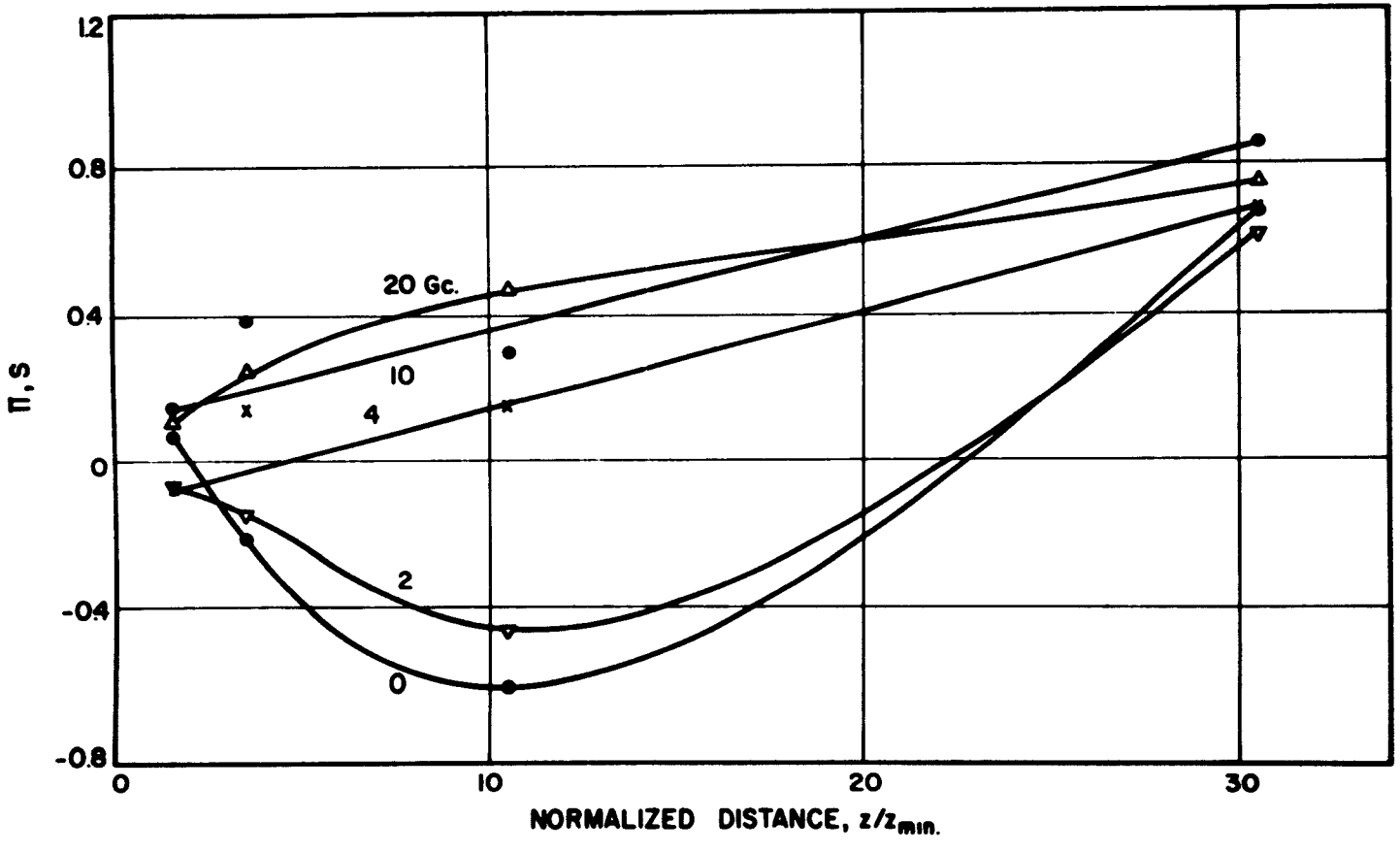

FIG. 5.28 Π/S VS. NORMALIZED DISTANCE FROM THE CATHODE (THE WHOLE BEAM).

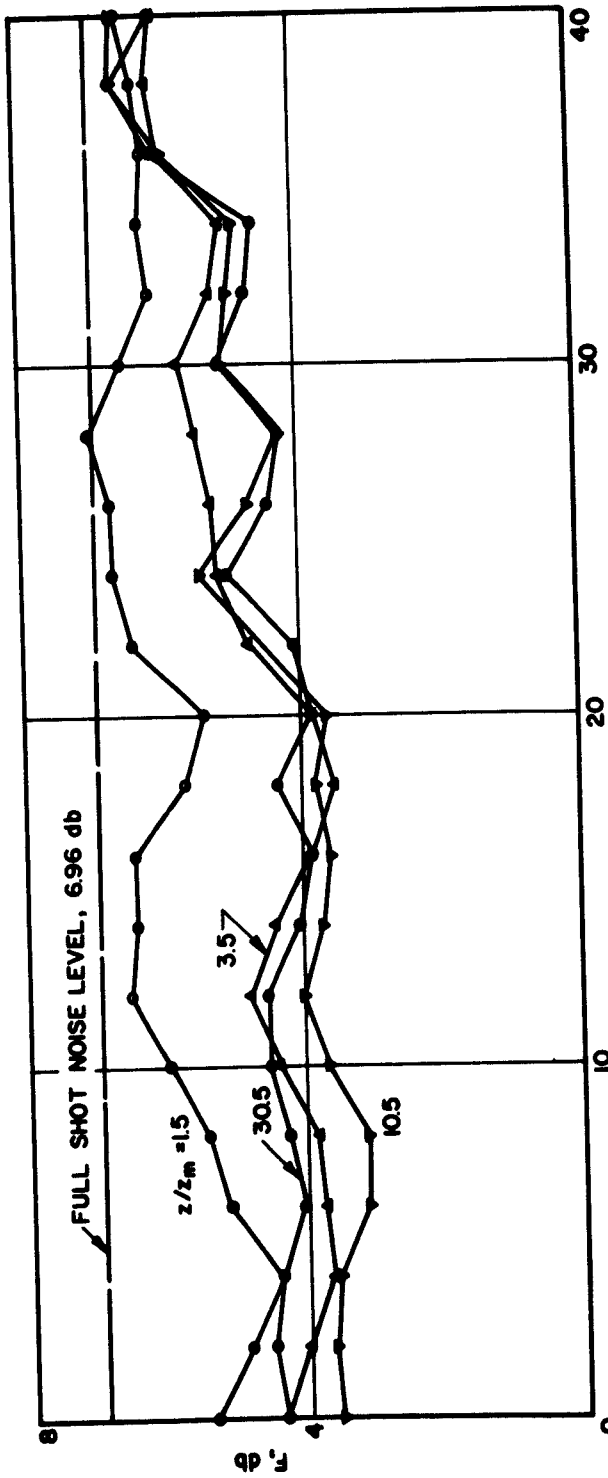

FIG. 5.29 THEORETICAL MINIMUM NOISE FIGURE VS. FREQUENCY (CENTER LAYER OF THE ELECTRON BEAM).

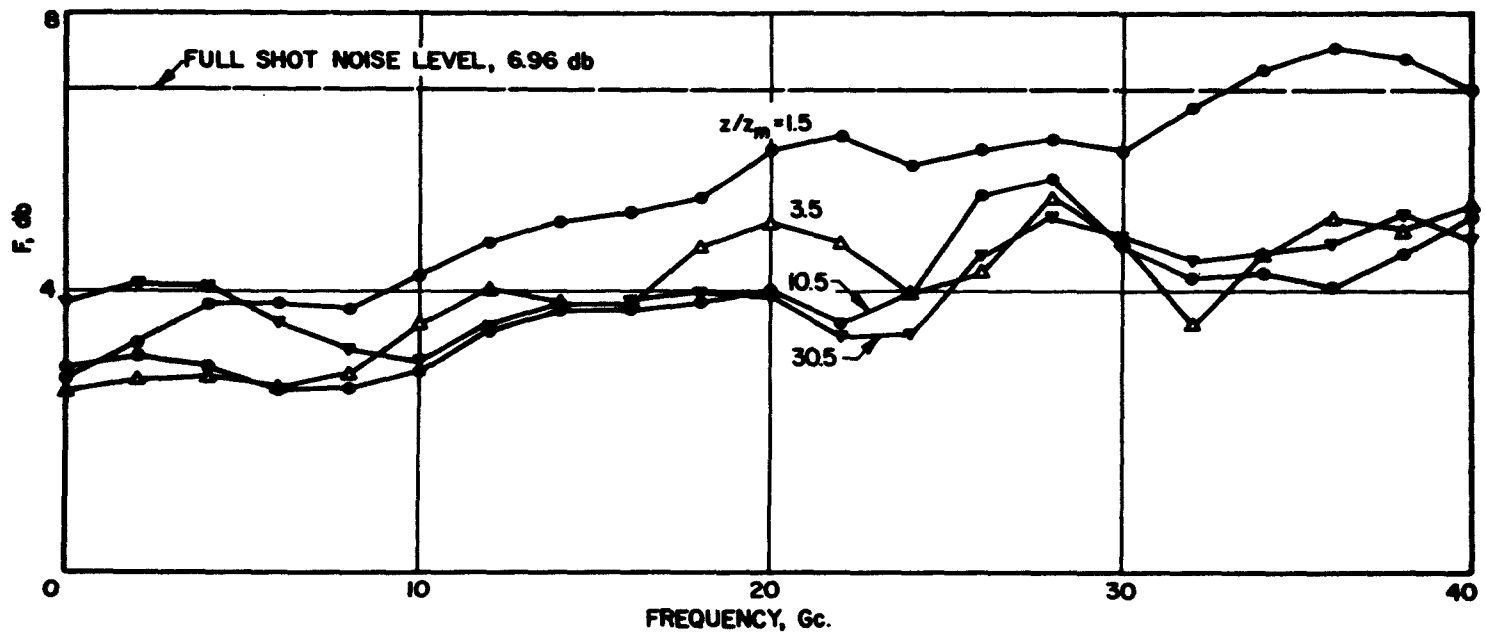

FIG. 5.30 THEORETICAL MINIMUM NOISE FIGURE VS. FREQUENCY (EDGE LAYER OF THE ELECTRON BEAM).

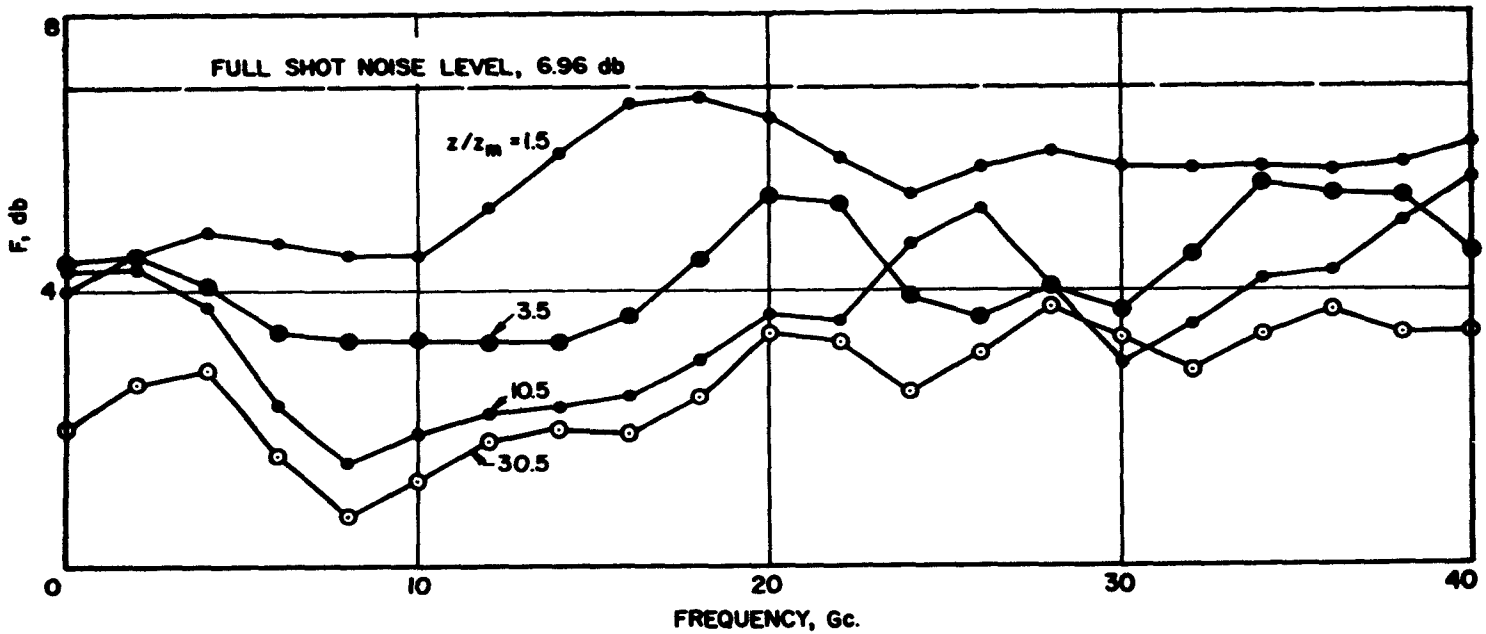

FIG. 5.31 THEORETICAL MINIMUM NOISE FIGURE VS. FREQUENCY (THE WHOLE BEAM).

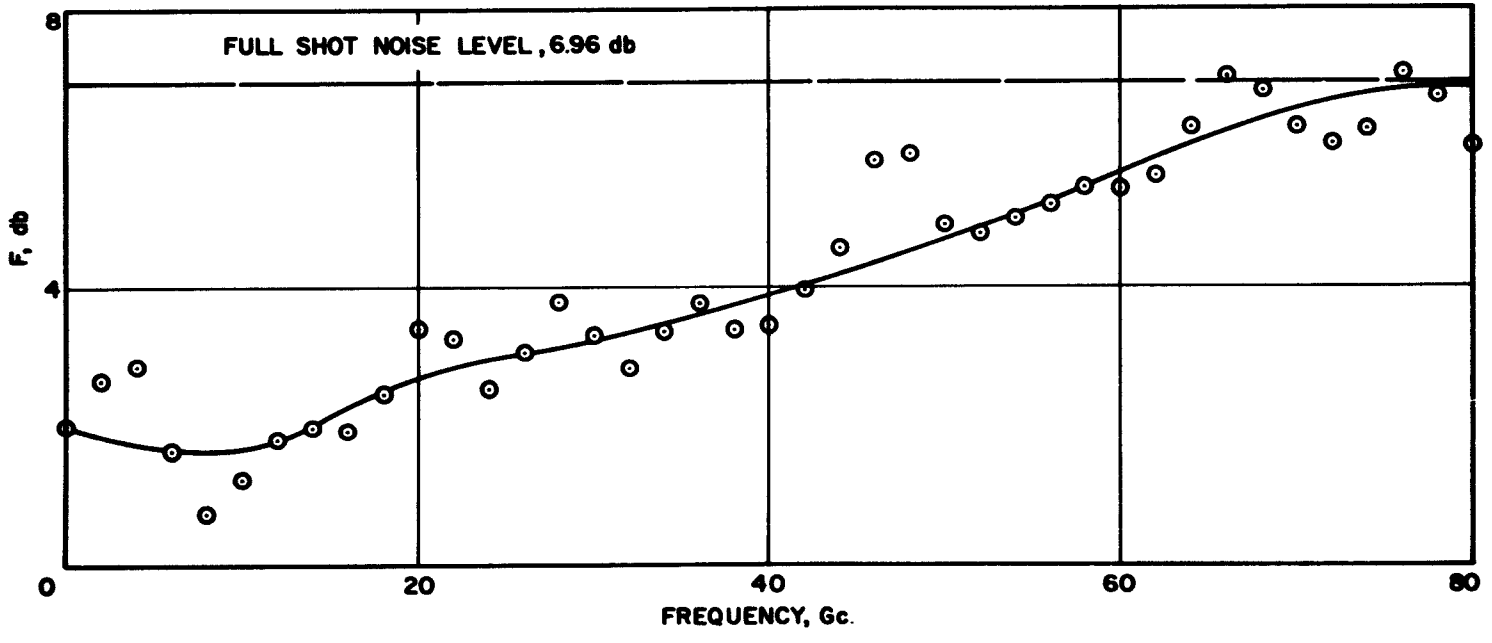

FIG. 5.32 THEORETICAL MINIMUM NOISE FIGURE FOR THE TWO-DIMENSIONAL SPACE-CHARGE-LIMITED DIODE VS. FREQUENCY (THE WHOLE BEAM).

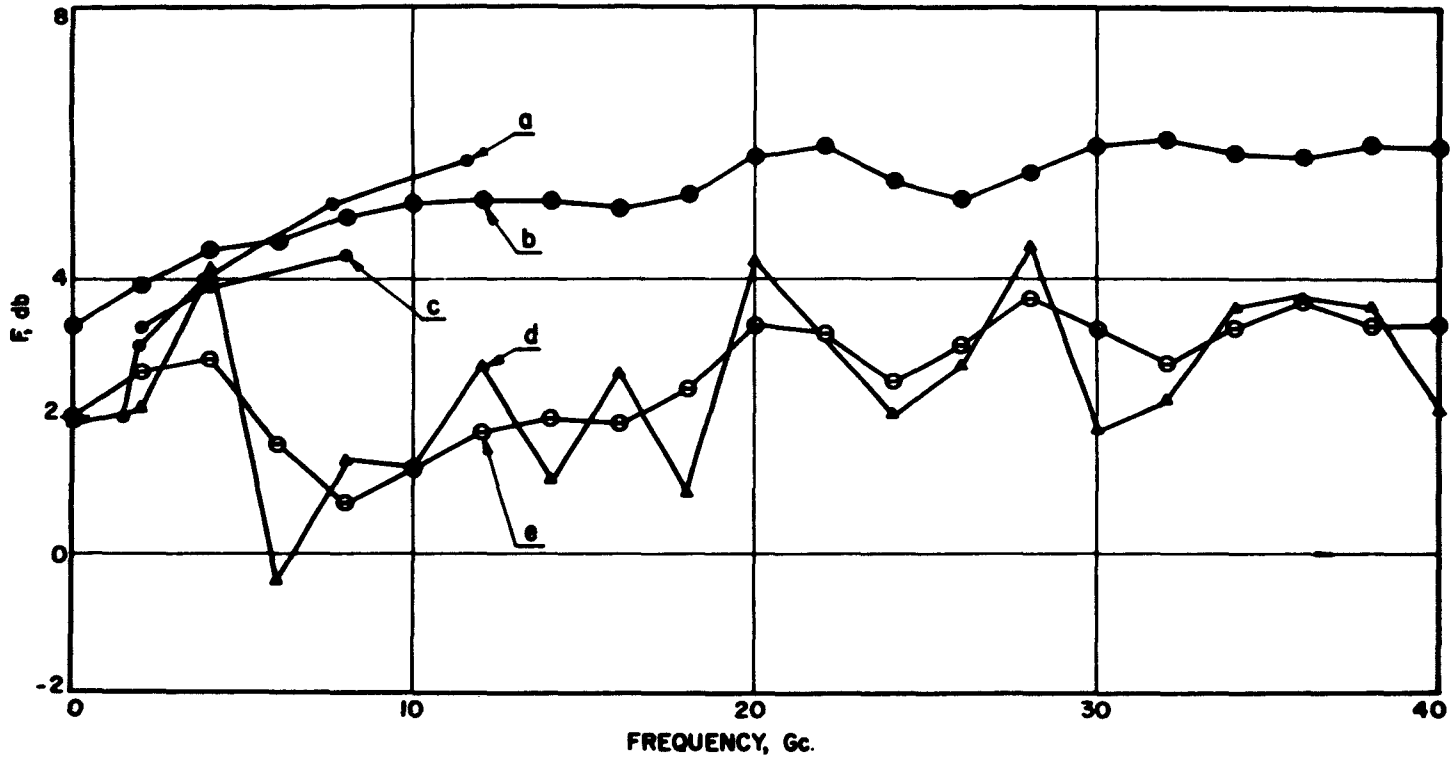

a. Vivian
b. Dayem and Lambert
c. Siegman, Watkins and Hsieh
d. Two-Dimensional Diode
e. Two-Dimensional Diode Lag Window Average

FIG. 5.33 THEORETICAL MINIMUM NOISE FIGURE VS. FREQUENCY FOR ONE-DIMENSIONAL AND TWO-DIMENSIONAL DIODES.

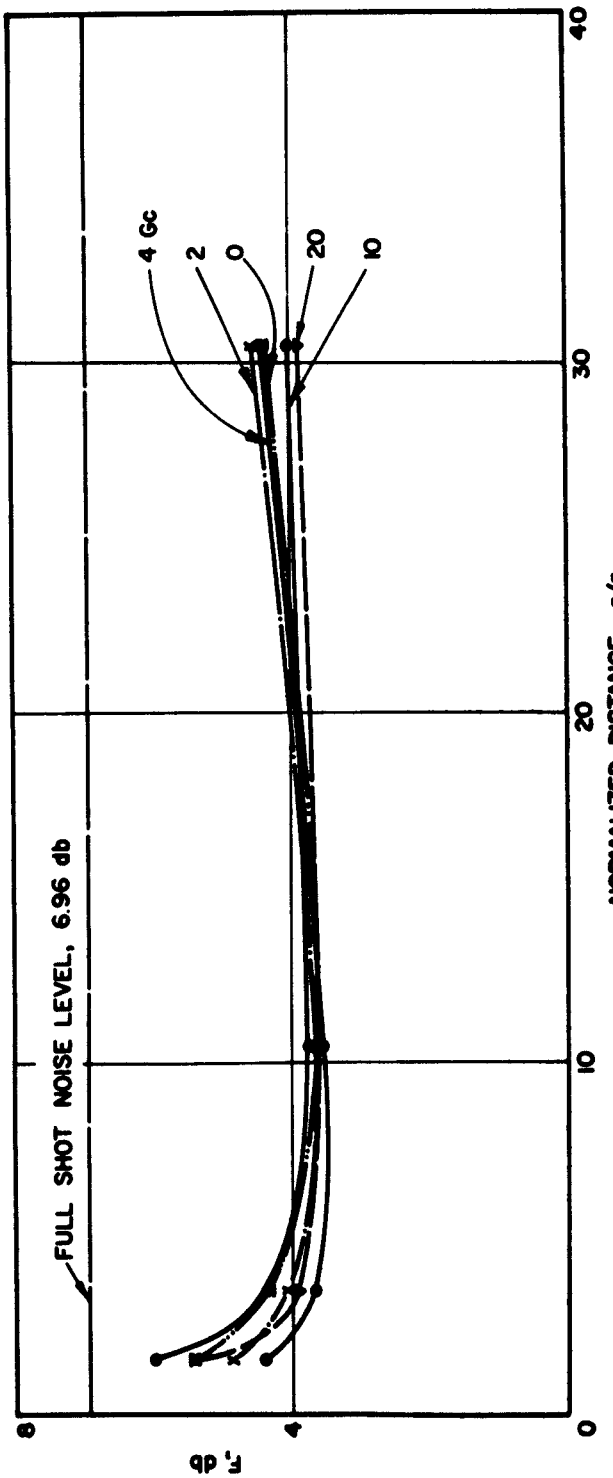

FIG. 5.34 THEORETICAL MINIMUM NOISE FIGURE VS. NORMALIZED DISTANCE FROM THE CATHODE (CENTER LAYER OF THE ELECTRON BEAM).

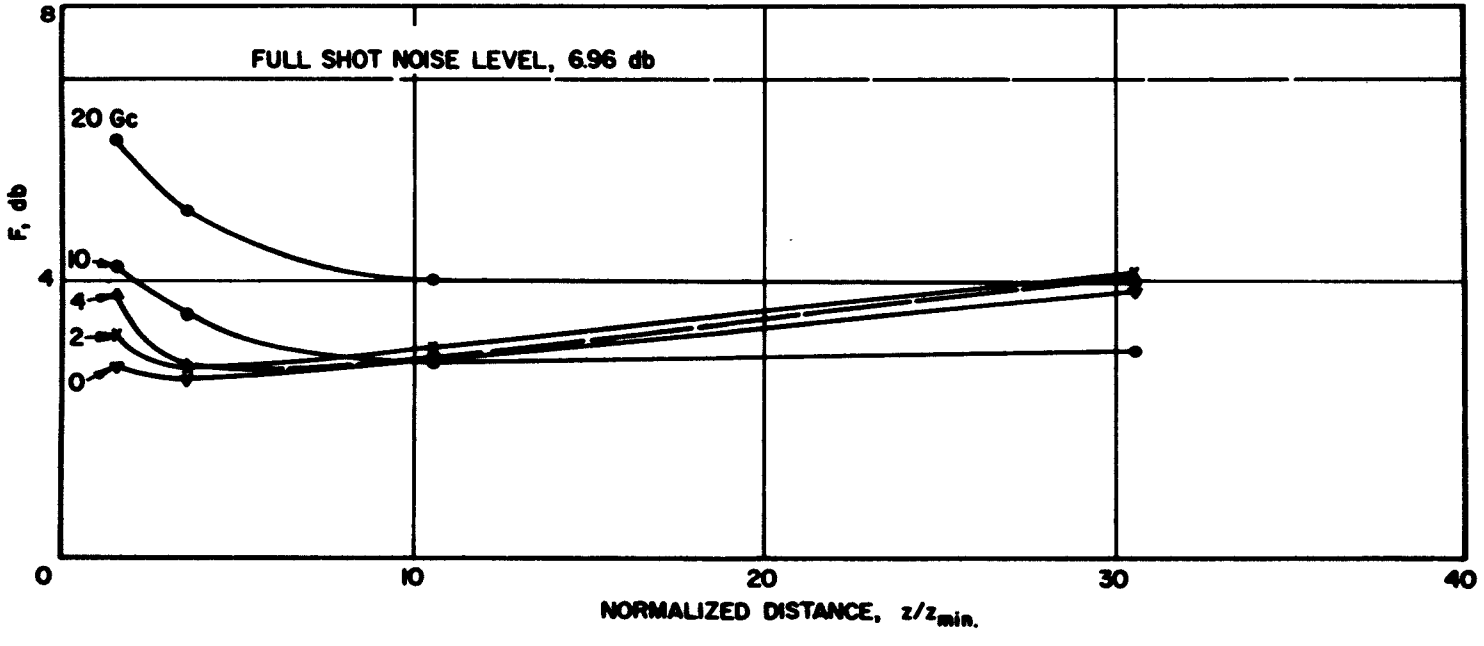

FIG. 5.35 THEORETICAL MINIMUM NOISE FIGURE VS. NORMALIZED DISTANCE FROM THE CATHODE (EDGE LAYER OF THE ELECTRON BEAM).

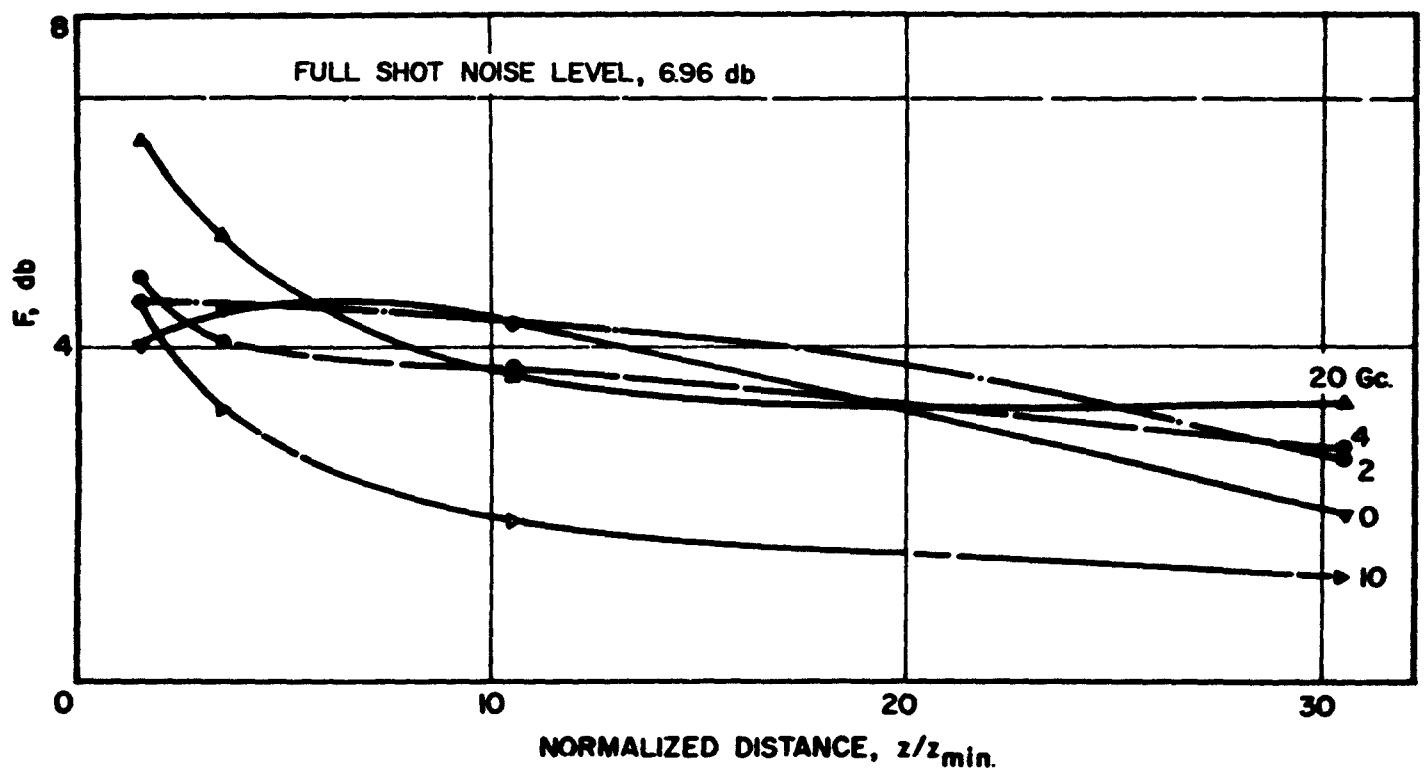

FIG. 5.36 THEORETICAL MINIMUM NOISE FIGURE VS. NORMALIZED DISTANCE FROM THE CATHODE (THE WHOLE BEAM).

possibly caused by the increase in S previously mentioned. As for the two-dimensional beam as a whole, less than 3 db minimum noise figure is predicted for frequencies below 20 Gc and it stays under 4 db up to 40 Gc. As expected, the noise figure of the two-dimensional diode tends to rise with frequency, reaching full shot noise level at approximately 70 Gc.

Results previously obtained for one-dimensional noise transport analyses are shown compared with the minimum theoretical noise figure of the two-dimensional diode. For the two-dimensional model both the spectral estimates and their lag window averages are presented. It is obvious that the point representing a noise figure of less than zero db is outside of the 32 percent confidence interval. Aside from a few points, the smoothed curve seems to be a good representation of the noise characteristics in the frequency domain. A theoretical minimum noise figure of less than 2 db is predicted for a small frequency range, and from the two-dimensional analysis the prediction appears to be in quantitative agreement with some experimental results recently reported. It is necessary to point out that the results for the one-dimensional analyses by Vivian[19], Dayem and Lambert[25] and Siegman, Watkins and Hsieh[11] are evaluated at a small distance beyond the potential minimum where the noise parameters are assumed to become invariant with distance, while the estimates for the two-dimensional diode are obtained at the anode plane. In the multi-velocity region created by the space-charge effects, substantial noise reduction is observed for the two-dimensional model at low frequencies.

It is clear from the foregoing comparison that the multi-dimensional effects may be substantial and should not be disregarded in noise transport analyses and the minimum noise figure of longitudinal beam-type

devices may be greatly reduced when an additional dimension is taken into account.

5.6 Space-Charge Effects at the Anode

In the two-dimensional theoretical model employed in the Monte Carlo calculation of noise transport analysis, the space-charge effect is approaching zero at the anode. As a result, the slopes of the noise parameters S and Π are expected to level off at the anode plane where the single-velocity theory begins to take over. Unfortunately, this phenomenon is not confirmed because of the lack of information concerning the transport characteristics of the electron beam between the anode and the third z-plane. In Fig. 5.23, no attempt is made to fit the S and Π curves with a prescribed zero gradient at the anode plane.

5.7 Errors in Electric Field Evaluation

The nature of errors introduced in the d-c electric field evaluation is actually two-fold. First of all, the method described in Appendix B involves certain averaging processes when the compartments are installed. Second, the replacement of the infinite series with an integral brings in a further approximation in the electric field computation. However, sampling of the crossing velocity at the z-planes shows good agreement between the d-c potential and the velocity of the slowest electrons. This, together with the average current and potential minimum characteristics, leads to the belief that the method for the d-c field computation is satisfactory.

CHAPTER VI. SUMMARY AND CONCLUSIONS

6.1 Summary and Conclusions

The noise transport phenomena in a hollow-beam thermionic diode operated under space-charge-limited conditions have been investigated by means of two different numerical methods. A two-dimensional mathematical discrete beam model was constructed to simulate the actual diode with a large beam radius to beam thickness ratio.

A small-signal linearized Boltzmann equation expressed in terms of the two-dimensional density function and the electric fields has been derived for an electron beam with an infinite axial magnetic field. Because of the discontinuity of the d-c density function in the velocity domain, Siegman's singularity extraction method was employed to take away the singularity factor from the transport equation; details of the extraction techniques are presented. To facilitate a solution for the transport equation by digital computer techniques, velocity classes are introduced as an approximation to the distribution function. Singularities brought forth by the velocity class approximations in the boundary conditions were investigated and their physical meanings are discussed in detail. Linear transform techniques were employed to solve the set of small-signal multi-coupled linear first-order differential equations governing the behavior of the density functions in phase space. Haus's small-signal noise theory was employed to evaluate the noise transport characteristics of the two-dimensional electron beam.

The two-dimensional beam noise transport phenomena was also treated by means of the Monte Carlo technique. Contrary to the density function calculations, the stochastic emission process at the thermionic

cathode was directly simulated and the electrons emitted were traced in phase space by numerical integration techniques until they left the diode. Random number transform techniques were presented and the merits of the Monte Carlo method of noise transport analysis is discussed. In Appendix B, the method employed to evaluate the d-c and a-c electric fields is described and the implication of the open-circuit assumption is elaborated. Following the thin beam assumption, the axial a-c electric field is taken to be uniform in the transverse direction across the electron beam, equivalent to a one-dimensional assumption for the a-c electric field. As a result, only the d-c multi-dimensional effects are included in the Monte Carlo calculations. A brief description of the generalized harmonic analysis and an introduction to sampling techniques are presented. Haus's noise parameters are estimated statistically by means of sampling techniques.

Results from the density function calculations carried out at three discrete frequencies are presented. Little or no reduction from the thermionic field emission shot noise is observed. There is no evidence of any multi-dimensional effects postulated and even the well known noise reduction mechanism due to the gating action of the potential minimum appears to be missing. A close examination of the two-dimensional coupling mechanism reveals that the induced a-c electric fields in the two-dimensional analysis decay too rapidly in the transverse direction to bring forth significant multi-dimensional effects. As a consequence of the velocity dependent characteristics of the coupling field, heavy emphasis is placed on the fluctuations associated with the slow electrons, causing a net reduction of the kinetic power carried by the electron beam and some deteriation in noise performance.

From the results of the Monte Carlo calculations, substantial noise reduction at a wide band of frequencies up to 20 Gc is observed. A minimum noise figure of less than 2 db is predicted for a small frequency range and the prediction appears to be in quantitative agreement with some experimental results recently reported. In addition to the noise current smoothing mechanism achieved by the fluctuation of the potential minimum, additional reduction of noise at frequencies several times the electron plasma oscillation frequency at the potential minimum is observed in the extended multivelocity region created by the multi-dimensional space-charge potential depression effects. Unusually large values of the ratio Π/S for the two-dimensional beam model are realized in the nonlinear multivelocity region beyond the potential minimum, resulting in a net reduction of the minimum achievable noise figure. Neither $S-\Pi$ nor $S+\Pi$ is found to be invariant with respect to distance from the cathode as predicted by the one-dimensional linearized single-velocity and multivelocity noise theories. The importance of the multi-dimensional d-c space-charge effects are clearly brought out in the Monte Carlo analysis.

It is evident from the discrepancy between the results from the two numerical methods of noise transport analysis in two-dimensional multivelocity electron beams that the coupling mechanism plays an influential role in the transport characteristics. Further improvement of the electron beam noise transport theory would depend on a more thorough understanding of the actual coupling mechanism in a multi-dimensional realistic beam model.

6.2 Suggestions for Further Study

It would be interesting to replace the two-dimensional a-c coupling term in the density function calculations by its one-dimensional counterpart and see if the results thus obtained would be similar to the results from the Monte Carlo calculations. The validity of the linearized analysis employed in the highly nonlinear region of the electron beam will be revealed.

Coupling mechanisms in multi-dimensional electron beams should be further investigated. It might even be feasible to construct experimental measurement to help determine the coupling a-c electric fields induced by the fluctuation of convection current densities.

APPENDIX A. A-C AND D-C ELECTRIC FIELDS IN A TWO-DIMENSIONAL DIODE AND SOME DETAILS IN THE DENSITY FUNCTION FORMULATION

A.I A-c Electric Fields

In a two-dimensional diode, the a-c electric fields induced by the moving space charge may be evaluated using Maxwell's equations. At high frequencies, because the electromagnetic field strength drops off rapidly with distance from the origin of the disturbance, effects due to the image currents are neglected in the following calculations. Consider $i_1(y',z)$ in Fig. A.1 to be the a-c current density of a z-directed sheet beam infinite in the x-direction.

$$i_1(y',z) = -e \int_{-\infty}^{\infty} \dot{z}\, F_1(y',z,\dot{z})d\dot{z} \quad . \tag{A.1}$$

If the convection current $i_1(y',z)$ is assumed to have an $e^{-j\beta' z}$ variation, according to the Laplace law, the tangential magnetic fields $H_{x1}(y,z)$ and $H_{x2}(y,z)$ may be expressed as

$$H_{x1}(y,z) = Ae^{\beta'(y-y')} \quad \text{for} \quad y < y' \quad , \tag{A.2}$$

$$H_{x2}(y,z) = Be^{-\beta'(y-y')} \quad \text{for} \quad y > y' \quad , \tag{A.3}$$

where $\beta' \equiv |\omega/u'|$ and $\beta' \neq 0$. Continuity of magnetic fields tangential to a sheet beam of infinitesimal thickness requires that

$$i_1(y',z)dy' = H_{x1}(y',z) - H_{x2}(y',z) \quad . \tag{A.4}$$

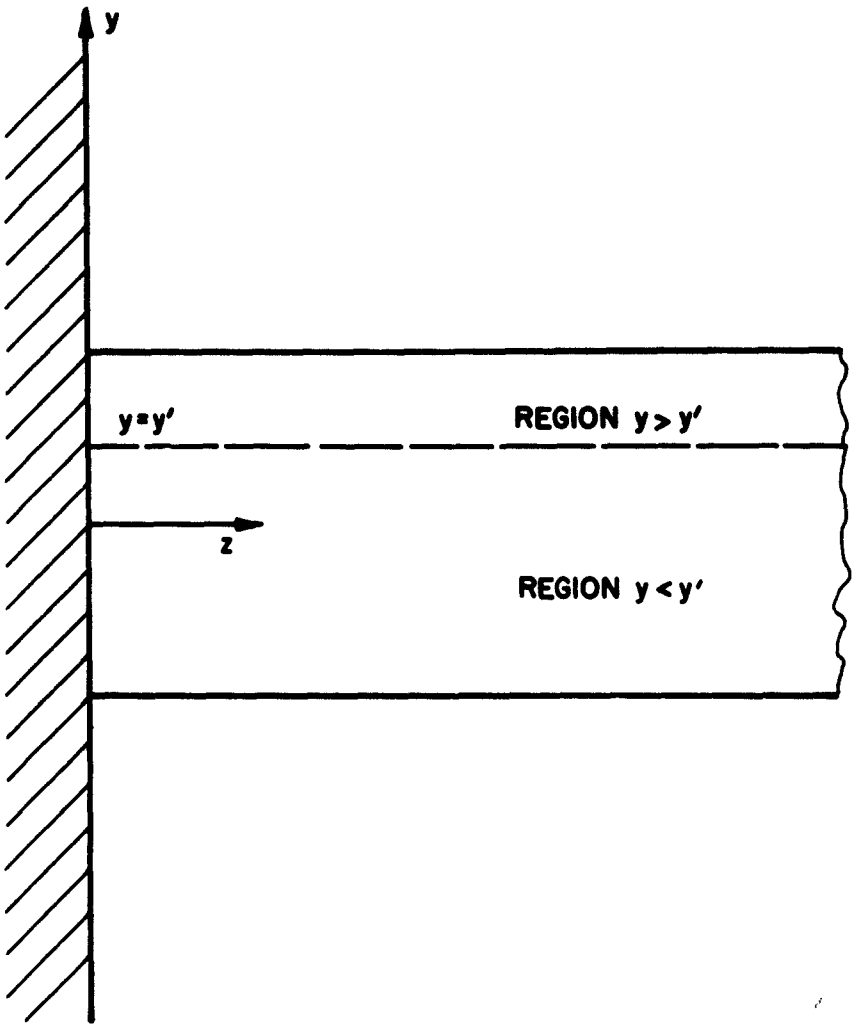

FIG. A.1 CALCULATION OF A-C ELECTRIC FIELDS ASSUMING A SHEET OF CURRENT AT y = y'.

Since the z-directed electric fields at y' associated with either H_{x1} or H_{x2} must be identical,

$$A = -B \tag{A.5}$$

and

$$i_1(y',z)\,dy' = 2A = -2B \ . \tag{A.6}$$

From Maxwell's equations

$$j\omega\epsilon_o E_{1z} = -\frac{\partial H_x}{\partial y} \ , \tag{A.7}$$

the z-directed electric field at (y,z) induced by a current sheet at (y',z) is therefore,

$$E_{1z}(y,z)_{y'} = -\frac{i_1(y',z)}{j2\omega\epsilon_o}\beta' e^{-\beta'|y-y'|}\,dy' \ , \tag{A.8}$$

and the total electric field at (y,z) is

$$E_{1z}(y,z) = \frac{e}{2j\omega\epsilon_o}\int_{-\infty}^{\infty}\int_{-\infty}^{\infty}\beta'\dot{z}'F_1(y',z,\dot{z}')\,e^{-\beta'|y-y'|}\,dy'\,d\dot{z}' \ . \tag{A.9}$$

This analysis assumes β' = constant, i.e., no acceleration.

A.II Potential Distribution of a Two-Dimensional Space-Charge-Limited Diode

Techniques similar to Langmuir's are employed to reduce Poisson's equation for a space-charge-limited two-dimensional diode to dimensionless form. Unfortunately, no general solution can be obtained corresponding to the one obtained in the one-dimensional case. Some arbitrary boundary conditions have to be applied to the top and bottom layers of the electron beam to facilitate obtaining a special solution.

For any sheet beam located at y with current flowing in the z-direction if the region between the cathode and the potential minima is

called Region I and the region beyond is Region II, the space-charge densities in respective regions are

$$\rho_I = -e\left[2\int_{\sqrt{\frac{-2eV}{m}}}^{v_o'} \frac{v_o F_o(v_o)dv_o}{v} + \int_{v_o'}^{\infty} \frac{v_o F_o(v_o)dv_o}{v}\right] ,$$

$$\rho_{II} = -e\int_{v_o'}^{\infty} \frac{v_o F_o(v_o)dv_o}{v} , \qquad (A.10)$$

where ρ = $\rho(y,z)$ space-charge density at (y,z),

$v^2(y,z)$ = $v_o^2 + 2hV(y,z)$; v is the velocity of electrons at (y,z) with v_o as initial velocity,

v_o = initial velocity of electrons,

v_o' = $\sqrt{-2hV'(y)}$, initial velocity of the slowest electrons in the layer located at y which possesses barely enough energy to reach the potential minimum,

$v_o F_o(v_o)dv_o$ = number of electrons emitted with their initial velocity between v_o and v_o+dv_o per unit area per second.

The initial velocities of the electrons emitted perpendicular to a thermionic cathode surface follow a Rayleigh distribution according to assumption 7 in Chapter II.

$$F_o(v_o)dv_o = -2\alpha I_{den.} v_o e^{-\alpha v_o^2} dv_o , \qquad (A.11)$$

$I_{den.}$ equals emission current density at the cathode. For an immersed flow diode, mixing of electrons originating from two different current

sheets is prohibited. If, in addition, the effect of collisions between electrons is neglected, Eqs. A.10 and A.11 may be combined to form

$$\rho_{\substack{I \\ II}} = 2\alpha I_{den.} \exp\left[\frac{2e\alpha V}{m}\right]\left\{\int_0^{\infty} e^{-v^2}\frac{dv}{\sqrt{\alpha}} \pm \int_0^{\sqrt{2h(V-V')\alpha}} e^{-v^2}\frac{dv}{\alpha}\right\} \tag{A.12}$$

or

$$\rho_{\substack{I \\ II}} = \sqrt{\alpha\pi}\ I_{den.} \exp\left[\frac{2e\alpha V}{m}\right]\left\{1 \pm \operatorname{erf}\sqrt{\frac{2\alpha e}{m}(V-V')}\right\} .$$

Poisson's equation may then be expressed in dimensionless variables.

$$\frac{\partial^2\eta(\zeta,\xi)}{\partial\xi^2} + \frac{\partial^2\eta(\zeta,\xi)}{\partial\zeta^2} + \frac{\partial^2\eta_m(\zeta)}{\partial\zeta^2} = \frac{1}{2}\frac{I_{den.}}{|I_o|}\exp(\eta+\eta_m)\left[1 \pm \operatorname{erf}\sqrt{\eta}\right] , \tag{A.13}$$

where $\eta_m(\zeta) = \frac{2e\alpha V'}{m}$,

the "±" signs are for Regions I and II respectively.

A.III A-c Transport Equation in Dimensionless Parametric Form

After the introduction of the excess energy parameter W, Eq. 2.6 is reduced by one term.

$$j\omega F_1(y,z,W) \pm \left\{W + 2h[V(y,z) - V'(y)]\right\}^{1/2} \left\{ \frac{\partial F_1(y,z,W)}{\partial z} \right.$$

$$\left. + \frac{\partial F_1(y,z,W)}{\partial W} \cdot \frac{\partial W}{\partial z} - 2hE_o(y,z) \frac{\partial F_1(y,z,W)}{\partial W} \right\} \mp 2hE_1(y,z) \left\{W + 2h[V(y,z) \right.$$

$$\left. - V'(y)]\right\}^{1/2} \frac{\partial F_o(y,z,W)}{\partial W} = 0 \quad , \quad (A.14)$$

where $W = \dot{z}^2 - 2h[V(y,z) - V'(y)]$.

But

$$\frac{\partial W}{\partial z} = -2h \frac{\partial V(y,z)}{\partial z}$$

$$= 2hE_o(y,z) \quad . \quad (A.15)$$

The transport equation is therefore,

$$j\omega F_1(y,z,W) \pm \left\{W + 2h[V(y,z) - V'(y)]\right\}^{1/2} \frac{\partial F_1(y,z,W)}{\partial z}$$

$$\mp 2hE_1(y,z) \left\{W + 2h[V(y,z) - V'(y)]\right\}^{1/2} \frac{\partial F_o(y,z,W)}{\partial W} = 0 \quad . \quad (A.16)$$

This equation combines with Eq. 2.7 to form an a-c transport equation expressed in terms of the density functions alone.

$$\pm \frac{\partial F_1(y,z,W)}{\partial z} = \frac{-j\omega F_1(y,z,W)}{\sqrt{W + 2h[V(y,z) - V'(y)]}}$$

$$\pm \left[\frac{-he}{2j\omega\epsilon_o} \int_{-\infty}^{\infty}\int_{-\infty}^{\infty} \beta' F_1(y',z,W') e^{-\beta'|y-y'|}\, dy'\, dW'\right]\left[\pm \frac{\partial F_o(y,z,W)}{\partial W}\right] . \tag{A.17}$$

Each term in Eq. A.17 may be put into dimensionless form, yielding,

$$\frac{\partial F_1(y,z,W)}{\partial z} = \beta\alpha^{3/4} \cdot \alpha \frac{I_o}{e} \cdot \frac{\partial P_1(\zeta,\xi,w)}{\partial \xi}$$

$$= \frac{\beta\alpha^{7/4} I_o}{e} \frac{\partial P_1(\zeta,\xi,w)}{\partial \xi} , \tag{A.18}$$

$$\frac{j\omega F_1(y,z,W)}{\sqrt{W + 2h[V(y,z) - V'(y)]}} = \frac{j\beta\alpha^{1/4} g \cdot \alpha \frac{I_o}{e} P_1(\zeta,\xi,w)}{\sqrt{\frac{w}{\alpha} + \frac{\eta(\zeta,\xi)}{\alpha}}}$$

$$= \frac{\beta\alpha^{7/4} I_o}{e} \frac{jgP_1(\zeta,\xi,w)}{\sqrt{w+\eta(\zeta,\xi)}} \tag{A.19}$$

and

$$\frac{he}{2j\omega\epsilon_o} \int_{-\infty}^{\infty}\int_{-\infty}^{\infty} \beta' F_1(y',z,W') e^{-\beta'|y-y'|}\, dy'\, dW' \cdot \frac{\partial F_o(y,z,W)}{\partial W}$$

$$= \frac{he}{2j\epsilon_o} \int_{-\infty}^{\infty}\int_{-\infty}^{\infty} \frac{P_1(\zeta',\xi,w)\exp\left[\frac{-g|\zeta-\zeta'|}{\sqrt{w(\zeta',\xi)+(\zeta',\xi)}}\right] d\zeta'\, dw}{\sqrt{w(\zeta',\xi)+\eta(\zeta',\xi)}}$$

$$\cdot \frac{\left(\alpha \frac{I_o}{e}\right)^{1/\alpha}}{\beta\alpha^{3/4}} \cdot \frac{\partial P_o(\zeta,\xi,w)}{\partial w_+} \cdot \left(\alpha \frac{I_o}{e}\right) \cdot \alpha$$

$$= -\frac{\beta\alpha^{7/4} I_o}{e}\left(\frac{1}{j8\sqrt{\pi}}\right) \int_{-\infty}^{\infty}\int_{-\infty}^{\infty} \frac{P_1(\zeta',\xi,w)\exp\left[\frac{-g|\zeta-\zeta'|}{\sqrt{w(\zeta',\xi)+\eta(\zeta',\xi)}}\right] d\zeta' dw}{\sqrt{w(\zeta',\xi)+\eta(\zeta',\xi)}}$$

$$\cdot \frac{\partial P_o(\zeta,\xi,w)}{\partial w} \quad . \quad \text{(A.20)}$$

The transport equation in dimensionless form is therefore,

$$\pm \frac{\partial P_1(\zeta,\xi,w)}{\partial \xi} = -\frac{jgP_1(\zeta,\xi,w)}{\sqrt{w+\eta(\zeta,\xi)}}$$

$$- \left\{\pm \frac{1}{j8\sqrt{\pi}} \int_{-\infty}^{\infty}\int_{-\infty}^{\infty} \exp\left[\frac{-g|\zeta-\zeta'|}{\sqrt{w(\zeta',\xi)+\eta(\zeta',\xi}}\right]\right.$$

$$\left. \cdot \frac{P_1(\zeta',\xi,w)}{\sqrt{w(\zeta',\xi)+\eta(\zeta',\xi)}}\, dw d\zeta'\right\} \left\{\pm \frac{\partial P_o(\zeta,\xi,w)}{\partial w}\right\} \quad . \quad \text{(A.21)}$$

A.IV Singularities in the A-c Density Functions

In a diode in which electrons have a half-Maxwellian velocity distribution, the d-c component of the density function may be expressed as

$$F_o(y,z,W) = -\frac{2\alpha I_o(y)}{e}\left\{\left[S(\alpha W_+ + \eta_c) - S(W_+)\right]^+ e^{-\alpha W_+} + S(W_+)\, e^{-\alpha W_+} + \left[S(\alpha W_- + \eta_c) - S(W_-)\right]^- e^{-\alpha W_-}\right\}, \quad (A.22)$$

where $W_+ \triangleq$ W for the forward going electrons, $\dot{z} \geq 0$,

$W_- \triangleq$ W for the backward going electrons, $\dot{z} < 0$,

η_c = the dimensionless potential parameter at the cathode,

$S(\alpha W_\pm + \eta_c)$ = a unit step function, and

$S(\alpha W_\pm + \eta_c) = 1$ for $\alpha W_\pm \geq \eta_c$,

$= 0$ for $\alpha W_\pm < \eta_c$.

The "±" superscripts of the square brackets correspond to the forward going and the backward going electrons respectively, and these two brackets vanish in the region beyond the potential minimum. Due to the existence of a step function, or step functions in the d-c density functions, one or more singularities are expected in any function involving the derivative of $F_o(y,z,W)$ depending on the discreteness of the velocity spectrum employed. If the d-c density function is reduced to dimensionless forms,

$$P_o(\zeta,\xi,w) = -2\left\{S(w_+)e^{-w_+} + \left[S(w_+ + \eta_c) - S(w_+)\right]^+ e^{-w_+} + \left[S(w_- + \eta_c) - S(w_-)\right]^- e^{-w_-}\right\}\frac{I_o(\zeta)}{I}, \quad (A.23)$$

The derivative of $P_o(\zeta,\xi,w)$ with respect to w_+ may be obtained in Dirac delta function form.

$$\frac{\partial P_o(\zeta,\xi,w)}{\partial w_+} = -\frac{2I_o(\zeta)}{I_o}\left\{\left[\delta(w_+) - S(w_+)\right] e^{-w_+}\right.$$

$$+\left[\delta(w_+ + \eta_c) - \delta(w_+) - S(w_+ + \eta_c) + S(w_+)\right]^{+} e^{-w_+}$$

$$\left.-\left[\delta(w_- + \eta_c) - \delta(w_-) - S(w_- + \eta_c) + S(w_-)\right]^{-} e^{-w_-}\right\}, \quad (A.24)$$

where $\delta(w)$ is a Dirac delta function.

A.V Kinetic Potential

If the definitions of the a-c and d-c density functions are substituted into the expression of Chu's kinetic potential V_1, the invariant characteristic over a d-c velocity jump gap is found missing once velocity spread is considered. However, a generalized form of this equivalent voltage fluctuation may be derived if the problem is approached from the energy standpoint.

In a two-dimensional multivelocity electron beam, the kinetic potential (or equivalent a-c voltage) V_1 of a sheet beam at y may be defined as the a-c energy expressed in electron volts.

$$V_1(y,z) \equiv -\frac{1}{2h}\left[-\frac{e}{I(y)}\int_0^{\infty} \dot{z}^3\left[F_o(y,z,\dot{z}) + F_1(y,z,\dot{z})\right]d\dot{z}\right.$$

$$\left.+\frac{e}{I_o(y)}\int_0^{\infty} \dot{z}^3\left[F_o(y,z,\dot{z})\right]dz\right], \quad (A.25)$$

where $I_o(y) = -\frac{e}{2} \int F_o(y,z,W)dW$,

$$I(y) = I_o(y) + I_1(y) ,$$

$$= -\frac{e}{2} \int_0^\infty F_o(y,z,W)dW - \frac{e}{2} \int_0^\infty F_1(y,z,W)dW ,$$

= current density of the beam layer at y.

The subscripts "0" and "1" are for d-c and a-c quantities respectively.

$$V_1(y,z) \cong \frac{e}{4h} \frac{1}{[I_o(y)]^2} \left[I_o(y) \int_0^\infty [W + 2\eta V(y,z)] F_1(y,z,W)dW \right.$$

$$\left. - I_1(y) \int_0^\infty [W + 2\eta V(y,z)] F_o(y,z,W)dW \right] \quad (A.26)$$

and

$$V_1(y,z) = \frac{e}{4hI_o(y)} \left[\int_0^\infty WF_1(y,z,W)dW \right.$$

$$\left. + \frac{\frac{e}{2} \int_0^\infty F_1(y,z,W)dW \int_0^\infty WF_o(y,z,W)dW}{I_o(y)} \right]$$

$$= \frac{e}{4hI_o(y)} \int_0^\infty (W+\bar{W}) F_1(y,z,W)dW , \quad (A.27)$$

where $\bar{W} = \frac{e}{2I_o(y)} \int_0^\infty \cdot WF_o(y,z,W)dW$.

A.VI Evaluation of the Weighting Factor R(ζ,w)

Evaluation of the weighting factor R(ζ,w) for the homogeneous part of the a-c density functions for an electron beam with a continuous velocity spectrum may be carried out in the following fashion. If the weighting factor R(ζ,w) is made up of two factors A(ζ) and e^{-w}, each a function of a single variable, by means of the shot noise formula and Eq. 2.18 for unit a-c current input per unit bandwidth, the following relationship may be derived.

$$2e|I_o(\zeta)|\Delta\zeta = \langle i_1^2(\zeta,0)\rangle$$

$$= \int_0^\infty R(\zeta,w)(\Delta\zeta)^2\,dw \qquad (A.28)$$

or

$$R(\zeta,w) = \frac{2e|I_o(\zeta)|}{\Delta\zeta}\,e^{-w} \quad . \qquad (A.29)$$

The value of the weighting factor R(ζ,w) thus obtained also satisfies the boundary conditions of the kinetic potential at the cathode. From Eq. 2.24

$$\langle V_1^2(\zeta,0)\rangle = \left(\frac{kT_c I_o}{eI_o(\zeta)}\right)^2 \int_0^\infty (w^2-2w+1)\,\frac{1}{I_o^2}\,R(\zeta,w)\,dw$$

$$= \left(\frac{kT_c I_o}{eI_o(\zeta)}\right)^2 \int_0^\infty (w^2-2w+1)\,\frac{2e|I_o(\zeta)|}{I_o^2\,\Delta\zeta}\,e^{-w}\,dw$$

$$= \frac{(2kT_c)^2}{2e|I_o(\zeta)|\Delta\zeta} \qquad (A.30)$$

and

$$< V_1(\zeta,0)\ i_1^*(\zeta,0) > \ = \ 0 \quad . \tag{A.31}$$

Similarly, the kinetic power theorem for the electron beam as a whole may also be verified.

$$< V(0)\ i^*(0) > \ = \ 0 \quad . \tag{A.32}$$

A.VII Points of Reflections

In the vicinity of the reflection points where $w+\eta$ approaches zero as a limit, the first term on the right-hand side of Eq. 2.15 in Chapter II tends to become infinity. It is necessary to show that the incremental change of $\rho_1(\zeta,\xi,w)$ stays in bound at the reflection points and the transport equation by itself is valid anywhere in the diode. If digital techniques are not employed in the numerical calculations, the assumption of $w+\eta \geq 0.002$ is absolutely unnecessary.

On the right-hand side of Eq. 2.15, all terms except the first one drop out in the neighborhood of a reflection point for a velocity class w_i leaving

$$\pm \left[\frac{dp_1(\zeta,\xi,w_i)}{d\xi} \right]_{w_i} \ = \ \frac{-j\beta p_1(\zeta,\xi,w_i)}{\sqrt{w_i + \eta(\zeta,\xi)}} \tag{A.33}$$

or

$$\pm \frac{dp_1(\zeta,\xi,w_i)}{p_1} \ = \ \frac{-j\beta d\xi}{\sqrt{w_i + \eta(\zeta,\xi)}} \quad , \tag{A.34}$$

where $\lim_{\xi \to \xi_r} w_i + \eta(\zeta,\xi) \to 0.$

As an example, the potential distribution curve for a one-dimensional beam is approximately

$$\eta(\xi) = \frac{1}{4}\xi^2 + 0.045\,\xi^4 + 0.0045\,\xi^6 \quad . \tag{A.35}$$

Equations A.34 and A.35 combine to give

$$\pm \frac{dp_1(\zeta,\xi,w_1)}{p_1(\zeta,\xi,w_1)} \cong \frac{-jgd\xi}{\sqrt{\frac{1}{4}(\xi^2-\xi_r^2) + 0.045(\xi^4-\xi_r^4)}} \quad , \tag{A.36}$$

$$\int_{p_{1,r}}^{p_{1,r+1}} \frac{dp_1(\zeta,\xi,w_1)}{p_1(\zeta,\xi,w_1)} \cong \int_{\xi_r}^{\xi_r+\Delta\xi} \frac{-jgd\xi}{\frac{1}{2}\sqrt{\xi^2 - \xi_r^2}} \quad , \tag{A.37}$$

$$\lim_{\xi \to \xi_r} \pm \ln \frac{p_{1,r+1}}{p_{1,r}} \cong -j2g \ln \left\{ \frac{\xi_r + \Delta\xi + \sqrt{(\xi_r+\Delta\xi)^2 - \xi_r^2}}{\xi_r} \right\}$$

$$= -j2g \frac{\sqrt{\Delta\xi}}{\xi_r} \left\{ \sqrt{\Delta\xi} + \sqrt{2\xi_r} \left(1 + \frac{\Delta\xi}{4\xi_r}\right) \right\} \quad , \tag{A.38}$$

$$\lim_{\xi \to \xi_r} p_{1,r+1} = p_{1,r} \exp\left[\mp j2g \left(\sqrt{\frac{2\Delta\xi}{\xi_r}} + \frac{\Delta\xi}{\xi_r} \right) \right] \tag{A.39}$$

or

$$\lim_{\substack{\xi \to \xi_r \\ \Delta\xi \to 0}} p_{i,r+1} = p_{i,r} \quad , \tag{A.40}$$

that is, the incremental change of p_i is zero when $\eta + w_i \to 0$ for the w_i velocity class.

APPENDIX B. POTENTIAL DISTRIBUTION IN A TWO-DIMENSIONAL DIODE AND GENERAL HARMONIC ANALYSIS

B.I The D-c Electric Field and Potential Distribution

Within a two-dimensional discrete-beam diode like the model employed in the density function method of noise transport investigation, it is possible to solve Poisson's equation for the instantaneous space-charge potential distribution if the solutions of a set of Laplace equations in Dirichlet form corresponding to the space-charge distribution in the diode are superposed on each other. Unlike the point charge assumption in a real three-dimensional model, electron are taken to be infinitely long uniform line charges extended in the x-direction. For a line charge located at (y_o,z_o), Poisson's equation may be written as

$$\nabla^2 V(y,z) = -\int_0^a \int_{-\infty}^{\infty} \frac{\rho_\ell}{\epsilon_o} \delta(z-z_o)\, \delta(y-y_o)\, dy\, dz \quad , \qquad (B.1)$$

where $V(y,z)$ = the d-c potential at (y,z),

a = the distance between the cathode and the anode,

ρ_ℓ = the charge per unit length in the x-direction,

$\delta(z-z_o) = \infty$ at $z = z_o$,

$= 0$ for $z \neq z_o$,

$\delta(y-y_o) = \infty$ at $y = y_o$,

$= 0$ for $y \neq y_o$,

$$\int_{-\infty}^{\infty} \delta(y-y_o)dy = 1,$$

$$\int_{-\infty}^{\infty} \delta(z-z_o)dz = 1,$$

with the following boundary conditions

$$V(0,y) = 0 \ , \tag{B.2a}$$

$$V(a,y) = 0 \ , \tag{B.2b}$$

$$V(z,\pm\infty) = 0 \ , \tag{B.2c}$$

$$\left.\frac{\partial V(z,y_o)}{\partial y}\right|_{y<y_o} - \left.\frac{\partial V(z,y_o)}{\partial y}\right|_{y>y_o} = \frac{\rho_\ell}{\epsilon_o}\,\delta(z-z_o) \ . \tag{B.2d}$$

If the Laplace equation is to be solved by the separation of variables method, a general solution of the potential function $V(z,y)$ is found such that

$$V(y,z) = \sum_n A_n \sin\frac{n\pi z}{a} \exp\left(\mp \frac{n\pi(y-y_o)}{a}\right) \ , \tag{B.3}$$

where the "-" sign is for the region $y > y_o$,

"+" sign is for the region $y < y_o$, from symmetry.

The Fourier coefficients A_n may be evaluated by means of the boundary condition of Eq. B.2d.

$$2A_n \int_0^a \frac{n\pi}{a} \sin^2\frac{n\pi z}{a}\,dz = \frac{\rho_\ell}{\epsilon_o} \int_0^a \delta(z-z_o) \sin\frac{n\pi z}{a}\,dz \tag{B.4}$$

or

$$A_n = \frac{\rho_\ell}{\epsilon_o} \cdot \frac{1}{n\pi} \sin\frac{n\pi z_o}{a} \tag{B.5}$$

and therefore

$$V = \sum_n \frac{\rho_\ell}{n\pi\epsilon_o} \sin\frac{n\pi z}{a} \sin\frac{n\pi z_o}{a} \exp\left[\mp \frac{n\pi}{a}(y-y_o)\right] \ . \tag{B.6}$$

Unfortunately, the Fourier series representation of potential distribution function V thus obtained is not differentiable at some boundaries where term-by-term differentiation of V(y,z) results in a divergent series. The electric field is not uniquely determined at z = 0 and z = a.

In order to arrive at a unique solution at all boundaries, the image method is employed to solve for the z-directed d-c electric fields instead. A line charge ρ_ℓ is placed at (y_o,z_o) between two infinitely extended conducting plates which are perpendicular to the z-axis and separated by a distance a. If both electrodes are kept at zero potential, the potential relative to either plate at a point (y,z) inside the diode due to the influence of the line charge may be computed by linear addition of the space-charge effects from the line charge itself and its infinite number of mirror images shown in Fig. B.1.

$$V(y,z) = \sum_{n=-\infty}^{\infty} \frac{-\rho_\ell}{2\pi\epsilon_o} \ln\sqrt{(z-2na-z_o)^2 + (y-y_o)^2}$$

$$+ \sum_{n=-\infty}^{\infty} \frac{\rho_\ell}{2\pi\epsilon_o} \ln\sqrt{(z-2na+z_o)^2 + (y-y_o)^2}$$

$$= \sum_{-\infty}^{\infty} \frac{\rho_\ell}{2\pi\epsilon_o} \ln \sqrt{\frac{(z-2na+z_o)^2 + (y-y_o)^2}{(z-2na-z_o)^2 + (y-y_o)^2}}$$

$$= \frac{\rho_\ell}{4\pi\epsilon_o} \ln\left[\frac{(z+z_o)^2 + (y-y_o)^2}{(z-z_o)^2 + (y-y_o)^2}\right] + \frac{\rho_\ell}{4\pi\epsilon_o} \sum_{-\infty}^{-1} \ln\left[\frac{(z+z_o-2na)^2 + (y-y_o)^2}{(z-z_o-2na)^2 + (y-y_o)^2}\right]$$

$$+ \frac{\rho_\ell}{4\pi\epsilon_o} \sum_{n=1}^{\infty} \ln\left[\frac{(z+z_o-2na)^2 + (y-y_o)^2}{(z-z_o-2na)^2 + (y-y_o)^2}\right]. \quad (B.7)$$

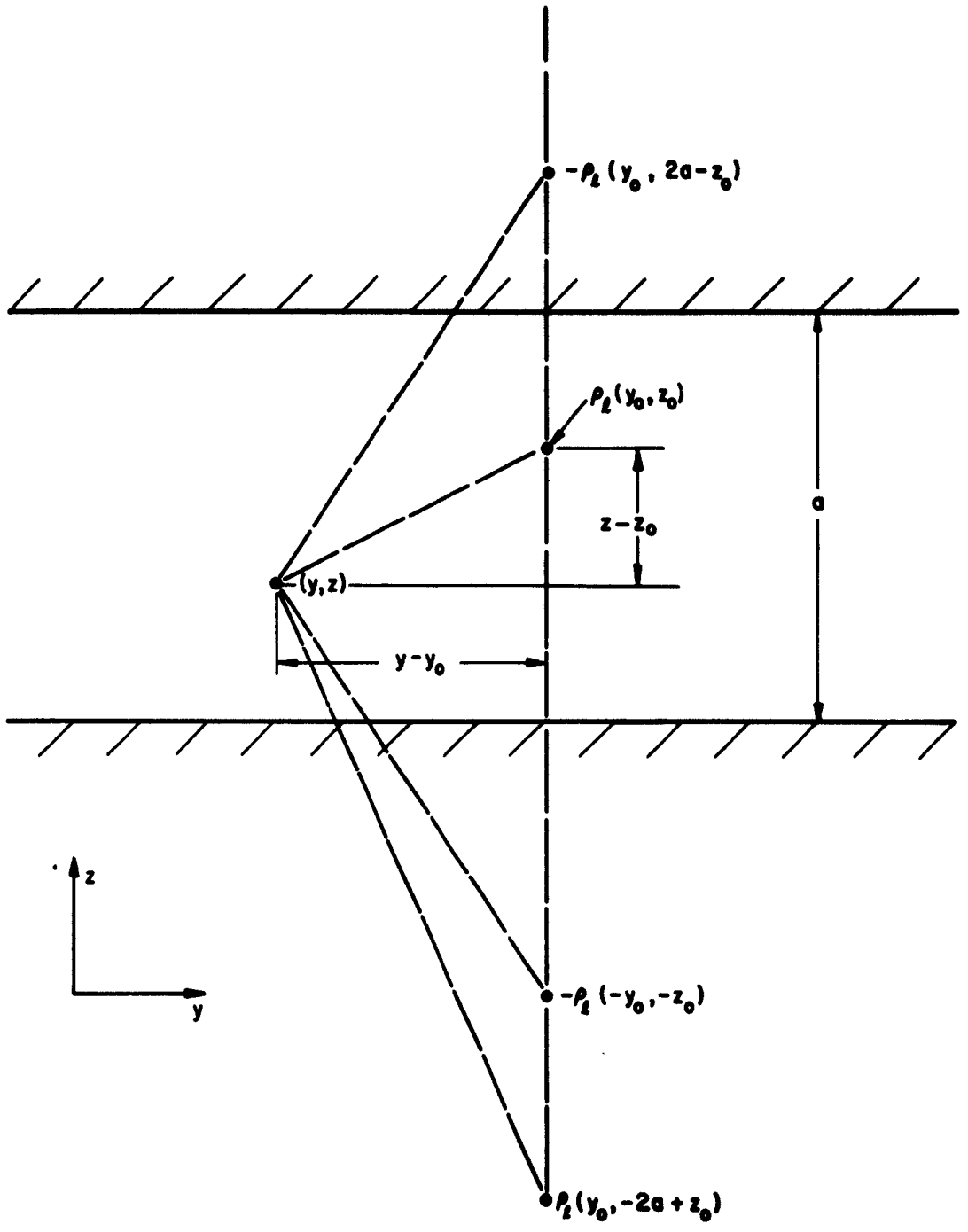

FIG. B.1 ELECTRIC FIELD DUE TO A LINE CHARGE BETWEEN TWO INFINITELY EXTENDED PARALLEL ELECTRODES.

Because $(y-y_o)^2 \ll (2na)^2$ for $n \neq 0$

$$V(y,z) \cong \frac{\rho_\ell}{4\pi\epsilon_o}\left\{ \ell n\left[\frac{(z+z_o)^2 + (y-y_o)^2}{(z-z_o)^2 + (y-y_o)^2}\right] + 2\sum_{n=-\infty}^{-1} \ell n\left[\frac{z+z_o-2na}{z-z_o-2na}\right] \right.$$

$$\left. + 2\sum_{n=1}^{\infty} \ell n\left[\frac{z+z_o-2na}{z-z_o-2na}\right]\right\} . \quad (B.8)$$

The series on the right-hand side are uniformly convergent as shown in Section B.I.1. As an approximation the summations may be replaced by integrals in which n is regarded as a continuous integration variable.

$$V(y,z) \simeq \frac{\rho_\ell}{4\pi\epsilon_o}\left\{ \ell n\left[\frac{(z+z_o)^2+(y-y_o)^2}{(z-z_o)^2+(y-y_o)^2}\right] + \ell n\left(\frac{z+z_o-2a}{z-z_o-2a}\right)\right.$$

$$+\frac{2}{2a}\int_{n=1}^{n=\infty} \ell n\left[\frac{(z+z_o)-2na}{(z-z_o)-2na}\right] d(2na) + \ell n\left(\frac{z+z_o+2a}{z-z_o+2a}\right)$$

$$\left.+\frac{2}{2a}\int_{n=-\infty}^{n=-1} \ell n\left[\frac{2na-(z+z_o)}{2na-(z-z_o)}\right] d(2na)\right\}$$

$$\simeq \frac{\rho_\ell}{4\pi\epsilon_o}\left\{ \ell n\left[\frac{(z+z_o)^2+(y-y_o)^2}{(z-z_o)^2+(y-y_o)^2}\right] + \ell n\left[\frac{(2a)^2-(z+z_o)^2}{(2a)^2-(z-z_o)^2}\right]\right.$$

$$+\frac{1}{a}\lim_{T\to\infty}\int_{n=1}^{n=T} \ell n\left[\frac{(z+z_o)-2na}{(z-z_o)-2na}\right] d(2na)$$

$$\left.-\frac{1}{a}\lim_{T\to\infty}\int_{n=T}^{n=1} \ell n\left[\frac{2na+z+z_o}{2na+z-z_o}\right] d(2na)\right\} . \qquad (B.9)$$

But,

$$\frac{1}{a}\int_{n=1}^{n=T} \ln\left[\frac{2na-(z+z_o)}{2na-(z-z_o)}\right] d(2na) = \frac{1}{a}\left\{ [2na-(z+z_o)]\ \ln[2na-(z+z_o)] \right.$$

$$\left. - [2na-(z+z_o)] \right\} - \frac{1}{a}\left\{ [2na-(z-z_o)]\ \ln[2na-(z-z_o)] - [2na-(z-z_o)] \right\}$$

$$= \frac{1}{a}\left\{ [2Ta-(z+z_o)]\ \ln[2Ta-(z+z_o)] - [2Ta-(z+z_o)] \right.$$

$$- [2a-(z+z_o)]\ \ln[2a-(z+z_o)] + [2a-(z+z_o)]$$

$$- [2Ta-(z-z_o)]\ \ln [2Ta-(z-z_o)] + [2Ta-(z-z_o)]$$

$$\left. + [2a-(z-z_o)]\ \ln[2a-(z-z_o)] - [2a-(z-z_o)] \right\}$$

$$= \frac{1}{a}\left\{ [2Ta-(z+z_o)]\ \ln[2Ta-(z+z_o)] - [2Ta-(z-z_o)]\ \ln[2Ta-(z-z_o)] \right.$$

$$\left. - [2a-(z+z_o)]\ \ln[2a-(z+z_o)] + [2a-(z-z_o)]\ \ln[2a-(z-z_o)] \right\} . \quad (B.10)$$

Similarly,

$$\frac{1}{a}\int_{n=1}^{n=T} \ln\left[\frac{2na+(z+z_o)}{2na+(z-z_o)}\right] d(2na) = \frac{1}{a}\left\{ [2Ta+(z+z_o)]\ \ln[2Ta+(z+z_o)] \right.$$

$$- [2Ta+(z-z_o)]\ \ln[2Ta+(z-z_o)] - [2a+(z+z_o)]\ \ln[2a+(z+z_o)]$$

$$\left. + [2a+(z-z_o)]\ \ln[2a+(z-z_o)] \right\} . \quad (B.11)$$

The last two terms combine to give

$$\lim_{T\to\infty}\left\{\frac{1}{a}\int_{n=1}^{n=T} \ell n\left[\frac{2na-(z+z_o)}{2na-(z-z_o)}\right] d(2na) + \frac{1}{a}\int_{n=1}^{n=T} \ell n\left[\frac{2na+z+z_o}{2na+z-z_o}\right] d(2na)\right\}$$

$$= \lim_{T\to\infty}\frac{1}{a}\left\{2Ta\ \ell n\left[\frac{[2Ta-(z+z_o)][2Ta+(z+z_o)]}{[2Ta-(z-z_o)][2Ta+(z-z_o)]}\right]\right.$$

$$+ (z+z_o)\ \ell n\left[\frac{2Ta+(z+z_o)}{2Ta-(z+z_o)}\right] + (z+z_o)\ \ell n\left[\frac{2a-(z+z_o)}{2a+(z+z_o)}\right]$$

$$+ (z-z_o)\ \ell n\left[\frac{2Ta-(z-z_o)}{2Ta+(z-z_o)}\right] + (z-z_o)\ \ell n\left[\frac{2a+(z-z_o)}{2a-(z-z_o)}\right]$$

$$\left. + 2a\ \ell n\left[\frac{[2a-(z-z_o)][2a+(z-z_o)]}{[2a-(z+z_o)][2a+(z+z_o)]}\right]\right\}$$

$$= 2\ \ell n\left[\frac{(2a)^2-(z-z_o)^2}{(2a)^2-(z+z_o)^2}\right] + \frac{z}{a}\ \ell n\left[\frac{[2a+(z-z_o)][2a-(z+z_o)]}{[2a-(z-z_o)][2a+(z+z_o)]}\right]$$

$$+ \frac{z_o}{a}\ \ell n\left[\frac{[2a-(z+z_o)][2a-(z-z_o)]}{[2a+(z+z_o)][2a+(z-z_o)]}\right] . \qquad \text{(B.12)}$$

The potential at (y,z) is therefore

$$V(y,z) = \frac{\rho_\ell}{4\pi\epsilon_o}\left\{ \ell n\left[\frac{(z+z_o)^2 + (y-y_o)^2}{(z-z_o)^2 + (y-y_o)^2} \right] + \ell n\left[\frac{(2a)^2 - (z-z_o)^2}{(2a)^2 - (z+z_o)^2} \right] \right.$$

$$+ \frac{z}{a}\,\ell n\left[\frac{[2a+(z-z_o)][2a-(z+z_o)]}{[2a-(z-z_o)][2a+(z+z_o)]} \right]$$

$$\left. + \frac{z_o}{a}\,\ell n\left[\frac{[2a-(z+z_o)]}{[2a+(z+z_o)]}\,\frac{[2a-(z-z_o)]}{[2a+(z-z_o)]} \right] \right\} . \quad (B.13)$$

For $z+z_o \leq 0.2a$

$$\ell n\left[\frac{(2a)^2 - (z-z_o)^2}{(2a)^2 - (z+z_o)^2} \right] \simeq \ell n\left[1 - \left(\frac{z-z_o}{2a} \right)^2 + \left(\frac{z+z_o}{2a} \right)^2 + \ldots \right]$$

$$\approx \left(\frac{z+z_o}{2a} \right)^2 - \left(\frac{z-z_o}{2a} \right)^2 = \frac{4zz_o}{4a^2} = \frac{zz_o}{a^2} , \quad (B.14)$$

$$\frac{z}{a}\,\ell n\left[\frac{[2a+(z-z_o)][2a-(z+z_o)]}{[2a-(z-z_o)][2a+(z+z_o)]} \right] = \frac{z}{a}\,\ell n\left[\frac{\left(1 + \frac{z-z_o}{2a}\right)\left(1 - \frac{z+z_o}{2a}\right)}{\left(1 - \frac{z-z_o}{2a}\right)\left(1 + \frac{z+z_o}{2a}\right)} \right]$$

$$= \frac{z}{a}\,\ell n\left[\left(1 + \frac{z-z_o}{a}\right)\left(1 - \frac{z+z_o}{a}\right) \right] = \frac{z}{a}\,\ell n\left[1 + \frac{z-z_o}{a} - \frac{z+z_o}{a} + \ldots \right]$$

$$= \frac{z}{a}\,\ell n\left[1 - \frac{2z_o}{a} \right] \approx \frac{-2zz_o}{a} , \quad (B.15)$$

$$\frac{z_o}{a} \ln \left[\frac{[2a-(z+z_o)][2a-(z-z_o)]}{[2a+(z+z_o)][2a+(z-z_o)]} \right] = \frac{z_o}{a} \ln \left[\left(1 - \frac{z+z_o}{a}\right)\left(1 - \frac{z-z_o}{a}\right) \right]$$

$$= \frac{z_o}{a} \ln \left[1 - \frac{z+z_o}{a} - \frac{z-z_o}{a} \right] = \frac{z_o}{a} \ln \left[1 - \frac{2z}{a} \right]$$

$$= - \frac{2zz_o}{a^2} \quad . \tag{B.16}$$

The last three terms add up to be $-(3zz_o/a^2)$.

$$V(y,z)_{z+z_o \leq 0.2a} = \frac{\rho_\ell}{4\pi\epsilon_o} \left\{ \ln \left[\frac{(z+z_o)^2 + (y-y_o)^2}{(z-z_o)^2 + (y-y_o)^2} \right] - \frac{3zz_o}{a^2} \right\} \tag{B.17}$$

and

$$\left| \frac{3zz_o}{a^2} \right| \leq 0.12 \quad .$$

Since a majority of the electrons inside the diode at any moment are within 0.2a from the cathode, the simplified equation may help to save much computing time.

The d-c electric field at any point (y,z) may be derived by taking term-wise differentiation of the potential curve. E(y,z) due to a line change ρ_ℓ at (y_o,z_o) is then

$$E(y,z) = - \frac{\partial V}{\partial z}$$

$$= \sum_{n=-\infty}^{\infty} \frac{\rho_\ell}{2\pi\epsilon_o} \left[\frac{z-z_o-2na}{(z-2na-z_o)^2 + (y-y_o)^2} - \frac{z+z_o-2na}{(z+z_o-2na)^2 + (y-y_o)^2} \right] \quad .$$

(B.18)

For n approaches $\pm \infty$

$$E_n(y,z) = \frac{\rho_\ell}{2\pi\epsilon_o}\left\{\left[\frac{1}{z-z_o-2na} - \frac{1}{z+z_o-2na}\right] + \left[\frac{1}{z-z_o+2na} - \frac{1}{z+z_o+2na}\right]\right\}$$

$$= \frac{\rho_\ell}{2\pi\epsilon_o}\left\{\frac{z-z_o}{(z-z_o)^2 - (2na)^2} - \frac{z+z_o}{(z+z_o)^2 - (2na)^2}\right\} . \quad (B.19)$$

Each term is increasing with $1/(2na)^2$; as a result, $E(y,z)$ is a uniformly convergent series, validating the term-wise differentiation procedure. It also allows the replacement of part of the summation by an integration as an approximation, treating $E_n(y,z)$ as a continuous function of n.

$$E(y,z) = \frac{\rho_\ell}{2\pi\epsilon_o}\left\{\frac{z-z_o}{(z-z_o)^2 + (y-y_o)^2} - \frac{z+z_o}{(z+z_o)^2 + (y-y_o)^2}\right.$$

$$+ \sum_{n=-\infty}^{-1}\left[\frac{1}{z-z_o-2na} - \frac{1}{z+z_o-2na}\right]$$

$$\left. + \sum_{n=1}^{\infty}\left[\frac{1}{z-z_o-2na} - \frac{1}{z+z_o-2na}\right]\right\} , \quad (B.20)$$

$$E(y,z) = \frac{\rho_\ell}{2\pi\epsilon_o}\left\{ \frac{z-z_o}{(z-z_o)^2 + (y-y_o)^2} - \frac{z+z_o}{(z+z_o)^2 + (y-y_o)^2} \right.$$

$$+ \frac{1}{2}\left[\frac{1}{z-z_o+2a} - \frac{1}{z+z_o+2a} + \frac{1}{z-z_o-2a} - \frac{1}{z+z_o-2a} \right]$$

$$+ \int_{n=-\infty}^{n=-1} \left[\frac{1}{z-z_o-2na} - \frac{1}{z+z_o-2na} \right] dn$$

$$+ \int_{n=1}^{n=\infty} \left[\frac{1}{z-z_o-2na} - \frac{1}{z+z_o-2na} \right] dn$$

$$= \frac{\rho_\ell}{2\pi\epsilon_o}\left\{ (z-z_o)\left[\frac{1}{(z-z_o)^2 + (y-y_o)^2} + \frac{1}{(z-z_o)^2 - (2a)^2} \right] \right.$$

$$-(z+z_o)\left[\frac{1}{(z+z_o)^2 + (y-y_o)^2} + \frac{1}{(z+z_o)^2 - (2a)^2} \right] + \frac{1}{2a}\ell n \left[\frac{2na-(z+z_o)}{2na-(z-z_o)} \right]_{n=-\infty}^{-1}$$

$$\left. + \frac{1}{2a}\ell n \left[\frac{2na-(z+z_o)}{2na-(z-z_o)} \right]_{n=1}^{\infty} \right\} , \qquad (B.21)$$

$$E(y,z) = \frac{\rho_\ell}{2\pi\epsilon_o}\left\{ (z-z_o)\left[\frac{1}{(z-z_o)^2 + (y-y_o)^2} + \frac{1}{(z-z_o)^2 - (2a)^2} \right] \right.$$

$$- (z+z_o)\left[\frac{1}{(z+z_o)^2 + (y-y_o)^2} - \frac{1}{(z+z_o)^2 - (2a)^2} \right]$$

$$\left. + \frac{1}{2a}\ell n \left[\frac{(2a+z+z_o)\,[2a-(z-z_o)]}{(2a+z-z_o)\,[2a-(z+z_o)]} \right] \right\} . \qquad (B.22)$$

For $z+z_o \leq 0.2a$, some of the terms in Eq. B.22 may be dropped.

$$E(y,z) \cong \frac{\rho_\ell}{2\pi\epsilon_o} \left\{ \frac{z-z_o}{(z-z_o)^2 + (y-y_o)^2} - \frac{z+z_o}{(z+z_o)^2 + (y-y_o)^2} \right.$$

$$\left. + \frac{1}{2a} \ln \left[\frac{\left(1 + \frac{z+z_o}{2a}\right)\left(1 - \frac{z-z_o}{2a}\right)}{\left(1 + \frac{z-z_o}{2a}\right)\left(1 - \frac{z+z_o}{2a}\right)} \right] \right\}$$

$$\cong \frac{\rho_\ell}{2\pi\epsilon_o} \left\{ \frac{z-z_o}{(z-z_o)^2 + (y-y_o)^2} - \frac{z+z_o}{(z+z_o)^2 + (y-y_o)^2} \right.$$

$$\left. \frac{1}{2a} \ln \left[1 + \frac{z+z_o}{a} - \frac{z-z_o}{a} \right] \right.$$

$$\cong \frac{\rho_\ell}{2\pi\epsilon_o} \left\{ \frac{z-z_o}{(z-z_o)^2 + (y-y_o)^2} - \frac{z+z_o}{(z+z_o)^2 + (y-y_o)^2} + \frac{z_o}{a^2} \right\} . \quad (B.23)$$

B.I.1 Uniform Convergence of the Series Representation of the Potential Function V. Uniform convergence of the infinite series representing the potential V may be shown by taking the partial sum of the series for large n. The nth term V_n of the series is

$$V_n = \frac{\rho_\ell}{2\pi\epsilon_o}\left[\ell n \sqrt{\frac{(z-2na+z_o)^2 + (y-y_o)^2}{(z-2na-z_o)^2 + (y-y_o)^2}} + \ell n \sqrt{\frac{(z+2na+z_o)^2 + (y-y_o)^2}{(z+2na-z_o)^2 + (y-y_o)^2}}\right]$$

$$= \frac{\rho_\ell}{2\pi\epsilon_o}\ell n \left[\frac{\left(\frac{z+z_o}{2na} - 1\right)^2 + \left(\frac{y-y_o}{2na}\right)^2}{\left(\frac{z-z_o}{2na} - 1\right)^2 + \left(\frac{y-y_o}{2na}\right)^2} \cdot \frac{\left(\frac{z+z_o}{2na} + 1\right)^2 + \left(\frac{y-y_o}{2na}\right)^2}{\left(\frac{z-z_o}{2na} + 1\right)^2 + \left(\frac{y-y_o}{2na}\right)^2}\right]$$

$$\simeq \frac{\rho_\ell}{2\pi\epsilon_o}\ell n \left[\frac{1 - \frac{z+z_o}{2na}}{1 - \frac{z-z_o}{2na}} \cdot \frac{1 + \frac{z+z_o}{2na}}{1 + \frac{z-z_o}{2na}}\right]$$

$$\simeq \frac{\rho_\ell}{2\pi\epsilon_o}\ell n \left[\frac{1 - \left(\frac{z+z_o}{2na}\right)^2}{1 - \left(\frac{z-z_o}{2na}\right)^2}\right]$$

$$\simeq \frac{\rho_\ell}{2\pi\epsilon_o}\ell n \left[1 - \left(\frac{z+z_o}{2na}\right)^2 + \left(\frac{z-z_o}{2na}\right)^2\right]$$

$$\simeq \frac{\rho_\ell}{2\pi\epsilon_o}\left[\left(\frac{z-z_o}{2na}\right)^2 - \left(\frac{z+z_o}{2na}\right)^2\right]$$

$$\simeq \frac{\rho_\ell}{2\pi\epsilon_o}\ \frac{-4zz_o}{4n^2a^2}$$

$$\simeq \frac{-\rho_\ell}{2\pi\epsilon_o}\ \frac{zz_o}{n^2a^2} \quad . \qquad \text{(B.24)}$$

Since V_n is proportional to $1/n^2$ for a given ϵ, there exists an n_o such that for $> n_o$, for all $n' > n$ and $a > 0$

$$\sum_{n > n_o}^{n'} \left| V_{\pm n} \right| < \epsilon \quad , \tag{B.25}$$

The series representing V is uniformly convergent.

B.I.2 Location of the Effective Centroids for the Electric Field and the Space-Charge Potential Distribution Calculations. In the vicinity of the cathode, the electric field experienced by a charged particle at (y,z) due to a line charge located at (y_o,z_o) is approximately

$$E(y,z) \simeq \frac{\rho_\ell(y_o,z_o)}{2\pi\epsilon_o} \left\{ \frac{z-z_o}{(z-z_o)^2 + (y-y_o)^2} - \frac{z+z_o}{(z+z_o)^2 + (y-y_o)^2} + \frac{z_o}{a^2} \right\}$$

$$\simeq \frac{\rho_\ell(y_o,z_o)}{2\pi\epsilon_o} \frac{2z_o}{z^2 - z_o^2} \tag{B.26}$$

for $y = y_o$. Now if the electric line charges are uniformly distributed inside a compartment of size Δz, the weighted centroid for the electric field computation at the edge of the compartment will deviate from the geometric centroid of the compartment considerably because of the manner by which the influences of the electrons are weighted.

$$\frac{2\bar{z}_o}{z^2 - \bar{z}_o^2} = \frac{\sum_{j=1}^{N} \frac{2z_{o,j}}{z^2 - z_{o,j}^2}}{N} \quad , \tag{B.27}$$

where $\bar{z}$ is the z-coordinate of the weighted centroid.

$\overline{z}_o \cong 0.066$ for $z = 1$ and $z_{oj} = 0.1, 0.2, 0.3 \ldots 0.9$

or

$$\overline{z}_o = \frac{2}{3}\Delta z \quad \text{for} \quad z > z_o$$

$$= \frac{1}{3}\Delta z \quad \text{for} \quad z < z_o \tag{B.28}$$

if $z - z_o < \Delta z$.

The weighting factor for the potential computations are also evaluated according to the average effect. From Eq. B.17, if $y = y_o$,

$$V(y,z) \cong \frac{\rho_\ell}{4\pi\epsilon_o} \cdot 2 \ln\left(\frac{z+z_o}{z-z_o}\right) . \tag{B.29}$$

Similar numerical approximation will yield an effective value of z_o for the potential distribution calculations.

$$\overline{z}_o = 0.45\,\Delta z \quad \text{for} \quad z < z_o ,$$

$$\overline{z}_o = 0.55\,\Delta z \quad \text{for} \quad z > z_o , \tag{B.30}$$

where $z - z_o < \Delta z$.

B.II Dimensions of the Two-Dimensional Diode

B.II.1 Physical Dimensions. The size and d-c characteristics c the diode employed in the Monte Carlo method of noise analysis are identical to those used in the density function method.

Cathode anode distance = 0.01852 cm

$V_{cathode} = 0$

$V_{anode} = 10$ volts

$T_c = 1160.6°$ Kelvin

Thickness of one layer of electron beam $\Delta y = 6.35 \times 10^{-4}$ cm

$I_{den.}$(emission current density) = -1.5 amp/cm^2.

B.II.2 Choice of Unit Electron Beam Area. Theoretically, a sample area may be selected to represent each layer of the electron beam. For an ergodic random process, the length of the time period over which statistical averages are taken is inversely proportional to the sample area, yet the computing time required for the d-c electric fields goes up as the square of the number of electrons inside the diode. As a result the sample area should be kept to a minimum so as to save time and, on the other hand, the average number of electrons emitted per time interval per unit sample area must be maintained large enough so that Poisson's distribution for electron emission may be applied effectively. Sample area ΔA is chosen here to be the square of a beam layer thickness

$$\Delta A = (\Delta y)^2 \quad . \tag{B.31}$$

For $\Delta t = 2 \times 10^{-12}$, the number of electrons emitted per time interval per unit area is

$$n = 7.5509 \text{ electrons.} \tag{B.32}$$

B.II.3 Choice of the Sizes of Compartments. The sizes of the compartments Δz_j are chosen subject to the following restrictions:

1. Δz_j must be large enough so that each compartment (i,j) contains enough electrons to make the fluctuations from the mean small.

2. It is also necessary to limit the sizes of the compartments to avoid unnecessary error in the computation of the d-c electric fields. Lumping of all charges at the centroid of a compartment is valid only if the separations between the electrons are small.

3. Δz_j should be small enough to assure that identical a-c electric fields are experienced by all the electrons inside the same compartment.

4. A final condition imposed upon the choice of Δz's is that

$$z_{min} > \Delta z > v_{avg} \Delta t$$

in the vicinity of the potential minimum.

As shown in Fig. B.2 there are a total of twenty-four compartments in each layer of the two-dimensional electron beam model and their dimensions are listed in the following table.

Table B.1

Compartment Size

Δz	Range	Number of Compartments
1.5×10^{-4} cm	$0 \leq z \leq 1.5 \times 10^{-3}$ cm	10
6.0×10^{-4} cm	$1.5 \times 10^{-3} \leq z \leq 4.5 \times 10^{-3}$ cm	5
1.5×10^{-3} cm	4.5×10^{-3} cm $\leq z \leq 1.65 \times 10^{-2}$ cm	8
0.02×10^{-3} cm	1.65×10^{-2} cm $\leq z \leq 1.852 \times 10^{-2}$ cm	1

B.III Velocity of Electrons

Fluctuations of the velocities at some preselected z-planes are recorded throughout the Monte Carlo calculations. During a time interval between t_i and $t_i + \Delta t$, the velocity of the ℓth electron at the z_n-plane and layer y_m is defined as $v_\ell(y_m, z_n, t_{ic})$.

For crossing to occur, it is necessary to have

$$z_\ell(t_i) \leq z_n ,$$

$$z_\ell(t_{i+1}) < z_n ,$$

where $z_\ell(t_i)$ is the position of the ℓth electron at t_i. Usually, $z_\ell(t_i) \geq z_{n-1}$ if the compartment sizes are adequately chosen, i.e.,

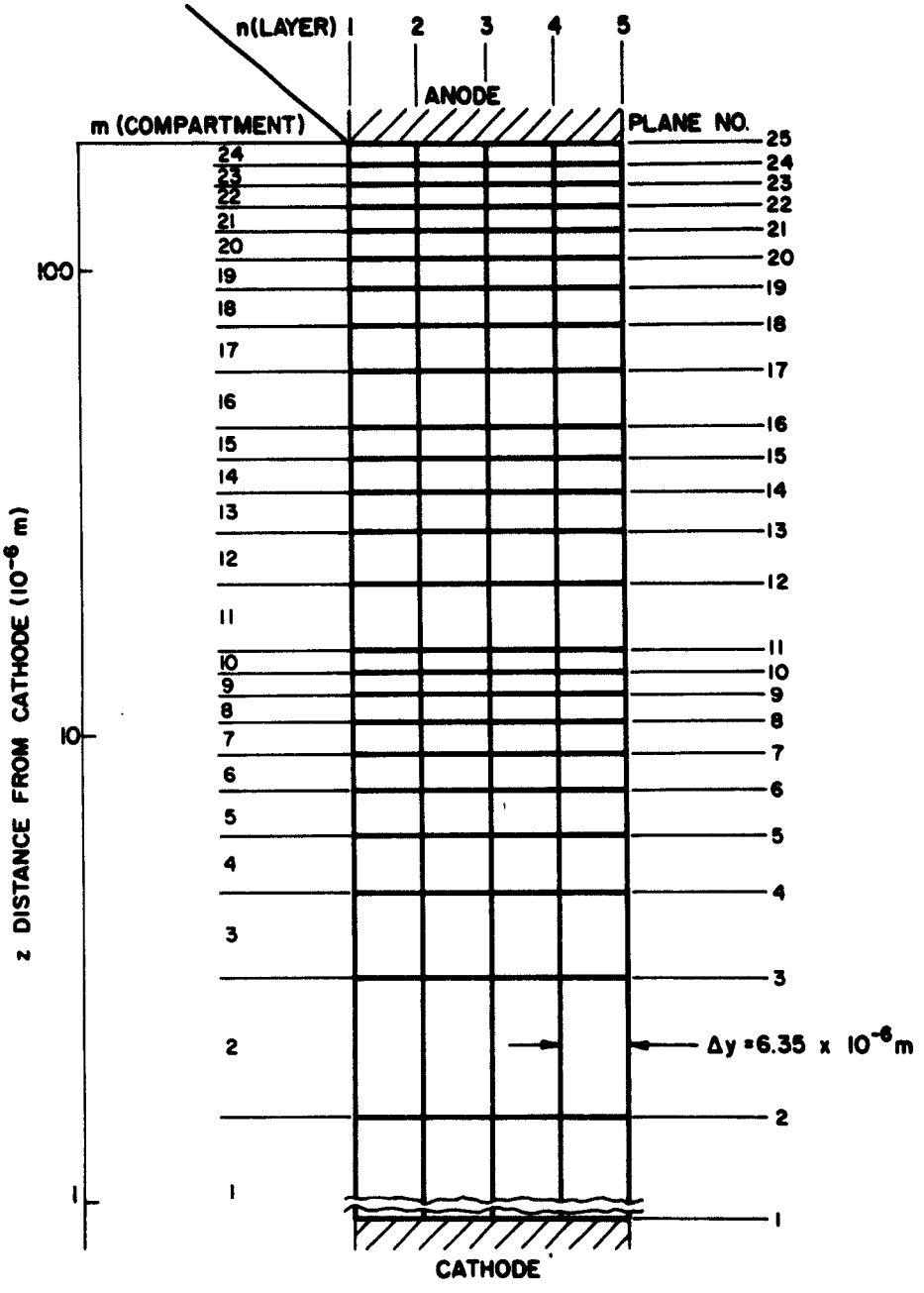

FIG. B.2 COMPARTMENTS IN A TWO-DIMENSIONAL DIODE FOR ELECTRIC FIELD COMPUTATIONS.

electrons do not cross more than one compartment boundary during unit time interval Δt. Then, the crossing time $t_i + \delta t$ is evaluated by means of the equation of motion such that

$$z_n - z(t_i) = v_\ell(y_m, z_n, t_i) \cdot \delta t - \left(h \frac{E_{d-c}}{2}\right) \delta t^2 \qquad (B.33)$$

or

$$\delta t = \frac{v_\ell(y_m, z_n, t_i) \pm \sqrt{v_\ell^2(y_m, z_n, t_i) - 2hE_{d-c}(z_n - z(t_i))}}{hE_{d-c}} \quad . \qquad (B.34)$$

Since E_{d-c} is negative, the lower sign will have to be used in order to bring forth a positive δt such that $0 \leq \delta t \leq \Delta t$. The velocity is therefore

$$v_\ell(y_m, z_n, t_{ic}) = v_\ell(y_m, z_n, t_i) - hE_{d-c}(\delta t) \qquad (B.35)$$

by definition.

B.IV General Harmonic Analysis

B.IV.1 Auto-Correlations and Cross-Correlations. For stationary random process with a sample function $x(t)$, the time auto-correlation function $R_{xx}(\tau)$ is defined such that

$$R_{xx}(\tau) = \lim_{T \to \infty} \frac{1}{2T} \int_{-T}^{T} x(t)\, x(t+\tau)\, dt \quad , \qquad (B.36)$$

where τ is the time interval between any two samples taken for the random variable $x(t)$. This is, according to the ergodic theorem, equal to the ensemble correlation function $\tilde{R}_{x_1, x_2}(\tau)$ which is the expected value of $x_1 x_2$

$$\tilde{R}_{x_1,x_2} = E[x_1,x_2]$$

$$= \int_{-\infty}^{\infty}\int_{-\infty}^{\infty} x_1(t)\, x_2(t+\tau)\, f_2(x_1,t;x_2,t+\tau)dx_1dx_2 \ , \qquad (B.37)$$

where $f_2(x_1,t;x_2,t+\tau)$ is the probability density of finding x between x_1 and x_1+dx_1 at t and between x_2 and x_2+dx_2 at $t+\tau$.

For x(t) assuming only a discrete set of values corresponding to a discrete set of t's equally spaced, the random process is called a random time series and its auto-correlation can be rewritten as

$$R_{xx}(s) = R_{xx}(s\Delta t) = \lim_{n\to\infty} \frac{1}{2N+1} \sum_{t=-N}^{N} x(t)\, x(t+s\Delta t) \ . \qquad (B.38)$$

Similarly, the cross-correlation function between two stationary random time series x(t) and y(t) with a discrete parameter t is

$$R_{xy}(s) = \lim_{N\to\infty} \frac{1}{2N+1} \sum_{t=-N}^{N} x(t)\, y(t+s\Delta t) \ . \qquad (B.39)$$

Some interesting characteristics of the foregoing equations may be revealed by replacing s with -s.

$$R_{xx}(-s) = \lim_{N\to\infty} \frac{1}{2N+1} \sum_{t=-N}^{N} x(t)\, x(t-s\Delta t) \ , \qquad (B.40)$$

$$R_{xy}(-s) = \lim_{N\to\infty} \frac{1}{2N+1} \sum_{t=-N}^{N} x(t)\, y(t-s\Delta t) \ . \qquad (B.41)$$

Now if $t' = t - s\Delta t$,

$$R_{xx}(-s) = \lim_{N\to\infty} \frac{1}{2N+1} \sum_{t'=-N-s\Delta t}^{N-s\Delta t} x(t'+s\Delta t)\, x(t)$$

$$= R_{xx}(s) \quad . \tag{B.42}$$

$$R_{xy}(-s) = \lim_{N\to\infty} \frac{1}{2N+1} \sum_{t'=-N-s\Delta t}^{N-s\Delta t} x(t'+s\Delta t)\, y(t)$$

$$= R_{yx}(s) \quad . \tag{B.43}$$

The auto-correlation functions are therefore even functions of time while the cross-correlation functions are not.

B.IV.2 Self-Power Spectral Density and Cross-Power Spectral Density of Ergodic Random Processes. For a random time series $x(t)$ such that

$$\lim_{T\to\infty} \frac{1}{2T} \int_{-T}^{T} |x(t)|^2 \, dt < \infty \tag{B.44}$$

there exists a Fourier transform of the correlation function $R(\tau)$ such that

$$S(f) = \frac{1}{2\pi} \int_{-\infty}^{\infty} R(\tau)\, e^{-j\omega\tau} d\tau \quad , \tag{B.45}$$

where $S(f)$ = the power spectral density function of the sample function $x(t)$ in the frequency domain, and

$\omega = 2\pi f$.

Similar to this, the power spectral density of a discrete parameter random process may be written as follows:

$$R(\tau) = R(\tau)\ \delta(\tau - s\Delta t) \quad . \tag{B.46}$$

Therefore

$$S(f) = \frac{\Delta t}{2\pi} \sum_{s=-q}^{q} R(s)\ [\cos \omega s\Delta t - j \sin \omega s\Delta t] \quad . \tag{B.47}$$

Whenever R(s) is an even function of s, the imaginary term drops out.

$$S(f)_{even} = \frac{\Delta t}{2\pi} \left\{ \sum_{s=1}^{p-1} 2\ R(s)\ \cos \omega s\Delta t + R(0) + R(p)\ \cos \omega q\Delta t \right\} \tag{B.48}$$

or when R(s) is an odd function of s such as the cross-correlation function

$$S(f)_{odd} = \frac{\Delta t}{2\pi} \sum_{s=-q}^{q} [R_{xy}(s) + R_{yx}(s)]\ \frac{1}{2}\ (\cos \omega s\Delta t - j \sin \omega s\Delta t)$$

$$= \frac{\Delta t}{2\pi} \left\{ \sum_{s=1}^{q} [R_{xy}(s) + R_{yx}(s)] \cos \omega s\Delta t \right.$$

$$\left. + R_{xy}(0) + \frac{1}{2} [R_{xy}(q) + R_{yx}(q)] \cos \omega q\Delta t \right\} - j \frac{\Delta t}{2\pi} \left\{ \sum_{s=1}^{q} [R_{xy}(s) \right.$$

$$\left. + R_{yx}(s)] \sin \omega s\Delta t + \frac{1}{2} [R_{xy}(q) + R_{yx}(q)] \sin \omega q\Delta t \right\} \quad . \tag{B.49}$$

APPENDIX C. KINETIC POWER IN AN ELECTRON BEAM

By means of the transmission-line analog[13], the existence of two wave solutions in a small-signal modulated electron beam may be illustrated. They are designated as the fast space-charge wave and the slow space-charge wave depending on their respective phase velocity compared to the average velocity $\dot{z}$ of the electrons. The kinetic potential V_1 and the convection current density i_1 may be expressed in terms of the two wave amplitudes, such that[30],

$$V_1 = \left[u_+ e^{j\beta_p z} + u_- e^{-j\beta_p z} \right] e^{-j\beta_e z} \tag{C.1}$$

and

$$i_1 = \frac{1}{W} \left[u_+ e^{j\beta_p z} - u_- e^{-j\beta_p z} \right] e^{-j\beta_e z} , \tag{C.2}$$

where u_+ is the amplitude of the fast space-charge wave whose propagation constant is $\beta_e - \beta_p$,

u_- is the amplitude of the slow space-charge wave whose propagation constant is $\beta_e + \beta_p$,

$W \triangleq 2V_o/I_o\,(\beta_p/\beta_e)$, the characteristic impedance of the electron beam,

$\beta_e \triangleq \omega/\dot{z}$,

$\beta_p \triangleq \omega_p/\dot{z}$, and

ω_p = the radian plasma frequency corresponding to the concentration of charge in the electron beam.

From the definition of the noise parameter Π in Eq. 2.31,

$$\Pi \triangleq \frac{1}{2} \mathrm{Re}\,[i_1^* V_1]$$

$$= \frac{1}{4}[i_1^* V_1 + i_1 V_1^*]$$

$$= \frac{1}{2W}[|u_+|^2 - |u_-|^2] \quad . \tag{C.3}$$

The right-hand side of Eq. C.3 represents the real kinetic power density in the electron beam. The two terms $|u_+|^2/2W$ and $|u_-|^2/2W$ may be regarded as the absolute value of the kinetic power density carried by the fast space-charge wave and the slow space-charge wave respectively.

BIBLIOGRAPHY

1. Schottky, W., "Spontaneous Current Fluctuations in Various Conductors", Ann. Physik, vol. 57, pp. 541-567; 1918.

2. Rack, A. J., "Effect of Space Charge and Transit Time on the Shot Noise in Diodes", B.S.T.J., vol. 17, pp. 592-619; 1938.

3. Llewellyn, F. B. and Peterson, L. C., "Vacuum Tube Networks", Proc. IRE, vol. 32, pp. 144-166; March, 1944.

4. Llewellyn, F. B., Electron Inertia Effects, Cambridge, London; 1941.

5. Pierce, J. R., "Noise in Resistances and Electron Streams", B.S.T.J., vol. 27, pp. 158-174; 1948.

6. Thompson, B. J., North, D. O. and Harris, W. A., "Fluctuations in Space-Charge-Limited Currents at Moderately High Frequencies", RCA Review, Part I, vol. IV, pp. 269-285; 1940: Part II, vol. IV, pp. 441-472; 1940.

7. Peterson, L. C., "Space Charge and Transit Time Effects on Signal and Noise in Microwave Tetrodes", Proc. IRE, vol. 35, pp. 1264-1272; 1947.

8. Pierce, J. R., Traveling-Wave Tubes, Chapter X, D. Van Nostrand Co., New York; 1950.

9. Whinnery, J. R., "Noise Phenomena in the Region of the Potential Minimum", Trans. IRE-PGED, vol. ED-1, pp. 221-236; 1954.

10. Watkins, D. A., "Noise at the Potential Minimum in the High Frequency Diode", JAP, vol. 26, pp. 622-624; May, 1955.

11. Siegman, A. E. and Watkins, D. A., "Potential-Minimum Noise in the Microwave Diode", Tech. Report No. 19, Stanford Electronics Labs.; July 2, 1957.

12. Watkins, D. A., "Noise Reduction in Beam Type Amplifiers", Proc. IRE, vol. 40, pp. 65-70; 1952.

13. Bloom, S. and Peter, R. W., "Transmission-Line Analog of a Modulated Electron Beam", RCA Review, vol. 15, pp. 95-100; March, 1954.

14. Bloom, S. and Peter, R. W., "A Minimum Noise Figure for the Traveling-Wave Tube", RCA Review, vol. 15, pp. 252-267; June, 1954.

15. Haus, H. A., "Noise in One Dimensional Electron Beams", JAP, vol. 26, pp. 560-571; May, 1955.

16. Haus, H. A. and Robinson, F. N. H., "A Minimum Noise Figure of Microwave Beam Amplifiers", Proc. IRE, vol. 43, pp. 981-991; August, 1955.

17. Siegman, A. E., "Analysis of Multivelocity Electron Beams by the Density-Function Method", JAP, vol. 28, No. 10, pp. 1132-1138; October, 1957.

18. Siegman, A. E., Watkins, W. A. and Hsieh, H. C., "Density-Function Calculations of Noise Propagation on an Accelerated Multivelocity Electron Beam", JAP, vol. 28, No. 10, pp. 1138-1148; October, 1957.

19. Vivian, W., "Transport of Noise at Microwave Frequency Through a Space-Charge-Limited Diode", Ph.D. Dissertation, The University of Michigan; 1959.

20. Currie, M. R. and Forster, D. C., "A New Mechanism of Noise Reduction in Electron Beams", Tech. Memo No. 512, Hughes Research Laboratories; May, 1958.

21. Berghammer, J. and Bloom S., "On the Nonconservation of Noise Parameters in Multivelocity Beams", JAP, vol. 31, pp. 454-458; March, 1960.

22. Hok, G., "Conservation Principles in Multivelocity Electron Flow", Trans. IRE-PGED, vol. ED-8, No. 6, pp. 452-461; November, 1961.

23. Shaw, A. W., "Investigation of Noise Reduction in Electron Beams by Means of Low Potential Regions", Tech. Report No. 401-2, Electron Devices Lab., Stanford Electronics Laboratories, Stanford, California; May 25, 1960.

24. Tien, P. K. and Moshman, J., "Monte Carlo Calculation of Noise Near the Potential Minimum of a High Frequency Diode", JAP, vol. 27, pp. 1067-1078; September, 1956.

25. Dayem, A. H. and Lambert, C. A. (Mrs.), "Noise Near the Potential Minimum of an Open Circuit Diode", Private Communication.

26. Berghammer, J., "Noise Smoothing by Reactive Damping in Finite Multivelocity Electron Beams", RCA Review, vol. 23, No. 1, pp. 185-194; March, 1961.

27. Hahn, W. C., "Small-Signal Theory of Velocity-Modulated Beams", Gen. Elec. Rev., vol. 42, pp. 258-270; 1939.

28. Ramo, S., "Space Charge and Field Waves in an Electron Beam", Phys. Review, vol. 56, pp. 276-283; 1939.

29. Kaplan, W., Advanced Calculus, Chapter VI, Addison-Wesley Publishing Co., Inc., Cambridge, Mass.; 1953.

30. Smullin, L. D. and Haus, H. A., Noise in Electron Devices, Chapter III, The Technology Press of Massachusetts Institute of Technology and John Wiley and Sons, Inc., New York; 1959.

LIST OF SYMBOLS

A	Cathode area.
A	Constant.
A_n	Fourier coefficient for the nth space harmonic.
a	Distance between the cathode and the anode of the two-dimensional diode.
B	Constant.
$D_o(\tau)$	Lag window, defined as $D_o(\tau) = 1$ for $\lvert\tau\rvert < q\Delta t$ $= 0$ otherwise.
$D_1(\tau)$	Lag window, defined as $D_1(\tau) = (1/2)[1 + \cos \pi\tau/q\Delta t]$.
$E(i,j;m,n)$	z-directed d-c electric field at the boundary between compartment (i,j) and compartment $(i+1,j)$ due to the presence of space charge $\rho_{m,n}$ at the centroid of compartment (m,n), volts/m.
$E(i,j)$	z-directed space charge electric field at the boundary between compartment (i,j) and compartment $(i+1,j)$, volts/m.
E	Total electric field, volts/m.
$E(x_1,x_2)$	Expected value of random variables x_1, x_2.
$E(y,z)$	Average z-directed space charge electric field at (y,z), volts/m.
$E_{applied}$	Applied d-c electric field in the z-direction, volts/m.
$E_{cathode}$	Electric field at the surface of the cathode, volts/m.
E_{d-c}	Total d-c electric field, volts/m.
$E(y,z,t)$	z-directed electric field at (y,z) at time t, volts/m.
$E_{oz}(y,z)$	z-directed d-c component of $E(y,z,t)$ volts/m.
$E_{1z}(y,z)$	The amplitude of the z-directed a-c component of $E(y,z,t)$, volts/m.
e	Absolute value of electron charge, coulombs.
$F(v)$	Integrated distribution function of a random variable v.

$F(y,z,\dot{y},\dot{z},t)$	Density function in a two-dimensional space.
$F(y,z,\dot{z},t)$	Density function in a two-dimensional space for $\dot{y} = 0$.
$F(y,z,W)$	Density function written in terms of excess energy parameter W.
$F_o(v_o)$	D-c density function of electrons with initial velocity v_o.
$F_o(y,z,\dot{z})$, $F_o(y,z,W)$	D-c component of $F(y,z,\dot{z},t)$.
$F_1(y,z,\dot{z})$, $F_1(y,z,W)$	Amplitude of the a-c component of $F_1(y,z,\dot{z},t)$.
$F_{min}(\zeta_j,\xi)$	Minimum noise figure for a beam layer at ζ_j and a distance ξ from the cathode.
$F_{min}(\xi)$	Minimum noise figure for the electron beam at a distance ξ from the cathode.
$F(y_m,z_n,\Omega)$	Minimum noise figure for the beam layer at (y_m,z_n) and frequency $f = \Omega/2q\Delta t$.
$F(z_n,\Omega)$	Minimum noise figure of the electron beam at z_n and frequency $f = \Omega/2q\Delta t$.
f	Frequency, cycles/sec.
f(v)	Distribution function of a random variable v.
f_c	Cut off frequency at which the ratio of the estimated spectral density and the actual spectral density falls to zero.
$G(\zeta_m,w_i;\zeta_n,w_\ell)$	Weighting factor for the response part of the a-c density function at layer n, velocity class ℓ corresponding to a unit current input at layer m, velocity class i of the homogeneous part of the density function.
g	Frequency parameter.
$H_x(y,z)$	A-c component of the x-directed magnetic field at (y,z), amp/m.
h	The absolute value of electron charge-to-mass ratio.
h	An integer.
$I_{den.}$	Average z-directed emission current density, amp/m^2.

I_o	Average z-directed convection current density in the beam, amp/m^2.
$I_o(y)$, $I_o(\zeta)$	Average z-directed convection current density at y or ζ, amp/m^2.
i	An integer.
i_c	z-directed convection current density, amp/m^2.
$i_1(y_m,z_n,t_i)$	z-directed a-c convection current density at the mth layer and nth plane during the time interval between t_i and $t_i+\Delta t$, amp/m^2.
$i_1(z_n,t_i)$	z-directed a-c convection current density at the nth plane during the time interval between t_i and $t_i+\Delta t$, amp/m^2.
$i_{1H}(\zeta_j,\xi;$ $_{1R}$ $\zeta_m,w_i)$	z-directed a-c convection current density at (ζ_j,ξ) per unit bandwidth associated with a unit homogeneous or response current input at the ith velocity class of the mth layer, amp/m^2.
$i_{1H}(\xi;\zeta_m,w_i)$ $_{1R}$	z-directed a-c convection current density at ξ per unit bandwidth associated with a unit homogeneous or response current input at the ith velocity class of the mth layer, amp/m^2.
J_{d-c}	z-directed d-c current density, amp/m^2.
j, k, ℓ, m	Integers.
m	Mass of an electron, kg.
N	Number of electrons in a compartment.
$N(y_m,z_n,t_i)$	The number of electrons crossing the nth plane at the mth layer during the time interval between t_i and $t_i+\Delta t$.
$N_o(y_m,z_n)$	Average number of electrons crossing the nth plane at the mth layer per unit time interval Δt.
n	An integer.
$P(\zeta,\xi,w)$	Dimensionless density function parameter defined as $P(\zeta,\xi,w) = [\alpha\ (I_o/e)]^{-1}\ F(y,z,W)$.
$P_o(w)$	D-c component of the dimensionless density function parameter $P(\zeta,\xi,w,t)$.
$P_1(\zeta,\xi,w)$	A-c component of the density function parameter $P(\zeta,\xi,w)$.

$P_{1H}^{\pm}(\zeta_j,\xi, {}_{1R}w_k;\zeta_m,w_i)$ Dimensionless a-c density function parameters at (ζ_j,ξ) associated with the kth velocity class induced by a unit homogeneous or response current input at the ith velocity class of the mth layer. "±" sign stands for the forward going and backward going electrons respectively.

$p_{1H}^{\pm}(\zeta_j,\xi, {}_{1R}w_k;\zeta_m,w_i)$ The response part of the dimensionless a-c density function parameter defined such that

$$P_1(\zeta_j,\xi,w_k;\zeta_m,w_i) \equiv \left[-\frac{\partial P_o(w)}{\partial w}\right]\frac{I_o}{I_o(\zeta_j)} \times p_1(\zeta_j,\xi,w_k;\zeta_m,w_i) - \frac{2\delta(w-w_i)e^{-j\theta_i}}{|I_o|}.$$

p Total number of computer time intervals employed in the Monte Carlo calculations.

$Q_o(f)$ The Fourier transform of $D_o(\tau)$, a spectral density weighting factor.

$Q_1(f)$ The Fourier transform of $D_1(\tau)$, a modified spectral density weighting factor.

q The number of time intervals $q\Delta t$ is defined such that two samples of a random variable taken at a time interval greater than $q\Delta t$ apart are completely uncorrelated.

R_i, R_s Random numbers.

$R(\tau)$ A correlation function between samples of a random process taken at a time interval τ apart.

$\overline{R(\tau)}$ Average value of $R(\tau)$ between $\tau - \Delta\tau/2$ and $\tau + \Delta t/2$.

$R_{xx}(\tau)$ Time auto-correlation function for a stationary random process with a sample function $x(t)$.

$R_{xx}(s)$ Same as $R_{xx}(s\Delta t)$.

$R_{xy}(s)$ Time cross-correlation function for two stationary random processes with sample functions $x(t)$ and $y(t)$ respectively.

$\tilde{R}_{x_1x_2}(\tau)$ Auto-correlation function for a random process with sample functions x.

S A noise parameter defined by Haus.

$S_1(f)$ Power spectral density of the convection current density fluctuations.

$S_2(f)$ Power spectral density of the equivalent velocity fluctuations created by shot effect from a thermionic cathode.

$S_R(f)$ Power spectral density, Fourier transform of $R(\tau)$.

$S_{\bar{R}}(f)$ Power spectral density, Fourier transform of $\bar{R}(\tau)$.

$S_R(s)$ Power spectral density corresponding to $R(\tau)$; s is a complex number.

$S_\delta(s)$ Power spectral density corresponding to a set of delta functions equally spaced in the time domain.

$S(s)$ $S(s)$ is defined as $S(s) = (1/2\pi j) \oint S_R(s-u)S_\delta(u)du$.

$S(w+\eta_c)$ A unit step function, $S(w+\eta_c) = 0$ for $w < \eta_c$.
$= 1$ for $w \geq \eta_c$.

$S(\zeta_j,\xi)$ Noise parameter at (ζ_j,ξ).

$S(\xi)$ Noise parameter at ξ.

$S(y_m,z_n,\Omega)$ Noise parameter at (y_m,z_n) and frequencies $f = \Omega/2q\Delta t$.

$S(z_n,\Omega)$ Noise parameter at z_n and frequencies $f = \Omega/2q\Delta t$.

s Complex frequency, cps.

s An integer.

T Ambient temperature in degrees K.

T A dummy variable employed during the evaluation of certain improper integrals.

T_c Cathode temperature in degrees K.

t Time measured from some reference point, sec.

t_i At the end of the ith time interval.

U_+ The amplitude of the fast space-charge wave.

U_- The amplitude of the slow space-charge wave.

u Velocity of electrons in the beam, m/sec.

u_o Average velocity of the electrons in the beam, m/sec.

$V(i,j,m,n)$ Potential depression at the boundary between compartment (i,j) and compartment $(i+1,j)$ due to the presence of space charge $\rho_{m,n}$ at the centroid of compartment (m,n), volts.

$V(i,j)$ Potential depression at the boundary between compartment (i,j) and compartment $(i+1,j)$ due to space charge, volts.

$V(y,z)$	Potential at (y,z) relative to the cathode potential, volts.
$V'(y)$	Potential at the potential minimum of the beam layer centered at y, volts.
V_{anode}	D-c potential at the anode (applied voltage).
V_{d-c}	D-c potential, volts.
V_{a-c}	A-c voltage across the diode, volts.
V_1	Chu's kinetic potential, volts.
$V_{1H}(\zeta_j,\xi;\ \zeta_m,w_i)$	z-directed kinetic potential at (ζ_j,ξ) per unit bandwidth associated with a unit homogeneous or response current input at the w_i velocity class of the mth layer, volts.
$V_{1H}(\xi;\zeta_m,w_i)$	z-directed kinetic potential at ξ per unit bandwidth associated with a unit homogeneous or response current input at the w_i velocity class of the mth layer, volts.
v_o	Initial velocity of electrons, m/sec.
$\overline{v_o^2}(y_m,z_n)$	Mean square velocity of electrons at (y_m,z_n).
v_o'	Initial velocity of the electrons which possess barely enough energy to reach the potential minimum, m/sec.
v_1	Amplitude of a-c velocity, m/sec.
v_i	Initial velocity of the ith electron, m/sec.
$v_\ell(y_m,z_n,\ t_{ic})$	Velocity of the ℓth electron crossing the nth plane at the mth layer at t_{ic}, m/sec.
W	Excess energy parameter defined as $W \triangleq \dot{z}^2 - 2h[V(y,z)-V'(y)]$.
W	Electron beam characteristic impedance defined as $W \triangleq (2V_o/I_o)(\beta_p/\beta_e)$, ohms.
$\overline{W}$	Average excess energy parameter.
W	Dimensionless excess energy parameter corresponding to W $w \triangleq \alpha W$.
w_k	Dimensionless excess energy parameter of the kth velocity class.
$X(\eta,w)$	A switch defined such that $X(\eta,w_h) \triangleq 1$ if $w < 0$, $w+\eta > 0.02$ $\triangleq 0$ otherwise.
x	Real space coordinate, meters.

$\dot{x}$ — Time derivative of x; x-directed velocity, m/sec.

$Y(\eta,w)$ — A switch defined such that
$Y(\eta,w) \triangleq 1$ if $w > 0$ or $w < 0$ and $w+\eta \geq 0.02$
$\triangleq 0$ otherwise.

y — Real space coordinate, meters.

$\dot{y}$ — y-directed velocity, m/sec.

Z — R-f impedance of the diode, ohms.

z — Real space coordinate, meters.

$\dot{z}$ — z-directed velocity, m/sec.

$\ddot{z}$ — z-directed acceleration, m/sec.

$z_{\ell}(t_i)$ — z-directed space coordinate of the ℓth electron at t_i meters.

z' — Space coordinate, a dummy variable, meters.

$\dot{z}'$ — z-directed velocity of electrons at a layer $y = y'$, m/sec.

α — A constant defined as $\alpha \triangleq m/2kT_c$.

β — A constant defined as $\beta \triangleq 2\pi^{1/4} (e|I_o|/\epsilon_o m)^{1/2}$

β' — Phase constant defined as $\beta' \triangleq \omega/\dot{z}$, m^{-1}.

β_e — Phase constant for a single velocity electron beam, $\beta_e \triangleq \omega/\dot{z}$, m^{-1}.

β_p — Plasma phase constant defined as, m^{-1}. $\beta_p = \omega_p/\dot{z}$.

$\delta(j,m)$ — Delta function defined as $\delta(j,m) \triangleq 1$ if $j = m$
$\triangleq 0$ if $j \neq m$.

$\delta(w-w_i)$ — Delta function defined as
$\int_{w_i-\epsilon}^{w_i+\epsilon} \delta(w-w_i)\, dw = 1$, $\delta(w-w_i) = 0$ for $w \neq w_i$
$= \infty$ for $w = w_i$.

δt — Incremental change in time.

Δt — Unit time interval $\Delta t = 2 \times 10^{-12}$ sec.

ΔA — Sample emission area of an electron beam layer, m^2.

Δz — Incremental change in z, meters.

$\Delta\theta$ — Incremental change in phase angle.

ϵ_o — Dielectric constant of the free space.

ζ — Dimensionless real space coordinate parameter.

$\dot{\zeta}$ — Time derivative of ζ.

$\eta(\zeta,\xi)$ — Potential parameter.

η_c — Potential parameter at the cathode.

$\eta_m(\zeta)$ — Potential parameter defined as $\eta_m(\zeta) = 2e\alpha V'/m$.

$\Theta(y_m,z_n,\Omega)$ — Cross-power spectral density of the convection current density fluctuations and the kinetic potential per unit bandwidth at (y_m,z_n) and frequency $f = \Omega/2q\Delta t$.

$\theta(y,z,s)$ — Cross-correlation function between the convection current density fluctuations and the kinetic potential at (y,z).

$\theta_i^{\pm}(\zeta,\xi,w_i)$ — Phase shift of the original disturbance associated with the ith velocity class.

$\theta_i^{\pm} \triangleq \pm a \int_0^{\xi} \frac{d\xi}{\sqrt{w_i+\eta(\zeta,\xi)}}$. The negative sign is for the backward going electrons.

$\Lambda(y_m,z_n,\Omega)$ — Imaginary part of $\Theta(y_m,z_n,\Omega)$.

$\Lambda(\zeta_j,\xi)$ — Imaginary part of the cross-power spectral density of the current fluctuations and the kinetic potential at (ζ_j,ξ).

$\Lambda(\xi)$ — Imaginary part of the cross-power spectral density of the current fluctuations and the kinetic potential at ξ.

ν — Frequency, dummy variable.

ξ — Dimensionless real space coordinate parameter.

$\dot{\xi}$ — Time derivative of ξ.

$\ddot{\xi}$ — Second time derivative of ξ.

$\Pi(y_m,z_n,\Omega)$ — Real part of $\Theta(y_m,z_n,\Omega)$.

$\Pi(\zeta_j,\xi)$ — Real part of the cross-power spectral density of the convection current density fluctuations and the kinetic potential at (ζ_j,ξ).

$\Pi(\xi)$ — Real part of the cross-power spectral density of the convection current density fluctuation and the kinetic potential at ξ.

ρ_{I} ρ_{II}	Space-charge density in regions I and II respectively coul./m^2.
ρ_{ℓ}	Space charge per unit length in the x-direction, coul./m^2.
$\rho_{m,n}$	Space charge per unit length in the x-direction at the centroid of compartment (m,n), coul./m.
$[\rho v](y,z)$	z-directed convection current density in compartment (y,z), amp/m^2.
τ	Time measured from some reference point, sec.
$\Phi(y_m,z_n,\Omega)$	Self-power spectral density of the kinetic potential at (y_m,z_n) and frequency $f = \Omega/2q\Delta t$.
$\varphi(y,z,s)$	Auto-correlation function of the kinetic potential at (y,z).
$\Phi(\zeta_j,\xi)$	Self-power spectral density of the kinetic potential at (ζ_j,ξ).
$\Phi(\xi)$	Self-power spectral density of the kinetic potential at ξ.
$\Psi(y_m,z_n,\Omega)$	Self-power spectral density of the convection current density fluctuations at (y_m,z_n) and frequency $f = \Omega/2q\Delta t$.
$\psi(y_m,z_n,s)$	Auto-correlation of the convection current density fluctuations at (y_m,z_n).
$\psi(\zeta_j,\xi)$	Self-power spectral density of the convection current density at (ζ_j,ξ).
$\psi(\xi)$	Self-power spectral density of the convection current density at ξ.
Ω	Frequency parameter defined as $\Omega = \Omega/2q\Delta t$, $sec.^{-1}$
ω	Radian frequency defined as $\omega = 2\pi f$.

DISTRIBUTION LIST

No. Copies	Agency
7	Aeronautical Systems Division, Attn: ASRNET-1, Wright-Patterson Air Force Base, Ohio
1	Air Force Cambridge Research Laboratories, Attn: Tube Group, L. G. Hanscom Field, Bedford, Massachusetts
1	Chief, Bureau of Ships, Code 691A4, Attn: Mr. H. J. Riegger, Department of the Navy, Washington 25, D. C.
1	Chief, Bureau of Ships, Attn: Mr. Charles Walker, Department of the Navy, Washington 25, D. C.
1	Commanding Officer, Diamond Ordnance Fuze Laboratories, Attn: Microwave Tube Branch, Washington 25, D. C.
1	Electronic Systems Division, Attn: ESRDE, Major J. W. Van Horn, L. G. Hanscom Field, Bedford, Massachusetts
1	Rome Air Development Center, Attn: RALTP, Mr. H. Chiosa, Griffiss Air Force Base, New York
1	Commanding Officer, USAERDL, Attn: Mr. Harold J. Hersh, SIGRA/SL-PRM, Ft. Monmouth, New Jersey
1	Commanding Officer, USAERDL, Attn: Mr. Irving Reingold, Microwave Tubes Branch, Ft. Monmouth, New Jersey
1	Commanding Officer, U. S. Naval Ordnance Laboratory, Attn: Miss Virginia L. Parker, Corona, California
30	ASTIA (TISIA), Arlington Hall Station, Arlington 12, Virginia
4	Advisory Group on Electron Devices, Attn: Mr. H. N. Serig, 346 Broadway, 8th Floor, New York 13, New York
1	Bendix Corporation, Systems Planning Division, Ann Arbor, Michigan, Attn: Technical Library
1	Mr. A. G. Peifer, Bendix Corporation, Research Laboratories, Northwestern Hwy. & 10-1/2 Mile Rd., Detroit 35, Michigan
1	Bendix Corporation, Research Laboratories, Northwestern Hwy. & 10-1/2 Mile Rd., Detroit 35, Michigan, Attn: Technical Library
1	California Institute of Technology, Department of Electrical Engineering, Pasadena, California, Attn: Professor R. Gould

No. Copies	Agency
1	Dr. Om P. Gandhi, Central Electronics Engineering Research Institute, Pilani, Rajasthan, India
1	Dr. Peter T. Kirstein, CERN, European Organization for Nuclear Research, Geneve 23, Switzerland
1	Cornell University, Department of Electrical Engineering, Ithaca, New York, Attn: Professor L. Eastman
1	Dr. Rajindar P. Wadhwa, Electron Tube Division, Litton Industries, 960 Industrial Way, San Carlos, California
1	Dr. G. Branch, General Electric Research Laboratories, Schenectady, New York
1	General Electric Company, Electron Tube Division of Research Laboratory, Schenectady, New York, Attn: Dr. E. D. McArthur
1	Dr. David C. Prince, Jr., General Electric Company, Flight Propulsion Laboratory Department, Cincinnati 15, Ohio
1	General Electric Microwave Laboratory, 601 California Avenue, Palo Alto, California, Attn: Mr. S. Webber
1	Dr. Kurt Amboss, Hughes Research Laboratories, Malibu, California
1	Dr. George R. Brewer, Electron Tube Laboratory, Hughes Research Laboratories, Malibu, California
1	Hughes Aircraft Company, Florence and Teals, Culver City, California, Attn: Mr. Nicholas E. Devereux, Technical Document Center
1	University of Illinois, Department of Electrical Engineering, Urbana, Illinois, Attn: Professor Paul D. Coleman
1	Dr. J. R. Hechtel, Litton Electron Tube Corporation, 960 Industrial Road, San Carlos, California
1	Litton Industries, 960 Industrial Way, San Carlos, California, Attn: Dr. Joseph Hull
1	Massachusetts Institute of Technology, Research Laboratory of Electronics, Cambridge 39, Massachusetts, Attn: Documents Library
1	Microwave Electronics Corporation, 4061 Transport Street, Palo Alto, California, Attn: Dr. S. F. Kaisel

No. Copies	Agency
1	Microwave Associates, Attn: Dr. P. Chorney, Burlington, Massachusetts
1	University of Minnesota, Department of Electrical Engineering, Minneapolis, Minnesota, Attn: Dr. W. G. Shepherd
1	Polytechnic Institute of Brooklyn, Documents Library, Brooklyn, New York
1	Raytheon Company, Spencer Laboratory, Burlington, Massachusetts, Attn: Mr. W. Teich
1	RCA Laboratories, Princeton, New Jersey, Attn: Library
1	Sperry Corporation, Electronic Tube Division, Gainesville, Florida, Attn: Library
1	Sperry Gyroscope Company, Great Neck, New York, Attn: Engineering Library
1	Dr. A. D. Sutherland, Sperry Electronic Tube Division, Gainesville, Florida
1	Stanford University, Microwave Laboratory, Stanford, California, Attn: Dr. M. Chodorow
1	Dr. K. J. Harker, Stanford University, W. W. Hansen Laboratories of Physics, Stanford, California
1	Stanford University, Electronics Laboratories, Stanford, California, Attn: Dr. A. E. Siegman
1	Sylvania Microwave Tube Laboratory, 500 Evelyn Avenue, Mountain View, California, Attn: Dr. J. Needle
1	Sylvania Electric Products Inc., Applied Research Laboratory, 40 Sylvan Road, Waltham 54, Massachusetts, Attn: Mrs. Mary E. Bufka, Librarian
1	Varian Associates, 611 Hansen Way, Palo Alto, California, Attn: Technical Library
1	Watkins-Johnson Company, 3333 Hillview Avenue, Palo Alto, California, Attn: Dr. D. A. Watkins
1	Mr. Gerald Klein, Manager, Microwave Tubes Section, Applied Research Department, Westinghouse Electric Corporation, Box 746, Baltimore 3, Maryland

No. Copies	Agency
1	Westinghouse Electric Corporation, P. O. 284, Elmira, New York, Attn: Mr. Daniel Buck
1	The University of Michigan, Office of Research Administration, Mortimer E. Cooley Building, Ann Arbor, Michigan, Attn: Project Files
62	The University of Michigan, Electron Physics Laboratory, 3505 East Engineering Building, Ann Arbor, Michigan

AD______________

The University of Michigan, Electron Physics Laboratory, Ann Arbor, Michigan. NOISE IN MULTI-DIMENSIONAL ELECTRON STREAMS, by C. P. Wen. March, 1963, 202 pp. incl. illus. (Proj. No. 4156, Task No. 415603)

The purpose of this investigation is to study the noise transport and reduction phenomena in multivelocity electron beams with significant potential variations in the transverse direction. The study was carried out by means of a high-speed digital computer employing two different numerical methods.

Details of the derivation of a small-signal linearized Boltzmann equation in terms of a statistical electron density function and the electric field in a two-dimensional space-charge-limited diode are presented.

The noise transport phenomena are also treated using the Monte Carlo technique in which random numbers are generated to simulate the stochastic emission process and each electron emitted from the thermionic cathode is traced in phase space by numerical integration methods.

Substantial noise reduction is found by the Monte Carlo method yielding a noise figure of less than 2 db. No reduction from shot noise if found in the density function calculation. This is attributed to the approximations made in numerically evaluating the velocity dependent coupling fields.

UNCLASSIFIED

1. Introduction
2. Density-Function Formulation
3. Monte Carlo Formulation
4. Results and Interpretations of the Density Function Calculations
5. Results and Interpretations of the Monte Carlo Calculations
6. Summary and Conclusions
I. Wen, C. P.

UNCLASSIFIED

AD______________

The University of Michigan, Electron Physics Laboratory, Ann Arbor, Michigan. NOISE IN MULTI-DIMENSIONAL ELECTRON STREAMS, by C. P. Wen. March, 1963, 202 pp. incl. illus. (Proj. No. 4156, Task No. 415603)

The purpose of this investigation is to study the noise transport and reduction phenomena in multivelocity electron beams with significant potential variations in the transverse direction. The study was carried out by means of a high-speed digital computer employing two different numerical methods.

Details of the derivation of a small-signal linearized Boltzmann equation in terms of a statistical electron density function and the electric field in a two-dimensional space-charge-limited diode are presented.

The noise transport phenomena are also treated using the Monte Carlo technique in which random numbers are generated to simulate the stochastic emission process and each electron emitted from the thermionic cathode is traced in phase space by numerical integration methods.

Substantial noise reduction is found by the Monte Carlo method yielding a noise figure of less than 2 db. No reduction from shot noise is found in the density function calculation. This is attributed to the approximations made in numerically evaluating the velocity dependent coupling fields.

UNCLASSIFIED

1. Introduction
2. Density-Function Formulation
3. Monte Carlo Formulation
4. Results and Interpretations of the Density Function Calculations
5. Results and Interpretations of the Monte Carlo Calculations
6. Summary and Conclusions
I. Wen, C. P.

UNCLASSIFIED

AD______________

The University of Michigan, Electron Physics Laboratory, Ann Arbor, Michigan. NOISE IN MULTI-DIMENSIONAL ELECTRON STREAMS, by C. P. Wen. March, 1963, 202 pp. incl. illus. (Proj. No. 4156, Task No. 415603)

The purpose of this investigation is to study the noise transport and reduction phenomena in multivelocity electron beams with significant potential variations in the transverse direction. The study was carried out by means of a high-speed digital computer employing two different numerical methods.

Details of the derivation of a small-signal linearized Boltzmann equation in terms of a statistical electron density function and the electric field in a two-dimensional space-charge-limited diode are presented.

The noise transport phenomena are also treated using the Monte Carlo technique in which random numbers are generated to simulate the stochastic emission process and each electron emitted from the thermionic cathode is traced in phase space by numerical integration methods.

Substantial noise reduction is found by the Monte Carlo method yielding a noise figure of less than 2 db. No reduction from shot noise if found in the density function calculation. This is attributed to the approximations made in numerically evaluating the velocity dependent coupling fields.

UNCLASSIFIED

1. Introduction
2. Density-Function Formulation
3. Monte Carlo Formulation
4. Results and Interpretations of the Density Function Calculations
5. Results and Interpretations of the Monte Carlo Calculations
6. Summary and Conclusions
I. Wen, C. P.

UNCLASSIFIED

AD______________

The University of Michigan, Electron Physics Laboratory, Ann Arbor, Michigan. NOISE IN MULTI-DIMENSIONAL ELECTRON STREAMS, by C. P. Wen. March, 1963, 202 pp. incl. illus. (Proj. No. 4156, Task No. 415603)

The purpose of this investigation is to study the noise transport and reduction phenomena in multivelocity electron beams with significant potential variations in the transverse direction. The study was carried out by means of a high-speed digital computer employing two different numerical methods.

Details of the derivation of a small-signal linearized Boltzmann equation in terms of a statistical electron density function and the electric field in a two-dimensional space-charge-limited diode are presented.

The noise transport phenomena are also treated using the Monte Carlo technique in which random numbers are generated to simulate the stochastic emission process and each electron emitted from the thermionic cathode is traced in phase space by numerical integration methods.

Substantial noise reduction is found by the Monte Carlo method yielding a noise figure of less than 2 db. No reduction from shot noise is found in the density function calculation. This is attributed to the approximations made in numerically evaluating the velocity dependent coupling fields.

UNCLASSIFIED

1. Introduction
2. Density-Function Formulation
3. Monte Carlo Formulation
4. Results and Interpretations of the Density Function Calculations
5. Results and Interpretations of the Monte Carlo Calculations
6. Summary and Conclusions
I. Wen, C. P.

UNCLASSIFIED